PB96-143136

June 1995 Final

Seismic Rehabilitation of Framed Buildings Infilled with Unreinforced Masonry Walls Using Post-Tensioned Steel Braces

NSF Grant No. BCS-9221527

Teran-Gilmore, Amador
Bertero, Vitelmo V. and
Youssef, Nabih

Earthquake Engineering Research Center
University of California at Berkeley
1301 S. 46th Street
Richmond, CA 94804

UCB/EERC-95/06

National Science Foundation
1800 G Street, N.W.
Washington, D.C. 20550

This report is organized in four chapters and one appendix. Chapter 1 provides an introduction to the seismic performance of unreinforced masonry (URM) buildings and framed buildings with URM infills based on a discussion of their performance during previous earthquake ground motions (EQGMs) and of recent research results obtained worldwide. Chapter 2 describes the mechanical properties and dynamic characteristics of an existing reinforced concrete (RC) framed building with URM infills located in the Los Angeles urban area. In Chapter 3, the desirable performances associated with different levels of EQGMs are discussed for framed buildings with URM infills. Finally, in Chapter 4 some observations, conclusions and recommendations are presented, with emphasis on the advantages and disadvantages of using post-tensioned (PT) braces to upgrade existing framed buildings with URM infills. Appendix A describes how the seismic inputs (corresponding to the safety level EQGM) for the design of the PT braces upgrading scheme was established.

281

unclassified unclassified unclassified

Page Intentionally Left Blank

REPORT NO.
UCB/EERC-95/06
JUNE 1995

EARTHQUAKE ENGINEERING RESEARCH CENTER

SEISMIC REHABILITATION OF FRAMED BUILDINGS INFILLED WITH UNREINFORCED MASONRY WALLS USING POST-TENSIONED STEEL BRACES

by

AMADOR TERÁN-GILMORE
VITELMO V. BERTERO
NABIH YOUSSEF

COLLEGE OF ENGINEERING

UNIVERSITY OF CALIFORNIA AT BERKELEY

For sale by the National Technical Information Service, U.S. Department of Commerce, Springfield, Virginia 22161

See back of report for up to date listing of EERC reports.

PB96-143136

SEISMIC REHABILITATION OF FRAMED BUILDINGS INFILLED WITH UNREINFORCED MASONRY WALLS USING POST-TENSIONED STEEL BRACES

by

Amador Terán-Gilmore
Vitelmo V. Bertero
and
Nabih Youssef

A Report to the National Science Foundation

Report No. UCB/EERC-95/06
Earthquake Engineering Research Center
College of Engineering
University of California at Berkeley
June 1995

TABLE OF CONTENTS

LIST OF TABLES

LIST OF FIGURES

ABSTRACT

It has been noted by several researchers that the most significant seismic hazards in our urban and rural areas are produced by the interaction between the seismic activity at the given site and the built environment (all human-made facilities). The great life and economic losses that occur during earthquake ground motions (EQGMs) are not produced by the ground motion itself, but by the failure and collapse of the structures that constitute the built environment. Given our inability to control the seismic activity that affects a given region, the most effective way to reduce its seismic hazards to an acceptable level is the upgrading (retrofitting) of existing hazardous structures. The urgency of the need to carry out this upgrading has been emphasized by the occurrence in recent years of moderate EQGMs in California, such as the Loma Prieta 1989 and Northridge 1994 events. Society as a whole and some members of the structural engineering community suddenly became aware of the vulnerability of their built environment and started wondering about the safety of this environment once they realized that the damage potential of the recent seismic events was significantly lower than that which can be expected from the "big one" (large seismic event with magnitude of 8 or larger).

Unreinforced masonry (URM) buildings and framed buildings infilled with URM walls, which were designed and constructed before the development and flourishing of seismic design, constitute an important part of the vast inventory of high-risk structures in many California cities. Currently, there is a need to develop simple and efficient (from a technical and economical point of view) retrofitting schemes to upgrade these buildings in such a way that they can have adequate performance during strong EQGMs.

In recent years, several researchers and practitioners have shown that the seismic performance of existing buildings when subjected to strong EQGMs can be enhanced considerably by bracing the buildings with post-tensioned (PT) rods or cables. The use of this upgrading technique yields several advantages, such as versatility, low cost, fast and clean construction, and does not add any significant reactive mass to the existing facility. The implementation of this technique to the upgrading of framed buildings with URM infills will probably yield large economic advantages

in the rehabilitation of these buildings. Nevertheless, there are many aspects and issues that need to be studied and resolved before attempting such implementation.

The studies reported herein have the following objectives: First, to identify, study and discuss relevant issues in the evaluation of the seismic hazards of non-ductile frames infilled with URM walls; second, to investigate the use of PT steel braces to reduce these seismic hazards in framed buildings with URM walls located in regions of high seismic risk in California; third, to study and discuss the issues that need to be considered during the design process to attain efficient (technically and economically) retrofitted facilities using this technique; fourth, to assess the use of this technique by studying the seismic performance of a specific building with non-ductile reinforced concrete (RC) frames and URM infills before and after it has been upgraded with PT braces; and fifth, to offer some conclusions drawn from the study and recommendations regarding the research that is needed to improve the application of such technique.

This report is organized in four chapters and one appendix. Chapter 1 provides an introduction to the seismic performance of URM buildings and framed buildings with URM infills based on a discussion of their performance during previous EQGMs and of recent research results obtained worldwide. Then, the use of steel braces for the upgrading of existing buildings is discussed, focusing attention on the particulars of the use of PT braces. Finally, based on the information introduced in this chapter, a preliminary discussion of the advantages of using PT braces to rehabilitate framed buildings with URM infills is presented.

Chapter 2 describes the mechanical properties and dynamic characteristics of an existing RC framed building with URM infills located in the Los Angeles urban area. The building was selected to illustrate the upgrading of this type of building by introducing PT braces to the existing structure. Current knowledge regarding the modeling of framed buildings with URM infills is discussed, and the behavior of this building when subjected to the safety level EQGM is assessed by analyzing elastic and nonlinear models of the building. From the results obtained from the previous analyses, the need to upgrade this building is assessed.

In Chapter 3, the desirable performances associated with different levels of EQGMs are discussed for framed buildings with URM infills. A procedure for the design of upgrading schemes (based on the use of PT braces) that accounts for these desired performances is presented and applied to the building introduced in Chapter 2. Next, the seismic performance of the upgraded building is assessed by means of linear and nonlinear analyses.

Finally, in Chapter 4 some observations, conclusions and recommendations are presented, with emphasis on the advantages and disadvantages of using PT braces to upgrade existing framed buildings with URM infills. Research needs to improve the application of this upgrading technique are presented.

Appendix A describes how the seismic input (corresponding to the safety level EQGM) for the design of the PT braces upgrading scheme was established.

ACKNOWLEDGEMENTS

This investigation was supported by the National Science Foundation under Grant No. BCS-9221527. NSF program officials William Anderson, Shih-Chi Liu and M. P. Singh provided valuable encouragement and guidance for the development and publication of the seismic rehabilitation strategy and technique proposed herein. The authors are grateful to NSF Repair and Rehabilitation Research Group Coordinator Jim Jirsa for his direction and contributions. The first author is also indebted to the "Universidad Autónoma Metropolitana" of Mexico for partially supporting his graduate studies at the University of California at Berkeley, and particularly to Professor Jesús Iglesias for his moral support.

The studies presented in this report were carried out by Amador Terán Gilmore as a part of his Ph.D. dissertation studies under the supervision of Professor Vitelmo V. Bertero and with the help and long and fruitful discussions held with Nabih Youssef. The help of Brad Young in editing this report is gratefully appreciated.

1 INTRODUCTION

Perhaps no structural material has been used so extensively around the world as unreinforced masonry (URM) for the construction of structures located in zones of high seismicity. And perhaps, the behavior and seismic performance of no other structural material has been so misunderstood as that of URM. Given the poor performance of URM buildings during past earthquakes, the notion that URM is not good structural material to resist lateral loads is widely extended in the structural engineering community. Nevertheless, thanks to the work of several researchers, a new knowledge of the possible advantages obtained by using URM in earthquake-resisting structures has evolved and challenged this notion.

As with any other structural material, the use of URM to resist lateral loads induced by earthquake ground motion (EQGM) has advantages and disadvantages, depending on how the URM has been used in the earthquake-resisting structure. This simple assertion should be kept in mind when considering that an efficient seismic upgrading of a building is possible only if the structural elements and materials located in the original building are used efficiently to help resist the seismic demands induced in the upgraded structure. In the specific case of URM buildings and framed buildings infilled with URM walls, many of which form part of our vast inventories of hazardous existing structures, an efficient upgrade can be achieved if the large natural sources of strength, stiffness and viscous and hysteretic energy dissipation provided by the URM walls are taken advantage of. Within this context, the main challenge confronted by the structural engineer can be summarized with the following question: What changes can and should be introduced to the mechanical and dynamic properties of the URM building that needs to be upgraded in such a way that the URM is put to work according to its strengths rather than on its weaknesses? And more specifically according to the objectives of these studies: How can these changes be achieved by introducing post-tensioned (PT) braces into an non-ductile framed building with URM infills?

Chapter 1 provides an introduction to the issues discussed above, which are instrumental to the understanding of the discussions presented in the rest of this report. Section 1.1 identifies the need for the upgrading of URM buildings and framed buildings infilled with URM walls according to the extensive damage observed in them during real earthquakes.

Section 1.2 attempts to demistify the behavior of URM walls and infills according to recent world-wide research that has been carried out by several researchers. Within this context, an attempt to identify the weaknesses and strengths of URM as a structural material are discussed, and according to the identified strengths, the adequate use of the URM infills to enhance the lateral strength, stiffness and viscous and damping energy dissipating capacity of an infilled frame is also discussed.

Section 1.3 discusses the issues that need to be considered when upgrading an existing structure by introducing in it new steel braces. It is concluded that the use of steel braces for such purpose is an attractive option; nevertheless, it is noted that several issues should be considered carefully when attempting to do so. Based on the discussion carried out in Section 1.3, Section 1.4 discusses the use of PT cables or rods to brace an existing building, focusing attention to some aspects that are particular to the behavior of PT braces.

Finally, Section 1.5 uses the material developed in the previous sections to discuss the use of PT braces to accomplish the efficient upgrading of an existing non-ductile framed building with URM walls.

1.1 INTRODUCTORY REMARKS

As previously noted by Bertero (1992b), seismic hazards in our urban and rural areas are products of the interaction between the seismic activity at a given site [the earthquake ground motions (EQGMs) induced at that site by all relevant seismic sources] and the built environment (all human-made structures). The great life and economic losses that occur during an EQGM are not products of the seismic rupture itself, but of the failure and collapse of the structures that constitute the built environment. Given our inability to control the seismic activity that affects a given site, the only way to reduce seismic hazards to an acceptable level is to reduce the seismic risk in our urban and rural areas by improving current earthquake-resistant design (EQ-RD) and earthquake-resistant construction (EQ-RC) procedures for new buildings and for the upgrading and rehabilitation of existing hazardous structures.

It has long been recognized that URM buildings and framed buildings infilled with URM walls (otherwise denoted herein as URM infills) form part of the vast inventory of hazardous existing structures in our built environment. Following the 1989 Loma Prieta and 1994 Northridge earthquakes (EQs), a large number of URM elements and structures were found to be damaged (Beavers et al. 1992, Moehle et al. 1994). Given the simplicity of the construction process of URM elements and structures, as well as the low price of the material itself, URM elements have provided for many years an economical way to support gravity loads, to enclose and subdivide the interior architectonic space of a building, and to provide good acoustic and thermal insulation to existing buildings. The insulation properties of masonry have been conducive to extensive use of URM infills in framed reinforced concrete (RC) and steel buildings. Nevertheless, due to a lack of understanding of the mechanical properties of masonry in the past, URM elements have not been used properly in earthquake-resistant buildings. Thus, consistent with the above mentioned approach to reduce seismic hazard, there is the need to study, experimentally as well as analytically, promising techniques for the seismic upgrading and rehabilitation of existing URM structures and framed buildings with URM infills.

1.2 SEISMIC PERFORMANCE OF UNREINFORCED MASONRY BUILDINGS

It has been recognized that the presence of masonry infills that are not isolated from the structural elements can have a beneficial effect on the seismic performance of existing framed buildings. Proper introduction of such elements into the bare frames of a building can lead to a considerable increase in the ultimate strength and stiffness of the building, as has been shown consistently in experimental tests and analytical studies (Klingner and Bertero 1976, Brokken and Bertero 1981, Chrysostomou et al. 1992, Schuller et al. 1994, Mander et al. 1994) and by the seismic performance of framed buildings with URM infills during real EQGMs (Wakabayashi and Martinez 1988). In spite of these advantages, it has been generally accepted that this type of building has a poor seismic performance, given the spectacular and numerous failures observed in URM buildings in past earthquakes, e.g. San Francisco 1906, Tangshan 1976, etc.; and in URM buildings and framed buildings with URM infills in recent earthquakes, e.g. Chile 1985, Mexico 1985, Loma Prieta 1989, Philippines 1990, Iran 1990, Northridge 1994 (EEFIT 1986, NBS 1987, Cruz 1988, Bertero 1992b, Beavers et al. 1992, Molavi and Eshghi 1992, Kusukawa et al. 1992, Moehle et al. 1994). Thus, it can be concluded that masonry elements and structures can have good or poor seismic performance, depending on ***how the masonry is used in the earthquake-resistant structure*** and, obviously, on how they have been designed, detailed and constructed.

One of the main problems in dealing with the performance of URM elements and/or structures lies in defining what constitutes an adequate seismic performance. This issue has been considerably obscured in the past by building codes in the United States, which traditionally have specified that the capacity of URM, due to its brittle nature, should be limited to a stress less than that that produces initial cracking (Boussabah and Bruneau 1992). Thus, based on this code-adopted performance criterion, URM elements or buildings only perform well if they remain uncracked. However, URM buildings and framed buildings with URM infills can have a reasonably well understood behavior and a reasonable margin of safety while not meeting this criterion. Several researchers note that the overall earthquake-resistant capacity of unconfined and particularly confined URM walls and URM infills can be considerably higher than was previously thought (Beavers et al. 1992, Meli et al. 1992, Abrams 1992). Thus, not only can some cracking occur on the masonry elements without detrimental effects on the overall seismic performance of the building, but in some cases this performance can be significantly enhanced by allowing the masonry to go into its nonlinear range of behavior.

Currently, there is a need to rationally define different levels of performance for URM elements, so that performance based EQ-RD methods can be implemented taking into account the real deformation, strength, stability and energy dissipation capacities of URM elements. For instance, it has been recognized recently that URM walls and infills have a considerably larger strength than that at first cracking, a large inelastic deformation capability and, if their in-plane and out-of-plane deformations are controlled within certain limits, a stable hysteretic behavior and thus a stable energy dissipating capacity (Abrams 1992, Meli et al. 1992, Beavers et al. 1992). Thus, the potential role that URM infills may play in enhancing the strength, stiffness and energy dissipation capacity of infilled framed buildings should be considered in their EQ-RD. Nevertheless, the mechanical characteristics of the constructed masonry infills affect considerably their seismic performance, and the above mentioned enhancements can be only achieved if the infills are made out of masonry that does not exhibit fragile behavior (termed in this report as "soft masonry"). For instance, if the masonry is fragile and brittle ("hard" masonry), it exhibits an explosive type of failure. In such cases, the deformability of the masonry is limited **by its brittle compression or tension failure**, and its energy dissipating capacity is practically nonexistent. Besides the characteristics of the masonry itself, the previously mentioned enhancements can only be achieved if the infills are designed and confined in such a way that cracking takes place all across the infill (does not concentrate in few locations), and that the existing frame members do not fail in a brittle mode (Klingner and Bertero 1976).

Fortunately, the majority of URM infills in buildings have been built with "soft" masonry (i.e., does not exhibit explosive type of failure). Given the distinctions made above about the different types of masonry, it should be noted that in this report URM infills are assumed to be fabricated out of "soft" masonry. As mentioned before, these infills can undergo, if their in-plane deformation (which is a function of the story drift or interstory drift index) is limited to adequate values, inelastic deformation and dissipate energy through stable hysteretic behavior. Figure 1.1, which shows lateral force vs. lateral displacement curves obtained experimentally for URM infills and walls under in-plane lateral loads, is included to illustrate the deformability capacity of URM infills built with "soft" masonry. The study of framed buildings with "hard" (fragile) masonry should be treated separately and is not included in this report.

To discuss the performance of URM elements, it is necessary to discuss against what such performance is measured. For this purpose, it is important to address the general modes of failure observed in URM elements, which can be classified according to Boussabah and Bruneau (1992) as: lack of anchorage, anchor failure, in-plane failures, out-of-plane failures, combined in-plane and out-of plane failures and diaphragm-related failures. Only some of the previous modes are relevant to buildings with URM infills, and thus attention is concentrated in this report on in-plane, out-of-plane, and combined in-plane and out-of-plane failure modes. Another important issue to be addressed while assessing the performance of URM elements is the influence that their local behavior and performance have on the overall seismic performance of an entire building system. Within this context, it should be noted that given their large initial stiffness and strength, URM infills tend to attract and carry a large percentage of the total lateral load acting on infilled framed buildings. Thus, their influence on the structural and dynamic characteristics [period (T), strength, damping and energy absorption and dissipation capacities] of the infilled building needs to be assessed carefully. Also, infills can create large stiffness and strength irregularities in plan and along the height of the building, which in turn can induce large torsional response and/or the creation of soft stories, thereby imposing on structural elements loading conditions for which they were not designed.

Although a basic knowledge of the mechanical properties of URM as a construction material is necessary to address the issues mentioned in the previous paragraph, such discussion goes beyond the scope of this report. A discussion of the mechanical properties and behavior under lateral loads of URM elements and a discussion on the way in which URM elements interact with other earthquake-resisting elements in an infilled framed building is presented in the next section.

1.2.1 In-plane behavior of unreinforced masonry elements

In the last two decades, several researchers have concentrated their efforts on demystifying traditional concepts of the behavior of URM elements when subjected to in-plane lateral loads (such as extremely poor deformability and energy dissipation capabilities). To do so, they have studied the in-plane behavior of URM elements well beyond their point of first cracking. Although not unaccompanied by some controversies, a new understanding of the behavior of URM elements has flourished.

Experimental tests (pseudo-dynamic tests of specimens subjected to constant vertical loads and shaking table tests) carried out by several researchers around the world (Klingner and Bertero 1976, König et al. 1988, Meli et al. 1992, Abrams 1992, Pires and Cansado 1992, Schuller et al.

1994) have consistently shown that URM walls and infills possess considerable capacity for inelastic deformation independently of their in-plane failure mode (i.e., diagonal tension, flexural tension, etc., for URM walls; and sliding shear, diagonal tension, compressive crushing, etc., for URM infills). It has been observed in the majority of these tests that URM walls and infills are able to carry a large percentage of their peak strength (ultimate lateral load carrying capacity) for relatively large drifts (0.005 and larger), as shown in Figure 1.1.

Some researchers note that vertical load increases the shear capacity and stiffness of URM elements, although large vertical forces reduce their available ductility (Meli et al. 1992, König et al. 1988). König et al. (1988) offer an insight by analyzing the post-crack dynamic cyclic behavior of URM walls: under small axial load, cracking developed through the bed joints and separate portions of the wall slid on each other, resulting in large relative deformation and little strength degradation before failure; and, under higher axial loads, the friction resistance of the bed joints increased in such a way that diagonal cracking occurred through the masonry units, and the individual portions of the walls (separated by the cracks) tended to slide along straight regular diagonal cracks, which resulted in significant degradation of strength and reduced deformability capacity (i.e., unstable post-cracking response). Langenbach (1990) confirms this interpretation by observing that if the failure does not occur in the masonry units, the softness and higher deformability capacity of the mortar encourages a more wide-spread small-scale cracking across the mortar joints of the whole URM element, which allows it to absorb more energy and perform in a ductile rather than a brittle manner. It is important to note that although URM elements show better deformability capacity for small axial loads, this does not mean that axial forces are not important to attain such deformability capacity. Abrams (1992) notes that the vertical compressive stresses are instrumental in the apparent ductility of these elements by attributing the large post-cracking strength to friction along the bed joints. Although URM infills in framed buildings behave differently than URM walls when subjected to lateral loads, Meli et al. (1992) note a similar influence of axial load in the behavior of URM walls confined with RC elements.

Pires and Cansado (1992) have shown in experimental tests that the construction process of an URM infill within a RC frame affects its behavior when subjected to lateral load. Before discussing this issue, it important to clarify some concepts by discussing the differences between a *confined URM element* and an *URM infill*; and between *reinforced masonry* and *confined URM*. *Reinforced masonry* denotes those masonry elements directly reinforced with steel bars. *Confined URM* denotes those masonry elements that are not reinforced, but are confined with the aid of RC members that surround them. These RC members provide a good in-plane and out-of-plane connection between the URM elements and other structural elements and the roof system, and improve the energy dissipation and deformation capabilities of the *confined URM element* (Meli et al. 1992). In the design of masonry structures, these RC members are provided for no other purpose than to enhance the performance of the URM elements. In this case, the RC members are constructed simultaneously or after the masonry element has been built, and it is said that the RC members confine the masonry, i.e., we talk of *confined URM*. In other cases, RC or steel structural elements, designed to carry a large percentage (if not all) of the vertical and lateral loads, are constructed first, and then the URM infills are introduced into them. In the latter case, it is undeniable that the existing frame members provide, sometimes unintentionally, confinement to the infills. Based on the results obtained in the pseudo-static test carried out on several 2/3 scale one-story infilled RC frame models, Pires and Cansado (1992) confirmed that the addition of infills to RC frames can increase significantly the energy dissipating capacity of the RC frames, but more importantly, they note that the different construction processes used to build their models had an important influence on their response to lateral load. They note that when the masonry walls (*URM infills*) were added after the RC members were constructed, the models achieved higher distortion levels with less degradation of their original mechanical characteristics than when the RC members were constructed after the wall (*confined masonry*). These results show that URM elements perform better when built after the existing frame members, and thus, that URM infills made of "soft masonry" should have, in general, significant deformability capacity beyond first cracking.

The above observation has been repeatedly confirmed in experimental tests (Klingner and Bertero 1976, Pires and Cansado 1992, Meli et al. 1992, Schuller et al. 1994, Gergely et al. 1994, Mander et al. 1994). In these tests, URM infills exhibited a stable hysteretic behavior and good energy dissipation characteristics for relatively large drift (0.005 and sometimes larger).

To understand the significant deformability capacity and stable hysteretic energy dissipation capacity (under moderate interstory drift index, IDI, demands) of URM infills, it is necessary to discuss some relevant aspects of the in-plane behavior of "typical" URM infills when subjected to monotonically increasing deformation. Under very low levels of lateral displacement, URM infills do not crack. If the infill is bonded to the surrounding frame, the force-deflection behavior is linear and elastic while the infill behaves as a shear panel. As the lateral force and deformation increase, some cracks are developed along the interface between the frame and the infill (i.e., a gap between the infill and the frame members starts to develop), and the frame-infill contact starts to concentrate at the corners of the infill. As the lateral displacement increases, diagonal cracking occurs in the infill and a compression strut develops. It can be concluded that at some stage of their behavior, the majority of URM infills behave as a diagonal element (strut) in their own plane. In this case, all of the resisting force carried by the infill is transmitted to the existing frame by the pressure delivered to the top of the columns, just below their intersection with the beam. Thus, the strut mechanism leads to high stress concentrations at the corners of the infill and the point at which the infill delivers the load to the frame. As the lateral deformation increases, the behavior of the infill depends more and more on the relative strength and stiffness of the frame and infill, and on the mechanical characteristics of the masonry itself. On one hand, if the strength of the infill is low or the frame members (mainly the columns) have been designed to avoid early failure, the masonry located at the corners starts to crush. Depending on the mechanical characteristics of the masonry, an increase in lateral deformation can lead to local crushing failure of the masonry in the corners or, if the post-peak compressive strength of the masonry does not drop rapidly with increasing deformation, to a degradation of the stiffness and strength of the masonry in these zones and to a widespread small-scale cracking over a large portion of the infill (Klingner and Bertero 1976, Pires and Cansado 1992, Mander et al. 1994, Gergely et al. 1994). In the latter case (widespread small-scale cracking), as the masonry located at the corners is crushed after several load cycles, the diagonal strut loses much of its original stiffness and load carrying capacity, and a large percentage of the lateral load is likely to be transferred to, and thus resisted by, other regions of the infill, such as off-diagonal masonry struts (Mander et al. 1994, Gergely et al. 1994). This mechanism of lateral load redistribution is usually accompanied by the opening of gaps between infill and existing frame members and the sliding of the infill within these members, and makes it possible for the infilled frame to reach higher levels of lateral displacement with less degradation of its strength and energy dissipating capacity. In the other hand, if the strength of the infill is high, it could cause the shearing failure of the existing columns (Klingner and Bertero 1976, Langenbach 1990, Schuller et al. 1994), which eventually is reflected in a smaller deformability capacity of the whole infill frame and to a faster drop of post-peak resistance with increasing lateral displacement.

It should be mentioned that there are several more modes of failure for URM infills than those discussed in the previous paragraph. Depending on the loading condition, the relative strength and stiffness of the frame and infill, the bond between the infill and the existing elements, and the mechanical characteristics of the masonry itself, a number of failure mechanisms (some of them summarized in Figure 1.2) are possible in an infilled frame (Mehrabi and Shing 1994). Although discussing all these mechanisms goes beyond the scope of this report, it is useful to discuss some tendencies observed by several researchers:

■ An increase in the strength of the infill is usually reflected by an increase in the overall lateral strength of the infilled frame, although usually this increase in strength is accompanied by a faster post-peak drop of resistance as the lateral displacements increase (Klingner and Bertero 1976, Schuller et al. 1994).

■ In general, as the strength of the masonry decreases, extensive horizontal and diagonal cracking occur in the infill before failure of the infilled frame. Also, in general, as the strength of the masonry increases, damage tends to concentrate at specific locations of the infill, usually at its corners (Gergely et al. 1994, Klingner and Bertero 1976).

It has been observed experimentally that URM walls and infills suffer considerable stiffness degradation with increasing drift, after which their stiffness reaches a value that remains fairly constant with further increase in drift (Brokken and Bertero 1981, Meli et al. 1992). Based on these and similar observations, several researchers suggest that seismic analysis and design procedures should consider material mechanical characteristics consistent with the expected strain level (Scalleti et al. 1992, Brokken and Bertero 1981). Brokken and Bertero (1981) have noted that the lateral stiffness and strength of masonry infills are very sensitive to the quality control of the material and to workmanship (including that on the interfaces of the infill and the existing frame elements).

Several issues of the in-plane behavior of URM elements are yet to be understood. Among them, it is necessary to gain a better understanding of the cyclic behavior of URM walls and infills. For instance, Abrams (1992) notes that the behavior for loading in one direction of URM walls did not appear to be influenced by previous damage in the other loading direction, which led him to conclude that the cyclic behavior of the walls can be fairly characterized by its behavior when subjected to monotonically increasing loads. Nevertheless, Klingner (1980) notes from experimental results that after reaching a given resistance level in one direction, an infilled frame model was not able to develop more than this resistance in the other direction upon load reversal. In other words, the resistance that a masonry infill has in one direction in some cases depends on the deformation demands on that infill in the opposite direction. At this stage, there is not enough information to explain the difference between the above observations, and thus this issue needs clarification. Another issue that deserves consideration is the in-plane behavior of URM infills with openings. Although some analytical efforts have been carried out to assess the effect that a large opening can have on the in-plane mechanical characteristics of an URM infill (Durrani and Luo 1994), and some experimental tests of URM elements with openings have been carried out (Meli et al. 1992), there is very little information about this topic if one considers the large percentage of real URM infills that have openings. This issue also needs clarification.

From the above results, it can be concluded that if certain conditions are met:

■ The lateral strength of a framed building with URM infills should not be estimated based on the lateral load that induces the initiation of cracking and/or crushing in the most loaded or weakest infill. Because the infills can usually deform inelastically after their first cracking and/or crushing, it is necessary to consider the overstrength that can be obtained due to the redistribution of internal forces when estimating the lateral strength of the whole frame-infill system.

■ URM infills can enhance considerably the strength and stiffness of a framed building.

■ URM infills can be used to dissipate energy through stable hysteretic behavior (several researchers that URM infills can undergo relatively high inelastic deformations while showing adequate hysteretic behavior). Nevertheless, to achieve this stable behavior, the in-plane drift index in the elements needs to be carefully controlled and certain modes of failure (for instance, brittle failure in the existing frame members) should be prevented from occurring.

1.2.2 Out-of-plane behavior of unreinforced masonry elements: importance of considering in-plane and out-of-plane demands simultaneously

From the information presented in the previous section, it can be concluded that the seismic capacities of URM infills and infilled framed buildings are considerably higher than was previously thought. Nevertheless, some of this information should be considered very carefully, given that the majority of the experimental results described above were obtained by applying seismic input (vibration or pseudodynamic loading) in the plane of the URM infills or walls, without specific concern for the multidirectional nature of real EQGMs. In analysis and design of URM elements, emphasis is usually put on in-plane behavior. Nevertheless, observed damage in real EQGMs brings attention to the out-of-plane behavior of URM infills. Real EQGMs simultaneously impose in-plane and out-of-plane demands on URM infills. Regarding this, Boussabah and Bruneau (1992) note that:

> ***EQ forces are multi-directional in nature, and thus each URM element is solicited in both its in-plane and out-of-plane direction. The on-site identification of combined in-plane and out-of-plane effects is nearly impossible, and observed such failures will generally be attributed uniquely and erroneously to the sole effect of out-of-plane forces.***

An insight into the above quote can be gained if one considers that, as mentioned before, URM infills tend to develop diagonal cracking when subjected to in-plane lateral load. When subjected to cyclic loads, they tend to develop an x crack pattern that extends all the way to the corners. This x crack pattern resulting from in-plane loading is similar to the crack pattern for a square panel subjected to out-of-plane forces, which implies that the out-of-plane strength can be weakened by in-plane cracking (Angel and Abrams 1994).

Inertial forces due to absolute accelerations and story drifts are the most significant out-of-plane and in-plane demands. When a frame with URM infills is subjected to drift on its own plane, the infill and/or its interface with the frame is forced to deform with the structural elements, which usually results in damage to the infill. In most cases, drift perpendicular to the plane of the infills is less significant, and as a consequence, their out-of-plane drift demands are usually neglected (Sakamoto 1978). While the use of peak absolute acceleration of the ground and/or floor motion is not a good measure to determine structural damage, it can be physically understood as a measure of the inertial force that must be resisted by a rigid, anchored object (Merz, 1977). URM infills are usually heavy enough as to be significantly affected by inertial forces. In this case, the out-of-plane effects of the inertial forces are usually more significant than those of the in-plane inertial forces, and thus some assessment of the out-of-plane behavior of the infills needs to be carried out (Sakamoto 1978). Obviously, out-of-plane effects increase with the size and flexibility of the wall. In this context, it should be considered that in some cases the response of the building sometimes amplifies the floor acceleration with respect to that of the input base motion.

Our understanding of out-of-plane failure is still limited. In this section, the work done by several researchers in this field will be briefly discussed. In some cases, the conclusions reached by some researchers almost seem to contradict those reached by other researchers. These contradictions reflect the state of our current knowledge, and thus, the need to devote more research to clarify this situation.

Beavers et al. (1992) note that out-of-plane failure should not cause as much concern as it traditionally has, given that test results show that the in situ out-of-plane seismic capacity of URM infills is very high (at least 13 and up to 30 times that obtained using conventional design methods as suggested by the experimental results obtained by Fricke et al. 1992). Mander et al. (1994) note that out-of-plane failure of infills with a height to thickness ratio of 18 was difficult to achieve under out-of-plane shaking, and that although previous in-plane damage somewhat reduced the out-of-plane strength of these infills, their residual out-of-plane strength was still substantial. Angel and Abrams (1994) conclude that out-of-plane strength of URM infills decreases as the in-plane cracking increases and that for the same in-plane damage, the out-of-plane strength reduction varies with the slenderness ratio of the infill. Angel and Abrams (1994) note that for severe in-plane damage and very slender infills, the out-of-plane strength is about half of that corresponding to the undamaged infill, while in-plane damage in infills with low slenderness ratio practically does not reduce their out-of-plane strength.

To understand the high out-of-plane strength of URM elements and infill walls, it is important to address the relatively new concept of out-of-plane dynamic stability, formulated following observations that URM walls properly anchored to floors and roof diaphragms can resist EQGMs more severe than otherwise predicted by traditional static analysis methods: after cracking, some portions of the walls behave as rigid-body members rocking on the wall through cracks; if gravity forces are sufficient to prevent overturning of these individual bodies, a condition of dynamic stability exists. In the case of framed buildings with URM infills, it should be noted that the infills are usually not anchored to the existing frame members, and that they are not supposed to carry the vertical loads (as would be the case of a masonry bearing wall, to which the out-of-plane seismic dynamic stability concept applies). Thus, it would appear that URM infills do not benefit from out-of-plane seismic dynamic stability. Nevertheless, some researchers (Paulay and Priestley 1992, Angel and Abrams 1994) note that infill panels' out-of-plane resistance is considerably enhanced by the compression membrane action (arching action) that they develop as they crack under lateral inertial accelerations, thanks to the confinement provided by the existing frame members and neighboring infills, or, in other words, that a condition of dynamic stability is likely to be developed.

Nevertheless, in the opinion of the authors, the experimental results that suggest a high out-of-plane strength of URM infills are not conclusive evidence that out-of-plane behavior should not be a concern in this type of element. The vast majority of the experimental results available were obtained in pseudo-dynamic tests that did not consider in-plane and out-of-plane demands simultaneously. In these tests, in-plane damage is usually induced first, and then the infill is subjected to out-of-plane loading. Liauw and Kwan (1992), after conducting shaking table tests on 1:3 scale four-story three-dimensional (3D) models, observe that their infilled model collapsed at a peak acceleration of 0.835g, because an infill panel located on the first story fell out of plane. They mention that although the input motion was parallel to the plane of the infills, out-of-plane effects amounting to 10 to 15% of the in-plane loads (resulting from the input motion) were produced. Liauw and Kwan conclude that the multidirectional excitations produced by real EQGMs should raise concern in view of the out-of-plane behavior of their model. Thus, although a new phase in our understanding of the real behavior of masonry elements and structures has begun, there is an urgent need to assess realistically the effects of multidirectional excitations on their behavior.

1.2.3 PERFORMANCE OF FRAMED BUILDINGS WITH UNREINFORCED MASONRY INFILLS ACCORDING TO THEIR BEHAVIOR DURING REAL EARTHQUAKE GROUND MOTIONS

Before enough knowledge was acquired in the proper seismic design of masonry buildings, many URM buildings and framed buildings with URM infills were constructed. In early seismic designs, some, if not all, of the issues discussed in Sections 1.2.1 and 1.2.2 were ignored. Thus, the spectacular failures and poor behavior observed in URM buildings and framed buildings with URM infills that has been observed during intense EQGMs are more due to an improper use of masonry as a structural material than on intrinsic bad behavior of masonry elements. Given the extensive use of URM infills in framed buildings in Mexico City, a good evaluation of the seismic performance of these elements was obtained during the 1985 Mexico earthquake (EQ). During this EQ, several cases of adequate seismic performance, as well as of failure and poor behavior, were observed in a large number of modern medium-rise framed RC buildings with URM infills (EEFIT 1986, NBS 1987, Wakabayashi and Martinez 1988, Bertero 1992b). In general, it has been considered that the presence of URM infills was beneficial for the majority of infilled framed buildings, and prevented the collapse of several buildings in the zone of highest seismic intensity. This usually was the case when the URM infills were placed symmetrically in plan and within all the stories of the building. Although some of these infills showed extensive shear diagonal cracking after the earthquake, they resisted the majority of the lateral loads acting on the buildings, protecting the columns from a possible failure and helping dissipate the energy input by the EQGM (Wakabayashi and Romero 1988, NBS 1987). Nevertheless, in other cases, the masonry infills contributed to poor seismic performance of framed buildings. Some of the statistical data compiled after the 1985 Mexico EQ provide some insight into this issue (Wakabayashi and Martinez 1988):

■ 42% of all buildings that failed were located on street corners. Of these buildings, a large percentage were RC framed buildings infilled with URM elements in only two sides (the two sides facing neighboring buildings), while the two sides facing the street were left free. A large number of failures can be attributed to the significant plan irregularity produced by the asymmetrical distribution of infills, which leads to large torsional response and pounding with adjacent buildings.

■ A weak and soft first story was present in 8% of all buildings that failed. A large percentage of these buildings were infilled RC framed buildings, with URM infills in all stories with the exception of the first story. This created a large concentration of deformation and energy dissipation demands that led to the failure of the columns of the first story.

■ Short columns created by the improper use of URM infills were observed in 3% of all buildings that suffered heavy damage or collapsed.

■ Although not statistically documented, a large number of failures were caused by irregularities caused by the failure of URM infills. In several cases, URM infills with low strength or inadequate anchorage to the building fell out-of-plane. From the nonstructural point of view, this type of failure produces extreme danger to human life due to the falling masonry. From a structural point of view, sudden out-of-plane failure of the rigid infills produces an unpredictable change in the structural and dynamic characteristics (strength, stiffness and energy absorption and dissipation capacities) of the building, and thus of its behavior. This type of failure can produce soft stories and large torsional response, with the corresponding problems associated with this behavior. A large number of out-of-plane failures were caused by the large drifts suffered by several buildings during this EQGM.

To correct the above-mentioned deficiencies in the seismic performance of URM buildings, more stringent provisions have appeared in EQ-RD codes regarding the proper use of masonry. Some of the issues stressed by these new provisions follow:

■ If masonry infills are not isolated from the existing structural members, then they become structural elements themselves, and their contribution to the overall response of the structure should be evaluated, and they and the existing structural members should be designed accordingly.

■ If stiffness and strength irregularities are created due to the presence of masonry elements, the reduction of the elastic force demands that are allowed for estimating the design forces should be considerably reduced.

■ Design guidelines for the proper design and confinement, in-plane and out-of-plane, of masonry elements are stressed.

A problem with the above provisions is that they can only be applied to the design and construction of new buildings. When it comes to correcting the deficient behavior of existing framed buildings with URM infills, none of the above approaches can be applied effectively, and thus there is a need to develop efficient techniques to upgrade and rehabilitate these buildings.

1.3 USE OF STEEL BRACES IN THE SEISMIC REHABILITATION OF EXISTING BUILDINGS

It is out of the scope of this report to describe all aspects involved in the seismic rehabilitation and upgrading of existing buildings. It is assumed the reader has a basic knowledge regarding this subject. For an introduction to this topic, the reader is referred to Jirsa and Badoux (1990), Miranda (1991) and Bertero (1992a).

There are several elements that can be used to brace an existing structure. Some of these elements work by developing axial tension and compression, others by developing only tension. In the former case, the elements have a high axial stiffness (i.e., rolled steel sections, angles, channels, tubes, etc.) while in the latter, a low axial stiffness (PT steel rods or cables).

The rehabilitation of an existing building using steel braces is an attractive option. Usually it is possible to achieve large increases in the lateral stiffness and strength of an existing building. The use of this technique offers the following advantages:

■ **Stiffness and deformation capability of the bracing system.** A very attractive aspect of the use of steel braces to upgrade an existing building is the wide range of stiffness that can be considered in the design of the bracing system. Once the stiffness of the existing structure is evaluated, a bracing system with adequate stiffness can be developed such that the original system is allowed to resist a portion of the lateral forces induced by EQGM. In some cases, it is important for the existing structure and the braces to reach their ultimate strength simultaneously (i.e., at similar levels of deformation). Designing the bracing system with these characteristics will usually result in efficient EQ-RD, as shown in Figure 1.3a. In other words, it would not be efficient to reach a level of deformation at which the original elements of the structure start to fail, while the braces still remain far from reaching their ultimate capacity, as shown in Figure 1.3b. It will not be desirable in every case to accomplish compatibility of stiffness and/or deformation, as in the case where the purpose of the bracing system is to unload the existing elements as much as possible (Figure 1.3c).

■ **Loads induced in the foundation.** Under normal conditions, it will be possible to distribute the braces within the building and design them in such a way that the loads that the bracing system induces in the foundation are distributed over the whole foundation system. In this way, it is possible to rehabilitate the building without costly modification of the existing foundation.

■ **Lightness.** The weight of steel braces is usually small compared to that of the existing structure and that of other upgrading techniques that involve the addition or resizing of structural elements. Thus, there is a small increase in the weight of the structure and of its reactive mass.

■ **Other advantages.** There are other advantages that, although not important from a structural point of view, can have a considerable influence in the selection of this upgrading technique. Among them, the following can be mentioned: clean and fast construction process, the use of braces to achieve interesting-looking architectural patterns in the structure while allowing sunlight to reach the interior of the building, etc.

To achieve an adequate seismic performance of an existing framed building upgraded by means of a steel bracing system, it is necessary to check several aspects of the global and local behavior of the upgraded structure. Among them, the following can be mentioned.

■ **Change of behavior of the original frame members.** It is important to study the change in behavior and failure mode of the existing frame members when introducing the braces. In some cases, if the existing elements are not strengthened properly to avoid their premature failure due to this change of behavior, the structure can have a poor seismic performance. The introduction of steel braces into the existing structure usually reduces the lateral deformation of the structure when subjected to EQGM, and thus usually reduces the bending moments at the ends of the existing frame members. This reduction usually occurs simultaneously with an increase in their axial forces, as shown qualitatively in Figure 1.4. In this figure, the behavior of a one-story one-bay frame is qualitatively compared to the behavior of the same frame when it is braced. The comparison of strength demands on one end (top or bottom) of one of the columns of each of the two versions of the frame is shown in the same figure. As shown, an initial moment and an initial axial force (M_0 and P_0, respectively) exist in the column before lateral load is induced to the frame. Note that these initial forces usually are not the same in the bare and the braced versions of the frame. Once the frame is subjected to EQGM, there is a change in the moment and the axial force in the columns. As shown qualitatively, the moment variation is usually more significant than the variation of axial force in the bare frame, while the opposite can be said for the braced frame. In some cases, the change in behavior of the existing members helps to improve their seismic performance; nevertheless, an excessive increase in the axial forces (i.e., in tall slender buildings) can be detrimental to the members' performance. It is usually considered that the axial forces in the beams can be neglected in the design of the beams due to the presence of a slab that is rigid in its own plane. Nevertheless, if the forces in the braces are high, the axial force induced in the beam to equilibrate such force can be also high, and thus its effect should be assessed.

■ **Change in dynamic characteristics.** There is the need to assess the change in the dynamic characteristics of the building once it is upgraded in order to detect possible changes in its lateral response.

■ **Connection of braces to existing structure.** The connection of the steel braces to the existing structure should be done carefully in order to allow the bracing system to fully develop its lateral stiffness and strength. If the connection fails before the brace it attaches to the structure, this brace will not be able to develop its maximum strength and/or lateral stiffness.

■ **Buckling of the steel brace.** To achieve a good seismic performance of the rehabilitated structure, it is necessary to avoid inelastic buckling of the braces. When a brace suffers nonlinear buckling during cyclic loading, it can lose a large percentage of its original strength. Overall buckling of a stiff member can lead to local buckling, and this local buckling under reversals of deformation can lead to premature failure. Also, the unexpected components of deformation produced by the buckling of the brace can induce undesirable stress components that could lead to a premature failure of its connection to the existing structure (Badoux and Jirsa 1987).

1.4 USE OF POST-TENSIONED STEEL BRACES IN THE SEISMIC REHABILITATION OF EXISTING BUILDINGS

The use of post-tensioned steel braces in the seismic rehabilitation of existing buildings is a relatively new upgrading technique that has been applied successfully to rehabilitate several low-rise RC buildings (Rioboo 1989). Earthquake simulator tests carried out on a 0.3-scale model of a six-story moment-resistant steel frame and analytical studies on the use of this technique in low-rise buildings located on firm and soft soils have shown the efficiency of this technique for the rehabilitation of low-rise existing structures (Guh 1989, Miranda and Bertero 1990, Pincheira and Jirsa 1992). These studies have shown the feasibility and efficiency of obtaining significant increases in lateral strength and stiffness in existing low-rise buildings using this technique.

Although the use of PT braces has advantages and problems similar to the use of other types of steel braces, there are some aspects peculiar to PT brace behavior:

■ **Linear elastic behavior of the PT cables.** PT braces are usually designed to work in their linear elastic range of behavior. This is done to prevent them from yielding in tension and thus from losing their initial prestress. Figure 1.5a shows the basic axial deformation vs. axial force curve for a rod or cable (such as those used in PT bracing systems) with no prestress. As shown, the rod or cable buckles elastically for very low compressive forces, and is capable of developing its yielding strength under tensile strains. Note that this type of element dissipates energy when it yields, although it does not when it buckles. Figure 1.5b shows the behavior of the rod or cable under cyclic loading producing yielding and buckling. As shown, all inelastic tensile elongation accumulates with reversals of actions, i.e., the length of the brace increases every time it yields in tension.

Figure 1.6a shows a counterpart of Figure 1.5a for a prestressed rod or cable. As shown, both figures are basically the same, with the exception that there is an initial state of stress and strain (produced by the prestress) in the prestressed rod or cable which is accounted for in Figure 1.6a by shifting the origin of the axial force vs. axial displacement cartesian axes. As a consequence, the rod or cable can *resist* axial force under lateral forces that induce, due to a decrease in the initial tension in the rod or cable, shortening in the brace (this can be interpreted as the rod or cable developing a compressive force), as shown in Figure 1.6a. From this figure, it is clear that if the rod or cable loses its prestress, it loses its capacity to *resist* axial loads when subjected to compressive strains. Figure 1.6b shows that if the rod or cable yields, there is a loss of prestress. This is illustrated by following the load path OABC in Figure 1.6b. As shown, the rod or cable remain elastic in the OA portion of this path. Once it reaches its yielding strength (point A) it yields and follows AB. As soon as there is a load reversal, the rod or cable unloads and reaches point C, which corresponds to zero axial deformation. From comparison of the location O and C, it can be concluded that there has been a loss of prestress.

The above observations can be used to understand the consequences that yielding of the PT braces can have on their performance. First, excessive loss of prestress will reduce significantly the ability of the PT braces to *resist* lateral loads that will shorten them. Second, excessive elongation of a PT brace can result in a decrease of the lateral stiffness of that brace. These two effects are detrimental to the performance of the PT bracing system.

It is also convenient to assess the consequences of the PT braces' elastic behavior on the dynamic response of the structure. For example, if the braces carry the majority of the lateral loads, the structure will respond essentially elastically to the effects of an EQGM. Possible increases in the response of the entire building due to this effect should be carefully assessed.

■ **Yielding Strength.** The PT braces can be fabricated from steels with different yielding strengths, and thus they can easily be designed for a wide range of elastic deformation capacities. Even if the PT braces are designed to remain elastic, a variety of yielding strengths can be used in the design process to enhance the compatibility of strength and deformation between the existing structure and the new bracing system, as shown in Figure 1.7 (Rioboo 1989).

■ **Initial state of stresses in the PT braces.** The amount of prestress provided to the PT braces should be designed to prevent their yielding and/or buckling. Thus, it is necessary to have a good estimate of the maximum axial forces and interstory drifts that can be induced in the PT braces and the upgraded building, respectively, when the building is subjected to the design EQGM.

■ **Elastic buckling.** Due to their low axial stiffness, the PT braces do not buckle inelastically. If they are subjected to net compressive strains, the PT braces just buckle (bend) without developing compressive stresses, but as soon as the loads reverse (to tension) the brace can develop its full tension capacity. This behavior can be repeated through several cycles without degradation of the tensile axial strength of the brace. In some cases, it may be necessary to assess the consequences that the elastic buckling of the braces can have on the seismic performance of the building (i.e., changes in strength and deformation demands in the existing elements that can lead to demands for which they were not designed for).

■ **Whipping of the PT braces.** Due to their low axial stiffness, the PT braces deform out of plane when subjected to compressive strains (i.e. when they undergo elastic buckling). Even a small axial deformation in the braces can produce large out-of-plane deformations. Thus, it is necessary to provide out-of-plane support to the PT brace to avoid this deformation component, or better, to have a good estimate of the minimum axial force acting on the brace when the structure is subjected to the design earthquake, in such a way that buckling can be avoided.

■ **Initial state of stresses in the existing elements.** Due to the initial level of prestress in the PT braces, an initial state of stresses is induced to the existing elements. Thus, the level of prestress to use cannot be determined without studying its effects on the behavior of the existing members. The existing members are subjected to an initial state of compression, which in some cases will enhance their seismic performance (mainly in low-rise buildings). Nevertheless, if the transverse steel of the existing members is poorly detailed, especially in columns, the initial compressive forces can be detrimental to their behavior. In some cases, the existing elements should be upgraded to resist these forces.

■ **Energy dissipation capacity of the braced building.** The fact that the PT braces remain elastic does not mean that the members of the existing structure, rehabilitated by this technique, will exhibit elastic behavior. As shown in Figure 1.8, it is possible to achieve controlled energy dissipation in the existing members while the braces remain elastic. It should be emphasized that the braces by themselves do not contribute to the energy dissipation capacity of the upgraded structure, because they are supposed to remain elastic. Nevertheless, the braces may indirectly enhance the energy dissipation capacity of the upgraded structure by enhancing the seismic performance of the existing elements (Miranda and Bertero 1990).

■ **Inelastic behavior of the PT cables.** It has been suggested by some researchers that in some cases it is appropriate to use high levels of prestress for the PT cables, in such a way that the braces yield in tension at relatively small drifts. The bracing system is expected to dissipate energy through the braces' hysteretic behavior during the early stages of an extreme event. Pincheira and Jirsa (1992) note that this design criterion can be more effective than using lower levels of initial prestress, and they emphasize the importance of preventing the braces from becoming slack. Figure 1.9 shows the axial load vs. axial deformation behavior for a rod or cable with a high level of prestress. This figure shows that if the rod or cable yields, there is a loss of prestress. This is illustrated by following the load path OABC in Figures 1.9a and 1.9b, and comparing the location of points O and C. Nevertheless, it can be seen that if the initial level of prestress is high and the inelastic deformation demand is small, the remaining prestress is enough to allow the rod to adequately resist axial forces under relative compressive strains, as shown in Figure 1.9a. As shown in this figure, some plastic hysteretic energy has been dissipated in the process. Figure 1.9b shows a case in which the inelastic axial deformation of the rod or cable is excessive.

■ **Economy.** Usually, the only materials needed to implement this technique are the braces themselves and their connection. Considering other costs, such as equipment and qualified labor, the total cost of implementing this technique in the field is usually lower than that of other upgrading techniques.

1.5 USE OF POST-TENSIONED STEEL BRACES IN THE SEISMIC REHABILITATION OF FRAMED BUILDINGS WITH UNREINFORCED MASONRY INFILLS

The possible use of PT braces to upgrade existing framed buildings with URM infills is discussed conceptually (rather than quantitatively) in this section. The following are important aspects of this problem.

■ **Need to establish a rational performance criteria that takes into consideration the structural and mechanical characteristics of the URM infills.** Before attempting to discuss the use of PT braces in the rehabilitation of framed buildings with URM infills, it is necessary to define the desired performance of the upgraded building when subjected to EQGMs corresponding to the different relevant limit states (service, damageability, safety, etc.). One way of defining the desired performance of the building consists in establishing performance criteria, i.e., defining limits for the value that the global and local response of the building can have in such a way that the response of structural and nonstructural elements can be controlled within a certain acceptable range of behavior. For instance, damage in frame members and URM infills (in-plane) can be controlled by limiting their deformation and energy dissipation demands, while out-of-plane damage control in URM infills and the integrity of the contents of the building can be achieved by limiting the story accelerations in the building.

In particular, current code regulations do not provide enough information and/or regulations to allow for a rational EQ-RD that takes into consideration the desired performance of the building when subjected to different levels of EQGMs. Thus, it is necessary to define rational performance criteria based on the expected (real) behavior of the URM infills. As discussed in Section 1.2, URM infills can have beneficial effects on the seismic performance of existing framed buildings (increased global stiffness, lateral strength and energy dissipation capability), and thus, a rational performance criteria for framed buildings with URM infills should be based on allowing the infills to contribute to the global lateral load resistance of the building in a controlled manner (i.e. without suffering excessive damage and/or degradation of their mechanical characteristics).

As remarked in Section 1.2 and shown in Figure 1.1, URM walls and infills show stable hysteretic behavior without considerable degradation of their resistance and hysteretic energy dissipation capabilities for relatively large drift. Thus, it seems that a reasonable way to enhance the seismic performance of URM infills, and thus of the entire building, consists in controlling their interstory distortions by controlling the global lateral displacement of the building. Note that if the in-plane degradation of the mechanical characteristics of the URM infills is kept within reasonable values, the probability of occurrence of an out-of-plane failure due to in-plane effects diminishes considerably.

In some cases, damage control in URM infills can not be achieved by only limiting their interstory distortions, given that in some cases the nonlinear cumulative demands are relevant to their behavior. The fundamental period of translation (T) of low-rise buildings tends to be small, especially if they are infilled with URM walls and/or upgraded with a bracing system. In this range of T, the damage produced by nonlinear cumulative demands (such as the demand of hysteretic energy dissipation) is less relevant, in many cases, than that produced by interstory distortion (Terán-Gilmore 1993). In these cases, it is reasonable to attempt damage control by focusing on displacement control. For small T, one way to control the displacement of a structure is by decreasing its global ductility demands by increasing its lateral strength (Shimizaki 1988, Qi and Moehle 1991). Nevertheless, once the lateral strength of the system reaches a certain value, a further increase in strength will not significantly affect the displacement response of that system. Thus, for the upgrading of a framed building with URM infills, it seems reasonable to *increase adequately the strength and stiffness* of the building through the introduction of the PT braces, in such a way that the interstory drifts, and thus damage in the URM infills, can be controlled to acceptable values (which must be defined as part of the performance criteria). Note that this is not the case for structures with larger T and built in soft soils, in which case the nonlinear cumulative demands can be significant and the elastic displacement can be similar or even considerably larger than the inelastic displacement.

■ **Proposed performance criteria and philosophy of design for the PT braces.** The design of an adequate PT bracing system for the seismic upgrading of a building can be based on different performance criteria. Once these criteria have been established and quantified, different philosophies of design can be used to satisfy them. In this section, one approach to the upgrading of existing infilled frame buildings with PT braces is discussed.

First, it should be emphasized that a large percentage of infilled frame buildings is formed by buildings having non-ductile frames, which in past decades were designed for gravity loads only or using rudimentary EQ-RD provisions. In this type of building, there is no certainty that the frame members can undergo significant, and in some case even moderate, nonlinear demands. A performance criterion involving these frame members should focus in avoiding their non-ductile (brittle) failure, which implies limiting them to their elastic range of behavior. It has been suggested before that the PT braces should remain essentially elastic during a seismic event. It follows from the above observations that the PT braces should be designed and introduced into the building in such a way that they and the frame members remain elastic.

One of the drawbacks of keeping the frame members and PT braces elastic is the probable increase of the strength demand in the building when subjected to ground motion. One way of diminishing such demand is to provide energy dissipating devices to the structure. It should be noted that this is not necessary in the case of infilled frames, given that they have a large natural source of viscous and hysteretic energy dissipators in the URM infills. Nevertheless, to use the URM infills as energy dissipators it is necessary to make sure they can provide this dissipation in a stable manner throughout the duration of the response to the critical ground motion. From the discussions presented in Section 1.2.1, it can be concluded that this is achievable by controlling their in-plane deformation, and thus the maximum IDI in the building, within certain limits.

The proposed performance criteria for the upgraded building can be summarized as:

- Non-ductile frame members should not develop brittle failure.
- URM infills should not collapse.
- The PT bracing system should not lose stiffness or develop soft stories (prevent PT braces from becoming slack and/or from buckling in compression).
- The above criteria can be complemented with performance criteria for nonstructural elements as well as contents.

To achieve the above performance criteria, the following philosophy is suggested:

- Keep the PT braces and non-ductile frame members in their elastic range of behavior.
- Control the maximum IDI in the building in such a way as to achieve a stable hysteretic behavior in the URM infills.

It should be strongly emphasized that the good performance of the upgraded building can only be achieved by controlling its response. It is not enough to meet just the strength demands in the building to achieve such control. Thus, the design of the PT braces can not be based on a strength demand-supply approach, such as those stressed by current EQ-RD codes; rather, the PT bracing system **should be configured and designed taking into account simultaneously the expected strength, displacement (or IDI) and energy dissipation demands.** It was suggested before that the IDI in the upgraded building should be controlled to achieve a stable hysteretic behavior in the URM infills. If their hysteretic behavior is stable, it can be said that the URM infills possess a high energy dissipation capacity. In many cases, the large energy dissipation capacity in the structure provided by the URM infills would make unnecessary to consider the demand-supply balance of hysteretic energy dissipation in the EQ-RD of the upgraded building. In other words, in many cases, it would be enough to consider simultaneously the strength and displacement demands to design and configure the PT bracing system. The previous observation will not be true for EQGMs with very large duration of strong motion.

■ **Out-of-plane failure.** The upgraded building can have an adequate seismic performance only if the out-of-plane failure of the infills is avoided, given that its occurrence can induce sudden and very large stiffness and strength irregularities, and thus unpredictable and large changes in the dynamic properties of the building. It is important to address again the concept of out-of-plane dynamic stability introduced in Section 1.2. It has been noted by the researchers of the ABK Method (1984) that, if the movement of the whole building is dampened by the yielding and nonlinear behavior of some of its members, the out-of-plane forces are considerably reduced (Langenbach 1990). In the case of upgrading an infilled frame, the use of PT braces with high stiffness and strength will likely reduce the nonlinear demands (deformation and hysteretic energy dissipation) in the building, which in turn will likely increase the in-plane and out-of-plane lateral forces and accelerations in the building (with respect to those on the unstrengthened building). Nevertheless, given that in the upgraded building the URM infills are supposed to dissipate energy through controlled nonlinear hysteretic behavior, the likely increase of lateral forces and story accelerations may be controlled to acceptable values. This issue will be addressed in more detail later.

To summarize, two issues need to be addressed. First, the lateral stability of the URM infill accounting for in-plane damage and out-of-plane acceleration demands; and second, the change of the lateral forces and accelerations on the building (in-plane and out-of-plane) with respect to those on the original building.

■ **Efficient (optimal) relative stiffness and limiting deformation.** As mentioned in Section 1.3, in order to achieve efficient EQ-RD of the upgraded structure it is important to select an efficient stiffness for the bracing system, and to supply this system with a lateral deformation capability similar to that of the existing structure. The mechanical characteristics of the PT bracing system should be provided in such a way that it adds enough strength and stiffness to the upgraded building to achieve adequate control of the interstory drifts and nonlinear cumulative demands, and it should be flexible enough to allow the infills to resist a significant portion of the lateral loads, and thus to allow the infills to be used extensively to dissipate energy. In other words, the PT braces should add enough stiffness to control the maximum IDI in the building, but they should not be so stiff that they minimize the contribution of the URM infills to resist the ground motion.

■ **Stiffness and strength irregularities in existing framed buildings with URM infills.** As remarked before, URM infills have been commonly used as nonstructural elements. Given that in the past the contribution of these elements with such high stiffness and strength was usually neglected in the design process, no special consideration was given to their location within the existing frames of a building. Thus, large irregularities in plan and height of stiffness and strength usually exist in this type of building. ***The PT bracing system should attempt to correct the irregularities created by the infills, both in plan and height.***

■ **Difficulty in assessing the real behavior of framed buildings with URM infills.** Brokken and Bertero (1981) have noted that the lateral stiffness and strength of a masonry infill are very sensitive to the quality control of the material, as well as to the quality of their workmanship (including the interfaces of the infill and the existing frame elements). It should be mentioned that infill walls have a wide variety of configurations, depending on whether there are doors, windows, or other holes in the infill. The variability of the properties and geometry of the infills, as well as the large irregularities of strength and stiffness they may produce in the building, have to be considered carefully if a realistic prediction of the behavior of the infilled building needs to be obtained. Given the complexity of the models and our lack of knowledge about how to model adequately the characteristics and irregularities of infilled framed buildings, it is necessary to use simplified models with the corresponding introduction of uncertainty (which is considerably larger than that involved in evaluating the real behavior of regular framed buildings) in the results obtained in their analysis. This uncertainty needs to be assessed carefully given that it is essential to have a reasonable estimate of the behavior of the upgraded building in order to avoid the loss of prestress and/or the elastic buckling of the PT braces. Given our current limitations, it would be desirable at least to bound the response of the upgraded building by bounding some of the main structural and dynamic characteristics of the analytical model to be used in the final analysis, and to make the final design of the PT bracing system accordingly.

■ **Degradation of structural properties of URM infills during an EQGM, and its consequence in the use of elastic analysis to predict the response of a framed building with URM infills.** It has been observed experimentally that the cyclic loading of URM infills leads to degradation of stiffness and strength, and that the effective equivalent viscous damping coefficient of the virgin system increases considerably as soon as some cracking develops (Brokken and Bertero 1981). Therefore, the stiffness, strength and damping properties used to model the URM infills in the building need to be considered carefully according to the expected deformation and cumulative demands on those infills. This is especially true if elastic analyses, as required by current EQ-RD codes, are carried out to analyze the behavior of the building, given that even at small deformation levels, the stiffness of the URM infills can decrease considerably with respect to its uncracked stiffness (Brokken and Bertero 1981).

■ **Initial state of stress in the existing URM infills.** It is necessary to evaluate the consequences that the initial state of stresses (due to prestressing of the PT braces) has on the seismic performance of the URM infills. Two possible effects can be mentioned: an initial state of moderate in-plane compression in the infills will usually enhance their ultimate strength, deformation capability and overall stability, while high compressive stresses can be detrimental to their behavior. Because of the large plan area of the URM infills, the increase in compressive stress is not expected to be very large, and thus this initial state would probably enhance the behavior of the existing URM infills. If the initial state of compression enhances the behavior of the infills, it would be desirable (if possible) to locate the PT braces in the frames where the URM infills are located.

■ **Yielding of the PT braces.** If the inelastic deformation demands in the braces are large, in such a way that they become slack, their stiffness diminishes, and this decrease in stiffness can be reflected by an increase in the displacement of the building that can induce excessive damage to the URM infills. Heavy damage (or failure) in the URM infills can lead to large irregularities of strength and stiffness throughout the plan and height of the upgraded building, which may produce unpredictable changes in its dynamic characteristics and, very probably, detrimental changes in its behavior. Even if no irregularities are created by the excessive degradation of their mechanical characteristics, if the contribution of the infills to the strength and stiffness of the building is lost unexpectedly as a consequence of the excessive yielding of the bracing system, an important percentage of the lateral load will begin to be carried by the frame. This can produce a large combination of axial forces and moments in the frame elements: axial forces induced by the braces and flexural moments due to the increased lateral deformation of the building. This type of loading, for which the frame elements were not designed, can lead to non-ductile failures in the existing columns. The importance of avoiding excessive yielding of the braces lies in the need to control the displacement in the URM building to acceptable values in such a way that excessive damage to the infills and other vertical elements is avoided. If the PT braces are allowed to yield, it is necessary to limit this yielding in such a way that it will not be detrimental to the response of the building. As the forces to be induced in the braces depend on the interaction between the dynamic characteristics of the entire building system and those of the EQGM, the importance of having a reasonable estimate of the characteristics and intensity of the EQGMs at the site is emphasized.

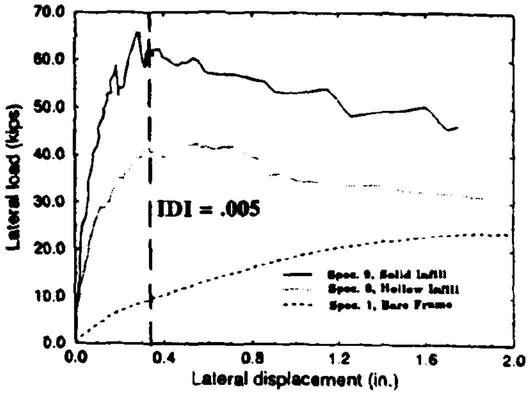

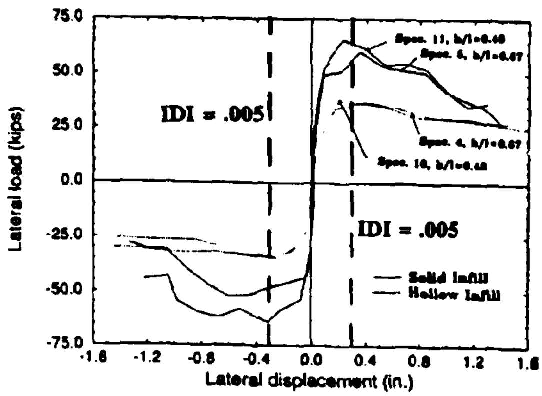

a) URM infill, monotonic (Schuller et al. 1994)

b) URM infill, cyclic envelope (Schuller et al. 1994)

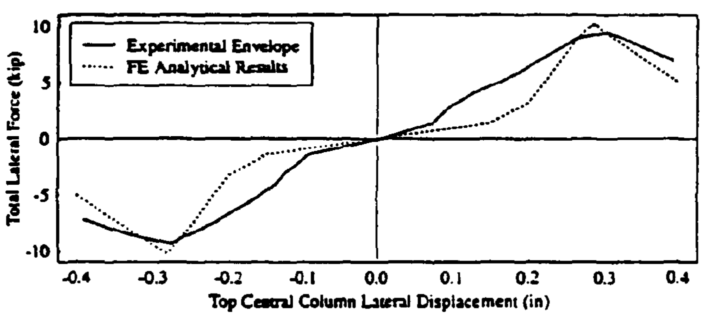

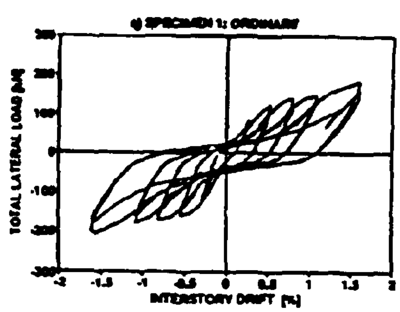

c) URM infill, cyclic envelope (Gergely et al. 1994)

d) URM infill, cyclic (Mander et al. 1994)

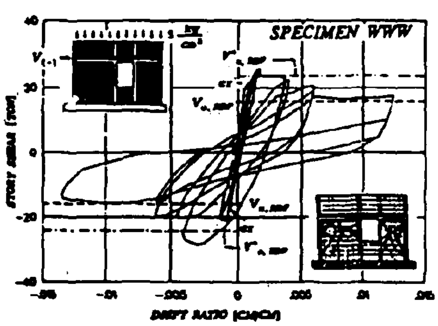

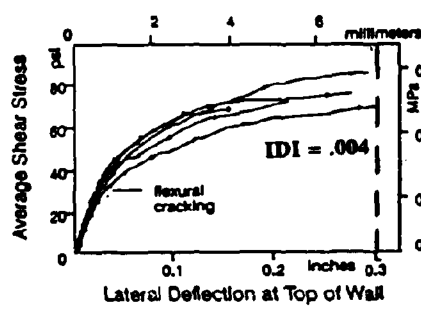

e) Confined URM wall, cyclic (Meli et al. 1992)

f) URM wall, monotonic (Abrams 1992)

Figure 1.1 Typical lateral load vs. lateral displacement curves and envelopes for URM infills and walls

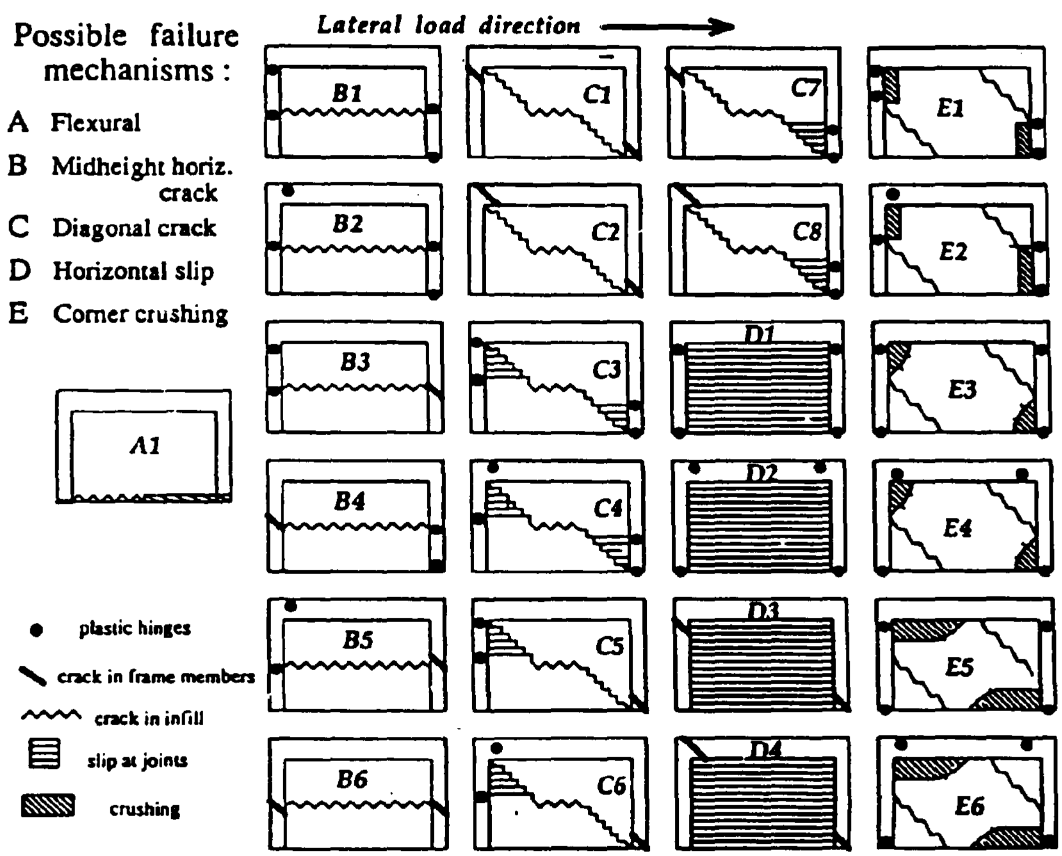

Figure 1.2 Failure mechanisms in frames with URM infills (Mehrabi and Shing 1994)

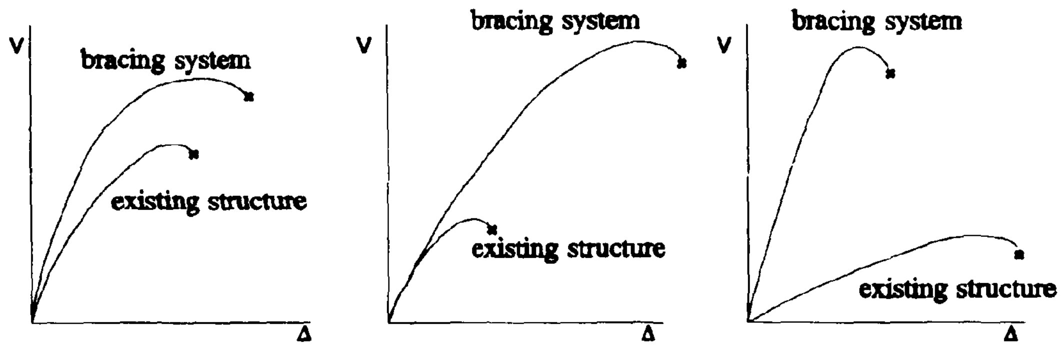

a) efficient use of braces   b) inefficient use of braces   c) use of braces to unload existing structure

Figure 1.3 Compatibility of stiffness and deformation capability between existing structure and the bracing system

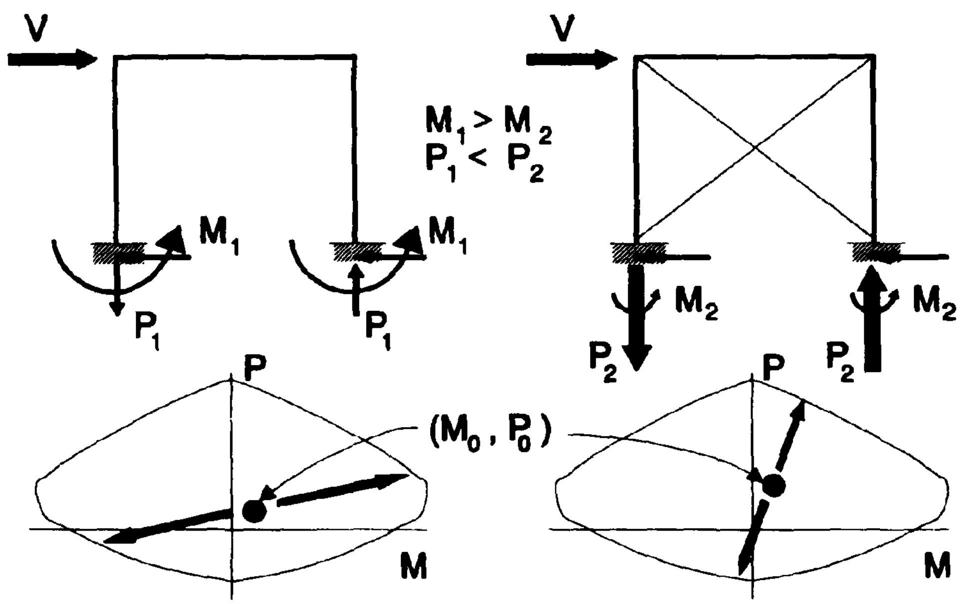

Figure 1.4 Change in behavior of existing elements

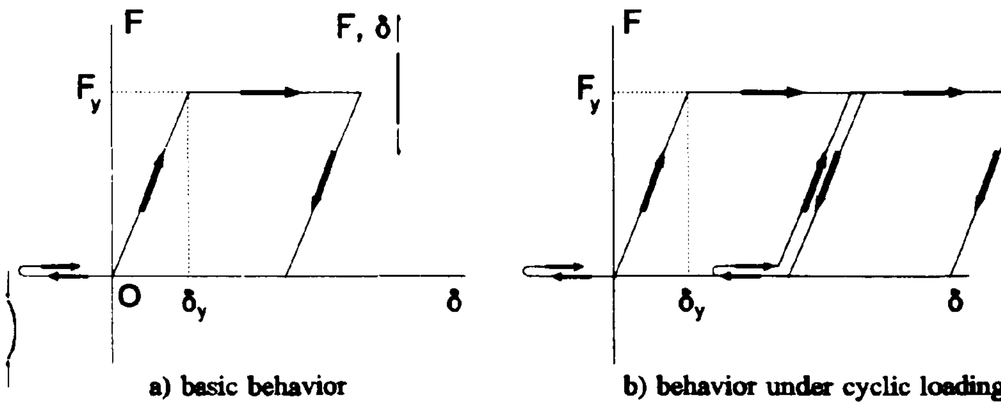

Figure 1.5 Axial displacement vs. axial load behavior of rod or cable with no prestress

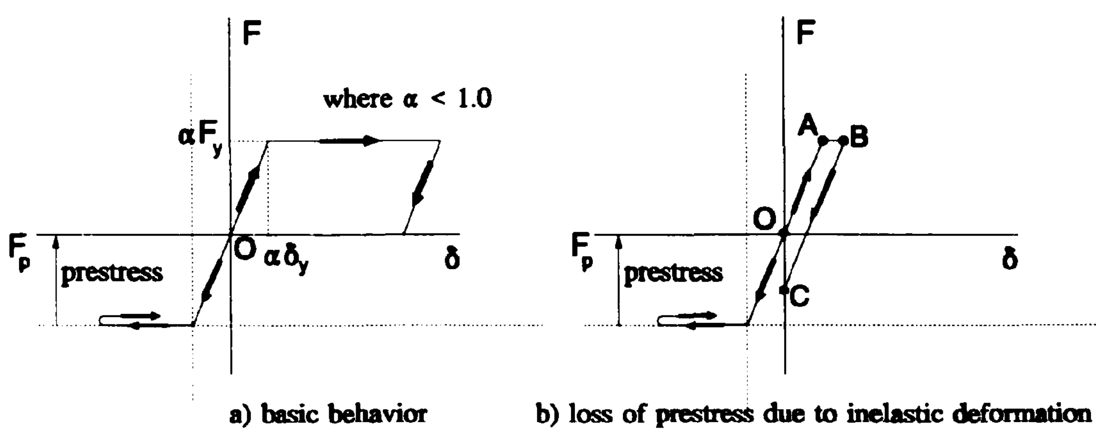

Figure 1.6 Axial displacement vs. axial load behavior of rod or cable with prestress

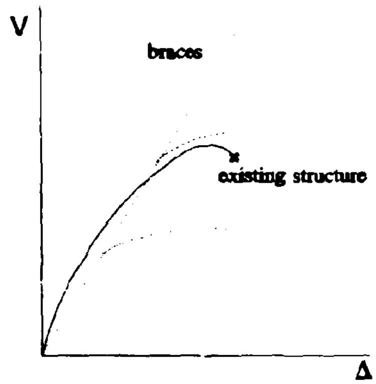

Figure 1.7 Use of different elastic deformation capabilities of PT braces to match the deformation capability of the existing structure

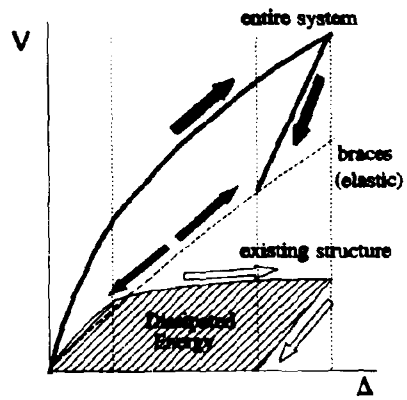

Figure 1.8 Energy dissipation in existing building upgraded with PT braces

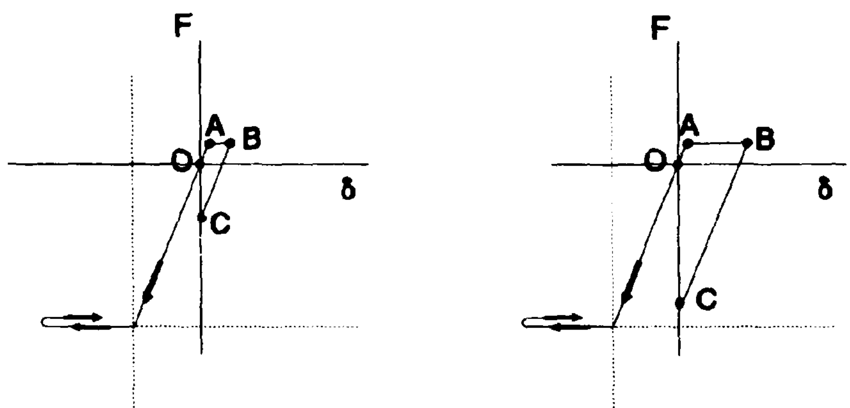

a) moderate loss of prestress

b) excessive loss of prestress

Figure 1.9 Axial displacement vs. axial load behavior of rod or cable with high prestress

2 CASE STUDY OF THE SEISMIC PERFORMANCE OF A FRAMED BUILDING WITH UNREINFORCED MASONRY INFILLS

The possible advantages and disadvantages, as well as the main design considerations for the use of post-tensioned (PT) braces to upgrade non-ductile frames with unreinforced masonry (URM) infills have been discussed in Chapter 1. Although from these discussions it can be established that the use of such upgrading technique may be attractive, there is a need to provide more concrete discussions that can aid the structural engineer to judge in a more realistic context the possible benefits and drawbacks associated with the use of this technique. This in turn, may help the engineer in deciding when can this upgrading technique may be used efficiently. At the heart of this issue lies the need to provide the practicing engineer with some quantification of the design and real mechanical properties of the bracing system (i.e., how many braces and their location, their size, their yielding strength, etc.) as well as of the global and local response of the upgraded building (and, of course, how does this response differs from that of the original building).

To make the above possible, it is necessary to provide some realistic examples of the use of PT braces in infilled non-ductile frame buildings. In this context, the best example that can be provided is to apply this technique to a real (existing) building, and discuss, while the earthquake-resisting design (EQ-RD) of the bracing system progresses, the relevant design considerations associated with its use. A great opportunity to accomplish this goal is provided by the fact that the Strong Motion Instrumentation Program of the California Department of Mines and Geology (CSMIP) has instrumented several buildings with infilled non-ductile frames.

After a brief search for a building that could provide a good example, a six-story commercial building with 12 channels of instrumentation and located in Pomona (CSMIP Station No. 23544) was selected. This building provides the opportunity to emphasize the benefits of the use of PT braces as an upgrading technique given that its infilled reinforced concrete (RC) frames have insufficient lateral strength and stiffness, as well as a large mass, stiffness and strength irregularities in plan and height. Also, the availability of the recorded response of the building to two earthquake ground motions (EQGMs) with different characteristics allows the study of its behavior and performance when subjected to different levels of EQGM, as well as the assessment of the reliability of current analytical tools to model such behavior. In this chapter, relevant information about the structural characteristics of the Pomona building is introduced, followed by a discussion of the problems found when modeling URM buildings for linear and nonlinear analysis. Finally, different analytical models of the Pomona building are analyzed when subjected to EQGMs of different intensity, and the results obtained from the analyses are discussed to assess its seismic performance and the need to upgrade it.

2.1 DESCRIPTION OF CASE BUILDING (POMONA BUILDING)

CSMIP Station No. 23544 is a six-story commercial building with a penthouse, a mezzanine and a basement level. This building was constructed in 1923 and has RC framed structure with unreinforced brick masonry infills in all its perimetral frames and three internal frames. At the ground level the building measures 65 feet (E-W direction) by 120 feet (N-S direction) in plan, as shown in Figure 2.1. Table 2.1 shows floor elevations and masses, along with the approximate locations in plan of the centers of mass and rigidity on each floor. The centers of mass corresponding to the second through fifth floor are close to the geometric centroid of the floor diaphragms, while large mass eccentricities exist in the mezzanine and sixth floors. In the mezzanine floor, the center of mass is displaced towards the northwest corner, and in the sixth floor (roof), towards the southwest corner. As shown in Table 2.1, the distance in the N-S direction between the centers of mass and stiffness in the mezzanine and second floors is very large, while in the third to sixth floors it is small. In the E-W direction, this distance is large for all floors.

The floor system consists of a three-inch thick one-way RC slab supported by RC joists spaced every two feet, while the structural system for gravity and lateral loads is formed by non-ductile RC frames (having beams, girders and columns) infilled with URM walls. Figure 2.1 shows schematic plan views of the different floors of the building, while Figure 2.2 shows schematic elevation views of the four perimetral frames and the notation used for floors and stories. As shown in Figure 2.2, there are URM infills in the perimetral frames, which probably contribute significantly to resist the lateral loads induced in the building by EQGMs. As shown, practically all infills in Frame 1 are full infills (without openings), while those located in Frame 6 have large openings, creating large stiffness and strength eccentricities in the E-W direction of the building, especially in the mezzanine and second floors (see Table 2.1). Infills located in the upper stories of Frames A and F show similar characteristics (openings); nevertheless in the lower stories (ground and mezzanine) the stiffness and strength of Frame A are lower than those of Frame F (by comparing Figures 2.2c and 2.2d, it can be seen that Frame A has a double-height first story and weaker and more flexible URM infills in this story than those in Frame F), creating large strength and stiffness eccentricities in these levels in the N-S direction (see Table 2.1). This eccentricity (N-S direction) is magnified by the presence of an L-shaped mezzanine (which as shown schematically in Figure 2.3 runs along Frames 1 and F), and a large mass eccentricity at the roof in this direction. It can be concluded that the building has large irregularities of mass, strength and stiffness in plan.

As shown in Figure 2.2, Frames A and 6, which correspond to the two facades facing the streets, show a double-height first level that has considerably fewer infills than the upper levels. As will be discussed in more detail later, this creates a weak and flexible first level, which produces a large irregularity in height, both in strength and stiffness.

The basement of the building is enclosed by a perimetral 12-inch thick concrete wall, which provides a stiff and strong support for the columns of the ground story, except those of Frame 6, because this perimeter wall has an offset of 7 feet 6 inches with respect to the plane defined by Frame 6, as shown in Figure 2.4.

The sizes of the beams are fairly constant over height, as shown in Table 2.2. Columns are square, and their sizes decrease considerably in higher stories, and become very small in the top story, as shown in Table 2.3. The sizes and reinforcement of columns are available, as well as some idea of the detailing of their transverse and longitudinal reinforcement. In the majority of the columns, transverse reinforcement was provided by closely spaced spirals. The sizes of the beams are available; nevertheless, because of the unavailability of information regarding their reinforcement, it was necessary to obtain estimates of their longitudinal and transverse reinforcement. To get a reasonable estimate of this reinforcement, it was considered necessary to look for information regarding the nature of the design procedures used in the year the building was designed (1923).

After a brief bibliographical search, it was found that the Building Laws of San Francisco (BLSF) of 1926 were the design regulations that came closest in time to the year 1923. According to these regulations, no considerations regarding lateral loads (including wind) should have been made in the original design of the six-story building (given its low height and large base-to-height ratio). Thus, there was reason to believe that this building had been designed for gravitational loads only. The structural drawings of this building include the axial loads for which its columns were designed, and it was found that these loads were very close to the axial strength of the columns obtained using the BLSF provisions for the design of axially loaded columns subjected to gravity loads. This fact confirmed that the structure was designed for gravitational loads only. Thus, an estimate of the longitudinal and transverse reinforcement of the beams was obtained by designing them according to the BLSF of 1926 and for gravitational loads only. Because the axial loads used in the original design of the columns were available, it was possible to reconstruct partially the gravitational loads for which the beams were designed. This process was facilitated by the extensive use of one-way slabs throughout the building.

It should be mentioned there are not enough available data to determine the type of anchorage and splicing used in the longitudinal reinforcement of beams and columns. Normally, it would be necessary to determine this information in the field; nevertheless, such information was not available. Thus, it is not possible to determine whether the detailing provided to the reinforcing bars would allow the RC elements to develop their maximum flexural strength. It is unlikely that the detailing used for the longitudinal reinforcement at the time of the design (1923), including the fact that the building was designed for gravitational loads only, will allow the RC elements to reach their ultimate and even their yielding flexural capacity. This fact introduces a large uncertainty into the analysis of the Pomona building; nevertheless, given that the existing frame members are supposed to remain elastic once the PT braces are introduced into the building, this issue is not expected to matter very much for the analysis of the upgraded building, as will be explained in Chapter 3.

2.2 MATERIAL PROPERTIES, MODELING OF MATERIAL BEHAVIOR

■ **Masonry.** The mechanical characteristics of the masonry are not known, because material tests have not been performed on the masonry of the Pomona building. These characteristics were estimated according to the values suggested by Kariotis et al. for the masonry in this building (1993):

Compressive strength	1.2 ksi
Compressive strain corresponding to compressive strength	.004 in/in
Elastic modulus (tension)	400 ksi
Cracking strength	0.1 ksi
Tensile strain	.00025 in/in

The stress-strain curve for the masonry was modeled according to the above mechanical properties and the following expressions (Ewing et al. 1990):

• ***Compression***: As shown in Figure 2.5, the stress-strain relation is described by two second-order polynomials and an exponential tail:

$$f(\epsilon) = f_m[A_1(\epsilon/\epsilon_0) - \lambda(A_1 - 1)(\epsilon/\epsilon_0)^2] \quad ; \quad 0 \geq \epsilon \geq \epsilon_p$$

$$f(\epsilon) = f_p\left[1 - \frac{(\epsilon - \epsilon_p)^2}{(A_2\epsilon_0 - \epsilon_p)^2}\right] \quad ; \quad \epsilon_p \geq \epsilon \geq \epsilon_e \tag{2.1}$$

$$f(\epsilon) = f_e\left[A'_3 + (1 - A'_3)\exp\left[-\gamma\frac{(\epsilon - \epsilon_e)}{\epsilon_e}\right]\right] \quad ; \quad \epsilon < \epsilon_e$$

where $f(\varepsilon)$ is the principal compressive stress; ε, the principal compressive strain; f_m, the uniaxial compressive strength; ε_0, the strain corresponding to f_m; f_p, the peak uniaxial compressive strength; ε_p, the strain corresponding to f_p; λ, a strength modification factor ($f_p = f_m / \lambda$); ε_e, the point of tangency between the second and third equations above; f_e, compressive stress at ε_e; A_1, A_2, A_3, A_4 are shape factors; and:

$$A'_3 = A_3(f_m/f_e)$$

$$\epsilon_e = \epsilon_0[1 + A_4(A_2 - 1)/\lambda] \tag{2.2}$$

$$\gamma = \frac{2f_m\epsilon_e(\epsilon_e - \epsilon_p)}{\lambda f_e(1 - A'_3)(A_2\epsilon_0 - \epsilon_p)^2}$$

• ***Tension***: As shown in Figure 2.6, the stress-strain relation is defined by a straight line plus an exponentially decaying tail as follows:

$$f(\epsilon) = E_t\epsilon_t \quad ; \qquad 0 \le \epsilon_t \le \epsilon_{cr}$$

$$f(\epsilon) = f_{cr}\left[B_1 + (1 - B_1)\exp\left[-\alpha\frac{\epsilon_t - \epsilon_{cr}}{\epsilon_{cr}}\right]\right] \quad ; \quad \epsilon_t > \epsilon_{cr} \tag{2.3}$$

where $f(\varepsilon)$ is the stress in the masonry due to tension stiffening; E_t, the modulus of elasticity in tension; ε_t, the tensile strain; ε_{cr}, tensile cracking strain; f_{cr}, tensile cracking stress; α, positive exponential parameter; and B_1, the lower limit for the exponential branch.

The compressive strength of the concrete and the yielding strength of the steel according to the structural drawings of the building are 3 ksi and 40 ksi, respectively. The stress-strain relationships for concrete and steel were modeled as follows:

■ **Concrete.** The stress-strain relationships for confined and unconfined concrete are described by the following equations (Park et al. 1982):

$$f_c = k f_c' \left[\frac{2\epsilon_c}{\epsilon_o k} - \left(\frac{\epsilon_c}{\epsilon_o k} \right)^2 \right] \qquad \epsilon_c \leq k\epsilon_o \tag{2.4}$$

$$f_c = k f_c' \left[1 - Z_m(\epsilon_c - \epsilon_o k) \right] \geq 0.2 k f_c' \qquad \epsilon_c > k\epsilon_o$$

where

$$k = 1 + \rho_s \frac{f_{yh}}{f_c'} \qquad Z_m = \frac{0.5}{\epsilon_{50u} + \epsilon_{50h} - \epsilon_o k}$$

$$\epsilon_{50u} = \frac{3 + \epsilon_o f_c'}{f_c' - 1000} \qquad \epsilon_{50h} = 0.75\ \rho_s \sqrt{\frac{h_1}{s}} \qquad \textit{units: psi}$$

and f_c is the longitudinal concrete stress; ε_c, the longitudinal concrete strain; f_{yh}, the yield stress for the hoop reinforcement; h_1, the width of the concrete core measured to the outside of the hoops; s, the center-to-center spacing of the hoops; and ε_o is typically assumed to be equal to 0.002. The maximum concrete strain is given by

$$\epsilon_{cmax} = 0.004 + 0.44\ \rho_s f_{yh} \qquad \textit{units: psi} \tag{2.5}$$

where ρ_s is the ratio of the volume of hoop reinforcement to volume of concrete core measured to the outside of the hoops.

The modulus of elasticity, E_c, and the modulus of rupture, f_t, were assumed to be (Mac Gregor 1988):

$$E_c = 57{,}000 \sqrt{f_c'} \qquad f_t = 7.5 \sqrt{f_c'} \qquad \textit{units: psi} \tag{2.6}$$

■ **Steel.** The steel reinforcement behavior was modeled by a straight line with slope E_s in its elastic range of behavior, by an horizontal straight line for plastic yield plateau and by a parabola once it strain-hardens:

$$
\begin{aligned}
&f_s = E_s \epsilon_s \qquad |\epsilon_s| \le \epsilon_y \\
&f_s = f_y \; sgn(\epsilon_s) \qquad \epsilon_y < |\epsilon_s| \le \epsilon_{sh} \\
&f_s = \left(a_2 \; \epsilon_s^2 + a_1 \; |\epsilon_s| + a_0\right) sgn(\epsilon_s) \qquad \epsilon_{sh} < |\epsilon_s| \le \epsilon_u \\
&\textit{where} \\
&sgn(\epsilon_s) \begin{cases} = 1 \; if \; \epsilon_s > 0 \\ = -1 \; if \; \epsilon_s < 0 \\ = 0 \; if \; \epsilon_s = 0 \end{cases} \\
&a_2 = \frac{f_u - f_y}{\epsilon_u^2 - \epsilon_{sh}^2 - 2\; \epsilon_u \; (\epsilon_u - \epsilon_{sh})} \qquad a_1 = -2 a_2 \epsilon_u \qquad a_0 = f_u - a_2 \epsilon_u^2 - a_1 \epsilon_u
\end{aligned}
\tag{2.7}
$$

For a reinforcement bar, an effective length of $s/\sqrt{2}$ was assumed to be laterally supported by stirrups. The critical buckling stress, f_{cr} , is given by the following relation (Filippou 1987):

$$
f_{cr} = 2 \; E_t(\epsilon_s) \; \pi^2 \; \frac{(.25\phi_L)^2}{s^2} \tag{2.8}
$$

where $E_t(\varepsilon_s)$ is the tangent modulus of the steel stress-strain relationship and ϕ_L the diameter of the bar.

The following values for steel Grade 40 were considered (Astaneh 1991):

Yielding stress,	f_y = 40 ksi
Ultimate stress,	f_u = 58 ksi
Strain at onset of strain-hardening	ε_{sh} = 0.012
Strain at ultimate,	ε_u = 0.20
Modulus of elasticity,	E_s = 29000 ksi

2.3 ANALYTICAL MODELING OF THE POMONA BUILDING

Although some suggestions regarding the modeling of buildings with URM infills are currently available, considerable research needs to be devoted to this issue. In several cases, the fact that some nonlinear analyses are carried out on a building raises the expectations of the engineer regarding the validity of the results obtained from such analyses. It must be mentioned that due to the large uncertainty involved in obtaining realistic analytical models for URM infills (especially in the case when the infills have openings and suffer several cycles of nonlinear behavior), the results obtained from the elastic and nonlinear analyses of infilled buildings need to be evaluated and judged carefully.

In this section, some suggestions made by several researchers to model URM infills and RC members when subjected to lateral deformations are presented. Within the framework provided by this information, the considerations involved in the modeling of the members of the building for performing elastic and nonlinear analyses of this building are discussed.

2.3.1 MODELING CONSIDERATIONS FOR ELASTIC ANALYSIS

As noted in Section 1.2.1, at some stage of their behavior URM infills usually suffer extensive diagonal cracking which helps in the formation of a mechanism in which lateral loads are resisted by a compression strut. Several researchers have suggested the possibility of modeling masonry infills using truss elements. Section 4.2.1 of "Guidelines for Analysis of Existing Frame Structures with Concrete or Masonry Infills" of SEAOC (1993) states: "*URM infills within frame elements shall be modeled as an equivalent strut developed from a rational analysis and using the strength and modulus characteristics as established by physical testing.*"

Klingner and Bertero (1976) discuss in detail the use of empirical formulas to determine the properties of an "equivalent" strut to be used in elastic analyses, while the use of the lateral force vs. lateral deformation curve of the infill (determined by using nonlinear finite element analysis) to estimate the properties of the strut has been discussed by Kariotis et al. (1993, 1994).

If an elastic analysis is performed, only the stiffness of the infill, and thus of the equivalent strut element, is required. Nevertheless, a question arises: Should the uncracked stiffness of the infill be considered in the analysis? Or, if an uncracked stiffness is used, how is this stiffness defined? To illustrate the difficulty involved in obtaining a definition of stiffness for an URM infill, the lateral deformation vs. lateral load curve for an URM infill (obtained from nonlinear finite element analysis) located in the building is shown in Figure 2.7. As shown, once the infill cracks considerable nonlinear behavior develops. Nevertheless, the lateral load-resisting capacity of an URM infill usually increases considerably with respect to the lateral load that produced the cracking. In some cases, it might be necessary to analyze the behavior of the building beyond first cracking by means of an elastic analysis, and thus the behavior of the infills beyond first cracking must be modeled in an appropriate manner (i.e., ***using an appropriate secant stiffness***). The problem that arises from the need to decide what secant stiffness should be used in the analysis is considerably obscured by the fact that the empirical equations given by different researchers to obtain the properties of the equivalent strut are usually not accompanied by relevant information regarding the deformation levels at which these equations are valid. A recent study (Jamal et al. 1992) suggests that several of these recommendations were obtained for different deformation levels, and thus cannot be applied freely to the modeling of URM infills. Therefore, it is convenient when possible to estimate the stiffness of the equivalent strut from the lateral force vs. lateral deformation curve of the URM infill. In some cases, nonlinear finite element programs have been used to estimate these curves, such as those shown in Figure 2.7, (Kariotis et al. 1993 and 1994). It should be mentioned that for this type of analysis, the modeling assumptions made to model the URM infill, surrounding elements and their interface should be done carefully given their influence on the final results.

Before establishing the properties of the equivalent strut once the lateral force vs. lateral deformation curve is available for a given URM infill, it is necessary to estimate its expected level of lateral deformation when the building is subjected to EQGM. Then, a secant stiffness can be estimated for use in the elastic analysis. But the lateral deformations in turn depend on the stiffness of the infill, which implies that to obtain reasonable results from an elastic analysis an iterative procedure must be used. To make this iterative procedure possible, the degradation of the strength and stiffness of the URM infills, and the energy dissipated during cyclic loading must be neglected or modeled according to simplifying assumptions.

A three-dimensional (3D) elastic model of the building was prepared by Kariotis et al. (1993). Kariotis et al. calibrated some structural parameters of the building, such as the effective stiffness of the RC members and URM infills (equivalent struts) and the percent of critical damping (ξ), in such a way that the response predicted analytically from the elastic model of the building matched as closely as possible the recorded response of the building during two EQGMs. The following are some of the modeling considerations made by Kariotis et al.

■ **Slab.** The RC slab was modeled as a rigid diaphragm.

■ **RC frame members.** The effective stiffness of RC members was estimated by reducing the moment of inertia of their gross section by a factor which accounts for cracking according to the expected interstory drift index (IDI) demands.

■ **URM infills.** The URM infills were modeled as diagonal truss elements, whose properties were estimated according to secant stiffness obtained from the curves shown in Figures 2.8a to 2.8h and the expected level of IDI.

■ **Damping.** ξ = 0.02 for all modes. Although higher values of ξ can be expected when URM cracks, Kariotis et al. found that the results obtained from the analysis of their elastic 3D model came closer to the recorded response of the building when a ξ = 0.02 was used.

■ **Mass.** The mass and location of the center of mass on each floor is shown in Table 2.1.

■ **Modal time history analysis.** Only the contributions of the first three modes were considered.

The dynamic characteristics according to the Kariotis et al. elastic 3D model are shown in Table 2.4. As shown, T_1 = 1.04 sec can be considered as the fundamental translation period in the E-W direction, while T_3 = 0.51 sec can be considered as the fundamental translational period in the N-S direction. T_2 = 0.70 is associated with a fundamental torsional mode of the building, which is coupled with the translational response of the building in the N-S direction.

Figure 2.9 shows the location of the sensors at CSMIP station No. 23544 (Pomona building). As shown, they are concentrated in the basement, at the second floor and on the roof. Figures

2.10 and 2.11 show story displacement envelopes estimated from the second floor and roof maximum displacements (interpolating linearly to obtain the maximum displacements of other stories) recorded during the Landers earthquake (EQ). Similar envelopes for the same EQGM were estimated from an elastic time-history analysis of the Kariotis et al. 3D model using the program SAP90 (Habibullah 1989). As shown in Figure 2.11, there is a close match between the analytical and recorded displacements in the N-S direction, while Figure 2.10 shows that a reasonable match was obtained in the E-W direction. It can be concluded that the maximum response of the building can be reasonably estimated using an elastic model.

A more detailed discussion of the modeling of the building, as well as further comparison between the estimated response and the recorded response, can be found in Kariotis et al. (1993).

2.3.2 Modeling Considerations for Nonlinear Analysis and Their Effects on the Reliability of the Expected Results

■ **Modeling Considerations.** The modeling of URM infills for nonlinear analysis is considerably more difficult than their modeling for elastic analysis. In the case of nonlinear analysis, the model of the infill should be able to predict the following: initial stiffness, first cracking and ultimate strengths, and degradation of stiffness and strength (including the pinching effect associated with the deterioration of initial stiffness). A comprehensive study regarding the modeling of the linear and nonlinear behavior of infilled RC frames using an equivalent truss element was carried out by Klingner and Bertero (1976) and Klingner (1980). Some researchers (Mander et al. 1994, Chrysostomou et al. 1992) have recently discussed the advantages of modeling the nonlinear behavior of URM infills without openings by using multi-strut models (one-diagonal and two off-diagonal struts acting simultaneously in compression only). Nevertheless it should be noted that very limited research effort has been devoted to the simplified modeling of the nonlinear behavior of URM infills with openings, and the applicability of the methods discussed previously to these type of infills has yet to be assessed. Given that the majority of the URM infills in the Pomona building have large openings in them, the definition of single or multi-truss models to capture the nonlinear behavior of these infills is beset with uncertainty.

Also, it has been observed experimentally that after an infilled framed reaches a given resistance level in one direction, the same infilled frame is not able to develop this same resistance in the other direction upon load reversal (Klingner 1980). In other words, the resistance that the infill has in one direction in some cases depends on the deformation demands on that infill in the opposite direction. Nevertheless, Abrams (1992) observed experimentally that this was not the case for URM walls subjected to lateral deformation. Although no direct comparison can be established between the experimental results obtained by the two researchers, it is clear that there is a need for further research to better determine the behavior of URM infills when subjected to lateral cyclic loading. Other sources of uncertainty are associated with the modeling of the behavior of the URM infills and their interaction with the existing frames, as well as with the modeling limitations inherent in the computer program used in the analysis.

Prior to deciding the considerations used to develop a model of the building, it is necessary to carefully define the objectives of the nonlinear analyses of the building:

- **Identify if there is a need to upgrade the Pomona building.**
- **Assess the performance of the upgraded building (in case that the building needs to be upgraded).**

It should be clearly stated that the above are the only objectives of the nonlinear analyses of the Pomona building, and other considerations go beyond the scope of this report. To accomplish the above objectives, it is necessary to develop a 3D model of the building, given the large irregularities in plan of this building.

Before performing 3D analyses, it was considered convenient to establish a frame of reference against which the modeling assumptions of the 3D model could be calibrated. This was done because the program DRAIN 3DX (Powell et al. 1994) used for the 3D analysis has been released only recently and no guidelines exist regarding its reliability and proper use. Also, it would be helpful to gain some insight into some aspects of the nonlinear behavior of the building that can aid in the interpretation of the results obtained from a 3D nonlinear analyses. Therefore, several planar (2D) nonlinear analyses of the Pomona building were carried out using the program DRAIN 2DX (Powell et al. 1992) to assess, in a economically feasible manner, the validity of some simplified modeling techniques for the behavior of the URM infills and to provide an insight into the nonlinear behavior of the building.

The DRAIN 2DX model consisted of an assemblage of two types of elements: beam-column elements to model the RC frame members, and truss elements to model the URM infills. In this section, the considerations involved in the creation of the DRAIN 2DX model of the building, as well as its limitations, are discussed.

• ***URM Infills.*** The URM infills were modeled using several truss elements in parallel having a linear piecewise idealization of the lateral force vs. displacement curves shown in Figure 2.8. These curves were estimated using a 2D nonlinear finite element program (Ewing et al. 1990), and the material properties and behavior described in Section 2.2. A detailed discussion of the considerations involved in modeling the infilled frame to obtain such curves can be found in Kariotis et al. (1993). All truss elements modelling a given URM infill were placed spanning only one of the diagonals of the bay where the infill was located on (as opposed to two in *X*), because it was found that in the analyses of isolated frames of the building this model yielded similar results to that where the infills were modeled with truss elements spanning both diagonals. This simplified modeling technique represented significant savings in computational effort.

One limitation of DRAIN 2DX is that it does not allow for stiffness or strength degradation on truss elements. Thus, only the initial stiffness and strength of the infills can be modeled reasonably well. The degradation ot these properties can not be modeled, nor can the effect that the deformation of the infill in one direction can have on its resistance in the opposite direction. If the cyclic deformation demands in the URM infills are large, the DRAIN 2DX model can not predict in a reasonable manner the response of the building; nevertheless, if the deformation demands on the building are limited to moderate values, the effects that the strength and stiffness degradations have on its response will diminish.

• ***Beams.*** A lumped plasticity model was used to model the beams. Thus, all inelastic deformations occurring at the beams are assumed to be concentrated at discrete points, usually at their ends. This is a reasonable modeling assumption for beams of structures subjected to lateral loads, given that their maximum moments usually occur at their ends if the effects of gravity loads are not very large.

The strength and stiffness of the beams were estimated considering the contribution of the slab. The strength was computed without the use of a strength-reduction factor. Miranda and Bertero (1990) note that experimental results suggest that if the beam gets further and further into its inelastic range of behavior, the reinforcement of the slab starts contributing more and more to the negative flexural strength of the beam. Thus, the amount of reinforcement of the slab that needs to be considered to compute the flexural strength of the beam depends on the level of inelastic deformation suffered by the beam, which is not known beforehand. It was assumed that the effect of the slab on the stiffness and strength of the beams can be considered by accounting for the mechanical characteristics of a section of the slab defined by its thickness and an effective flange width, which according to French and Moehle (1991) is the least of: a) the web width plus 16 times the slab thickness, b) the transverse separation between beams, and c) one fourth the span of the beam. It should be noted that, because of limitations on the modeling capacity of DRAIN 2DX, the beams have equal stiffness for positive and negative moments. These two values will usually be different due to different ratios of positive and negative steel and due to the fact that for positive moment the beams behave like T beams, while for negative moments they behave as rectangular beams. To estimate the stiffness at one end of a beam, an average of the positive and negative "cracked section" effective moment of inertias was used. The stiffness of the entire beam was computed as the average of the stiffness corresponding to both ends.

To model the hysteretic behavior of the beams, an elasto-plastic model was used because this type of behavior was the only option currently provided by DRAIN 2DX. Although a better option to estimate the response of RC structures is a stiffness-degrading model, usually elasto-plastic models lead to practically the same maximum responses (Mahin and Bertero 1981).

The moment-curvature relationships for the beams were computed using the material mechanical characteristics described in Section 2.2 and using the assumptions that plane sections remain plane after flexural deformation and that there exists complete compatibility of strains between steel and concrete. The moment-curvature relationship was approximated by a bilinear curve (elasto-plastic model). The beam yielding moment, M_y, and yield curvature, φ_y, were defined as the moment and curvature at which any bar of the section reaches first yielding. The ultimate bending moment, M_u, was defined as the moment when either: a) the maximum compressive strain is reached in the concrete; b) the ultimate strain is reached in any bar (for instance, fracture of the bar in tension); or c) the buckling stress is reached in any bar. The ultimate curvature, φ_u, was defined as the curvature at which M_u is reached. By connecting the origin to the point defined by (M_y, φ_y) with a straight line and connecting this point to the point defined by (M_u, φ_u) with another straight line, the bilinear moment curvature diagram was defined.

Shear deformations were accounted for in the behavior of the beams. For this purpose, the cracked shear area of the beam was estimated as $A_v/3$, where A_v is the gross area divided by 1.2 (Park et al. 1975). Due to modeling limitations, the shear stiffness remained constant throughout the analysis. The joint regions at the ends of the beams were modeled as infinite rigid links at these locations with a length equal to half the width (parallel to the plane of the frame) of the columns.

• ***Columns***. A lumped plasticity model was used to model the columns. Their moment of inertia was computed using the gross section. This seems a reasonable assumption, considering that the great majority of the columns in this building remain under axial compression even under the effect of lateral loads. Due to modeling limitations, the stiffness in the column remains constant throughout the analysis. Any redistribution of forces in the columns due to possible changes in their axial and flexural stiffness (which vary depending on the value of the axial force induced in the column) has not been modeled.

Shear deformations were accounted for by estimating the cracked shear area of the columns as $A_v/3$. As in the case of beams, shear stiffness remains constant throughout the nonlinear analysis. The joint region of the columns was modeled as an infinitely rigid link at their top end and having a length equal to the total depth of the beam. The strengths of the columns were computed using the program BIAX (Wallace 1992). The strain-hardening modulus of a column depends on the detailing of its longitudinal and transverse steel, and on the axial force acting on it. Because the axial force can change considerably in some columns, their post-elastic stiffness can vary significantly over time. DRAIN 2DX only allows one value of strain-hardening for the analysis, and thus the real inelastic behavior of the column cannot be captured. Given the good confinement provided to the columns of the Pomona building, no significant degradation in the strength of the column is expected even under moderately high axial loads, and thus a strain-hardening of zero was found reasonable.

• ***Story weights.*** The mass at each floor is shown in Table 2.1.

• ***Damping.*** For the nonlinear time-history analysis a Rayleigh damping matrix was used. The amount of damping provided to the model of the building varied from analysis to analysis as a function of the EQGM intensity. The amount of damping corresponding to a given analysis is specified in the section in which such analysis is discussed.

• ***Slab.*** The RC slabs were modeled as rigid diaphragms.

• ***Penthouse.*** Except for its weight, which was added to the weight of the roof diaphragm (sixth floor diaphragm), the penthouse was not considered.

■ **Reliability of the results to be obtained.** The reliability of the results to be obtained from a nonlinear analysis must be analyzed in the light of the assumptions made in the modeling of the real building. As mentioned before, not enough information regarding the anchorage of the longitudinal steel of the RC frame members (beams and columns) of the Pomona building was available for this project. Although the longitudinal and transverse reinforcement of the beams was estimated according to available information, some uncertainty is involved in the process of estimating it. Because of the above, it is difficult to assess the deformation capability of beams and columns, and thus their capability to form plastic hinges and to dissipate plastic hysteretic energy through their nonlinear behavior. This fact directly affects the validity of the results obtained from the nonlinear analysis, given that the nonlinear analysis is based on the assumption that the RC members are capable of hinging at their ends. Thus, the existing uncertainties in the determination of the mechanical characteristics of the RC members not only affect the assessment of their strength and deformability supplies, but also affects the determination of their demand counterparts. Nevertheless, it is important to keep in perspective the objective of the nonlinear analyses dealt with in this chapter: to assess the need to upgrade the Pomona building. Within this context it should be mentioned that if the analyses of the nonlinear analyses of the Pomona building yield significant ductility demands, as is expected in the existing RC members when subjected to the design EQGM, there is no question that the building has to be retrofitted, especially because the RC members form part of a non-ductile frame.

2.4 TWO-DIMENSIONAL NONLINEAR ANALYSIS

One important issue in the assessment and calibration of modeling techniques for the DRAIN 2DX model is to compare the results obtained in a 2D nonlinear analysis with the measured response of the building. Unfortunately, the measured response of the building has important 3D effects, and thus a direct comparison is not possible. To allow for a preliminary calibration of the modeling techniques used in the DRAIN 2DX model, the results obtained using this program were compared with those obtained from the elastic analysis (using SAP90) of the Kariotis et al. model. As discussed in Section 2.3.1, the Kariotis et al. model was calibrated so that its response to two EQGMs was close to the measured response of the building during those EQGMs. Nevertheless, as mentioned in Section 2.3.1, the Kariotis et al. elastic model accounts for 3D effects. To make a 2D comparison possible, the Kariotis et al. model was modified by fixing the rotational degree of freedom in each floor diaphragm, thus eliminating the 3D effects in the behavior of the building (and thus creating a Kariotis et al. 2D elastic model). Because the 3D elastic model gives a good estimate of the measured response, it is considered that the results obtained in the Kariotis et al. 2D elastic model can provide a reasonable frame of reference against which the modeling techniques for the DRAIN 2DX model can be calibrated. Planar nonlinear analyses were only carried out in the E-W direction (the building has smaller lateral strength and stiffness in this direction as compared to the N-S direction).

2.4.1 TWO-DIMENSIONAL PUSHOVER ANALYSIS

First, a pushover analysis considering P-Δ effects was carried out to determine the lateral displacement vs. lateral load characteristics of the building (neglecting torsion), as well as to establish the distribution of nonlinear demands (plastic hinging) throughout the building. The distribution of lateral loads over height for the pushover analysis was obtained by assuming a triangular distribution of accelerations over height.

Figure 2.12 shows the roof displacement (δ_{roof}) vs. base shear (V_b) curve obtained from the pushover analysis of the E-W direction. As shown, the building shows significant nonlinear behavior, even for very small displacements. To study separately the influences that the RC frame and the URM infills have on the global behavior of the building, the δ_{roof} vs. V_b curve for the same building without infills is included. As shown in Figure 2.12, if no torsional irregularities are considered in the analysis, the URM infills enhance considerably the behavior of the RC frame alone (considerable increases in stiffness and strength of the building).

The maximum base shear (V_{bmax}) for the E-W direction of the building with URM infills is around 1150 kip, which corresponds to 0.18 W, and would be reached at a $\delta_{roof} \approx 5"$ provided the brittle failure of its RC members can be avoided. It needs to be noted that the building can develop this base shear only if no torsion is present in its lateral response. For δ_{roof} of 5", the global ductility ratio demand (μ_g) in the RC frame without infills is around 2.5 (as can be seen in the idealized bilinear behavior of the RC frame in Figure 2.12). Considering that the building was designed for gravitational loads in the year 1923, it is likely that it will not be able to develop such μ_g. Thus, for δ_{roof} of 5", the RC members will probably exceed their deformation capabilities, or in other words, the building is not likely to reach its maximum strength given that it can not accommodate the deformability demands required to achieve it. Note that for δ_{roof} larger than 5", the RC frame *without* URM infills develops a mechanism that exhibits negative stiffness.

Figures 2.13 and 2.14 show the distribution of floor displacement and IDI over height for different values of δ_{roof}. As shown in both figures, as δ_{roof} increases, lateral deformation concentrates in the bottom two stories (corresponding to the ground and mezzanine stories).

When δ_{roof} reaches a value of 5 in, the maximum value of IDI (which corresponds to the second story) reaches a value of 0.01. Again, it is difficult to assess whether the RC members of the building will be able to reach this IDI value given the lack of information concerning their detailing.

Figures 2.15 to 2.20 show how nonlinear behavior progresses throughout the members of the building in the E-W direction as δ_{roof} increases. The lateral loads in the pushover analysis go from left to right in these figures. Each figure shows the six frames that constitute the lateral-resisting structural system in the E-W direction. The vertical lines represent the columns of the structure, the continuous horizontal lines the beams, the discontinuous horizontal lines a rigid diaphragm (slab), and the diagonal lines the truss elements representing the URM infills. As shown, the basement has been modeled for frames B, C, D and E. The basements of Frames A and F were not modeled given that these frames are supported by the RC perimetral wall surrounding the basement (see Figure 2.4), and thus they can be considered to be supported on a rigid base. Similar considerations were given to the central columns of Frame C because they are also supported by a RC wall. A small circle in the middle of a diagonal represents that that URM infill exhibits nonlinear behavior (i.e., has gone beyond cracking), while a small circle at either end of a beam or a column represents the formation of a plastic hinge. As shown, when δ_{roof} = 1", practically all walls in the structure have already cracked. When δ_{roof} = 2", extensive hinging of RC members is observed. It is noticeable that several of these hinges developed in columns and not in beams, especially in the perimetral frames (A and F), which have deep spandrel beams (see Table 2.2). Note that frame A is close to developing a mechanism that involves its first two stories (ground and mezzanine). As δ_{roof} increases, the hinging of RC members continues, especially those located in the perimetral frames and those located in the two lower stories. When δ_{roof} reaches values of 5" and 6", a mechanism involving the two lower stories has practically formed on all frames. It is interesting to note that in the perimetral frames (A and F) there is extensive hinging on columns located in several stories, while in the interior frames hinging of columns usually occurs only at the base of those columns located in the ground story.

2.4.2 TWO-DIMENSIONAL NONLINEAR TIME-HISTORY ANALYSIS

Planar nonlinear time history analyses were performed for the following EQGMs.

- An EQGM that would allow an assessment of the reliability of the nonlinear modeling techniques used to create the DRAIN 2DX model. For this purpose the Landers E-W EQGM was used and a $\xi = 0.02$ was used for the first two translational modes.
- An EQGM that is supposed to represent the safety level EQGM. For this purpose, the E-W component of the Landers EQGM was scaled to a peak ground acceleration (PGA) of 0.3g (i.e., scaled up by a factor of six) and a $\xi = 0.05$ was used for the first two translational modes. It should be mentioned that in general it is not enough to scale the PGA of an EQGM to define the safety level EQGM. Figure 2.21 shows a comparison between the strength demands corresponding to the design EQGM corresponding to the safety level (determined in Appendix A) and those corresponding to the scaled Landers E-W EQGM. As can be concluded from Figure 2.21, the scaled Landers E-W EQGM provides a close representation to the design EQGM for T equal or larger than 0.5 sec.

As mentioned before, the results obtained from the DRAIN 2DX model of the E-W direction will be compared to those obtained from a 2D version of the Kariotis et al. elastic model. Table 2.5 shows the dynamic properties of the Kariotis et al. 2D elastic model of the building. As shown, a value of 0.99 sec is associated with the fundamental translational period in the E-W direction, and this value is very similar to the value corresponding to the 3D elastic model (1.04 sec). In the N-S direction these values are 0.52 and 0.51 sec, respectively. It can be concluded that eliminating the rotational degrees of freedom in the 3D elastic model of the building does not affect considerably the values of the fundamental translational periods.

Figure 2.22 shows a comparison between the displacements at the center of mass of each floor diaphragm of the Kariotis et al. elastic models when considering and neglecting torsion (3D and 2D response, respectively) and subjected simultaneously to the Landers N-S and E-W EQGMs. As shown, when torsional response is neglected, the E-W displacements at the centers of mass decrease significantly (about 25% in the displacement at the roof). The results shown in Figure 2.22b will be compared with those obtained from the DRAIN 2DX model subjected to Landers

E-W EQGM. Figures 2.23 and 2.24 establish this comparison. As shown, the displaced shape for the elastic and nonlinear time history analyses are very similar; nevertheless, the displacements predicted by the nonlinear analysis are about 25% to 30% smaller than those predicted by the linear analysis. Figure 2.25, which qualitatively establishes a comparison between the cyclic behavior of the elastic and nonlinear models of the building, helps explain these results. As shown, the nonlinear model has considerably larger stiffness at small deformations, and thus if the EQGM excitation is not intense, the nonlinear model will predict smaller displacements; also, the nonlinear model tends to dissipate energy through its cyclic nonlinear behavior, which can be interpreted in an elastic model context as an increase in the value of its viscous damping coefficient.

The results obtained from the nonlinear analysis would be improved if degradation of stiffness and strength in the URM infills could be accounted for; nevertheless, the above results suggest that a very simple nonlinear model can be used to predict reasonably well the 2D response of the Pomona building.

Figures 2.26 and 2.27 summarize the results obtained from the DRAIN 2DX model subjected to the safety level EQGM (Landers scaled up by a factor of 6). These figures show in discontinuous lines the results obtained from the pushover analysis of the same building and the results obtained from elastic time-history analysis using the Kariotis et al. 2D elastic model (SAP90). The positive and negative envelopes of displacement and IDI obtained from the nonlinear time-history analysis are shown in these figures with continuous lines. Note that both the positive and the negative envelopes are plotted on the positive side of the displacement and IDI axis. This was done to facilitate a comparison between the results obtained in the pushover analysis and those obtained in the nonlinear time-history analysis and elastic time-history analysis. As shown in Figure 2.26, the shapes for the displacement envelopes obtained from the nonlinear time-history analysis are very similar to those obtained from the pushover analysis. The maximum δ_{roof} values obtained from DRAIN 2DX are 10" and 6" in the negative and positive direction, respectively. The maximum δ_{roof} displacement obtained from the elastic time-history analysis is about 75% of that obtained from DRAIN 2DX, which suggests that the elastic time-history analysis gives reasonable estimates of the displacement demands. Figure A.11b (Appendix A) shows the displacement spectra for the Landers E-W EQGM. As shown, for a $T \approx 1.0$ sec (fundamental period of the building in the E-W direction), the nonlinear displacement demands are larger than the elastic one. A simple observation like this can help decide on the adequacy of an elastic analysis to predict the global displacement demands of the building when subjected to the safety level EQGM.

As shown in Figure 2.27, the shapes for the IDI envelopes obtained from the nonlinear time-history analysis are similar in the lower stories to those obtained from the pushover analysis at a similar δ_{roof}; nevertheless, the IDI demands in the upper stories are underestimated in the pushover analysis (because it neglects upper-mode effects). As shown, the maximum IDI obtained from the nonlinear time-history analysis is about .02, which is very large if compared to the IDI limit ranging from 0.01 to 0.02 usually considered acceptable for buildings designed according to current earthquake-resistant design provisions (Qi and Moehle 1991, Bertero et al. 1991). As shown, the maximum IDI demands obtained from the elastic time-history analysis are about 67% those obtained using DRAIN 2DX. The IDI predicted by the elastic analysis for the upper stories is larger than that predicted from DRAIN 2DX in spite of the fact that the δ_{roof} predicted from the nonlinear analysis is larger than that predicted by the elastic analysis. The previous inconsistency is likely to be a product of the existence of a flexible and weak (soft) first story in the Pomona building: while the nonlinear model is able to consider further degradation of the mechanical properties of the soft story as its nonlinear demands increase (and viceversa), the elastic model, which was created to recreate the response of the building to less intense EQGMs, needs to be adjusted using an iterative procedure to account for the strong relation that exists between the degradation of the mechanical properties of the soft story and an increase in its seismic demands. In the elastic analysis, such calibration was not done, and thus, the elastic analysis is likely to underestimate the response in the lower (soft) story and, as a consequence, overestimate that of the upper stories.

In spite of the differences in the results obtained in the elastic and nonlinear time-history analysis of the E-W direction of the Pomona building, both type of analyses strongly suggest an inadequate seismic performance, and thus the need to upgrade the building. In this context, it should be stated that the torsional response of the building, which in view of the results presented in Figure 2.22 is expected to be large, has been neglected. Such effects will be assessed in the next sections.

2.5 THREE-DIMENSIONAL NONLINEAR ANALYSIS

Several nonlinear 3D analyses of a simplified model of the building were carried out to assess its behavior and performance when its torsional response is accounted for. For this purpose, the recently released DRAIN 3DX program (Powell et al. 1994) was used. To allow for the calibration of the DRAIN 3DX model, the results obtained using this program were compared with those obtained previously from the DRAIN 2DX model.

The considerations involved in creating a nonlinear 3D model of the Pomona building are similar to those discussed in Section 2.3.2. Nevertheless, there are some differences between the models created for DRAIN 3DX and DRAIN 2DX. In the next paragraphs, the main differences are discussed.

■ **URM Infills.** The URM infills were modeled using fiber elements, such as that shown in Figure 2.28a. As shown in Figure 2.28b and 2.28c, the curvature (or moment) in each segment is assumed to be constant. Each URM infill within a bay was modeled using two diagonal struts forming an X. The geometric and mechanical characteristics of each pair of struts in the X were assigned to them in such a way that their lateral force vs. displacement curve was equal to the piecewise linear representation of one of the curves shown in Figure 2.8. The fibers in a strut were defined so that it has a small moment of inertia so that in turn it may work axially (as a truss element). The fiber element in DRAIN 3DX allows for stiffness and strength degradation according to simple rules. The uncertainty about how degradation occurs during the nonlinear cyclic behavior of real URM infills (with and without openings) is large, and thus it is difficult to quantify or model such degradation. For the current model, the strength and stiffness degradation was neglected. It should be noted that this issue is less relevant for the analysis of the upgraded version of the building, given that its maximum IDI is limited in such a way as to insure stable hysteretic behavior in the URM infills.

■ **Beams.** The beams were modeled using fiber elements. A tributary width of slab equal to that specified in Section 2.3.2 was modeled (also using fibers) as part of a beam. It should be mentioned that the fiber element is able to model the different geometric properties of a given transverse section of a beam for positive and negative flexural moment (for negative moment the beam behaves as a rectangular section, while for positive, as a T section), as well as any possible variation of these properties throughout the length of the beam. Given that DRAIN D3X does not allow for element gravitational loads, these loads were idealized using nodal loads, as shown in Figure 2.29b. Figure 2.29c shows a comparison between the moment diagrams in a beam with fixed ends obtained by idealizing the gravity loads as distributed loads, Figure 2.29a, and as concentrated loads, Figure 2.29b. The moments at the end of the beam for both idealizations are the same; nevertheless, the moment diagram in the internal part of the beam can change considerably. Thus, if the beams are expected to yield at their ends, the model shown in Figure 2.29b would yield similar results to that shown in Figure 2.29a. If the beam is expected to hinge at an intermediate location, the results obtained from both models can be quite different. For a framed building subjected to lateral loads and relatively small gravity loads (dead and live loads), hinges are usually concentrated at the ends of the beams, and thus the model illustrated in Figure 2.29b for gravity load is believed to yield reasonable results.

The existence of intermediate nodes in a beam implied that each beam had to be idealized using three fiber elements, as shown in Figure 2.29b. In turn, each one of these three fiber elements was modeled using three segments. Given that DRAIN D3X assumes constant curvature in each one of these segments, and that the curvature diagram in the fiber model of the beam follow a linear pattern (there are only nodal loads, i.e. concentrated loads), the plastic hinges in the fiber model will tend to concentrate in the segments that have been shadowed in Figure 2.29b. The constant curvature assumption and the fact that the plastic hinges can only occur at certain locations of the fiber model of the beam will usually be reflected in an overestimation of the beam's flexural strength when subjected to lateral load:

• ***Constant curvature assumption.*** Figures 2.28b and 2.28c shows examples of the effect that assuming constant curvature in the different segments of a frame member can have on the prediction of the maximum moment demand. Take the case illustrated in Figure 2.28b, in which the maximum moments occur at the ends (M_1 and M_2). Given the constant curvature (i.e. constant moment) assumption, the moments at the segments located at the ends, M_{1cc} and M_{2cc}, are smaller than M_1 and M_2. From this example and that illustrated in Figure 2.28c, it can be concluded that the use of constant curvature segments to model a frame member will underestimate the maximum moment demand in the same. The underestimation of the moment demand has the same effects and thus can be interpreted as an overestimation the flexural capacity of the member.

• ***Fixed location of plastic hinges.*** This issue can be dealt with in a straightforward manner using the theory of plastic analysis of framed buildings. Although a detailed discussion goes beyond the scope of this study, it can be said that of all possible and meaningful collapse mechanisms for a frame loaded with lateral load and a known (and fixed) value of gravity load, the true collapse mechanism is that that yields the smallest lateral load (assuming the pattern of lateral loads is also fixed). For the true collapse mechanism, there will be an associated and specific pattern of location of plastic hinges. Any other mechanism having a different pattern of plastic hinges will yield a higher collapse load, and thus will tend to overestimate the lateral strength of the frame. In the fiber model shown in Figure 2.29b, the location of plastic hinges is fixed. In the case of the columns, this location is acceptable (shaded areas), as opposed to that of the beams, which is not necessarily that of the true collapse mechanism. It can be concluded that such model will tend to overestimate the lateral strength of the frame because it enhances the flexural strength of the beam.

Although a better option to estimate the response of RC structures is a stiffness-degrading model, usually elasto-plastic models lead to practically the same maximum responses (Mahin and Bertero, 1981). With this in mind and considering that the main response quantity used to measure the performance of the building is its maximum IDI (which is a function of the global displacement of the building), no degradation of stiffness was considered in the beams.

When using a fiber element model, there is no need to estimate the moment-curvature relationships for a flexural member, given that this information is computed from the fibers' mechanical properties (strain vs. stress curves), their location within the cross section and assuming that a plane section remains plane after the element has deformed in flexure. Depending on the stress vs. strain curves supplied for the concrete fibers, DRAIN 3DX can account for events such as cracking and crushing of the concrete of an RC flexural member.

The shear stiffness and the joint region were modeled according to the same assumptions described in Section 2.3.2.

■ **Columns.** The columns were also modeled using fiber elements. Each column was modeled using one element divided in three segments, as shown in Figure 2.29b. Note that small segments were defined at the ends of the columns to avoid overestimating their flexural strength (recall that the curvature is assumed to be constant in each segment). It is worth mentioning that the fiber element can estimate phenomena such as changes in the flexural stiffness and the strain hardening modulus of a column as a function of the axial load acting on it, thereby allowing the possible redistribution of forces in the columns due to possible changes in their flexural stiffness (produced by a change in their axial force) to be modelled. The shear area and the joint region of the columns were modeled using considerations similar to those described in Section 2.3.2. Figure 2.30 shows the potential of DRAIN 3DX's fiber element to model the behavior of RC columns subjected to different axial loads (P) by comparing the moment vs. curvature curves computed for one of the columns of the Pomona building using DRAIN 3DX and the program RCCOLA (Mahin and Bertero 1977). As shown, both programs give similar results, in spite of the fact that the number of fibers used in DRAIN 3DX was considerably less than that used in RCCOLA.

■ **Damping.** For the nonlinear time-history analysis a Rayleigh damping matrix was used. The amount of damping provided to the model of the building varied from analysis to analysis as a function of the EQGM intensity. The amount of damping corresponding to a given analysis is specified in the section in which such analysis is discussed.

■ **Slab.** Preliminary studies carried out using fiber elements to model RC beams suggest that the ultimate strength of the beams of a RC frame can be considerably overpredicted when the slab of the frame is modeled as a rigid diaphragm. To analyze a framed structure using an analytical model (computer model), it is necessary to define an axis for each beam. The geometric properties of each beam are then computed with respect to this axis. Figure 2.31a shows that when a beam of a frame is deformed in double curvature due to the effects of lateral load in the building, its axis will usually elongate. If the slab is modeled as a rigid diaphragm, the beam will not be allowed to deform axially, which means that a state of compression is induced in the beam. This compression is likely to enhance considerably the flexural strength of the beam, as shown in Figure 2.31b. Although the slab of a real building is likely to provide some axial restraint to the beams of a frame, our limited understanding of this effect does not allow its quantification. For the DRAIN 3DX model of the building, the slab was not modeled as a rigid diaphragm, but as mentioned before, a tributary width of slab was modeled as being part of each beam.

■ **Story weights.** The mass at each floor is shown in Table 2.1. Given that the slab was not modeled as a rigid diaphragm, the story mass was distributed among all nodes located in the corresponding floor diaphragm.

■ **Penthouse.** Except for its weight, which was added to the weight of the roof diaphragm (sixth floor diaphragm), the penthouse was not considered.

Although the DRAIN 3DX model is a very sophisticated model, this does not necessarily guarantee a substantial improvement (if any) in the estimation of the seismic response of the real Pomona building. As with any other model, the structural engineer should interpret carefully the results obtained using this program.

2.5.1 THREE-DIMENSIONAL PUSHOVER ANALYSIS

Several pushover analyses considering P-Δ effects were carried out to determine the lateral displacement vs. lateral load behavior of the building, as well as to establish the distribution of global displacement demands throughout the building. The distribution of lateral loads over height for the pushover analysis was obtained by assuming a triangular distribution of accelerations over height.

First, a pushover analysis in the E-W direction of the DRAIN 3DX model of the pomona building was carried out neglecting the effects of torsion. This was done to establish a direct comparison between the results obtained using the DRAIN 2DX and DRAIN 3DX models. Both models yielded practically the same value of ultimate base shear at a δ_{roof} of 6 in (V_b = 0.18 W and 0.19 W, respectively). Figures 2.32 and 2.33 compare the displacement and IDI distribution over height obtained from the DRAIN 2DX and DRAIN 3DX (without torsion) models. Note that given that the slab of the DRAIN 3DX model has not been idealized as a rigid diaphragm, the displacement at the top of two columns located in a given story are not necessarily the same, even if that floor is not allowed to rotate. The displacement and IDI distributions shown in Figure 2.32 and 2.33 for DRAIN 3DX correspond to the column line that is closest to the geometric centroid of the floor diaphragms. It can be concluded by analyzing Figures 2.32 and 2.33 that in spite of the different models used (DRAIN 2DX and DRAIN 3DX), both predict a similar global behavior, i.e., lateral deformation tends to concentrate in the bottom stories as δ_{roof} increases. Note in Figure 2.33 that the IDI demands predicted in the ground and mezzanine stories by DRAIN 3DX are slightly smaller than those predicted using DRAIN 2DX, while the opposite occurs in stories 2, 3 and 4.

Next, two more pushover analyses were carried out using the DRAIN 3DX model, but now allowing the floor diaphragms to rotate. Figures 2.34 to 2.38 summarize the results obtained from a 3D pushover analysis in which the lateral loads have been applied in the E-W direction only, while Figure 2.34 and Figures 2.39 to 2.43 summarize those of a similar analysis in which the loads were applied in the N-S direction. Figure 2.34 compares the δ_{roof} vs. V_b curves obtained from pushover analyses in the E-W direction of the original building using the DRAIN 2DX and DRAIN 3DX (with torsion) models. The curve that has been plotted for the DRAIN 3DX model corresponds to the node that is closest to the geometric centroid of the roof diaphragm. As shown, due to torsional effects, the initial lateral stiffness of the building is slightly reduced, although the building could reach practically the same ultimate V_b if it had enough deformation capability to undergo a δ_{roof} of 6 in. Figure 2.35 shows four δ_{roof} vs. V_b curves, one for each one of the four corners of the DRAIN 3DX model that accounts for torsion. It is clear from these curves that there is a significant torsional response in the E-W direction. Figures 2.36 and 2.37 show a comparison between the displacement and IDI distributions over height corresponding to the four corners of the DRAIN 3DX model (curves with continuous line) and those obtained using the DRAIN 2DX model (curves with discontinuous line). As shown in Figure 2.36, all four corner displacement distributions are similar to that corresponding to the DRAIN 2DX model. As expected due to torsional effects, the displacements of the corners located in Frame A (southeast and southwest corners) have larger displacements than those of DRAIN 2DX, while those of the corners located in Frame F (northeast and northwest corners) are smaller.

Figure 2.37 shows that the IDI distribution over height for the corners located in Frame A is similar to that corresponding to the DRAIN 2DX model, although DRAIN 3DX predicts a slightly larger IDI in the ground story and a smaller one around the second story. The IDI for the corners located in Frame F is considerably smaller than that of the DRAIN 2DX model in the ground and mezzanine stories, while it is larger for stories 2 and 3. To help explain such differences, Figure 2.38 has been included. This figure shows how the six floor diaphragms of the DRAIN 3DX model move relative to each other and to the ground as δ_{roof} increases in the E-W direction. For a given δ_{roof}, the discontinuous rectangle represents the position of the ground floor while the other six continuous rectangles represent the floor diaphragms of the building. The diaphragms' displacements illustrated in Figure 2.38 have been scaled up by a factor of 50 so that the relative movements between the floors can be perceptible. As mentioned before, as δ_{roof} increases, the deformation tends to accumulate in the lower two stories, specifically in Frame A. Note that the two bottom diaphragms are rotating clockwise around Frame F, which explains why the IDI predicted for the two bottom stories of Frame A using DRAIN 3DX are larger than those estimated using DRAIN 2DX, while those of Frame F are smaller. There is practically no interstory rotation in the upper four stories of the building, i.e., there is not a significant increase in the rotation of the roof relative to that of the second floor. This means that the portion of the building formed by the upper four stories is rotating practically as a rigid body with respect to the two lower stories. Studying Figure 2.38 closely, it is possible to note that the third and fourth floor diaphragms are actually rotating counterclockwise with respect to the second floor diaphragm. This small rotation helps to explain why the IDI in the second story of Frame A predicted by DRAIN 3DX is smaller than its DRAIN 2DX counterpart, while the opposite occurs with the IDI in the second and third stories of Frame F.

Figure 2.34 shows the δ_{roof} vs. V_b curve obtained from the 3D pushover analysis of the DRAIN 3DX model (with torsion) in the N-S direction. As shown, the lateral strength and stiffness of the Pomona building in this direction are considerably higher than those in the E-W direction. If the building does not develop a brittle failure, it may reach a V_b around 0.42W in the N-S direction. Figure 2.39 shows V_b vs. δ_{roof} curves for the four corners of the DRAIN 3DX model obtained from the 3D pushover analysis in the N-S direction. As shown, the torsional response of the building when loaded in the N-S direction is larger than its torsional response when it is loaded in the E-W direction. Figures 2.40 and 2.41 suggest that as δ_{roof} increases, the deformation in the N-S direction tends to accumulate in the two lower stories of the building, specifically in Frame 6 (southeast and northeast corners). It is interesting to note in Figures 2.40 and 2.41 that the southwest corner displaces very little at the mezzanine, second and third floor diaphragms, while there is sudden and large increase of the displacements of this corner in the upper floors. To help explain this, Figure 2.42 has been included. As shown, the small displacements of the bottom floors of the southwest corner occur because the building is practically rotating around the bottom stories of this corner when loaded in the N-S direction. Note that this is not so in the upper stories. Again, there is practically no interstory rotation in the upper four stories of the building, i.e., there is not a significant increase in the rotation of the roof relative to that of the second floor. The portion of the building formed by the upper four stories is rotating practically as a rigid body with respect to the two lower stories. The above behavior can be explained with the aid of Table 2.1 and Figures 2.2a, 2.2b and 2.3. As shown in Table 2.1, the location of the center of rigidity on every single floor is shifted towards the west end of the building, and this shift is specially large in the two bottom floors (mezz and second). Figures 2.2a and 2.2b show that these large shifts are produced because the west frame, Frame 1, is completely infilled with solid URM walls; while the east frame, Frame 6, have practically no infills in its two lower practically no infills in its two lower stories and infills with large openings in its upper stories. The presence of the mezzanine, shown in Figure 2.3, also helps explains the large shift in the center of rigidity in the E-W direction of the two lower floors, given that it creates a double height story in the lower part of Frame 6. Also, as shown in Table 2.1, the centers of mass of every single floor are shifted to the east of their respective center of rigidity, in such a way that the building develops large counterclockwise torsional moments when it starts deforming towards the north. The fact that the building has flexible and weak (soft) bottom two stories and a large eccentricity in the location of the center of rigidity in these same stories, together with the fact that large torsional moments develop when the building displaces in the N-S direction, it is no surprise that the building practically rotates in the bottom stories around Frame 1 (west frame) when loaded in the N-S direction (while simultaneously accumulating large deformation demands in the bottom stories of Frame 6). It should be noted that the N-S displacement in the bottom two floors of the northwest corner are clearly larger than those of the southwest corner. This difference can be explained because, as mentioned before, the 3D nonlinear model of the building did not considered the existence of a rigid diaphragm. As mentioned before, when the beams of the building are loaded, they tend to expand, and this expansion will create a difference in the displacement corresponding to both ends of a given frame.

The global displacement demands estimated from the DRAIN 3DX pushover analysis are consistent with those obtained using DRAIN 2DX and with the existing stiffness and strength irregularities in plan and height.

2.5.2 Three-dimensional nonlinear time-history analysis

Results of the 3D nonlinear time-history analysis of the DRAIN 3DX model are not available because of the extremely large time that this program needed to finish them. Although it was not possible to obtain the very valuable information provided by this type of analysis, the need to upgrade the Pomona building is clearly demonstrated by the results obtained from previous analyses. A new series of analysis will be carried out in the future with the help of a new program for the nonlinear 3D analysis of RC structures (Filippou, 1995).

Floor	Elevation (ft)	Mass (kip-sec^2/in)	Location of center of mass[1] (ft)		Location of center of rigidity [1] (ft)	
			N-S direction	E-W direction	N-S direction	E-W direction
mezz	13.0	1.51	74	45	88	55
second	25.5	3.24	58	32	86	55
third	36.0	2.84	57	30	56	48
fourth	46.5	2.84	57	30	55	39
fifth	57.0	2.84	57	30	53	42
sixth	71.0	3.55	49	38	53	46

(1) with respect to the southeast corner of the building

Table 2.1 Floor characteristics of the Pomona Building

Floor	Perimetral Frames		Internal Frames	
	Largest	Smallest	Largest	Smallest
mezz	8 x 53	8 x 42[2]	15.5 x 45	11.5 x 20
second	12 x 84	8 x 42	12.5 x 42	11.5 x 20
third	8 x 42	8 x 42	12.5 x 42	11.5 x 20
fourth	8 x 42	8 x 42	12.5 x 42	11.5 x 20
fifth	8 x 42	8 x 42	12.5 x 42	11.5 x 20
sixth	8 x 46.5[1]	8 x 46.25	12.5 x 42	11.5 x 24

(1) neglecting two beams of size 8 x 82.5
(2) neglecting one beam of size 8 x 20

Table 2.2 Summary of sizes of beams over height (inches)

Story	Largest	Smallest
ground	32	21(1)
mezz	26	19(2)
2	25	17
3	25	15
4	23	13
5	20	8

(1) neglecting one column of size 16
(2) neglecting one column of size 12

Table 2.3 Summary of sizes of columns over height (inches)

Mode	Period (sec)	mass participating in the mode (%)	
		N-S direction	E-W direction
1	1.04	1.01	87.64
2	0.70	19.21	5.55
3	0.51	69.30	0.06

Table 2.4 Dynamic characteristics of Pomona Building from 3D elastic model

Mode	Period (sec)	mass participating in the mode (%)	
		N-S direction	E-W direction
1	0.99	0.00	92.84
2	0.52	88.51	0.00

Table 2.5 Dynamic characteristics of Pomona Building from 3D elastic model restrained against rotation

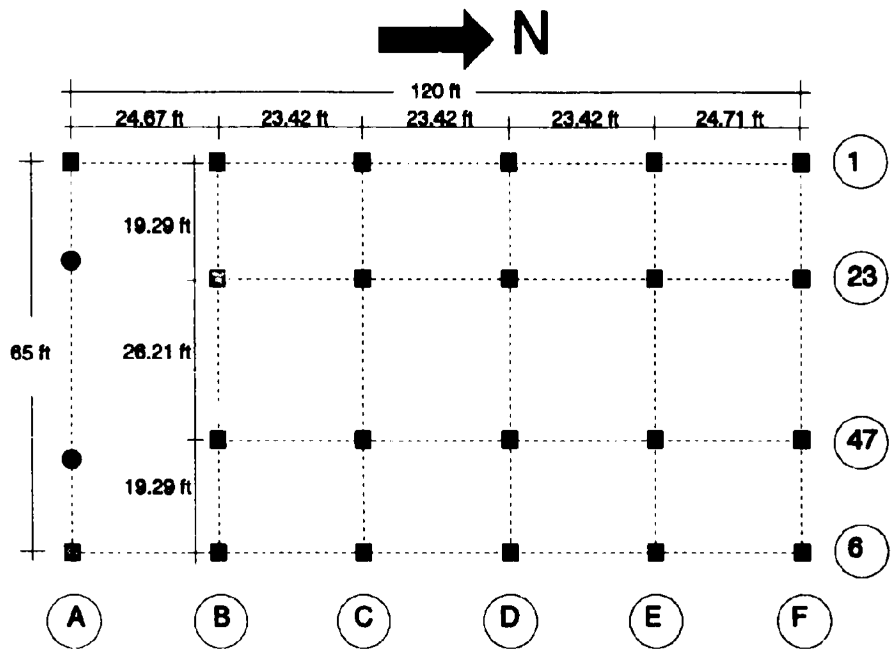

a) Mezzanine and second floor

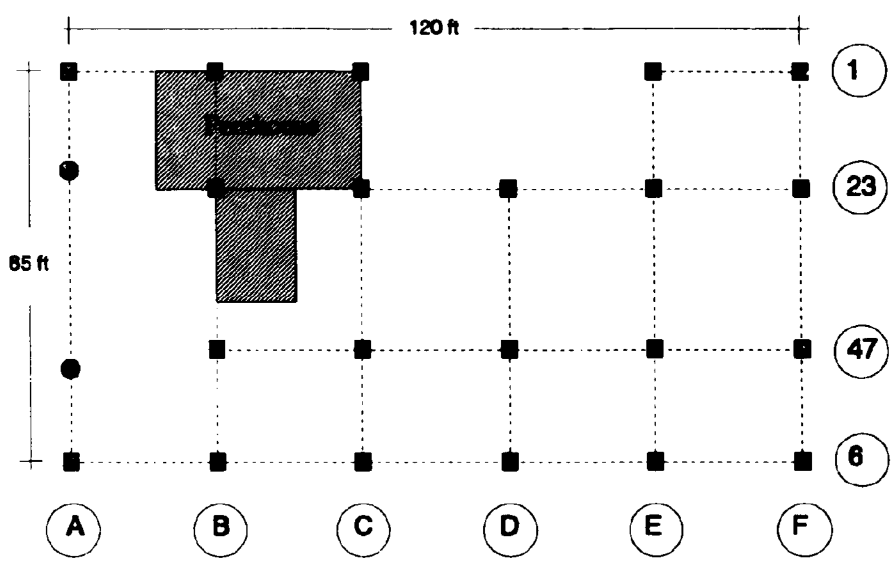

b) third floor through roof

Figure 2.1 Plan view of Pomona Building

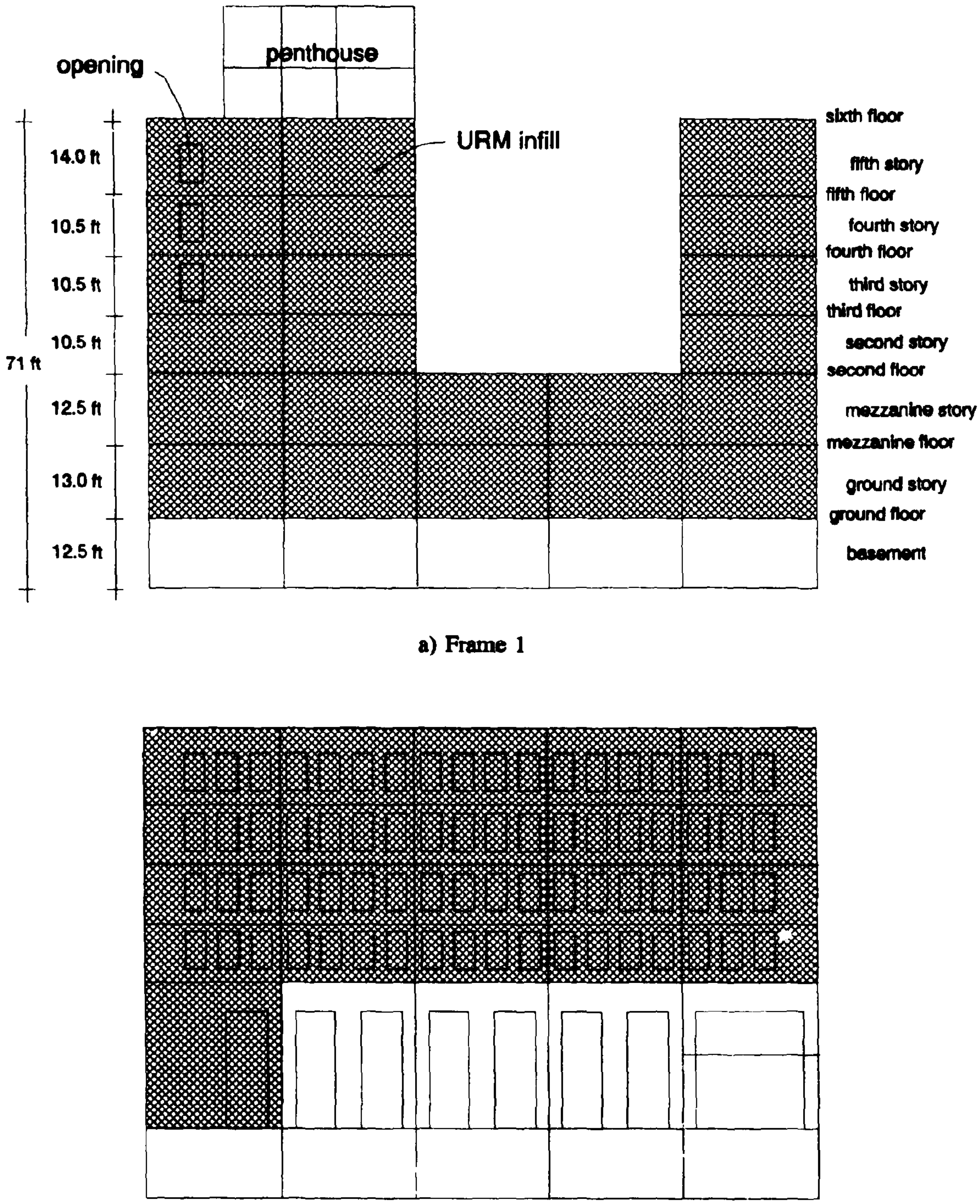

a) Frame 1

b) Frame 6

Figure 2.2 Elevation view of perimetral frames

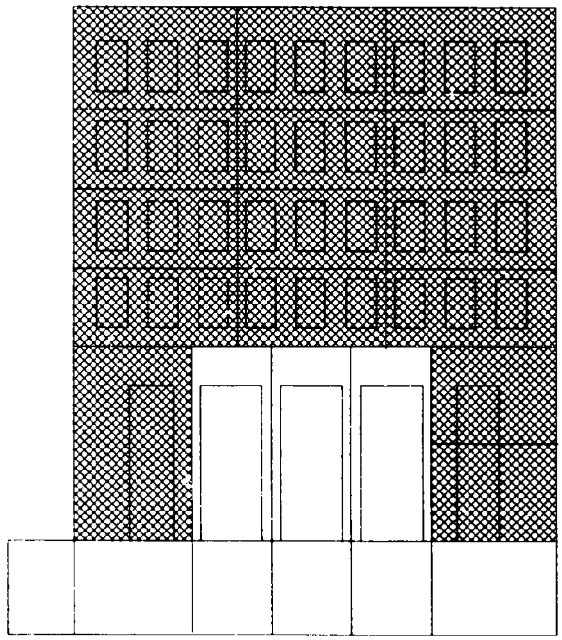

c) Frame A

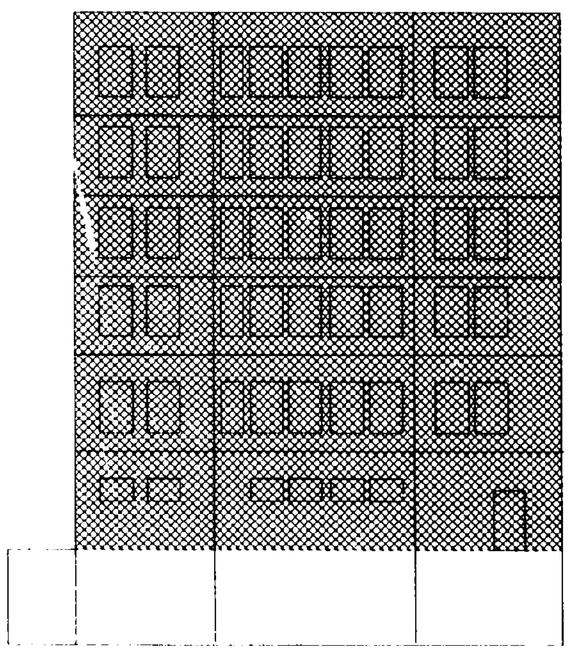

d) Frame F

Figure 2.2 continued

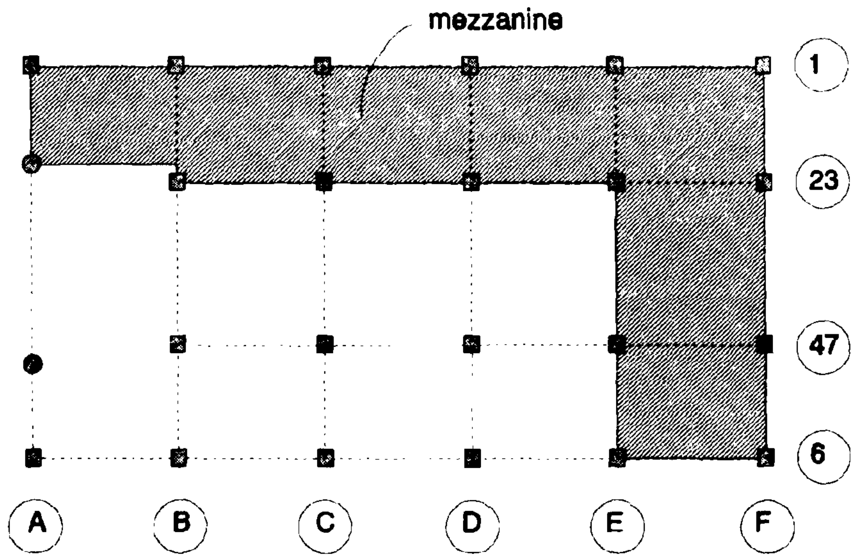

Figure 2.3 Plan view of mezzanine

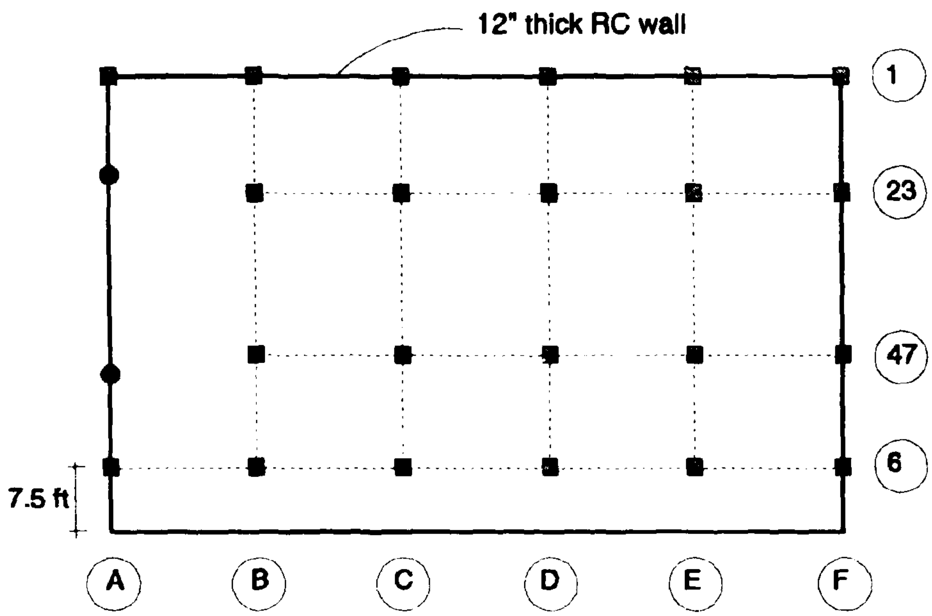

Figure 2.4 Plan view of basement perimetral wall

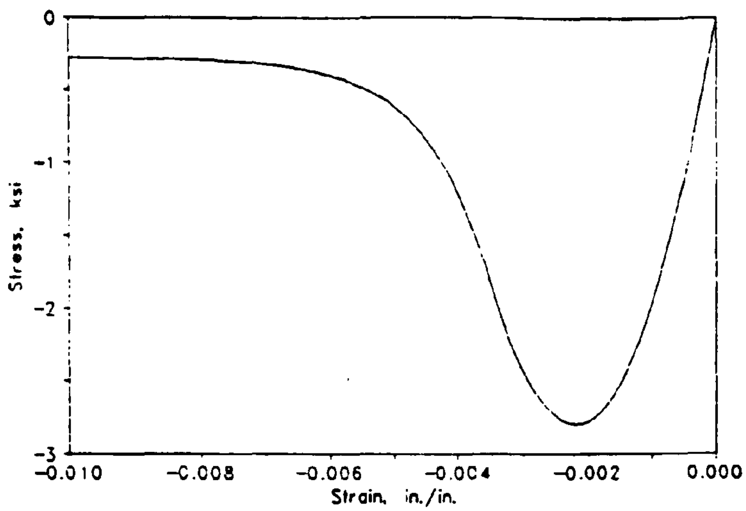

Figure 2.5 Compression model for masonry

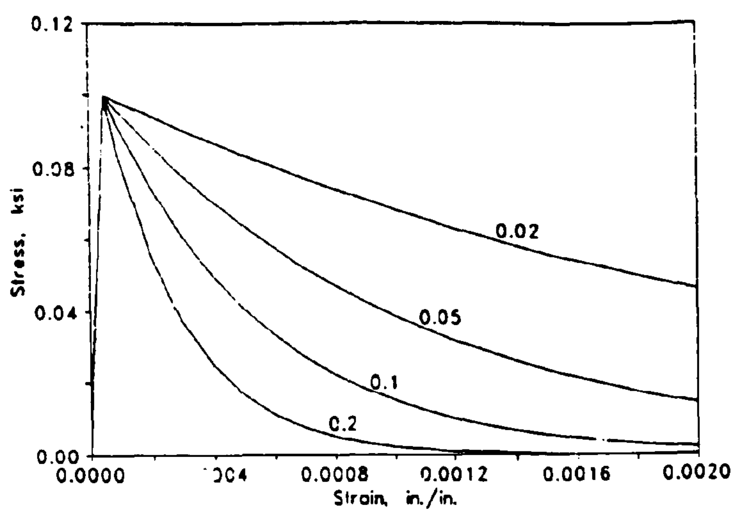

Figure 2.6 Tension model for masonry

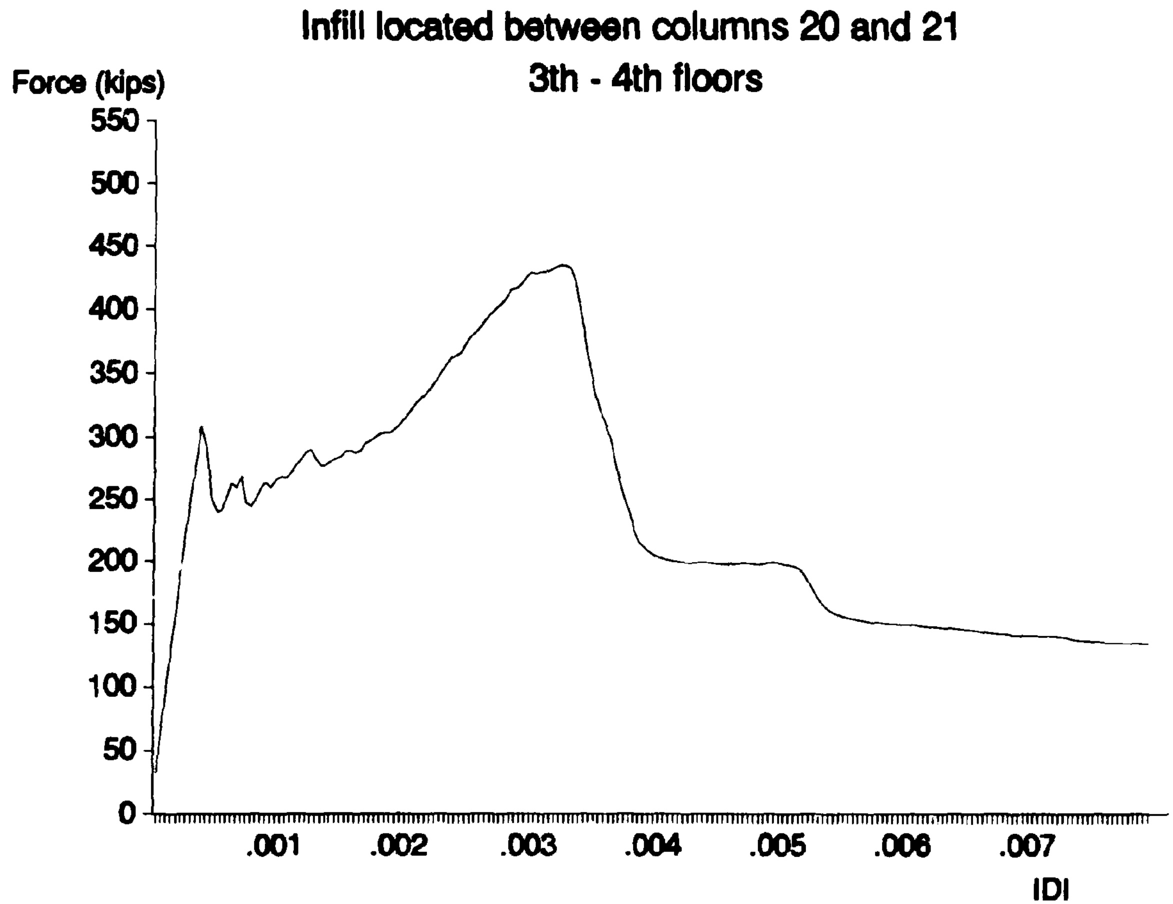

Figure 2.7 Lateral load vs. lateral displacement curve for URM infill in Pomona Building

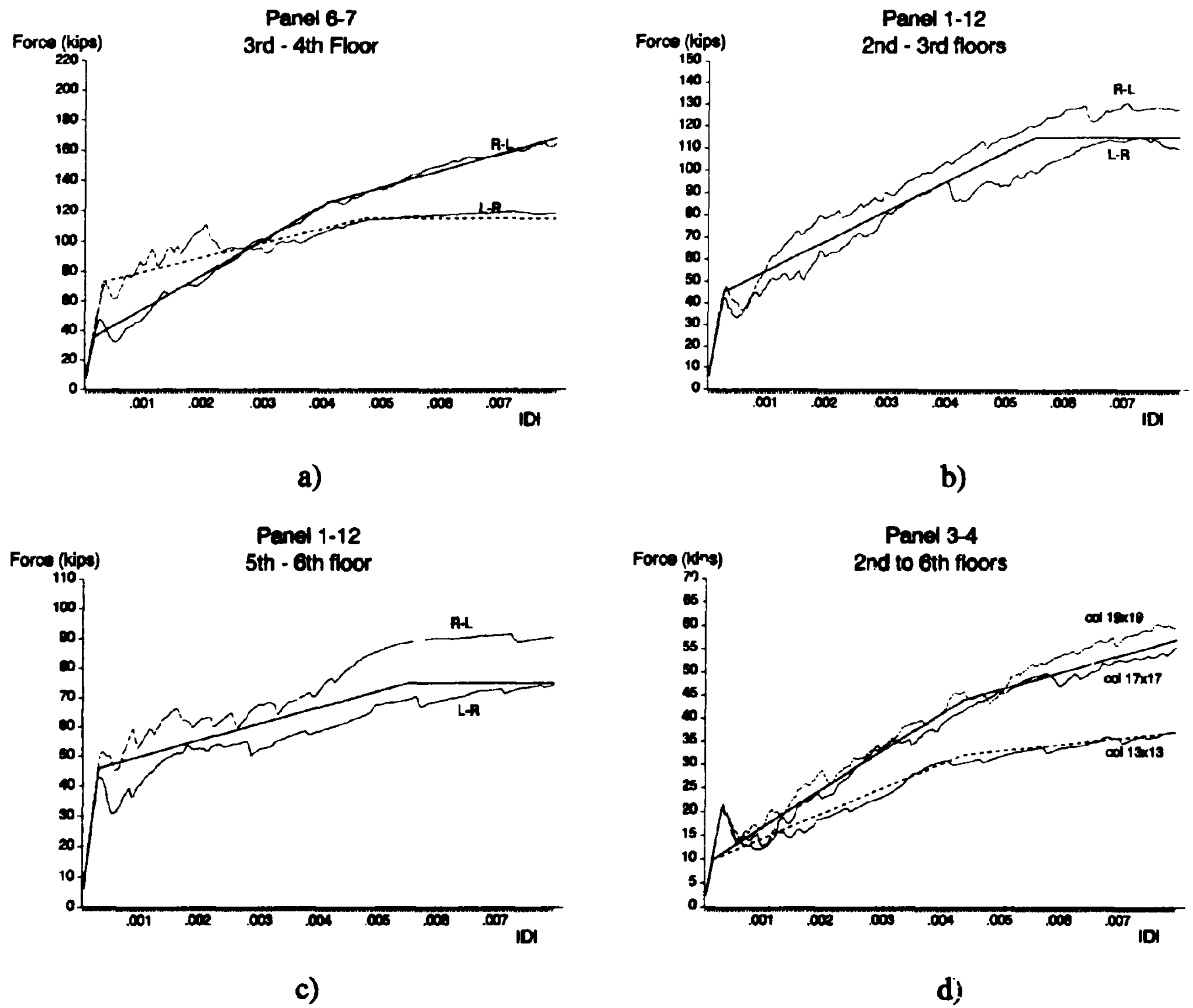

Figure 2.8 Lateral load vs. IDI curves for selected infills in Pomona Building, Kariotis et al. (1993)

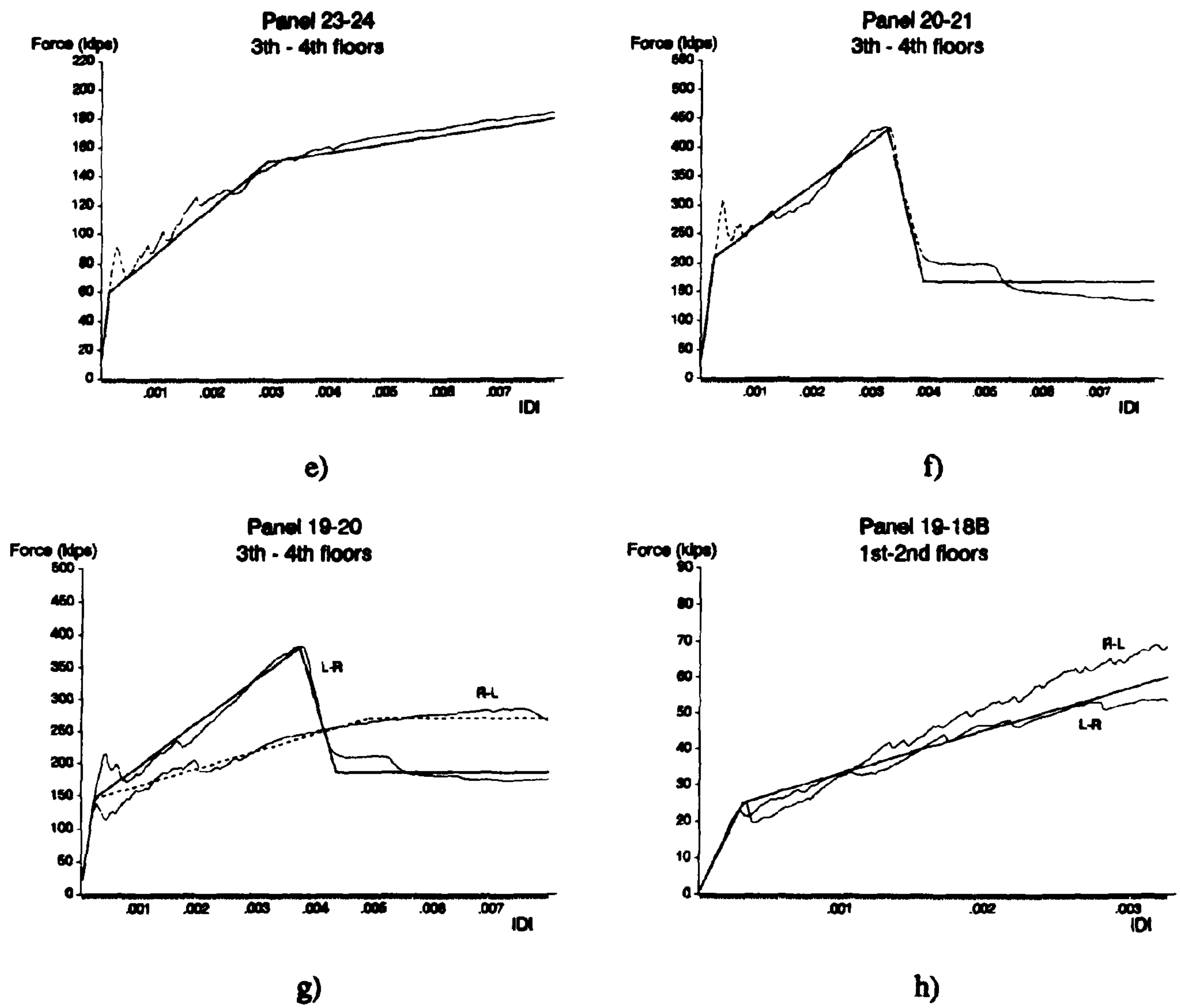

Figure 2.8 continued

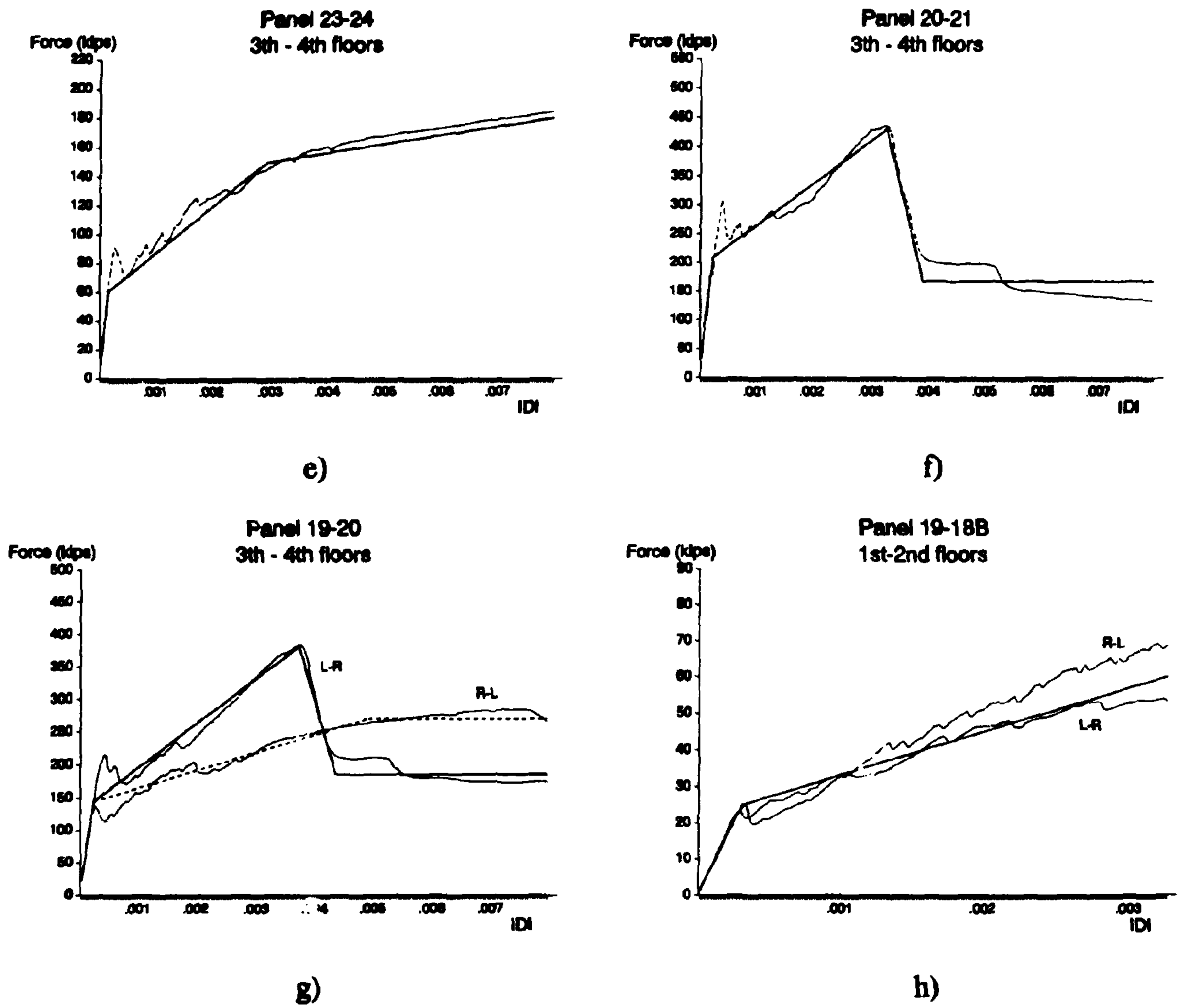

Figure 2.8 continued

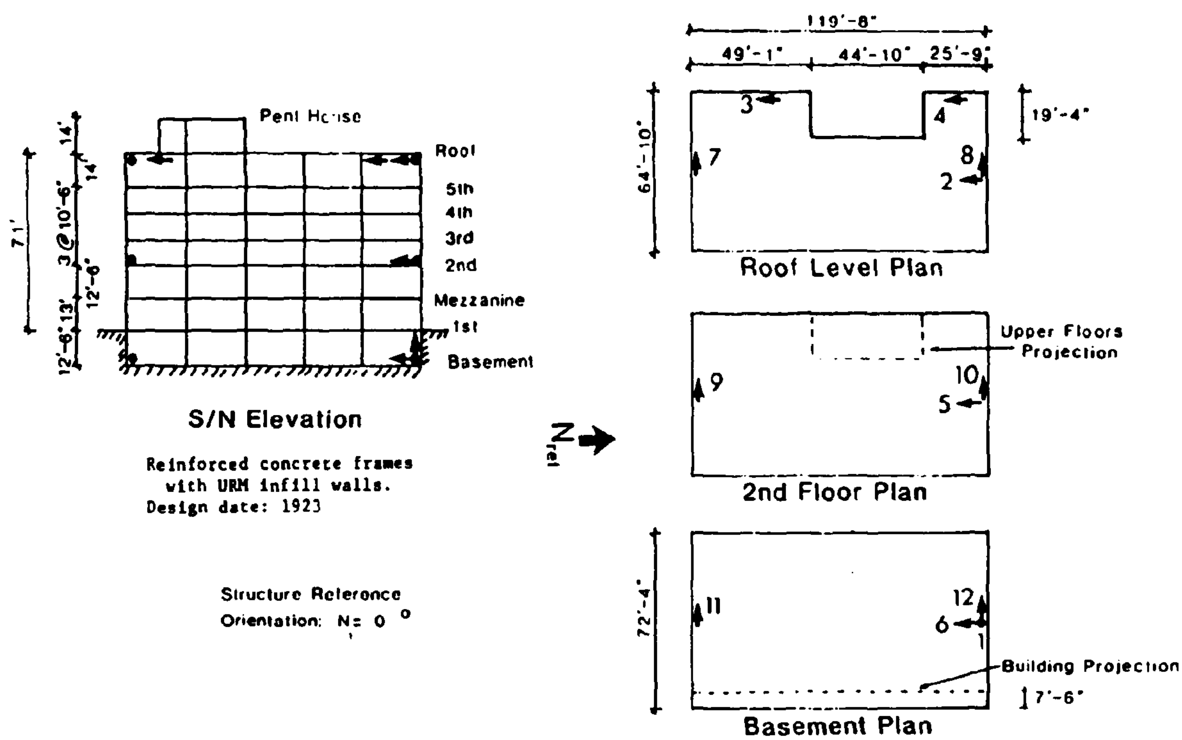

Figure 2.9 Sensor locations for CSMIP Station No. 23544

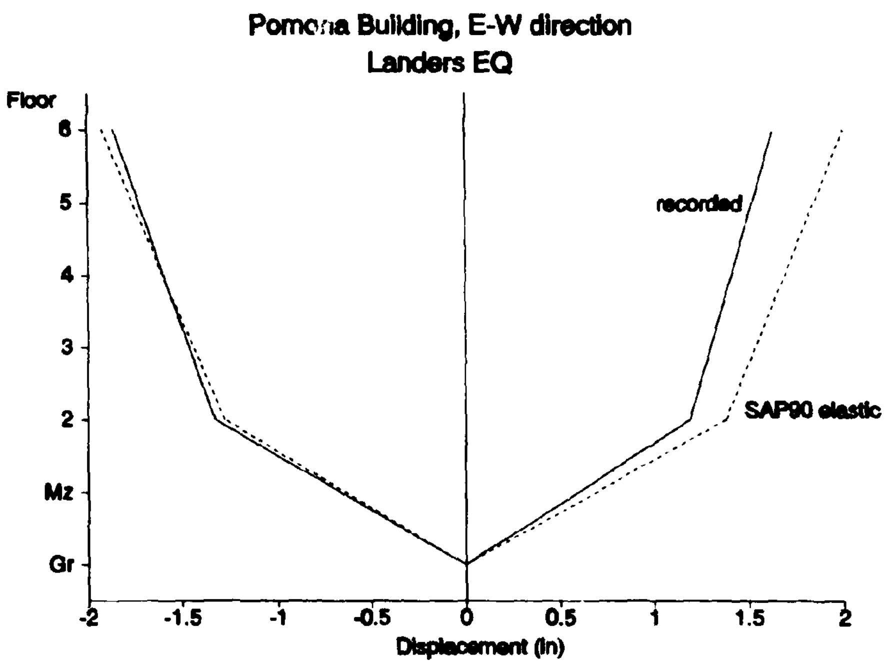

a) Frame A

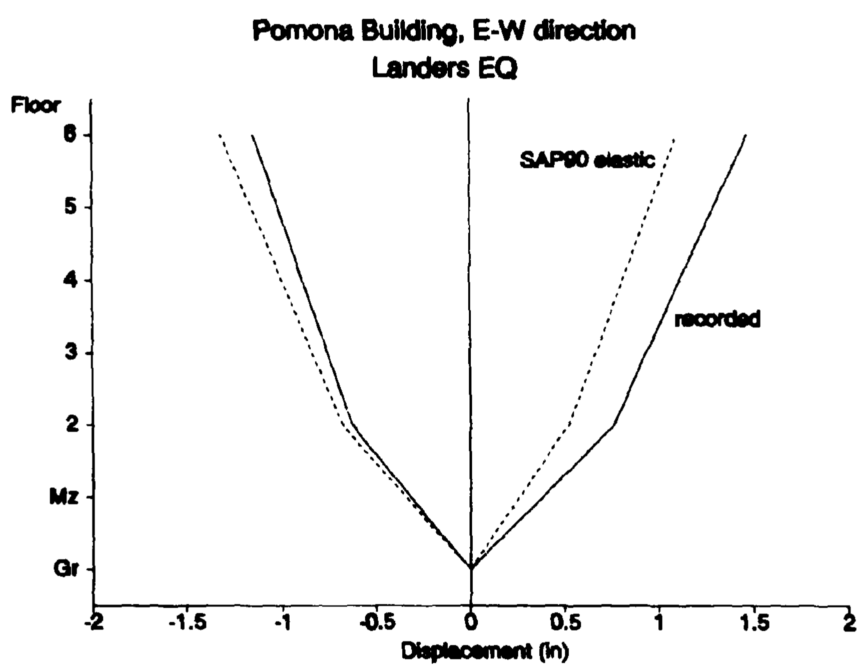

b) Frame F

Figure 2.10 Comparison of floor displacements obtained from measured response and elastic time-history analysis of building subjected to Landers EQ. E-W direction

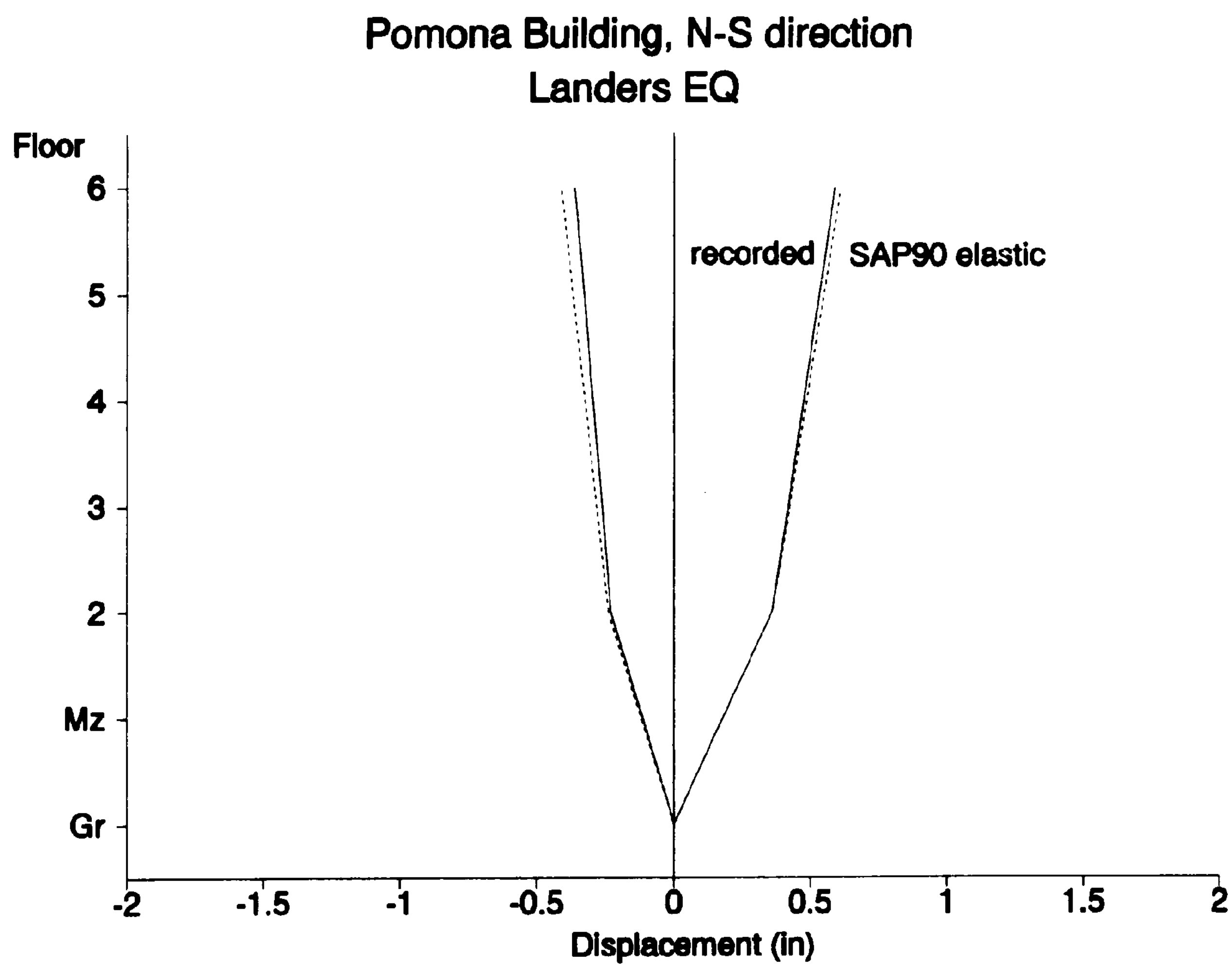

Figure 2.11 Comparison of floor displacements obtained from measured response and elastic time-history analysis of building subjected to Landers EQ, N-S direction

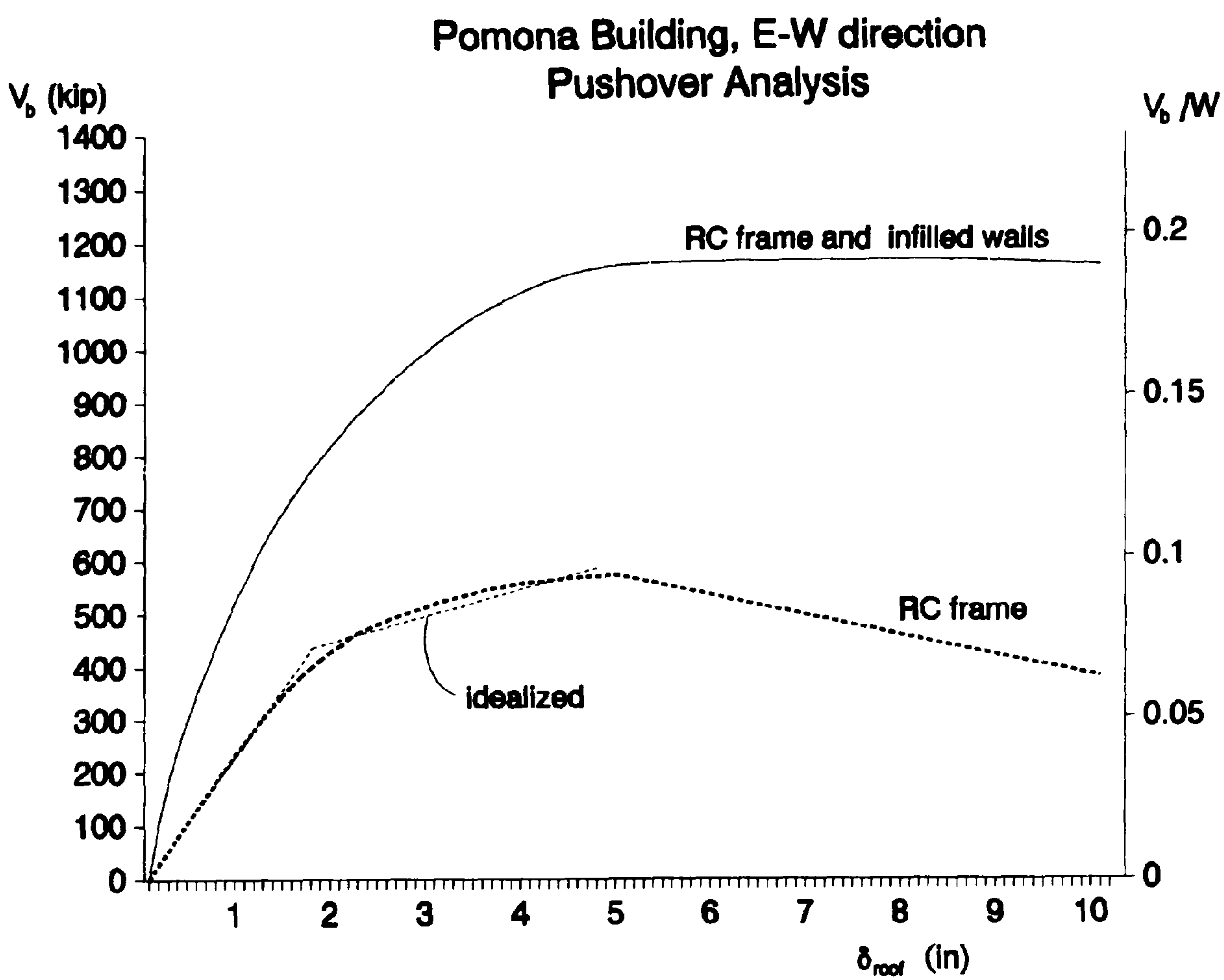

Figure 2.12 Roof displacement vs. base shear curve obtained from 2D pushover analysis of E-W direction

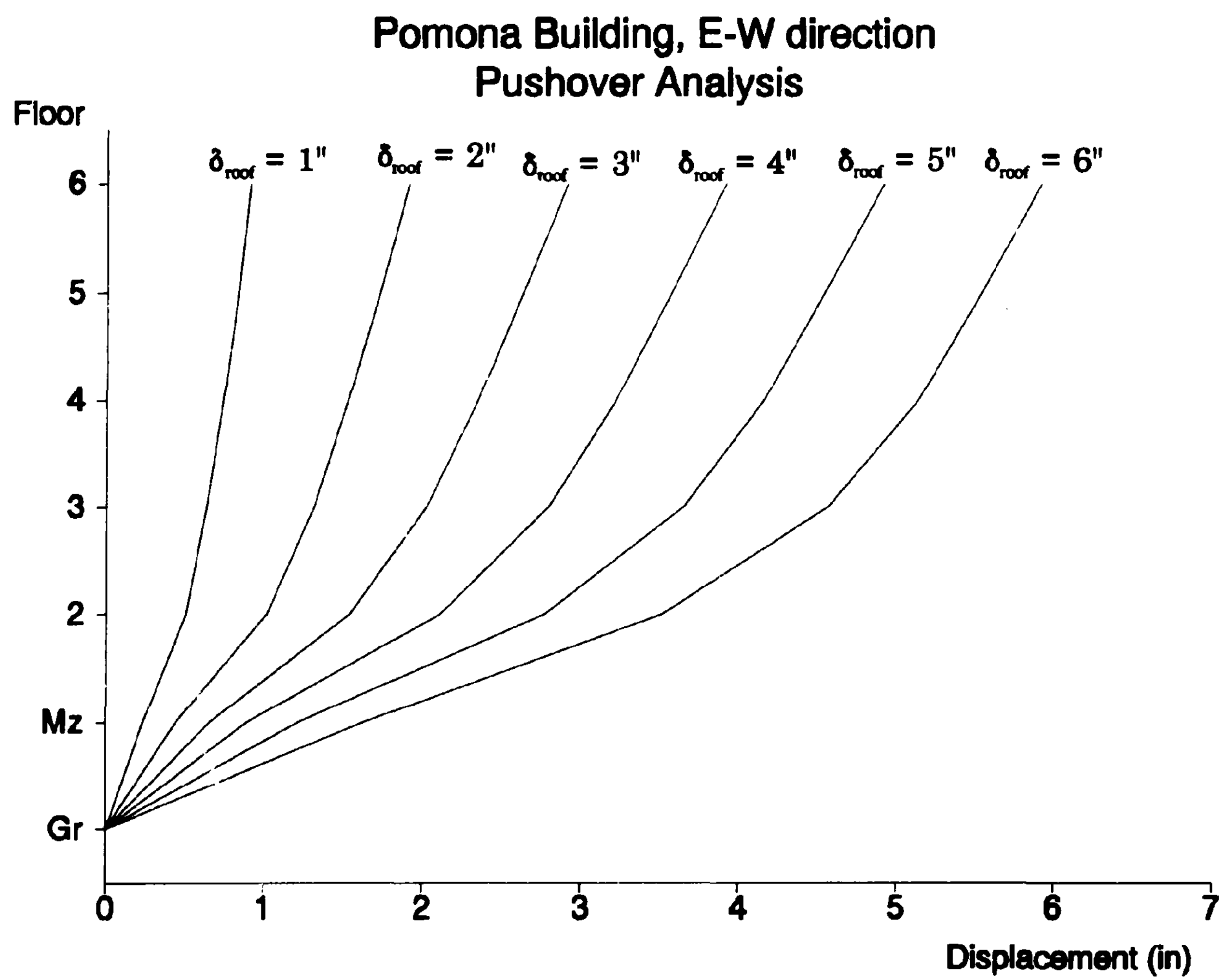

Figure 2.13 Floor displacement distribution over height obtained from 2D pushover analysis of E-W direction

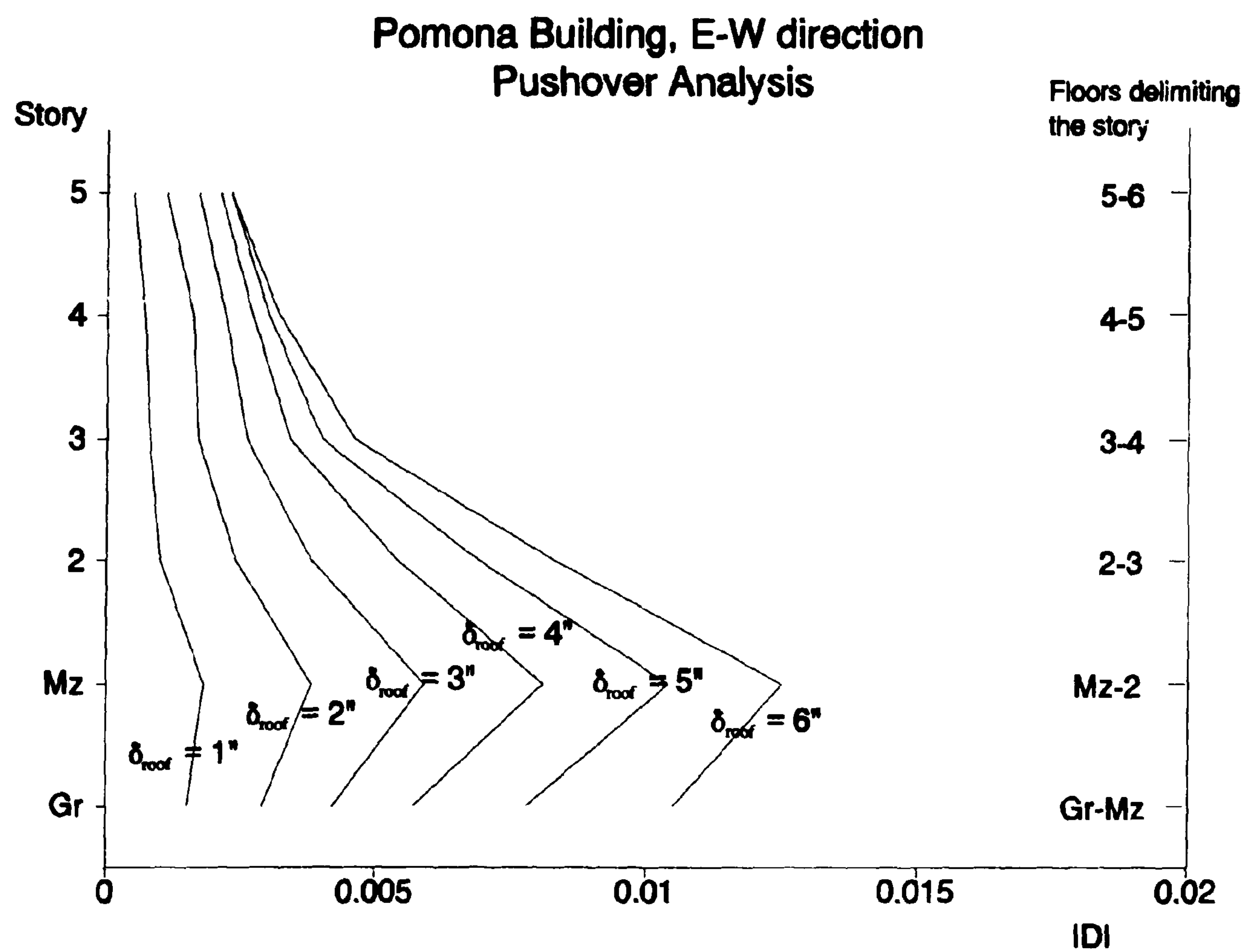

Figure 2.14 IDI distribution over height obtained from 2D pushover analysis of E-W direction

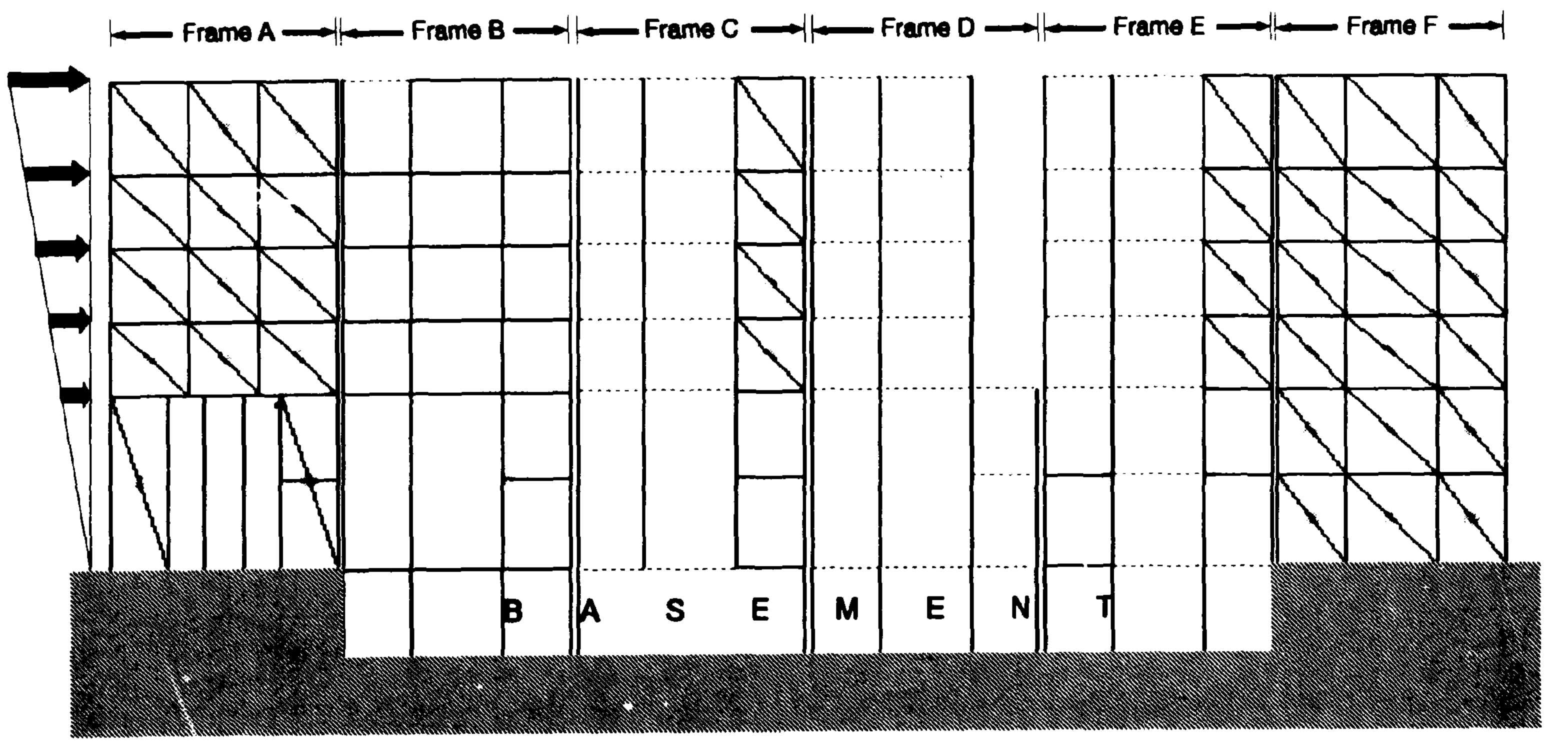

Figure 2.15 State of the E-W direction at $\delta_{roof} = 1''$ according to 2D pushover analysis

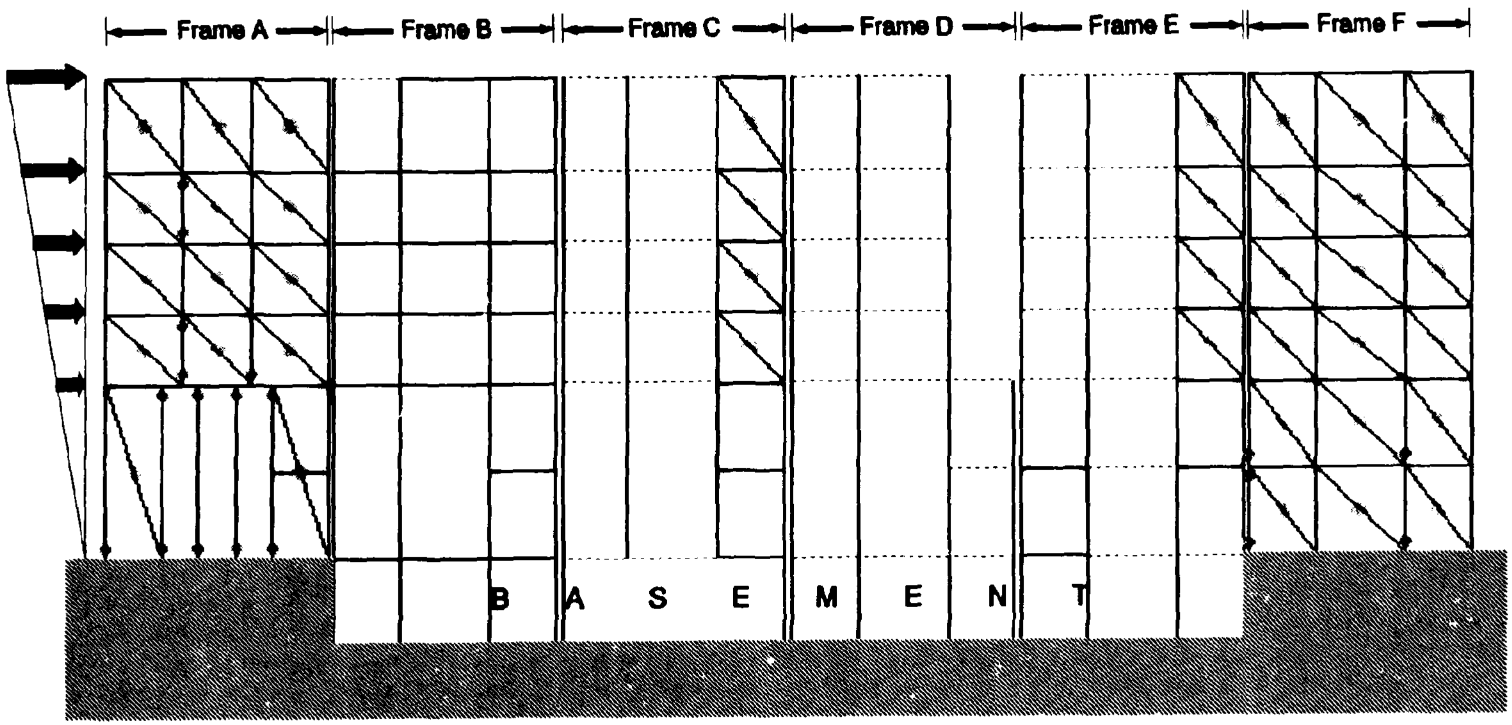

Figure 2.16 State of the E-W direction at δ_{roof} = 2" according to 2D pushover analysis

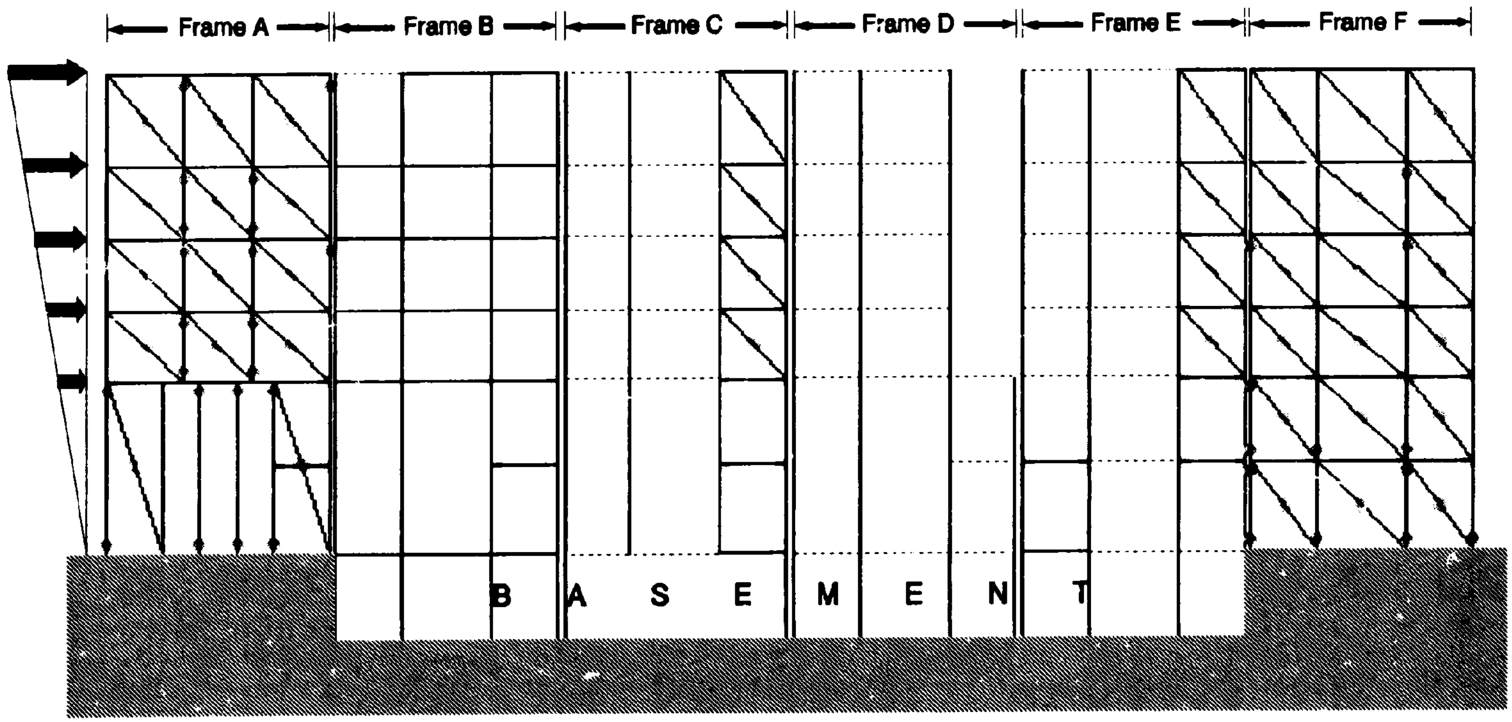

Figure 2.17 State of the E-W direction at δ_{roof} = 3" according to 2D pushover analysis

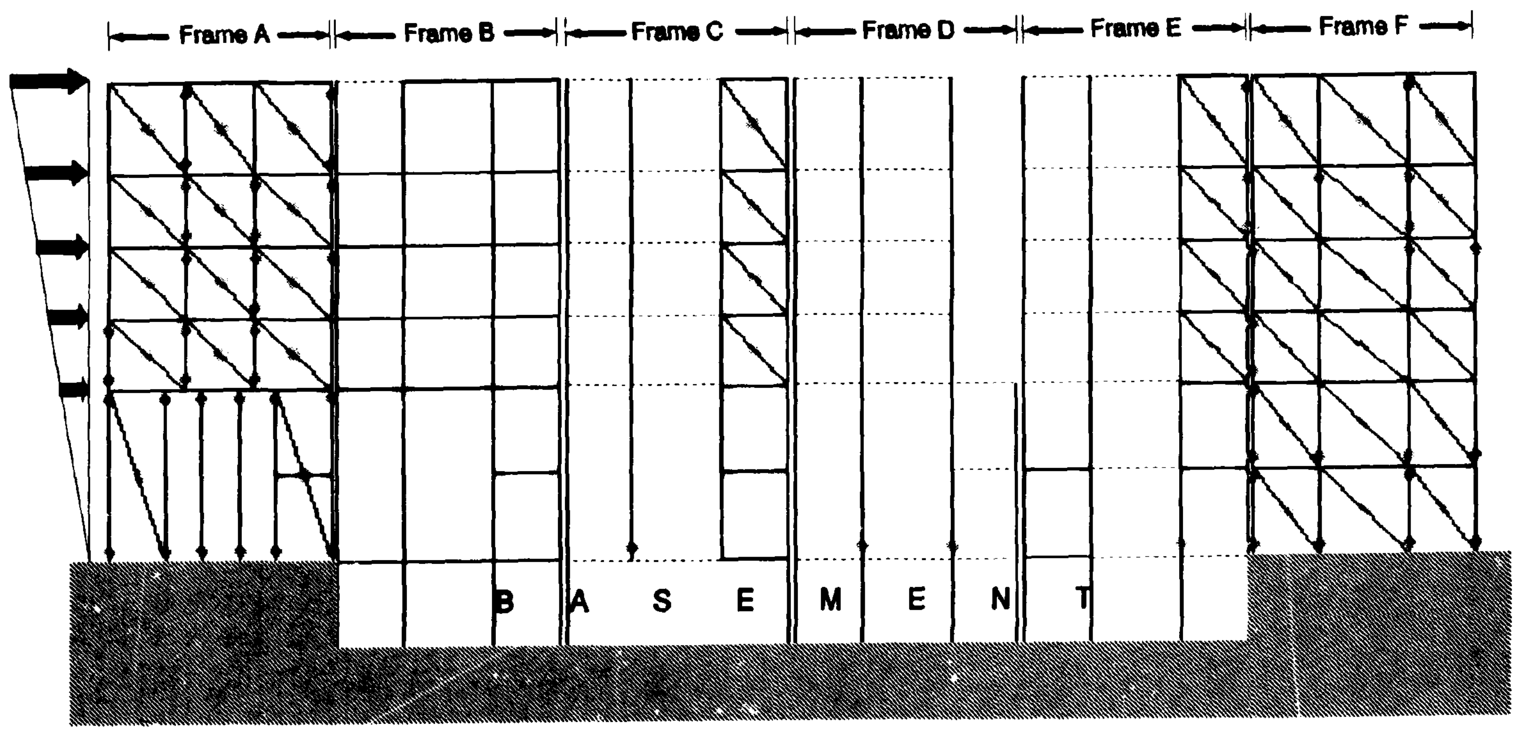

Figure 2.18 State of the E-W direction at δ_{roof} = 4" according to 2D pushover analysis

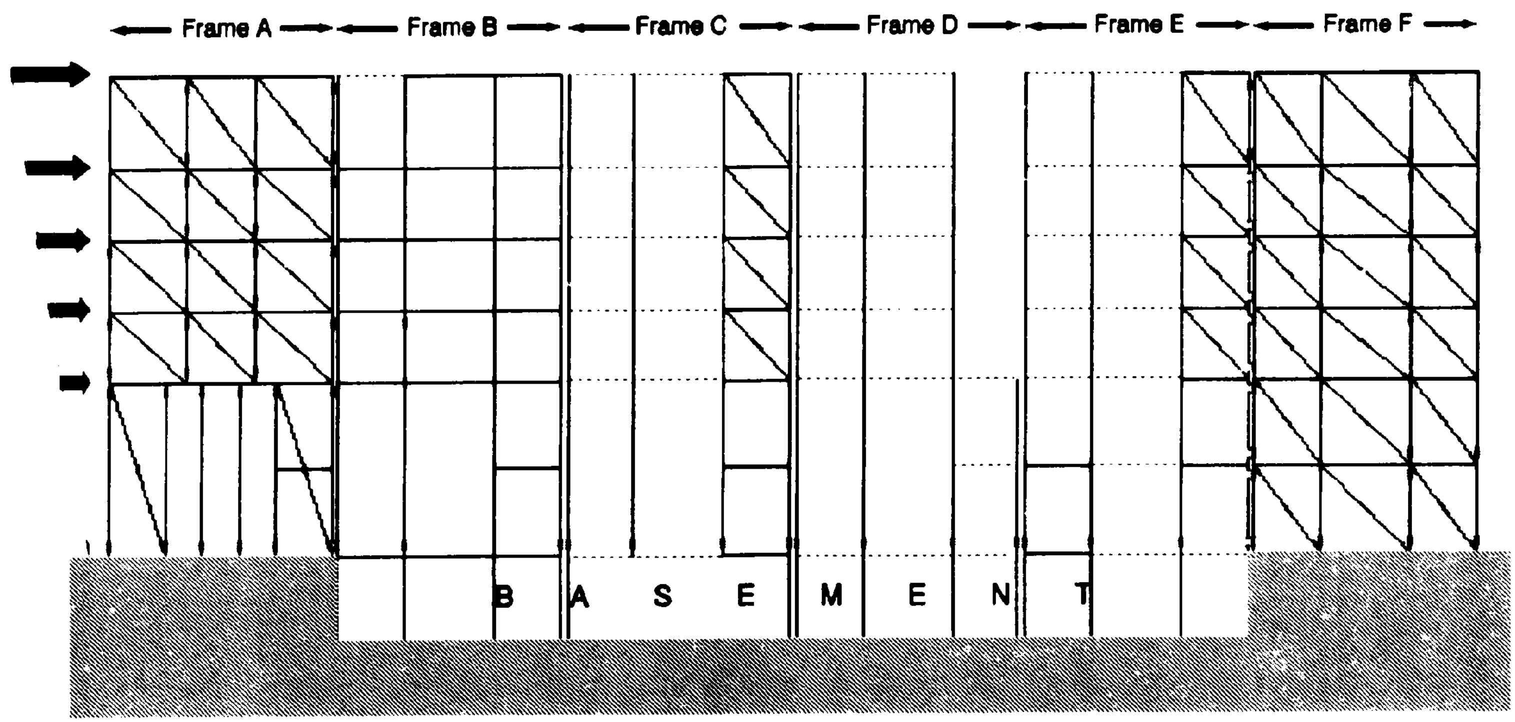

Figure 2.19 State of the E-W direction at $\delta_{roof} = 5''$ according to 2D pushover analysis

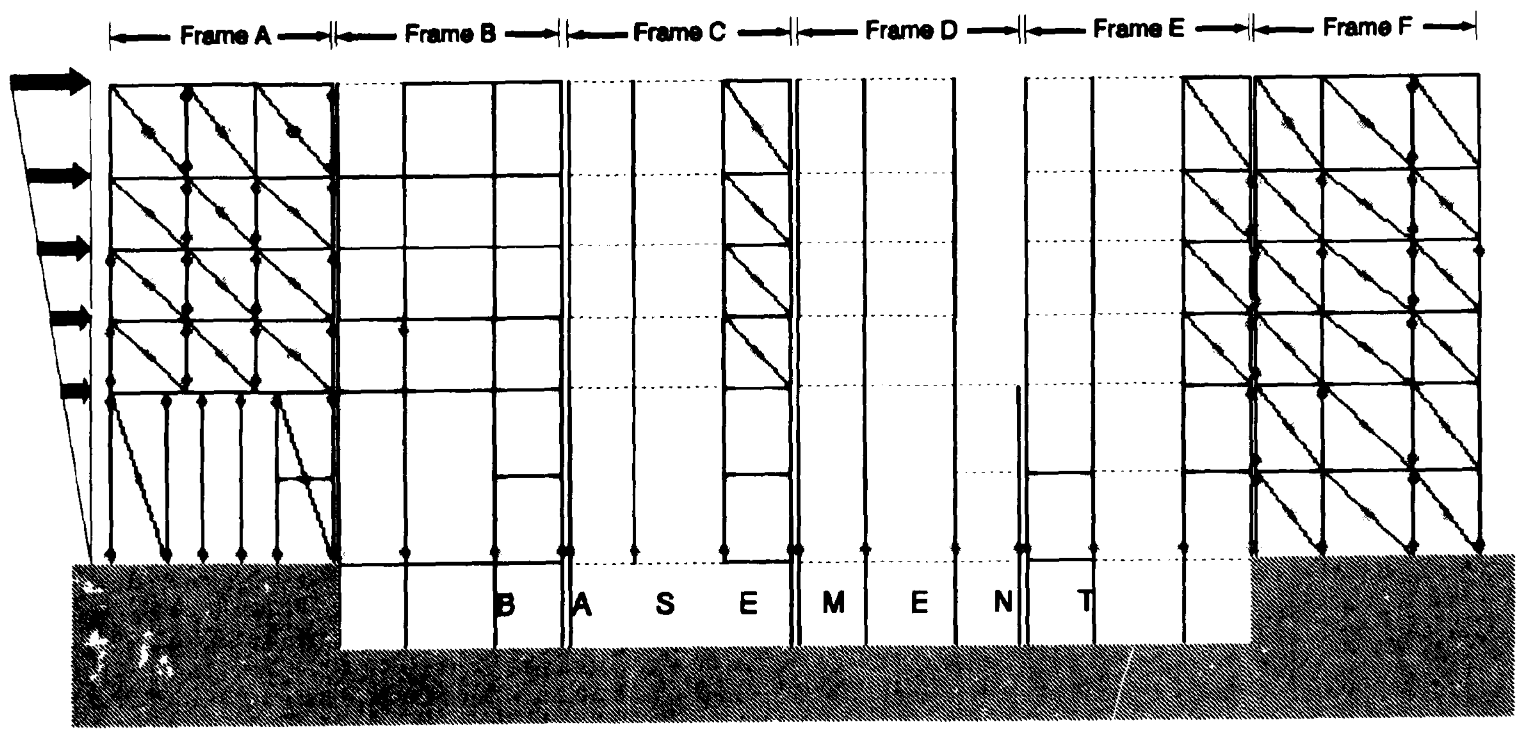

Figure 2.20 State of the E-W direction at $\delta_{roof} = 6''$ according to 2D pushover analysis

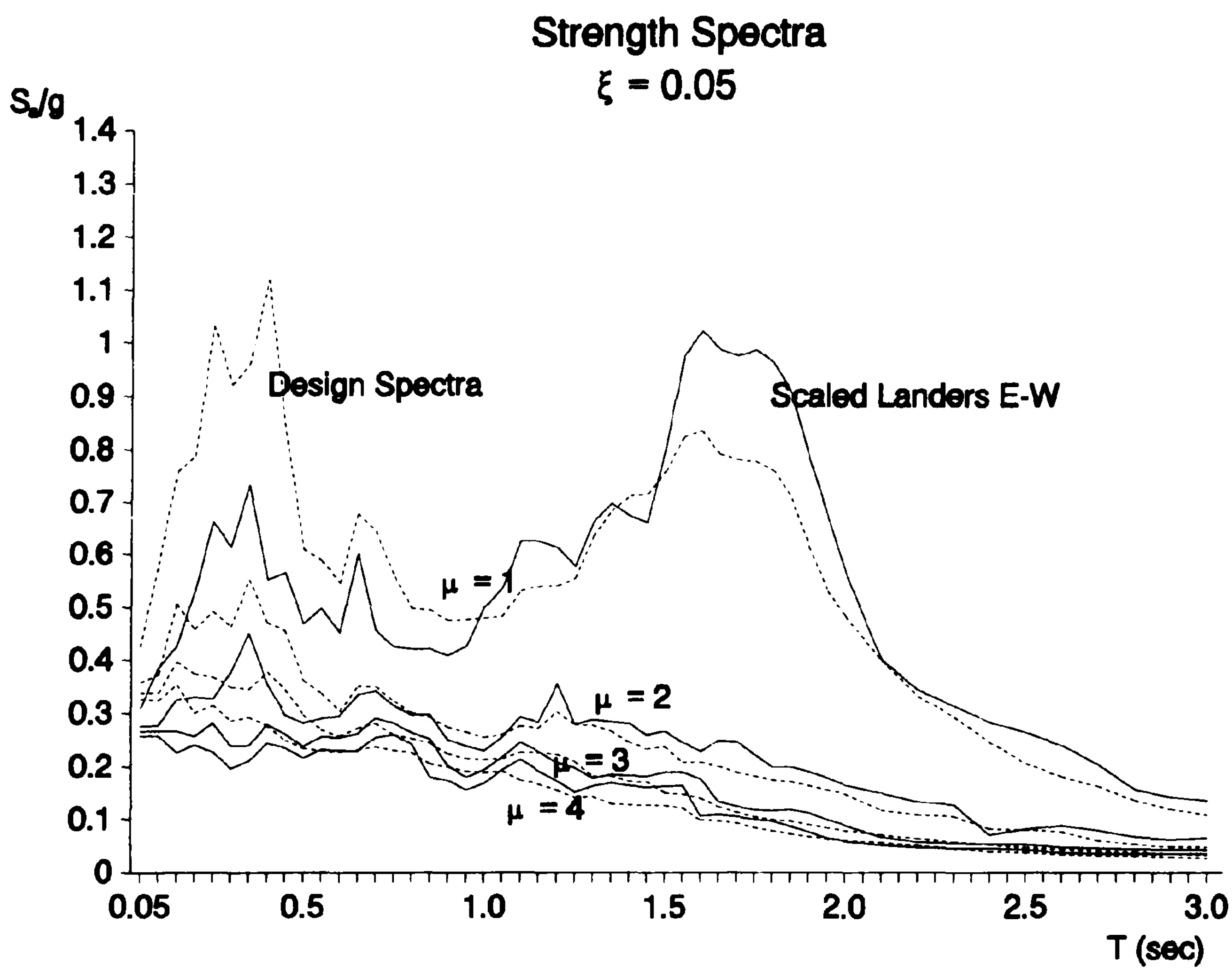

Figure 2.21 Comparison of design strength spectra and strength spectra of Landers E-W component scaled up by a factor of six

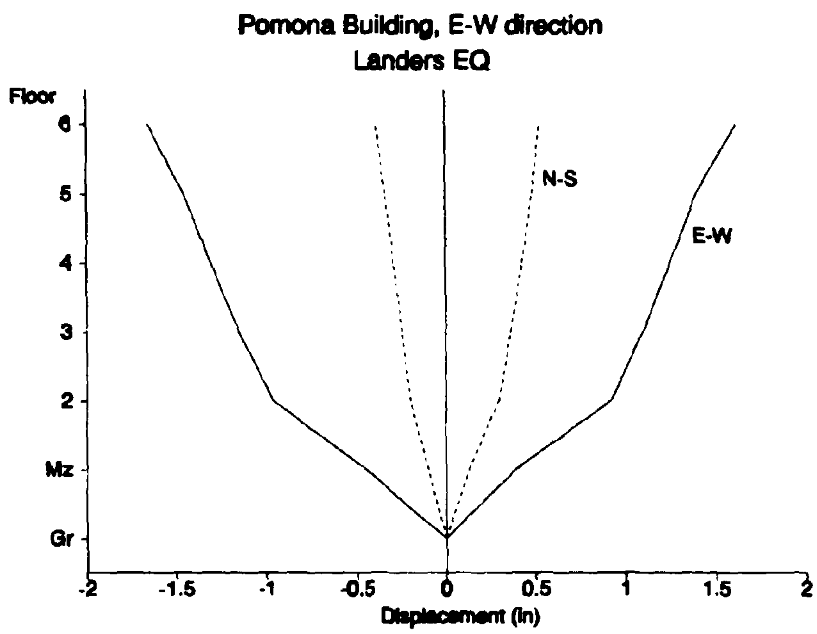

a) 3D Analysis

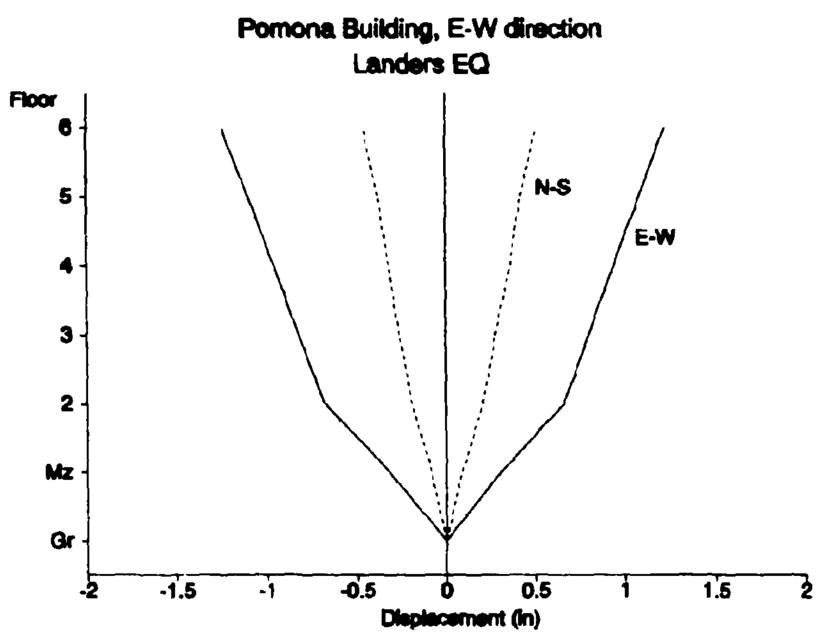

b) 2D Analysis

Figure 2.22 Floor displacements at center of mass obtained from elastic time-history analysis of building subjected to Landers EQ

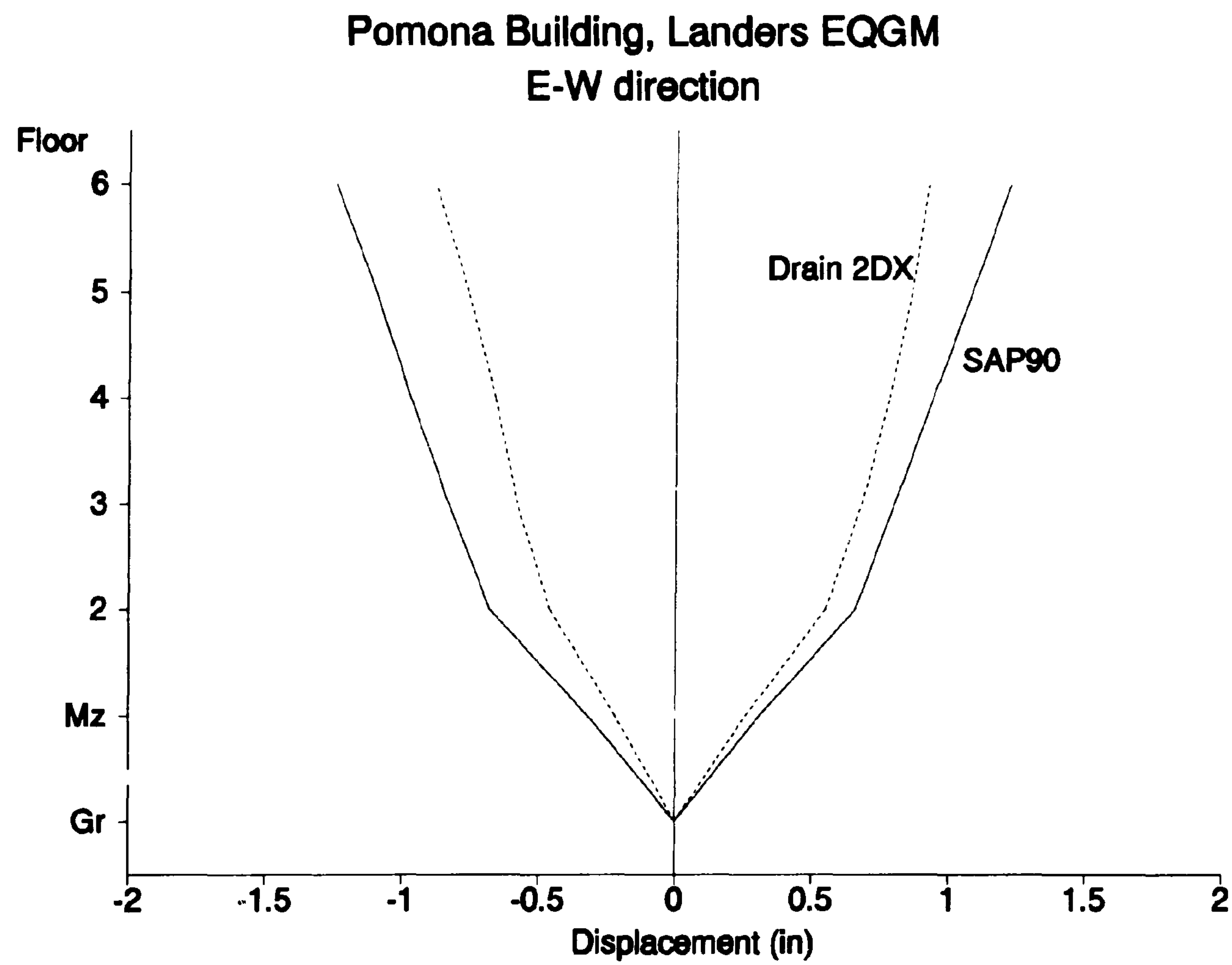

Figure 2.23 Comparison of floor displacements obtained from 2D elastic and 2D nonlinear time-history analysis

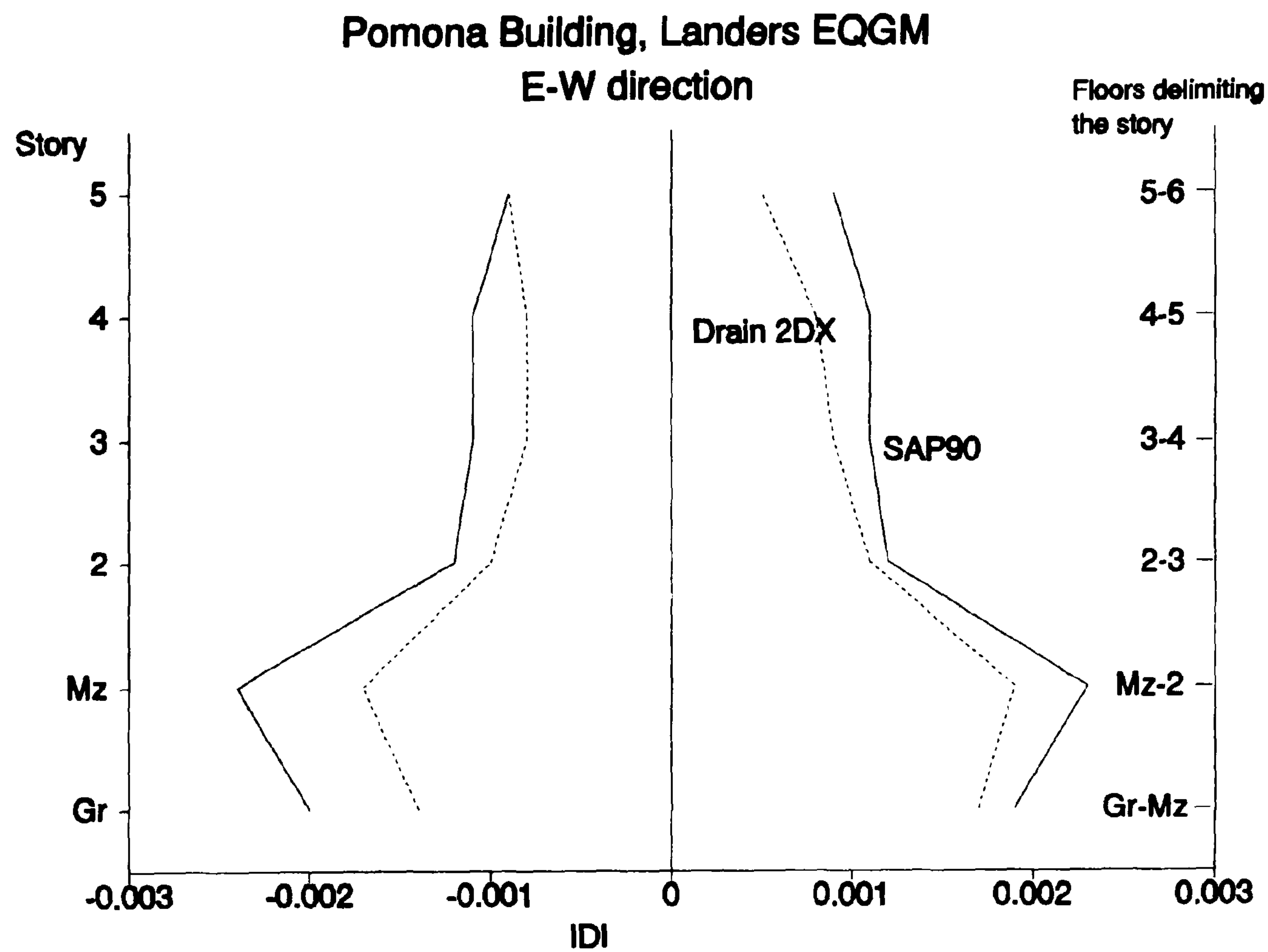

Figure 2.24 Comparison of IDI obtained from 2D elastic and 2D nonlinear time-history analysis

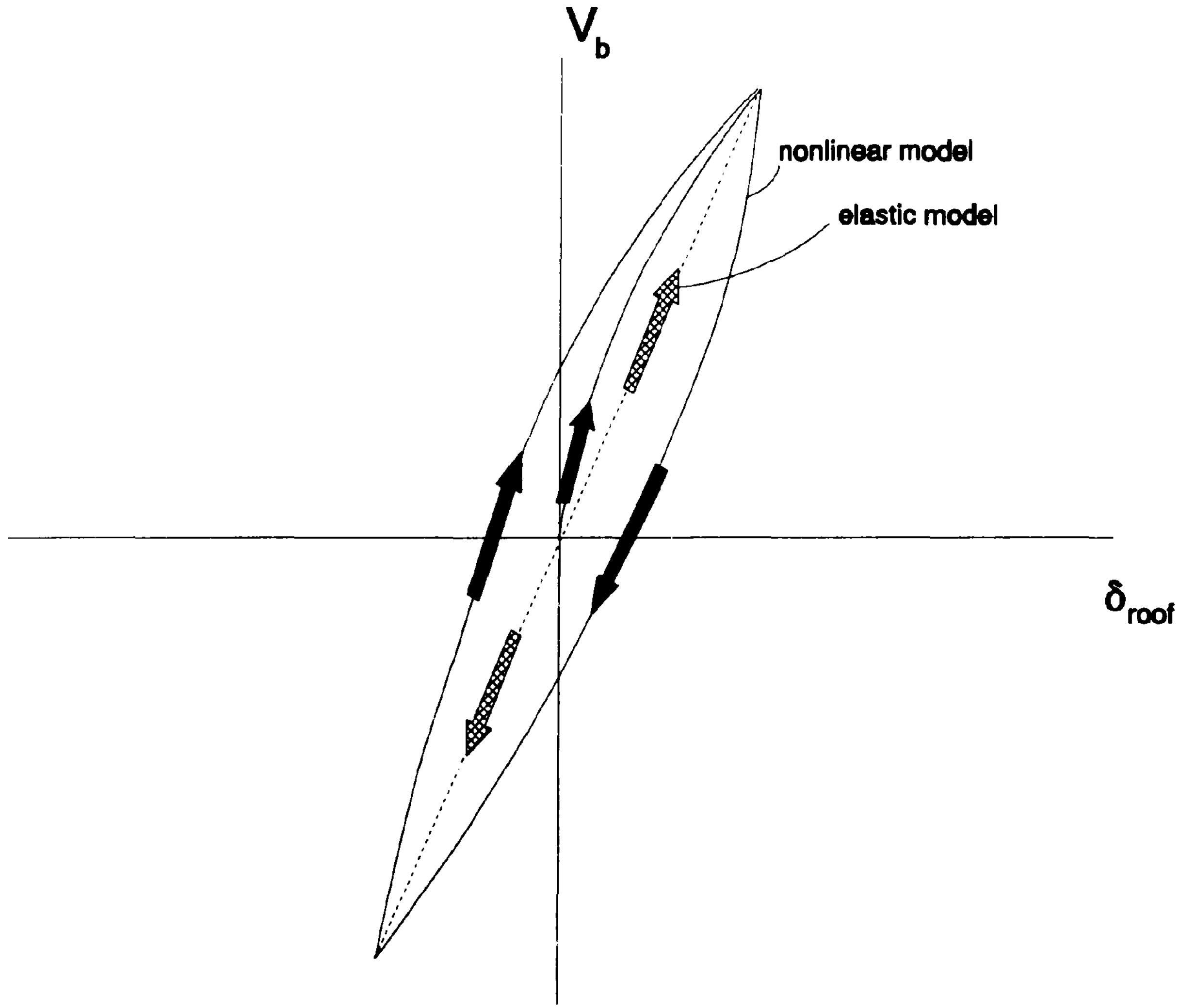

Figure 2.25 Comparison of idealized hysteretic behavior of elastic and nonlinear models

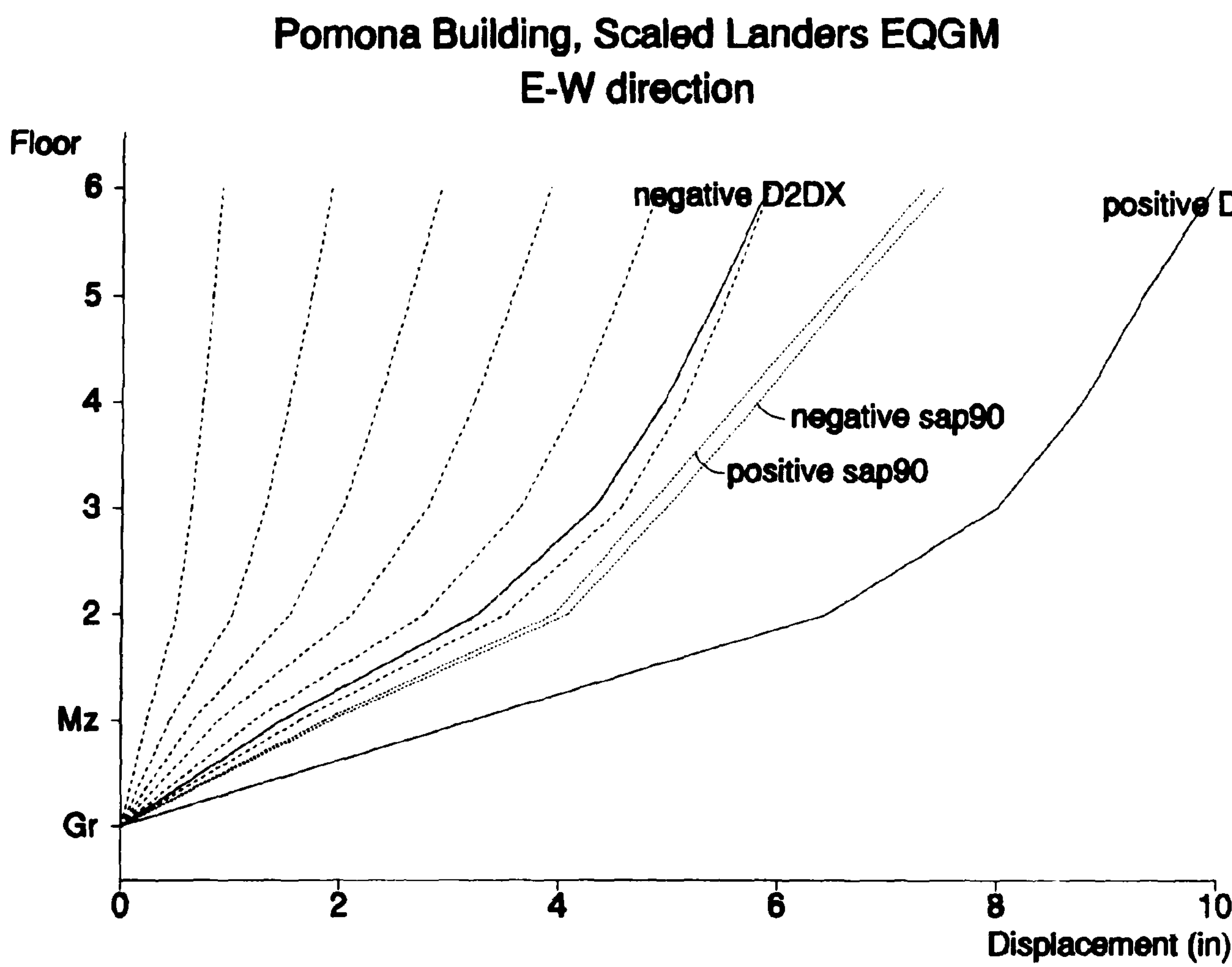

Figure 2.26 Floor displacements in E-W direction obtained from 2D nonlinear time-history analysis using the Landers E-W EQGM scaled up by a factor of six

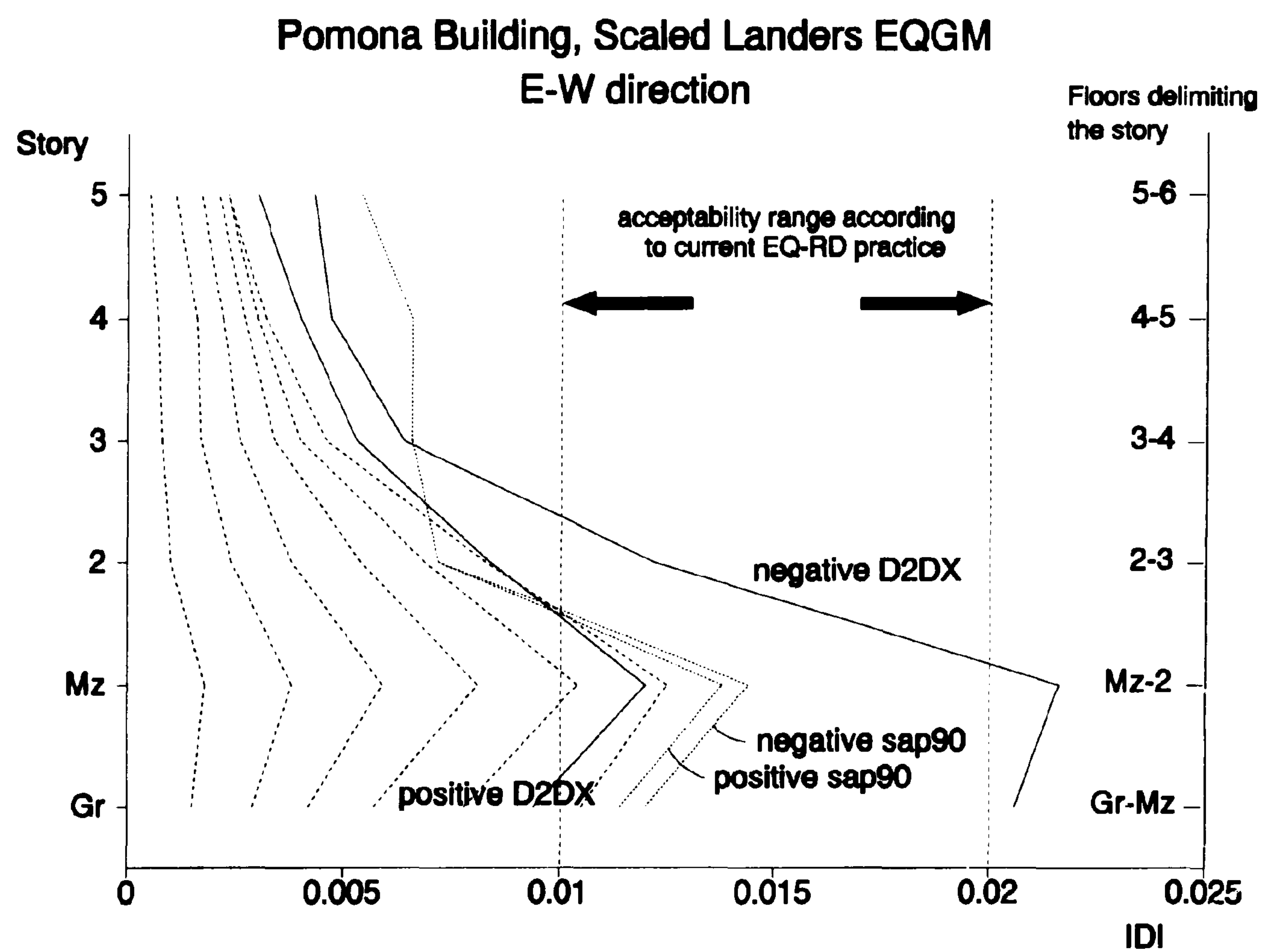

Figure 2.27 IDI in E-W direction obtained from 2D nonlinear time-history analysis using the Landers E-W EQGM scaled up by a factor of six

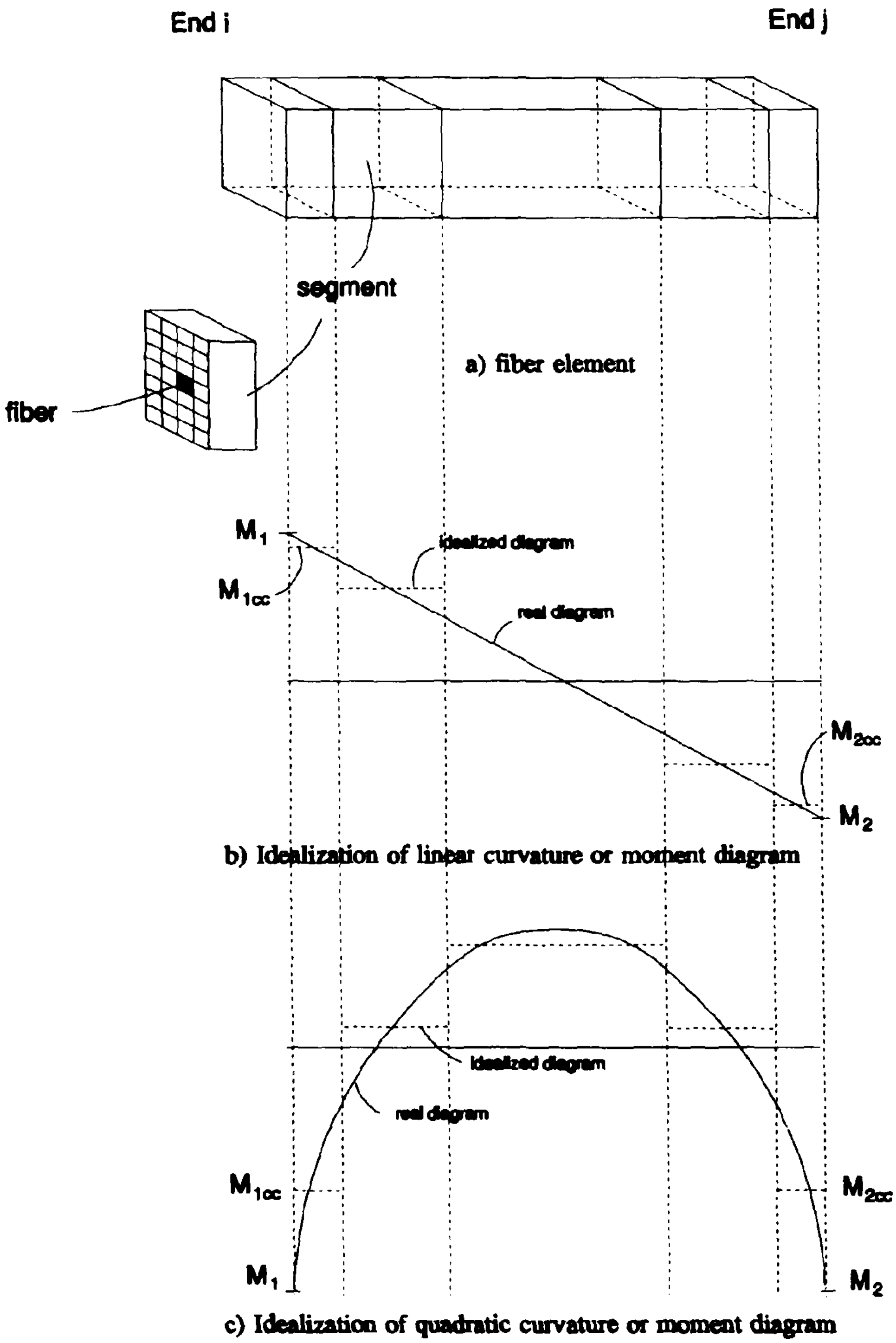

Figure 2.28 Fiber element with segments having constant curvature

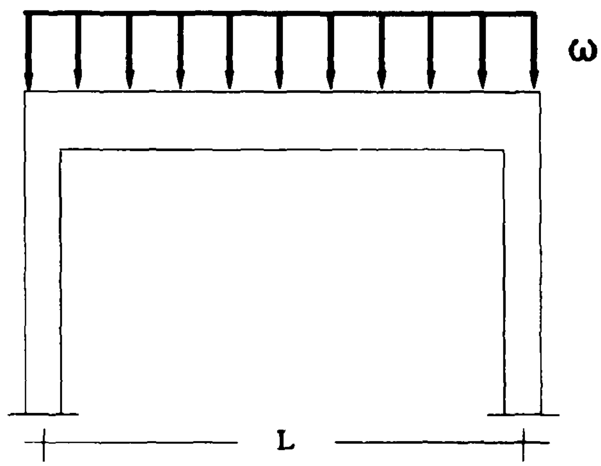

a) distributed load on beams

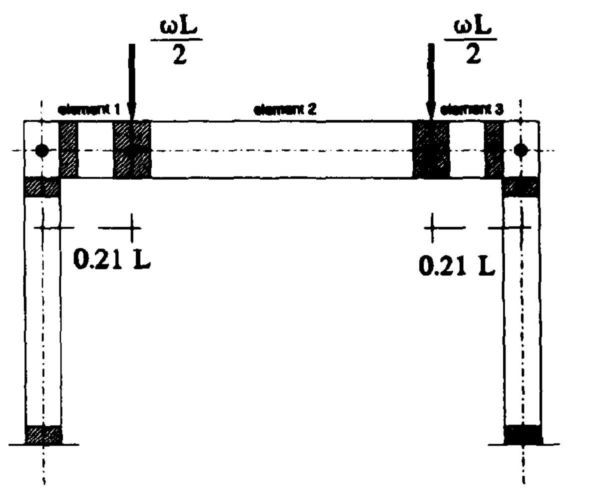

b) idealization of gravitational loads for Drain 3DX

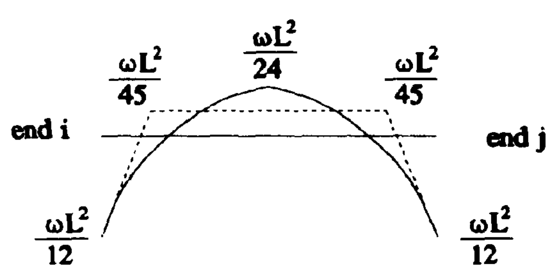

c) moment diagrams of beam with fixed ends subjected to loads shown in a) and b)

Figure 2.29 Comparison of moment diagrams in beam with fixed ends subjected to different idealizations of gravity loads

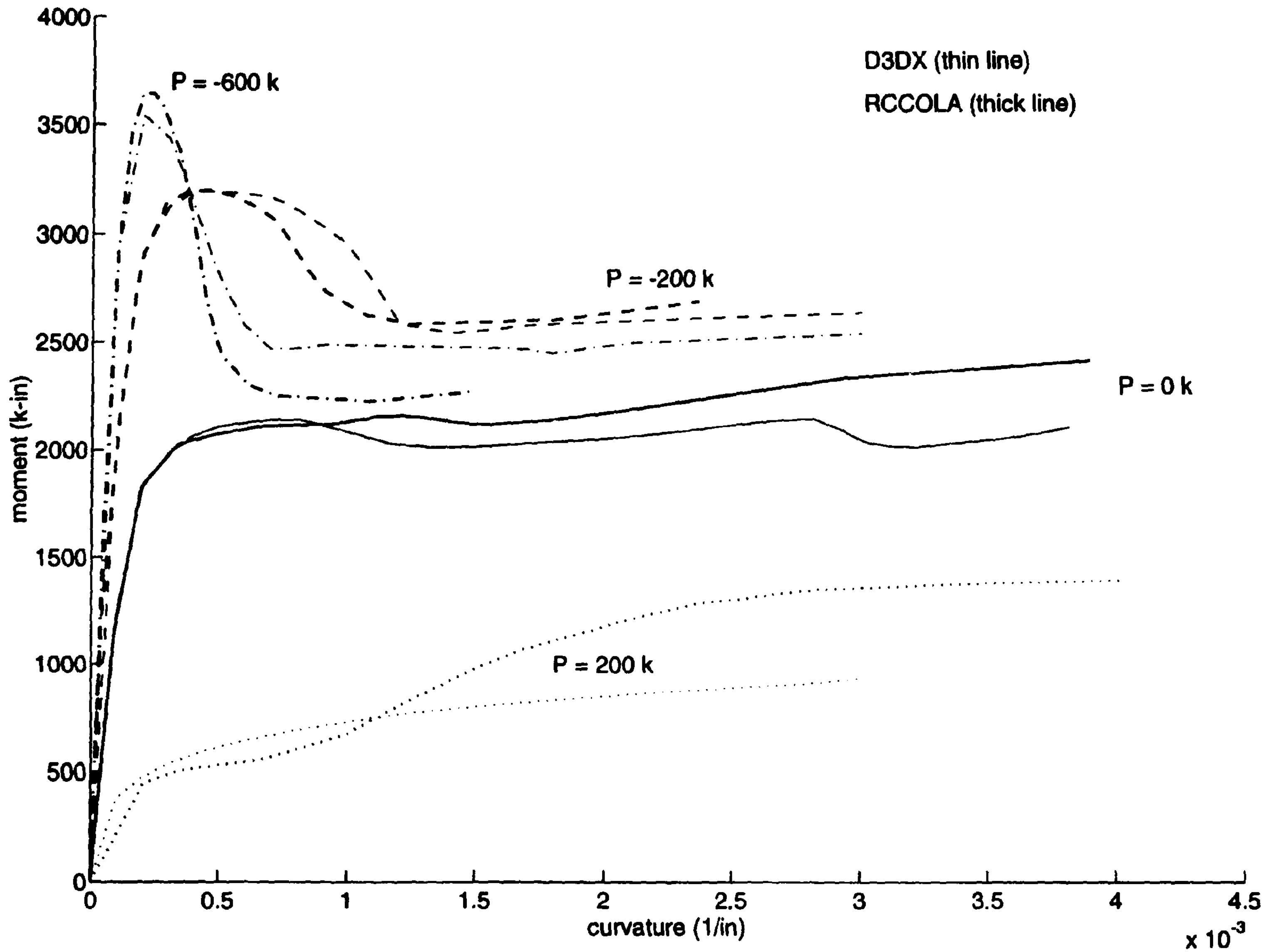

Figure 2.30 Comparison of moment-curvatures curves obtained using DRAIN 3DX and RCCOLA

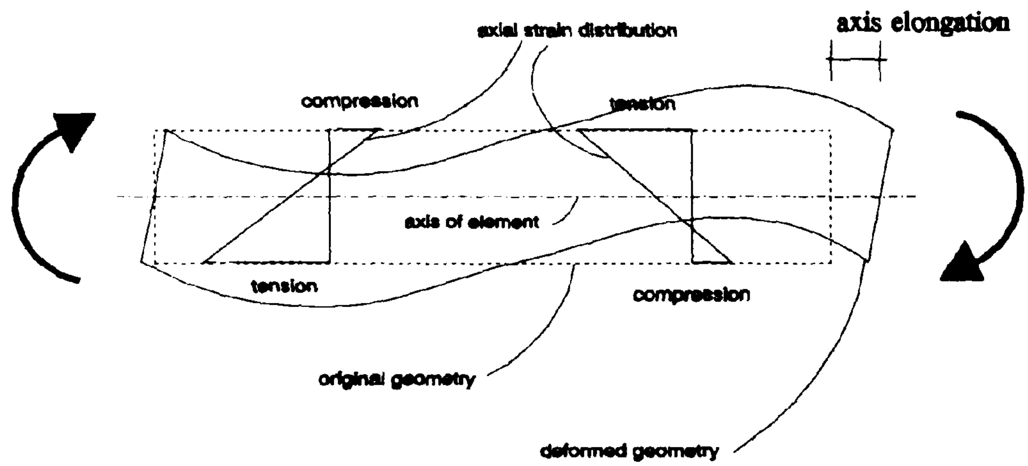

a) elongation of beam's axis due to flexural deformation

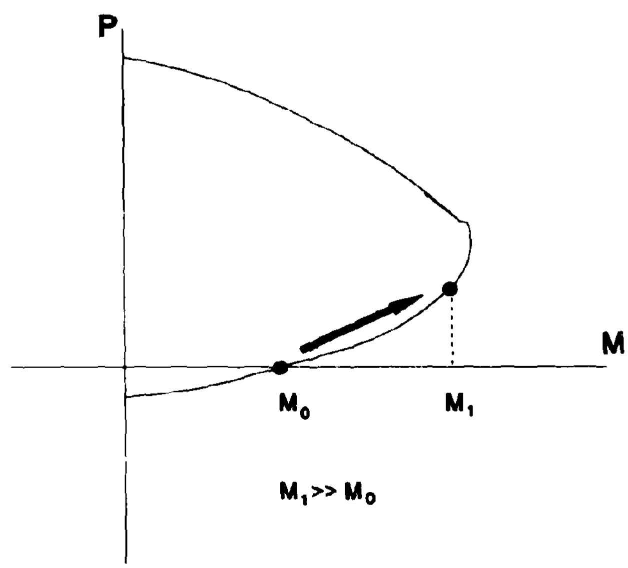

b) Effect of increasing axial force on beam's flexural strength

Figure 2.31 Effect of axial restraint on the flexural strength of a RC beam that exhibits double curvature

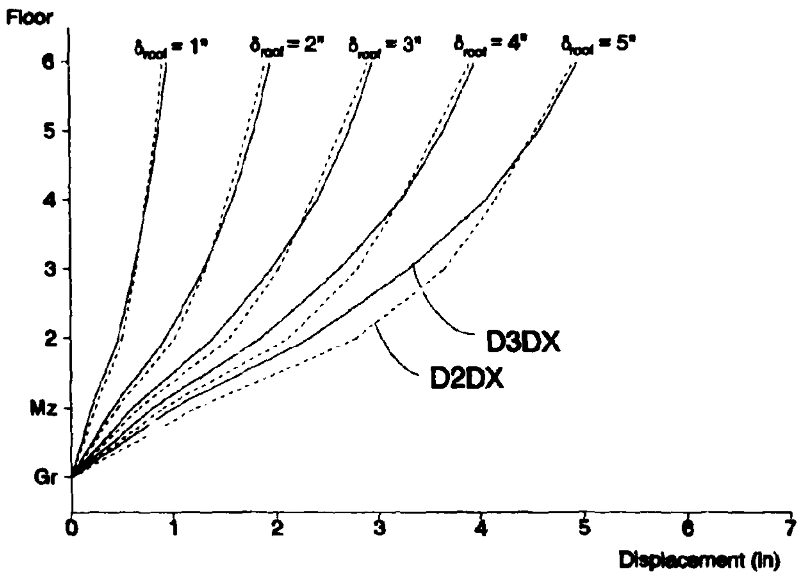

Figure 2.32 Comparison of floor displacements obtained from 2D and 3D pushover analysis, E-W direction

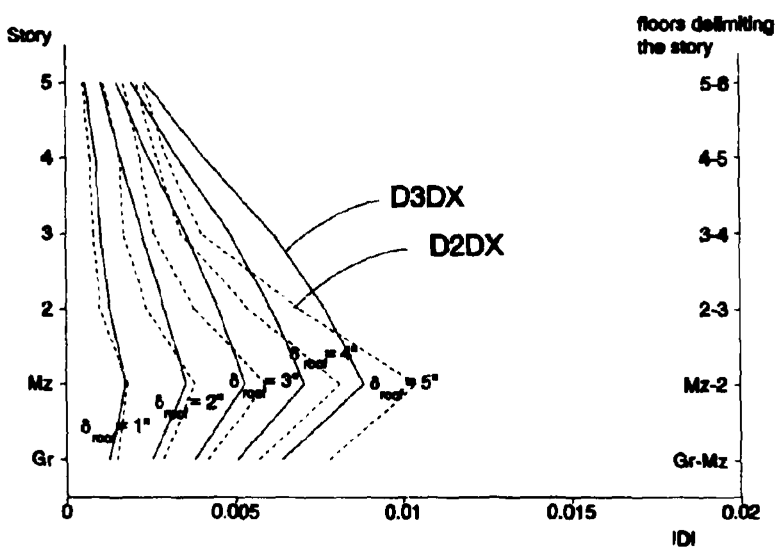

Figure 2.33 Comparison of IDI obtained from 2D and 3D pushover analysis, E-W direction

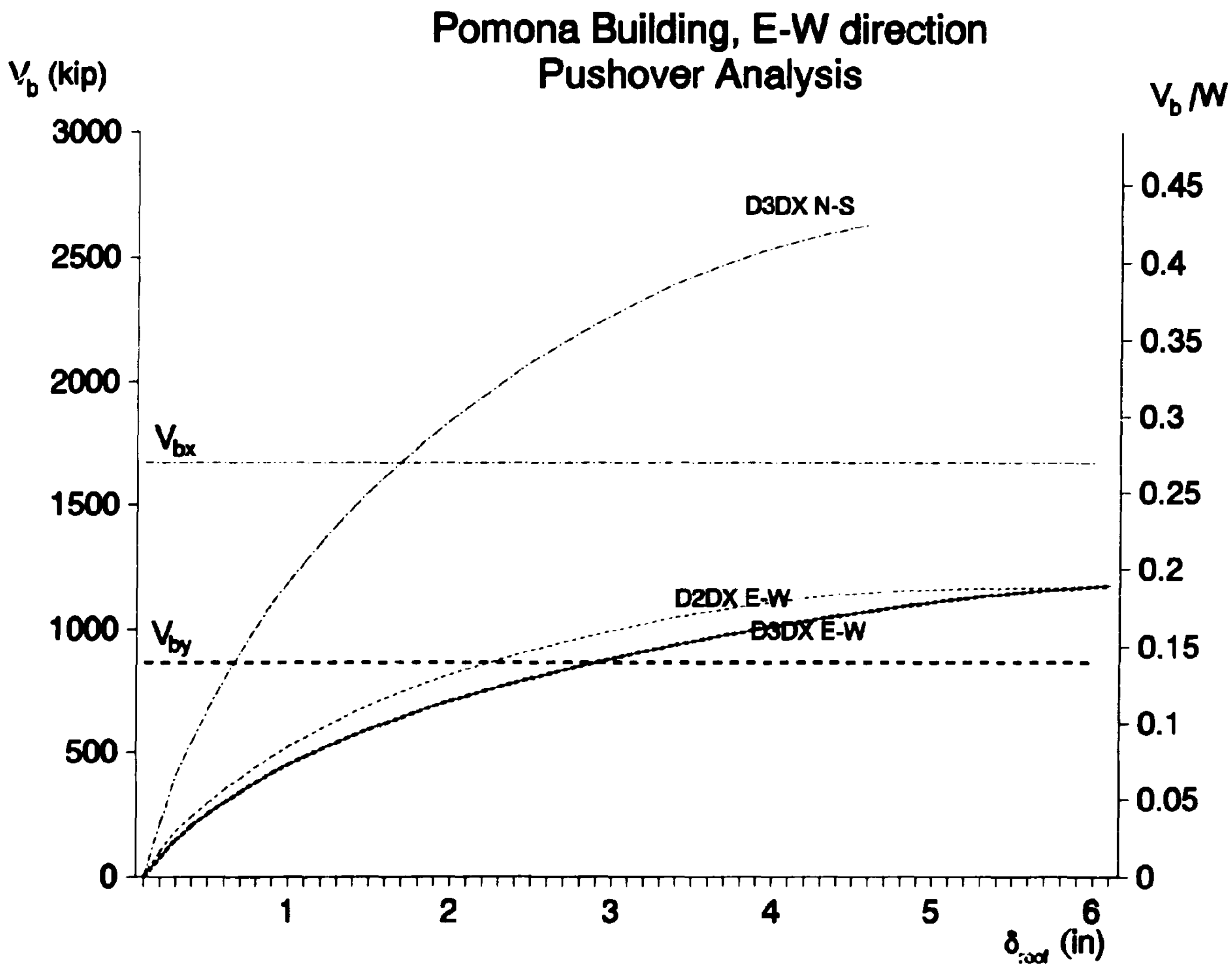

Figure 2.34 Roof displacement vs. base shear curves obtained from 2D and 3D pushover analyses

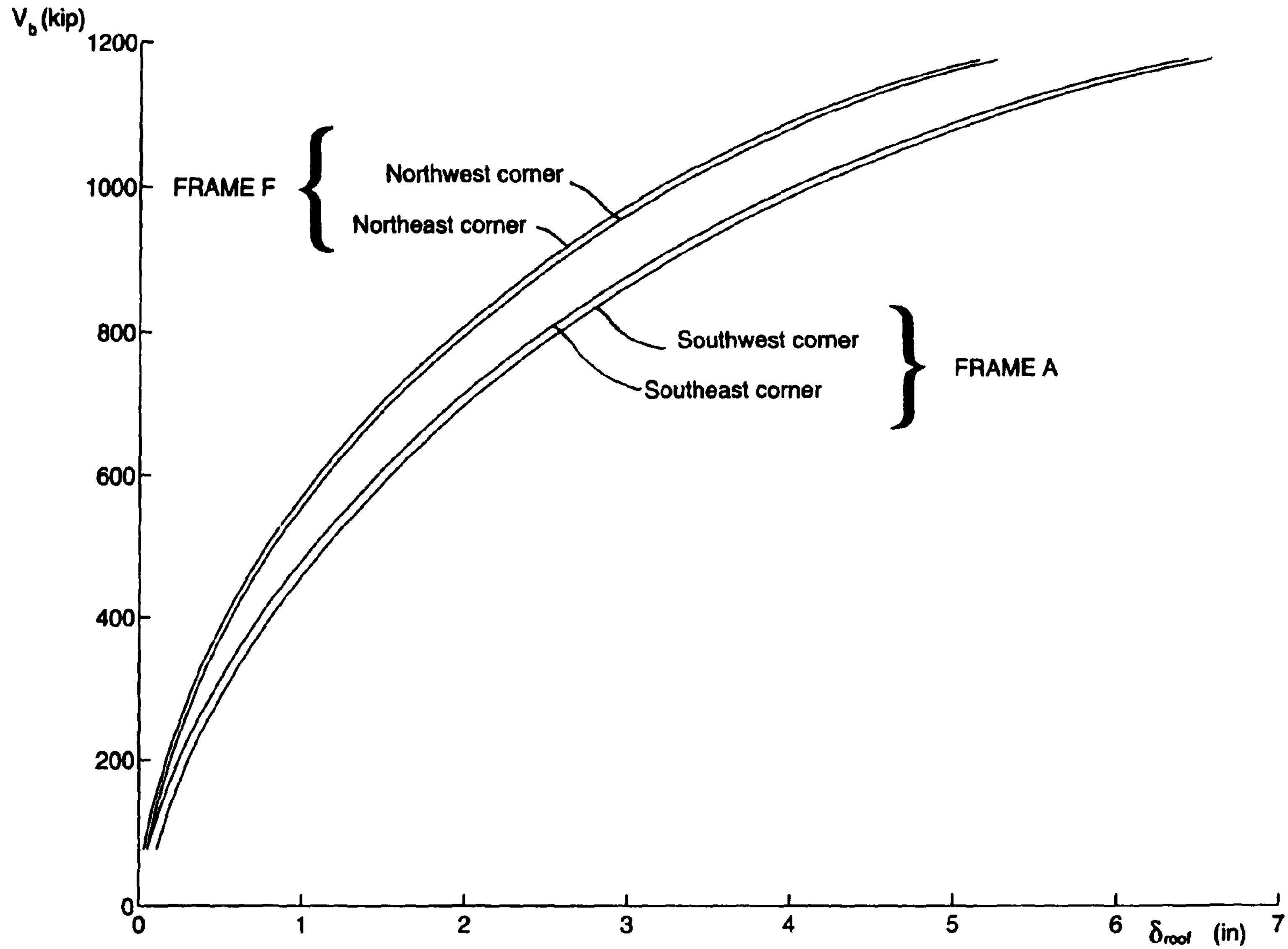

Figure 2.35 Roof displacement vs base shear curves from 3D pushover analysis of E-W direction of original building

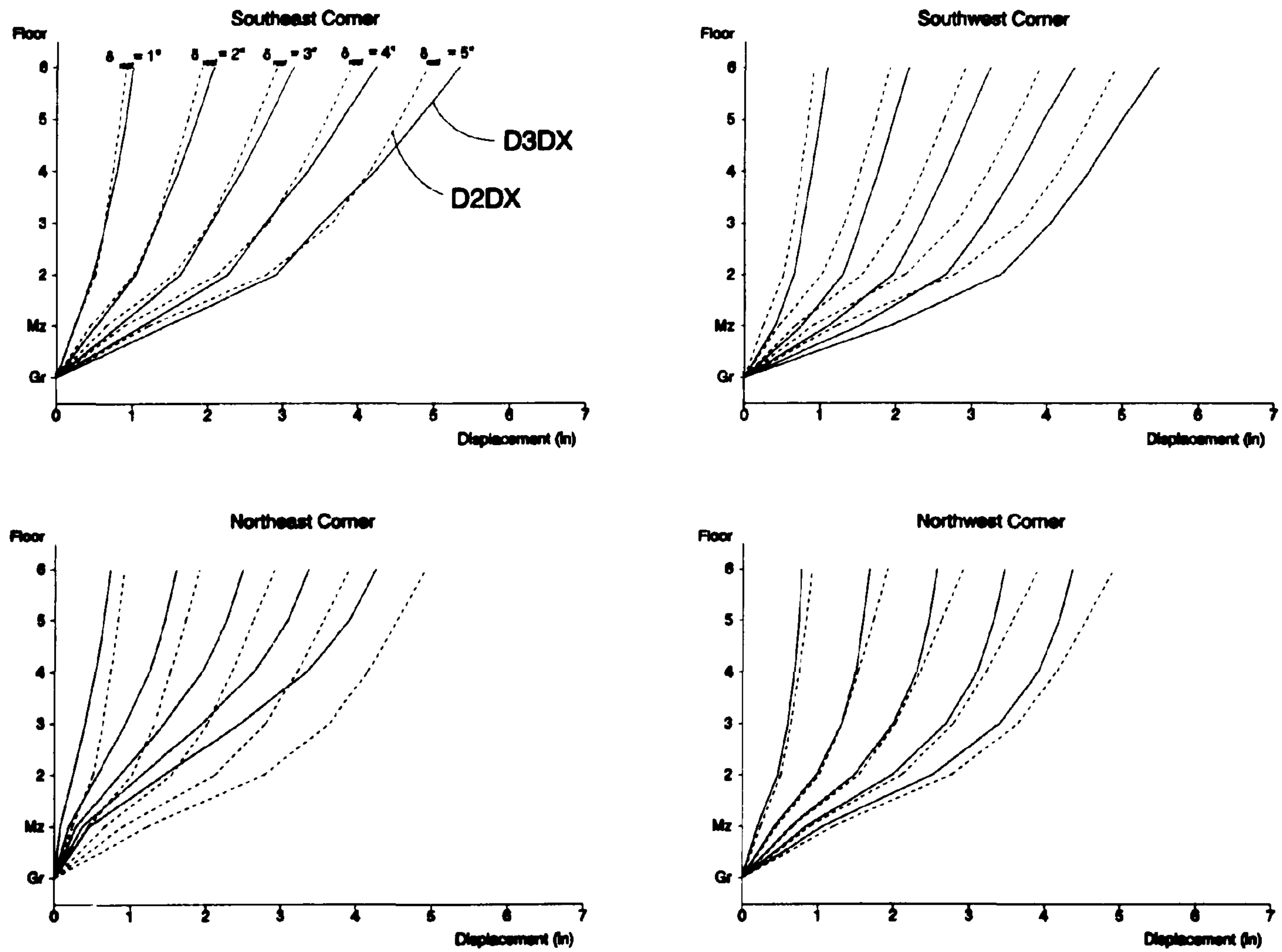

Figure 2.36 Comparison of floor displacements obtained from 2D and 3D (including torsional effects) pushover analysis, E-W direction

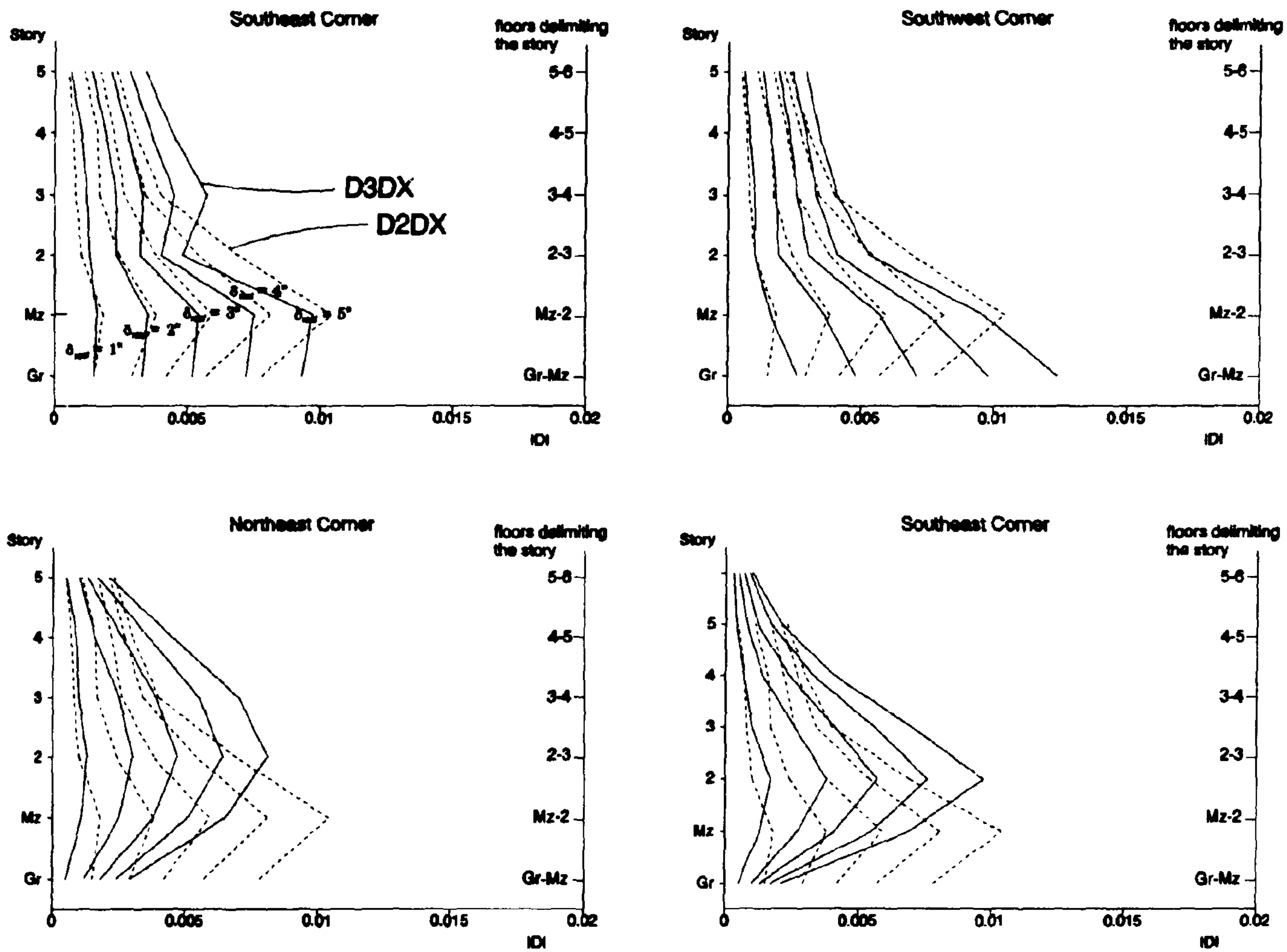

Figure 2.37 Comparison of IDI obtained from 2D and 3D (including torsional effects) pushover analysis, E-W direction

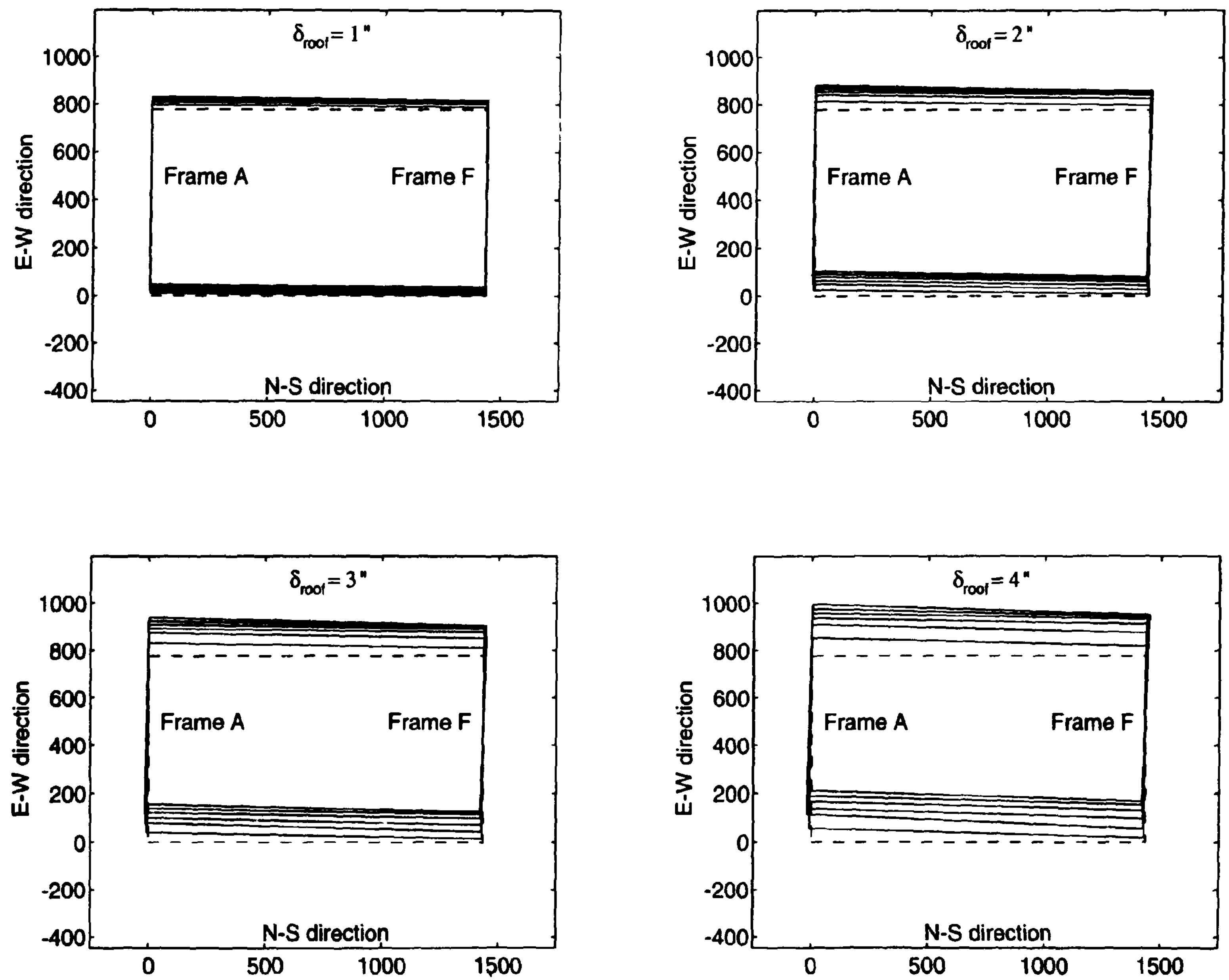

Figure 2.38 Displaced floor diaphragms from 3D pushover analysis of E-W direction of original building

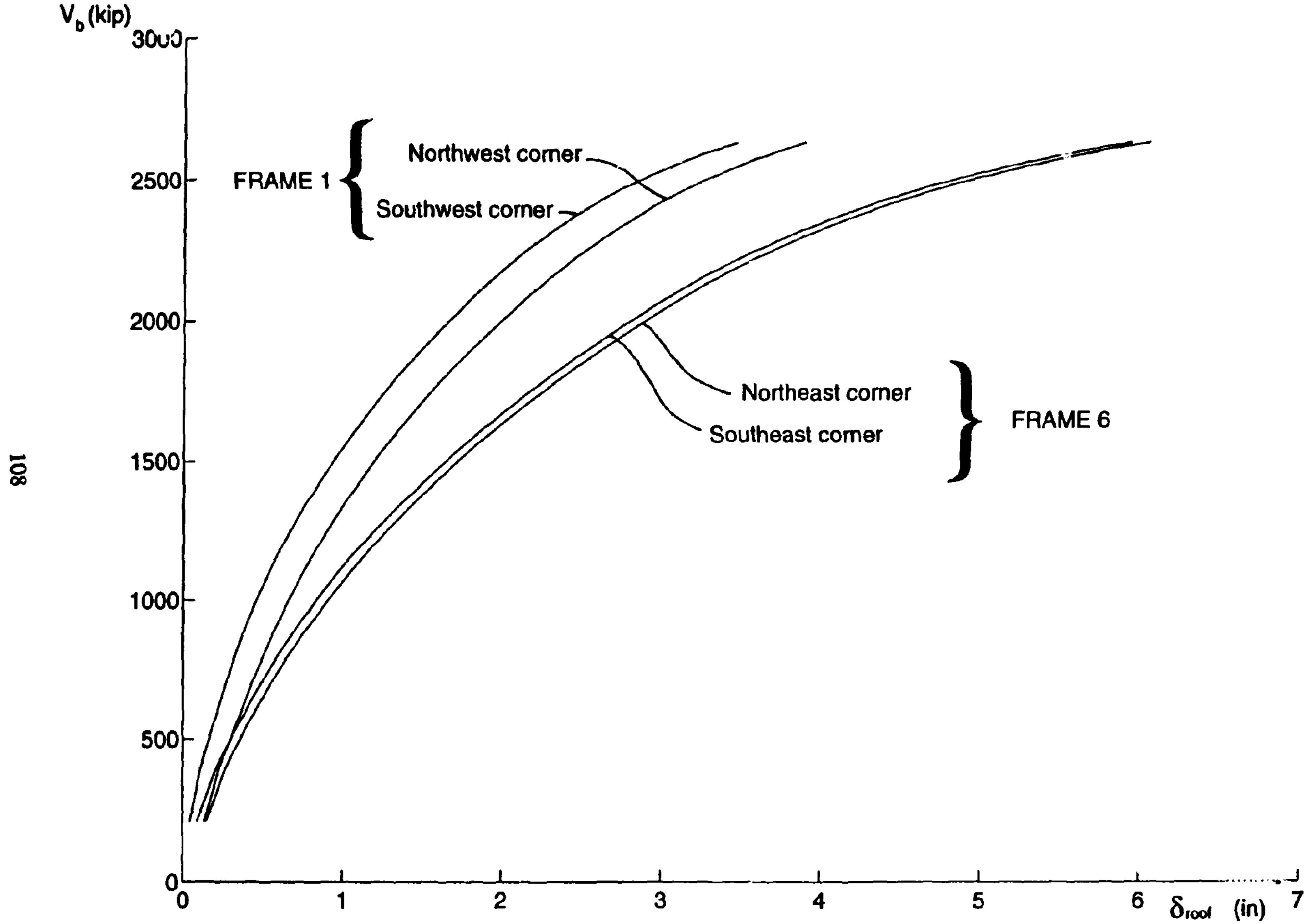

Figure 2.39 Roof displacement vs base shear curves from 3D pushover analysis of N-S direction of original building

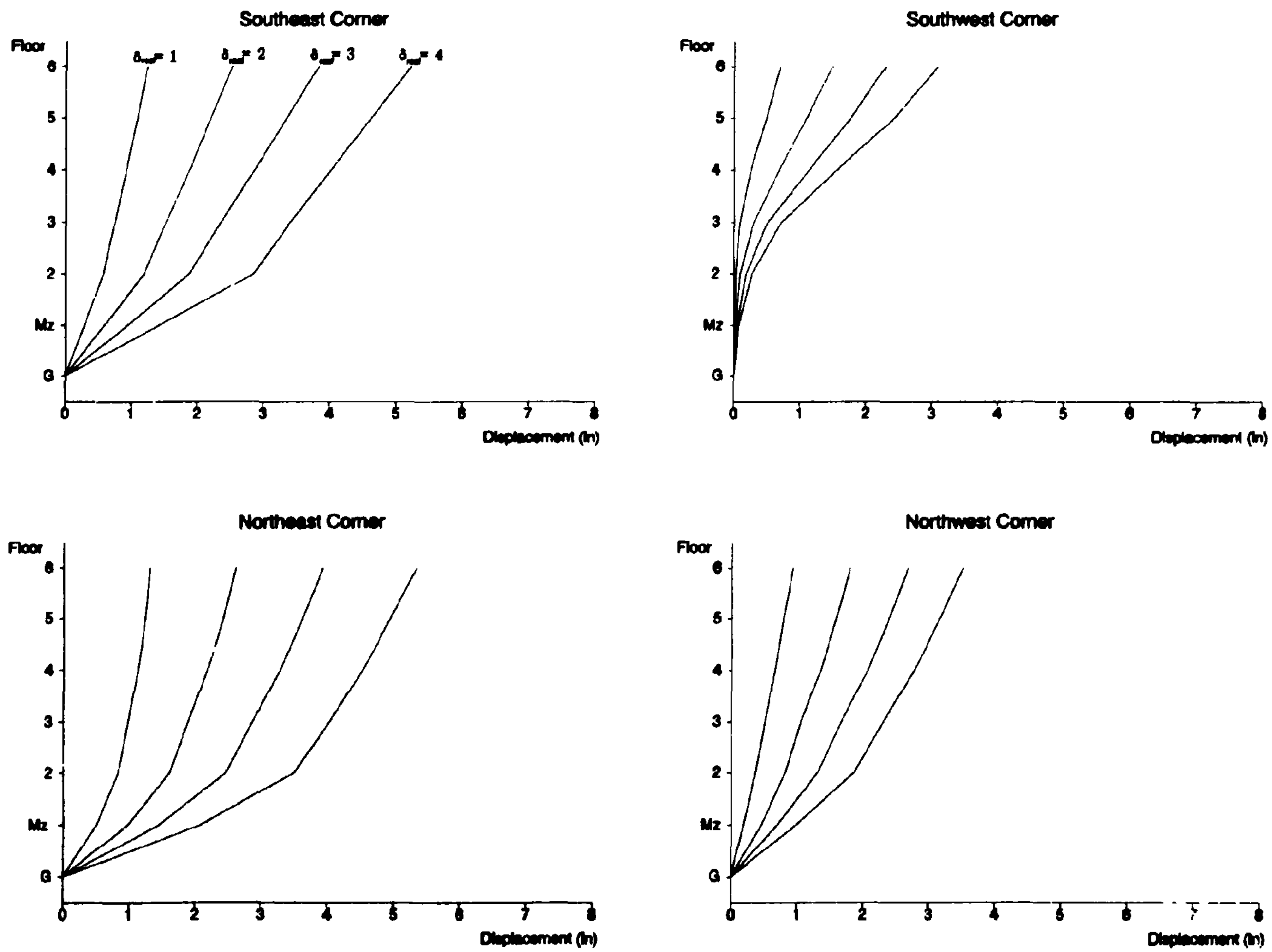

Figure 2.40 Floor displacements obtained from 3D (including torsional effects) pushover analysis, N-S directiion

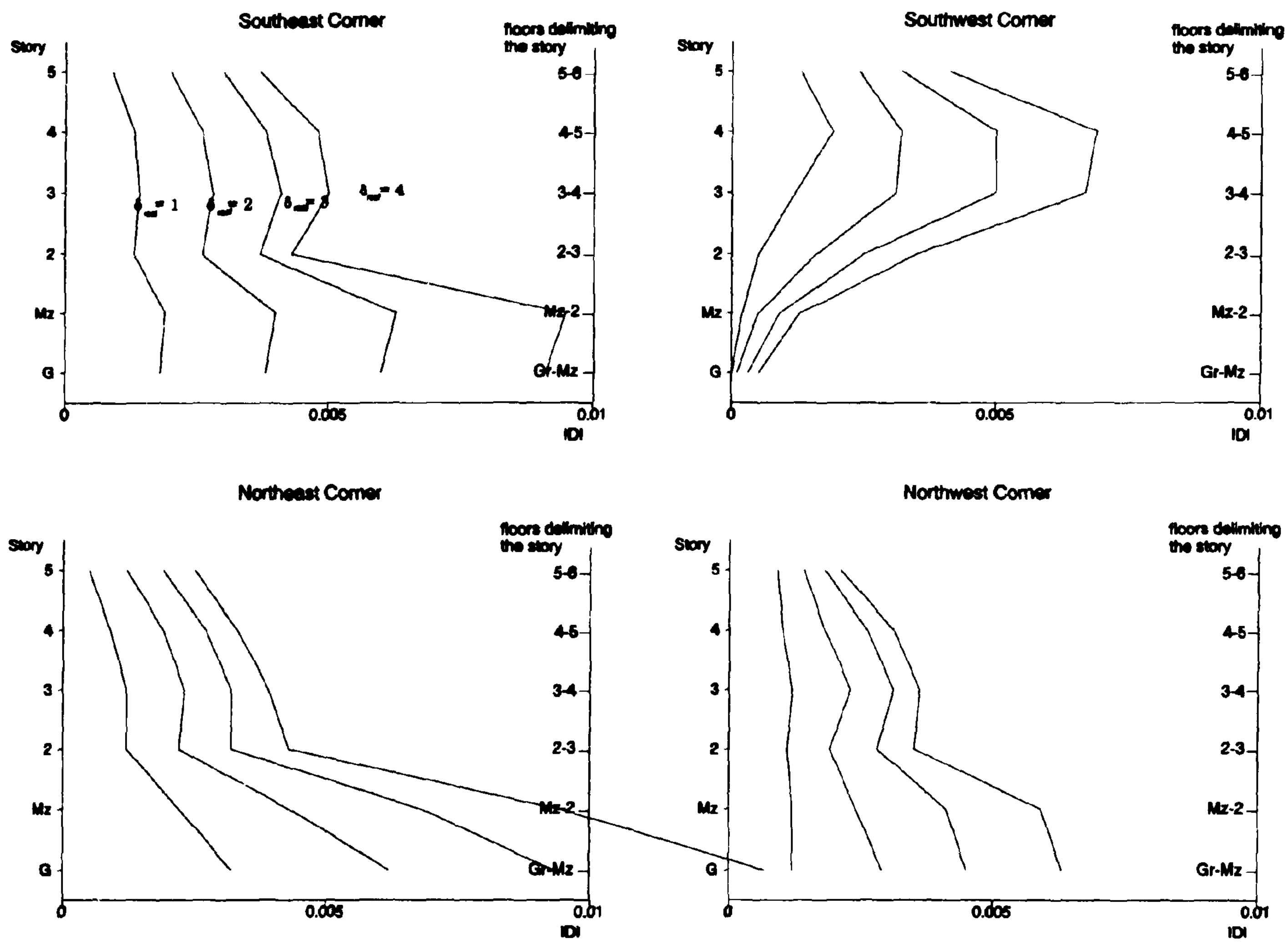

Figure 2.41 IDI obtained from 3D (including torsional effects) pushover analysis, N-S direction

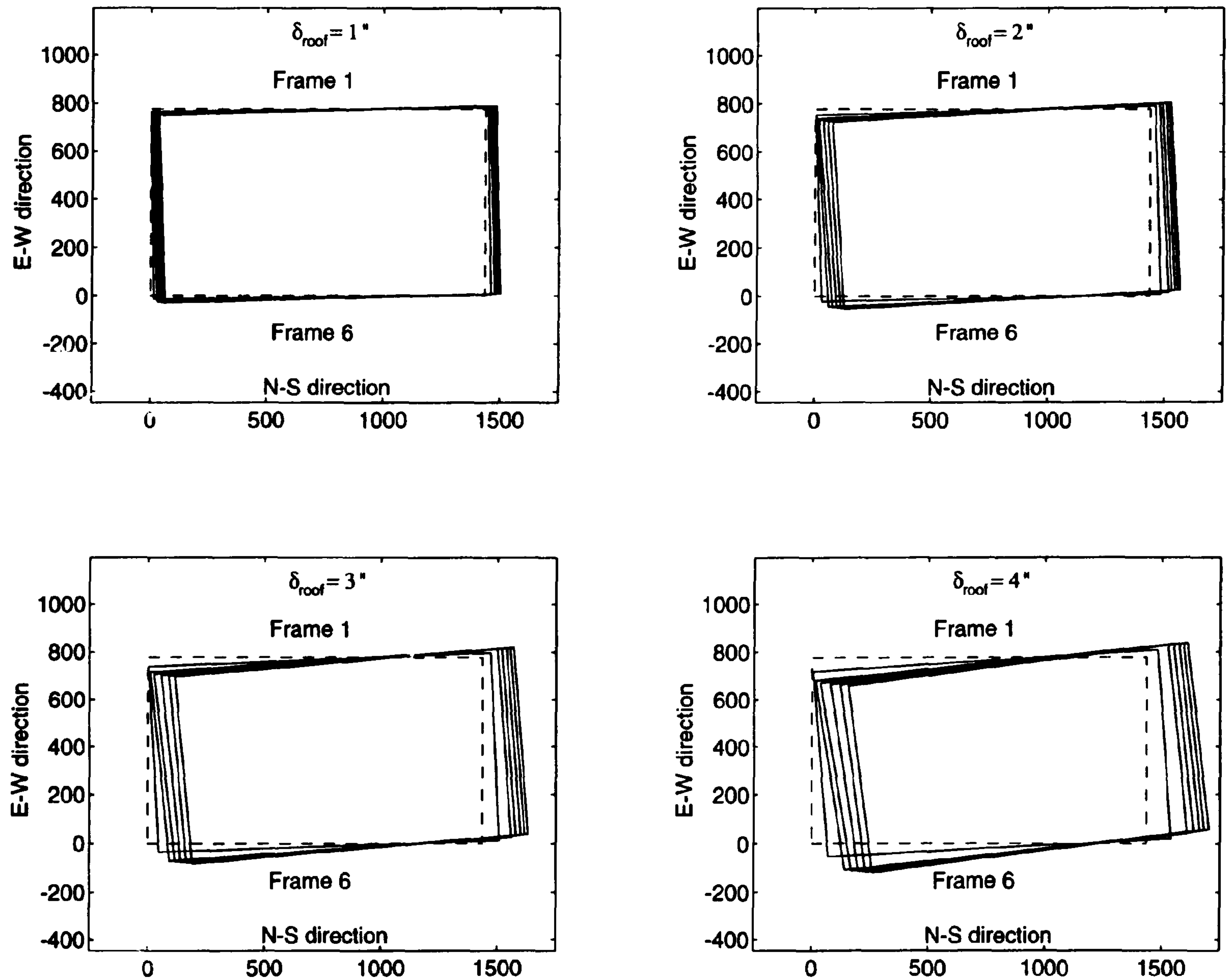

Figure 2.42 Displaced floor diaphragms from 3D pushover analysis of N-S direction of original building

3 REHABILITATION OF CASE BUILDING WITH POST-TENSIONED STEEL BRACES

In order to identify the advantages and disadvantages of using post-tensioned (PT) steel braces to upgrade the seismic performance of existing hazardous framed buildings with unreinforced masonry (URM) infills, the building described in Chapter 2 was considered for the application of this technique. In this chapter, a quantification of the target performance for the upgraded Pomona building is discussed. Then, an assessment of the performance of the existing Pomona building when subjected to the design earthquake ground motion (EQGM) and the design of a PT brace configuration to upgrade this building are carried out using a simplified methodology that is suitable for use in a practical context. Finally, the performance of the upgraded Pomona building is assessed based on the results obtained from several two-dimensional (2D) and three-dimensional (3D) elastic and nonlinear analyses.

3.1 TARGET SEISMIC PERFORMANCE

Several issues need to be addressed when defining the target performance of a structure at its different relevant performance levels. In the case of the Pomona building, an extra difficulty arises from the fact that the deformability capacity of its reinforced concrete (RC) members can not be established with precision. In this report, the definition of target performance will be based on limiting damage in structural and nonstructural elements within preestablished limits. To accomplish this purpose, it is necessary to provide a quantitative measure to the qualitative definition of damage in these elements. One way to accomplish this is by establishing relationships between the qualitative definition of damage and the global and local response of the building.

For instance, damage in RC members and URM walls can be estimated by using damage indexes, such as the Park and Ang damage index, DMI_{PA}, for RC members (Park et al. 1984) and the Kwok and Ang damage index, DMI_{KA}, for URM walls (Kwok and Ang 1987). In these indexes, damage in an element is computed as a linear combination of the damage produced by the maximum deformation demand and that produced by the cumulative hysteretic energy dissipation demand. Both indexes are computed with similar formulas:

$$DMI_{PA} = \frac{\delta}{\delta_{u,mon}} + \frac{\beta \int dE_H}{F_y \, \delta_{u,mon}}$$
$$DMI_{KA} = \frac{\delta}{\delta_{f,mon}} + \frac{\gamma \int dE_H}{F_u \, \delta_{f,mon}} \tag{3.1}$$

where δ = maximum deformation demanded by the EQGM; $\delta_{u,mon}$ = ultimate deformation capacity under monotonically increasing deformation; $\delta_{f,mon}$ = failure deformation capacity under monotonically increasing deformation; F_y = yield strength; F_u = ultimate shear capacity; dE_H = incremental dissipated hysteretic energy; and β and γ are non-negative parameters. Median values for β and γ are 0.15 and 0.075 (Cosenza and Manfredi 1990, Kwok and Ang 1987). Both damage indexes have been calibrated to quantify the level of damage in RC members and URM walls. For instance, a value of DMI_{PA} less or equal than 0.4 can be interpreted as reparable damage, larger than 0.4 as damage beyond repair, and larger or equal than 1.0 as collapse (Park et al. 1984).

In Section 1.5, it was mentioned that the main objective of introducing PT braces to an infilled framed building is to limit the displacement demands in the frames of the building in such a way that the existing beams and columns remain elastic (i.e., suffer small nonlinear demands) while the URM infills are used as stable energy dissipators. If, as discussed in that section, the frame members and PT braces remain elastic, there will be no hysteretic energy dissipation demands (cumulative nonlinear demands) in them; while the detrimental effects of these demands on the performance of the URM infills can be minimized if their maximum distortion is limited to values that enable these infills to exhibit a stable hysteretic behavior, and thus to exhibit a large supply of hysteretic energy dissipation. As a consequence, damage control in the existing elements can be achieved through drift control, and an adequate upgrading strategy consists in controlling the maximum demand of interstory drift index (IDI) in the building in such a way that the global hysteretic behavior of the upgraded building remains fairly stable during the ground motion.

From the above discussion, it is clear that the quantification of the performance criteria of RC elements and URM infills may be carried out by setting values for the maximum IDI allowed in the building. The level of damage in other nonstructural elements is usually associated with their maximum lateral deformation demand, and thus, damage in these elements can also be controlled by controlling the IDI in the building. In summary, damage control in structural and nonstructural elements of the Pomona building may be achieved by controlling the maximum IDI. Special attention should be given to story accelerations in the case of contents susceptible to acceleration. The following considerations were made to quantify IDI limits in the Pomona building:

■ **URM infills.** The IDI limit for damage control should be estimated according to the deformability capacity of the masonry. Kariotis et al. (1993) suggested a compressive strain at ultimate capacity (ε_u in Figure 3.1a) of 0.004 for the masonry in the building. This value is close to the average value of ε_u = .0042 obtained by Atkinson and Jan (1990) after an extensive statistical study of the mechanical properties of brick masonry. Thus, the deformability characteristics of the masonry of the Pomona building can be considered average. Figure 3.1b shows a lateral load vs. IDI curve, obtained using a nonlinear finite element program (Ewing et al. 1990) and monotonically increasing lateral deformation, for a typical URM infill without openings located in Frame 1 of the Pomona building. As shown in Figure 3.1b, the URM infill has a sudden and large decrease of lateral strength for IDI > 0.0035. This suggests that to avoid excessive degradation of stiffness and strength in this URM infill, its IDI demands should be limited to 0.0035. Figure 3.2 shows the IDI envelopes, obtained by analyzing the elastic 3D model described in Section 2.3.1, for the four perimetral frames of the building when it is subjected to the EQGMs recorded at the site during the Landers and Upland earthquakes (EQs). Figure 3.2c shows that the estimate of the maximum IDI in the ground story of Frame 1 during the Upland EQ reached values that exceeded 0.0020. While according to Figure 3.1b extensive cracking should have been expected in the URM infills of Frame 1 at IDI ≈ 0.002, no damage or cracking was reported in these URM infills after the Upland EQ. This suggests that the analytical procedure used in this report to predict the deformability capacity of the URM infills somehow underestimates this capacity, and that to limit the IDI of URM infills without openings to 0.0035 would probably be too conservative. As mentioned in Section 1.2.1, recent experimental results suggest that URM walls and infills show stable hysteretic behavior for relatively large values of IDI (0.005 and even larger). Thus, without ignoring the analytical results shown in Figure 3.1b, it would seem more realistic to limit the IDI in infills without openings to a value of 0.005. Finally, it is interesting to note that the lateral load vs. lateral displacement curve shown in Figure 3.1b has a shape similar to that corresponding to the masonry axial stress vs. axial strain curve shown in Figure 3.1a.

■ **RC members.** The deformation capacity of the existing RC members can not be established with precision due to the lack of information regarding the splicing and anchorage of their longitudinal reinforcement. As shown in Figures 3.2b and 3.2d, the IDI demands in the ground story of Frame A exceeded 0.005 during the Landers and the Upland EQs. Given that there was no report of damage in RC members during these EQs, it can be concluded that these members must be able to reach an IDI $\approx$ 0.005 without brittle failure.

■ **Nonstructural elements.** IDI limits strongly depend on the type of nonstructural element taken into consideration. For the current project, it was considered adequate to adopt the values suggested by Bertero and Bertero (1992). According to their recommendations, IDI in common nonstructural elements for the service and safety limit states must be limited to 0.003 and 0.0125, respectively.

From the analysis of the above values of IDI, it is clear that the controlling IDI at safety level is imposed by the URM infills, i.e. IDI $\leq$ 0.005. Although a multi-limit state performance criteria usually needs to be established to allow for a rational earthquake-resistant design (EQ-RD) of the upgraded building, the seismic rehabilitation of the Pomona building is based only on the safety limit state (see Appendix A). The target seismic performance chosen for the upgraded building is summarized in Table 3.1.

3.2 PRELIMINARY DESIGN OF THE POST-TENSIONED BRACING SYSTEM

In a practical context, it may be desirable to analyze not just one, but several alternatives to upgrade a building. If many alternatives are considered at the beginning of the EQ-RD process, it may be impossible to analyze each one in detail. In this case, it is desirable to establish simple preliminary analysis procedures that allow for the identification of the most promising alternatives. Once these have been identified, detailed analyses of each of them can be carried out to decide which can be implemented in the existing building.

In this section, the basis for a simplified analysis procedure based on the use of single-degree-of-freedom system (SDOFS) and stick models of the building is discussed. This simple procedure was used to study different upgrading alternatives using PT braces. To do so, it was necessary first to establish the validity of this approach. This was done by creating SDOFS and stick models of the existing building, and then checking if a procedure based in the use of these models is capable of predicting reasonably well the global response of the building when subjected to EQGM.

3.2.1 MECHANICAL PROPERTIES OF THE POMONA BUILDING

Before attempting to analyze the behavior of the Pomona building, it is necessary to determine its global and story strengths and stiffness. Also, it is important to determine other of its characteristics that may affect its seismic performance, such as plan and height irregularities.

Usually, the practical engineer would need to prepare a detailed 3D model of the building to assess the need to upgrade it. This type of model will also need to be available to assess the performance of the building once it has been upgraded. Usually, although not ideally, the practicing engineer will use elastic analyses to identify the dynamic and mechanical characteristics, as well as structural deficiencies, of the existing building. As mentioned in Section 2.3.1, a 3D elastic model of the building is available. This elastic model was created during a research project (Kariotis et al. 1993) to reproduce the recorded response of the Pomona building during the Landers and Upland EQs. Although this model could not capture exactly all aspects of the behavior of the building, it provided reasonable estimates of the maximum recorded response. It is considered that the steps needed to develop a model like the one mentioned above are fairly simple and straightforward, so that it is feasible for a practicing engineer to create a similar model when working on a practical project. In the next sections, it is assumed that one such model exists.

■ **Story stiffness.** The story stiffness can be estimated using the available 3D elastic model. Lateral story forces were estimated using a triangular acceleration distribution over height, as shown in Figure 3.3. Two static analyses (one for each of the N-S and E-W directions) of the 3D elastic model were performed by applying these lateral forces to the center of mass of the floor diaphragms. The story shears and drifts obtained from the above analyses were used to estimate the story stiffness in each direction. The story mass and stiffness for each story, in both directions, are summarized in Table 3.2. From this table, the existence of a flexible mezzanine story in both directions is noticeable. Figure 3.4 shows how the floors and stories are identified herein, and that due to the existence of the mezzanine, some vertical elements (columns and URM infills) start at the ground floor and end at the second floor. Therefore, the ground and mezzanine stories cannot be considered as two separate stories, but rather as forming part of a larger flexible double story that can be interpreted as a flexible *first story*. As shown in Figure 3.1b, the lateral stiffness of URM infills strongly depend on the deformation demands to which they are subjected. The story stiffness shown in Table 3.2 are secant stiffness that were obtained for the deformation demands that the Landers and Upland EQs induced in the building. If other deformation levels need to be considered, it is necessary to adjust the value of the story stiffness accordingly.

■ **Story secant stiffness.** In order to determine the stiffness of the PT braces, it is convenient to determine the lateral story stiffness at different deformation levels. Modifying the 3D elastic model to determine these stiffness would be very time consuming. Thus, it becomes necessary to come up with a simple method to estimate secant story stiffness. A simple and reasonable way to estimate the secant stiffness of the URM infills in a story is to establish a target value of IDI in the infills, and with this value of IDI and the IDI vs. lateral force curves corresponding to the different URM infills (shown in Figure 2.8) determine the secant stiffness for each individual infill. Then the total stiffness of all URM infills in a story can be estimated as the sum of the secant stiffness of all individual infills. The total story stiffness can then be estimated by adding that provided by the URM infills plus that provided by the RC members. Note that because the target IDI is restricted to small values (IDI < .005), and the RC members are supposed to remain elastic (have small nonlinear demands), it is reasonable to assume that their stiffness remains constant once the concrete cracks (i.e., no need to determine secant stiffness for RC members to estimate the total story secant stiffness). Using this simple method, the lateral story stiffness corresponding only to the infills and computed for the deformation demands associated with the Upland and Landers EQs are shown in column (2) of Tables 3.4 and 3.5.

The above method to estimate the story secant stiffness of the infills is based on the assumption that the infills are subjected exclusively to shear deformation. This is not always the case, especially for infills located in the top stories of slender buildings. In the latter case, the infilled frame would not behave as a shear beam, but flexural deformations can become relevant. A more formal way to estimate the contribution of the URM infills to the story stiffness is to use the available 3D elastic model of the building. For this purpose, a second analysis needs to be carried out on this model, but this time without URM infills. An estimate of the lateral stiffness of the infills can be obtained by subtracting the stiffness obtained from both 3D elastic models (with and without infills). These estimates are summarized in Table 3.3 and column (1) of Tables 3.4 and 3.5.

Note in Tables 3.4 and 3.5 that the approximate method [column (2) in the tables] yields reasonable estimates of the URM infills story stiffness obtained using the 3D elastic model [column (1) in the tables], except for the two top stories in the E-W direction. Thus, the simplified procedure might be used to estimate story stiffness of the URM infills for different target IDI. In this report, the URM infills' story stiffness for a target IDI of 0.005 were estimated using the simplified procedure by assuming a constant IDI of 0.005 over height. These values of the secant story stiffness of the infills for an IDI of 0.005 were then corrected using the factor shown in columns (3) of Tables 3.4 and 3.5. This correction will usually only be necessary for the infills located in the top stories of slender infilled frames. The corrected stiffness values for an IDI of 0.005 are shown in the last columns of Tables 3.4 and 3.5.

The important issue underlying the above discussion is not the way in which the secant story stiffness have been determined, but the fact that it is useful to establish a simple and reasonable method to do so. The existence of a flexible *first story* in the Pomona building can be noted in the values of story stiffness shown in Tables 3.4 and 3.5. It should be mentioned that in the original Pomona building the stiffness of the *first story* decreases relative to that of the other stories (the flexible *first story* becomes more pronounced) as the lateral displacement of the building increases. Figure 3.5, shows that because there is larger concentration of deformation in the two bottom stories, their secant stiffnesses depart more from their initial stiffnesses than those corresponding to stories 2 to 5.

■ **Story and global lateral strength**. To estimate the ultimate strength of the building, a simplified procedure was used. This procedure, originally proposed by the Japan Building Disaster Prevention Association, was modified by Iglesias et al. (1986) to apply it to Mexican RC construction. A simple adaptation of some of the values proposed by Iglesias et al. was carried out to address the difference between Mexican and American practices. The method assumes that the lateral strength of the ith story, V_{Ri}, of an existing low-rise building can be estimated as the sum of the shear resistance of the different vertical elements within that story (i.e., columns and URM infills) according to the following formula:

$$V_{Ri} = [\alpha_1 v_m \Sigma A_m + \alpha_2 v_M \Sigma A_M + \alpha_3 v_c \Sigma A_c] \tag{3.2}$$

where α_1, α_2, α_3 are the participation factors; v_m, v_M, v_c the resisting shear stress of masonry walls, RC walls and RC columns, respectively; ΣA_m, ΣA_M, ΣA_c total area on a story of masonry walls, RC walls and RC columns, respectively.

The ultimate strength in the ith story (V_{ui}) is obtained as:

$$V_{ui} = q_1\, q_2\, q_3\, q_4\, q_5\, V_{Ri} = 0.64\ V_{Ri} \tag{3.3}$$

where q_i are corrective factors from Table 3.6. The ultimate strength of a given story is considered to be reached when its URM infills reach their ultimate strength. For this case, α_1=1.0 and α_3=0.5 (note that A_M = 0 because there are no RC shear walls in the building). From the recommendations given by Iglesias et al., v_c = 7 kg/cm^2. The value of v_m was computed according to UBC 1991 as:

$$\begin{aligned} v_{mcr} &= (\ 3.5\ -\ 1.75\frac{M}{Vd}\sqrt{f_m}\ ) \\ v_{mu} &= (\ 5.0\ -\ 2.5\frac{M}{Vd}\sqrt{f_m}\ ) \end{aligned} \tag{3.4}$$

where v_{mcr}, v_{mu}, f_m and M/Vd are the cracking shear stress, the ultimate shear stress, the compressive strength and the shear span, respectively, of the masonry element. M/Vd was considered equal to one for values larger than one. The ultimate strength of the masonry can also be estimated from the available lateral force vs. IDI curves shown in Figure 2.8.

The estimated story strengths in the N-S and E-W directions are summarized in Tables 3.7 and 3.8, respectively. In these tables, the strength of the columns already include an α_3 of 0.50, and the total story strength is equal to 0.64 times the sum of the strength of the columns and infills. Also, in these tables, the story at which the building is likely to fail (critical story) and the base shear strength demand on the building when this failure occurs, 1729 kips in the N-S direction (V_{bx}=0.28W) and 863 kips in the E-W direction (V_{by}=0.14W), are outlined with an arrow. Note that the previous values are not the story shears corresponding to the critical stories, but the values of the base shear at the moment when the critical story fails (i.e. reaches its ultimate capacity). The critical stories were determined by assuming a linear distribution of accelerations over height. It should be noted that there is a weak *first story* in both directions (the ground and mezzanine stories are considered to form part of the weak *first story*). Adding this result to the fact that there is a *first soft story* in both directions (as shown in Table 3.2), it can be concluded that the building shows a weak and soft *first story*.

The values of V_{by} and V_{bx} estimated above are compared in Figure 2.34 to the values obtained from 3D nonlinear pushover analyses of the building. The pushover curves were obtained without consideration of the real deformability capabilities of the elements of the building. Considering that the Pomona building is formed by non-ductile RC frames, the maximum IDI that its RC elements can actually undergo without failure must be around .01. This IDI occurs when δ_{roof} is around 3", which means that the building is likely to reach its ultimate strength for this value of δ_{roof}. Taking this into consideration, it can be concluded from Figure 2.34 that the simple method described above yields reasonable estimates of the ultimate strength of the building.

■ **Plan irregularities.** The Pomona building has a very high torsional response, which is caused by pronounced plan irregularities. An attempt was made to account for these irregularities in a simple manner. For this purpose, it was necessary to determine the location of the center of stiffness (center of elastic resistance) for each story in the N-S and E-W direction. The center of elastic resistance is defined as the point on the floor diaphragm through which the application of a static horizontal force causes no rotation of the diaphragm, no matter in what direction the force is applied (Hejal and Chopra 1987). Two different methods were used to estimate the location of the centers of elastic resistance, a simple one and a formal one. This was done to establish whether the simple procedure yields reasonable estimates of the location of these points. The simple method consists in estimating the story stiffness for each frame in the building, and then estimating the location of the center of elastic resistance as follows:

$$(X_{cr}, Y_{cr})_j = \left(\frac{\Sigma x_j k_{xj}}{\Sigma k_{xj}}, \frac{\Sigma y_j k_{yj}}{\Sigma k_{yj}}\right) \tag{3.5}$$

where $(X_{cr}, Y_{cr})_j$ is the location of center of stiffness in the jth floor; x_j and y_j the location of frames contributing stiffness to the Y and X direction, respectively, in the jth story; and k_{xj} and k_{yj} the frame stiffness in the X and Y direction, respectively, in the jth story.

The formal method consists in trying to locate the centers of elastic resistance by using the 3D elastic model of the building. This was done by moving the points at which the story lateral forces are applied to their corresponding floor diaphragm, until no rotation (or very small rotation) of all the floor diaphragms is observed. A linear distribution of acceleration over height was assumed to obtain the story forces, and they were applied statically. One of the biggest problems involved in the determination of the centers of elastic resistance using the formal method was the fact that it was time consuming (the lateral and the torsional stiffness of the stories varied considerably as a function of the location of the point at which the static lateral forces were applied).

The location of the centers of mass and elastic resistance in each floor diaphragm, according to the simple and formal methods, is summarized in Table 3.9. The distances given in this table are measured from the southeast corner of the building and, as a remainder, the dimensions of the building are 120' and 65' in the N-S and E-W directions, respectively (see Figure 2.1).

It should be noted that the center of elastic resistance could not be estimated using the formal method for the bottom two stories in the N-S direction (at least not according to the definition given before). Riddell and Vasquez (1984) note that the existence of the center of elastic resistance is restricted to a particular class of buildings and that for a general multistory building such a concept is physically meaningless. They also note that when centers of resistance exist, they all lie in a vertical line, which implies certain plan regularity with height. It should be noted that stories 2 to 5 have very similar plan layouts, while the plan layouts of the ground and mezzanine stories are considerably different. The results obtained using the formal methods tend to support the Ridell and Vasquez conclusions: in the portion of the structure that has the same structural layout over height (stories 2 to 5, which correspond to floors 3 to 6), the center of elastic resistance exists and is on a vertical line; while in the lower stories, this center does not exist (the center of elastic resistance was not located within the floor diaphragm).

It can be seen that both methods yield similar locations for the centers of elastic resistance, which implies that the simplified method gives reasonable estimates of such locations. Table 3.9 also gives the location of the center of mass of each floor diaphragm. From this table, it can be concluded that the eccentricity in the E-W direction (perpendicular to N-S loading) is in general very large, while that in the N-S direction (perpendicular to E-W loading) is less significant, except in the ground and mezzanine stories. The results summarized in Figures 2.38 and 2.42 support the previous observations.

3.2.2 SIMPLIFIED ASSESSMENT OF THE POMONA BUILDING'S PERFORMANCE

In this section, the use of SDOFS and stick models to assess the performance of the Pomona building is discussed. This is done to introduce the notion that the global behavior of a building can sometimes be represented fairly well by using simple models. The availability of simple models becomes relevant when several alternatives for the upgrading system are being considered, because in this case it is not possible to study them all using a complex analysis model. The creation of the SDOFS will be carried in two steps. In a first step, the available information of the mechanical characteristics of the building is used to create a stick model as that shown in Figure 3.6a. Once this information has been condensed in the stick model, this model is used to create the SDOFS model.

The need to create the stick model will become clear in Section 3.2.3. In summary, the preliminary analysis and design of the PT bracing system is carried out with the aid of the stick model (the 3D elastic model is not used in this preliminary phase). The reason that it is convenient to create a SDOFS model from the stick model is to provide, with the use of the appropriate strength and displacement spectra, a graphical representation of the expected response of the building when subjected to EQGM (this will be illustrated later by using Figures 3.7 to 3.9).

Two stick models (one for each of the E-W and N-S directions) were created using the properties summarized in Table 3.2. To check the adequacy of the stick models, their dynamic characteristics were estimated by solving the following eigenvalue problem:

$$K\phi = \omega^2 M\phi \tag{3.6}$$

where K is the stiffness matrix, M the mass matrix, ω^2 the eigenvalue (square of the frequency) and ϕ the corresponding eigenvector.

The dynamic properties of the stick models of the Pomona building are summarized in Table 3.10. The fundamental periods of translation estimated using these stick models are 0.55 and 1.00 in the N-S and E-W directions, respectively. These values are close to those estimated using the 3D elastic model of the building (0.51 and 1.04 sec, respectively). As shown by the results in the table, the modal mass corresponding to the first translational mode in each direction is around 90% of the total mass. This implies that the base shear demand on the building can be estimated reasonably well from the response of the fundamental mode of translation of the stick model. The previous observation is very important, because it implies that the global response of the building can be represented fairly well using a SDOFS, which is obtained from the fundamental mode of translation of the stick model.

The creation of the SDOFS model once the stick model has been established is straightforward. The periods shown in Table 3.10, corresponding to the fundamental periods of translation of the stick models in both directions, are assigned to the SDOFS models used to capture the global response of the building in those directions. A damping coefficient (ξ) equal to 0.02 will be used to assess the response of the SDOFS models (to be consistent with the value of ξ used in section 2.3.1 for the analysis of the 3D elastic model). Given that practically all the building's mass is associated with the first translational mode of the building, the values of V_b given in Tables 3.7 and 3.8 are assigned as the strength of the SDOFS.

To assess the performance of the building using a SDOFS model, it is necessary to relate the maximum displacement demand on the SDOFS (δ_{SDOFS}) to the global displacement demands on the building itself. This can be done by defining a coefficient of distortion as IDI_{max}/IDI_{avg}, where IDI_{max} and IDI_{avg} are the maximum IDI and average IDI, respectively, in the building. An estimate of IDI_{avg} can be obtained by using the response of the SDOFS (in particular, δ_{SDOFS}) and the mode shape of the fundamental mode of vibration (ϕ_1) of the corresponding stick model as follows:

$$IDI_{avg} = \frac{\delta_{roof}}{H} = \frac{\Gamma\ \phi_1(H)\ \delta_{SDOFS}}{H}$$
$$where\ \ \Gamma = \frac{\phi_1^T M 1}{\phi_1^T M \phi_1} \tag{3.7}$$

and δ_{roof} is the displacement demand in the roof, H the total height of the building and the other variables have been defined before.

The coefficient of distortion (c.o.d.) can be approximately defined as the product of the coefficients of distortion in plan and height [$(c.o.d.)_\theta$ and $(c.o.d.)_H$, respectively]. The coefficient of distortion in plan for a given floor is defined as the ratio of the floor displacement at the end frame normalized by the floor displacement at the center of mass. The coefficient of distortion can be estimated directly from the results of a static analysis of the available 3D elastic model of the building. Nevertheless, estimating the coefficient of distortion using this method can be time consuming if several upgrading alternatives are considered.

A reasonable estimate of the coefficient of distortion in height can be obtained using the mode shape corresponding to the first mode of the stick model (i.e., ϕ_1). Also, if the lateral stiffness of all frames at a given story are available, it is possible to obtain the translational and torsional stiffness of every story, and with that, the translation and rotation of each diaphragm when the building is subjected to lateral loads. Using the translational and torsional stiffness of every story to estimate the coefficient of distortion in plan, and the first mode of the stick model to estimate the coefficient of distortion in height, the values summarized in Table 3.11 were obtained. As shown, values of 2.6 and 2.7 were obtained as coefficients of distortion in the E-W and N-S directions, respectively. The value of c.o.d. establishes a relation between IDI_{max} and IDI_{avg} as follows:

$$c.o.d. = (c.o.d.)_H \ (c.o.d.)_\theta = \frac{IDI_{max}}{IDI_{avg}} = \frac{IDI_{max}}{\frac{\Gamma \phi_1(H) \delta_{SDOFS}}{H}} \tag{3.8}$$

$$IDI_{max} = \frac{\Gamma \phi_1(H) \delta_{SDOFS}}{H} (c.o.d.)_H \ (c.o.d.)_\theta$$

where all variables have been defined before.

An IDI_{max} of 0.005 occurs when the value of δ_{SDOFS} is equal to 1.3" and 1.1" in the E-W and N-S direction, respectively. These δ_{SDOFS} correspond to roof displacements (δ_{roof}) of about 1.6" in both directions. Note that different values of δ_{SDOFS} in the E-W and N-S directions led to a similar value of δ_{roof} in both directions. This can be explained because of the different values of the product Γ ϕ_1(H) [see Table 3.11 and refer to equation (3.7)], which in turn reflect the fact that the fundamental mode shapes in both directions are different..

The values of coefficient of distortion obtained above are similar to those obtained using the elastic 3D model of the building. For the Landers EQ, the following results were obtained in the 3D elastic model: the maximum values of δ_{roof} (occurring at the center of mass of the roof diaphragm) in the N-S and E-W direction were 0.5" and 1.6" respectively, while the values of IDI_{max} were 0.0019 and 0.0057, respectively. Assuming a linear relationship between δ_{roof} and IDI_{max} in the N-S direction, a δ_{roof} of 1.6" would be associated with an IDI_{max} of 0.0058, while in the E-W direction a δ_{roof} of 1.6" is associated with an IDI of .0057. For the simple method proposed to estimate c.o.d., a δ_{roof} of 1.6" has been associated with an IDI_{max} of 0.005 in both directions. It can be concluded that the value of coefficient of distortion estimated according to a simple methodology gives reasonable quantification of the plan and height irregularities in the building.

Finally, the performance of the building can be assessed by using the properties of the SDOFS models (period, T, base shear strength, V/W, and maximum acceptable displacement, δ_{max}) in the appropriate strength and displacement spectra. This is shown in Figures 3.7 and 3.8. In Figure

3.7, it can be seen that the building has enough strength to survive the recorded EQGMs with a global displacement ductility demand (μ) around 1; nevertheless, as shown in Figure 3.7d, in case of the Upland EQ the elastic strength demand is very close to the ultimate strength of the building. The horizontal lines at 1.2" (3 cm) in Figure 3.8 represent the displacement of the SDOFS associated with an IDI_{max} = 0.005. As shown in Figures 3.8a and 3.8c, the displacements for the SDOFS and a μ of 1 are well below 1.2" for the N-S direction ($T \approx 0.5$ sec), while they are very close to this limit for the E-W direction ($T \approx 1.0$ sec). It can be concluded from the use of the SDOFS models that the stiffness and strength supplies in the building are adequate to limit IDI_{max} to values less than 0.005, although for the E-W direction IDI_{max} is practically equal to 0.005. As shown in Figures 3.2b and 3.2d, the maximum IDI predicted for these same EQs using the elastic 3D model of the building are slightly larger than 0.005, which emphasizes one more time that the SDOFS model can predict reasonably well the response of the building.

Large simplifications were made when idealizing the Pomona building as a SDOFS. Some of them are conservative, e.g., neglecting the energy dissipation capacity provided by the URM infills, assigning the total mass of the building to the SDOFS, etc.; while others are not conservative, e.g., assuming that the coefficient of distortion computed elastically will not increase with higher strength and displacement demands, etc. Nevertheless, it can be concluded that the simplified model gives a reasonable estimate of the building's global response.

According to Figures 3.7 and 3.8, it can be concluded that when the building is subjected to the Landers and Upland EQs, it remains basically elastic and its IDI_{max} is around 0.005. Thus, its performance can be considered satisfactory during these EQs. Nevertheless, this assessment changes considerably when the supplies in the building are compared to the demands produced by what has been defined in Appendix A as the design EQGM for safety (which was obtained for a ξ of 0.05). As shown in Figure 3.9a, the strength of the building is clearly insufficient in both directions to limit the value of μ to within reasonable values ($\mu > 4$ in the E-W direction and $\mu \approx 3$ in the N-S direction). Regarding the stiffness of the building, the continuous horizontal line labeled as *unbraced* in Figures 3.9c and 3.9d shows the δ_{roof} at which $IDI_{max} \approx 0.005$. As shown in Figure 3.9c, the demanded δ is larger than this value for both the N-S and E-W directions. Thus, IDI_{max} is larger than 0.005 in the N-S direction and considerably larger than that in the E-W direction.

3.2.3 Preliminary analysis and design of the post-tensioned bracing system

As mentioned, the advantage of creating the stick model becomes more apparent when the performance of different upgraded versions of the building need to be compared, because in this case very simple alterations to this model permit the analysis of a new version of the upgraded building. In this context, the complexity of the 3D elastic analysis would not allow the comparison of several alternatives. Once the range of possibilities has been reduced using the stick model, detailed analyses can be carried out on a few promising configurations. In this section, the use of the stick model to assess the *performance of the upgraded building* when subjected to the safety EQGM is illustrated.

In the design of the PT braces, it is not enough to meet the strength demands in the building because its seismic performance strongly depends on its displacement demands. Strength and displacement demands should be considered simultaneously in the preliminary design of the braces. The design for strength for life safety performance of the bracing system is simplified because the braces should be designed to remain elastic. As mentioned in Section 1.5, the *overall* stiffness of the PT bracing system depends on the following:

• For efficient EQ-RD, it is desirable for the bracing system to have stiffness such that the existing URM infills can contribute to carry an important percentage of the lateral load. In this way, the URM infills can dissipate part of the energy input to the building.

• The stiffness of the bracing system needs to control the lateral displacement of the building in order to control structural and non-structural damage, and to allow for stable hysteretic behavior in the URM infills (i.e. $IDI_{max} < 0.005$).

The *relative* stiffness of the bracing system in plan and height should attempt to correct the existing lateral stiffness and strength irregularities. In the case of the Pomona building, the braces should stiffen and strengthen considerably the first two stories as compared to the upper stories, and reduce the large plan eccentricities, particularly in the first two stories.

In a given story, the total area of braces (A_T) and their lateral stiffness are related as follows:

$$K_{br} = \Sigma \frac{A_i E}{L_i} \cos^2\alpha_i$$
$$A_T = \Sigma A_i \tag{3.9}$$

where K_{br} is the required stiffness of the bracing system; and α_i, L_i, A_i and E are defined in Figure 3.10.

The strength of the bracing system in a given story can be estimated as:

$$\sigma_{br_i} = \frac{E\,\Delta}{L_i} \cos\alpha_i$$
$$V_{br} = \Sigma \sigma_{br_i} A_i \cos\alpha_i \tag{3.10}$$

where Δ is the interstory displacement and V_{br} the lateral strength of the bracing system.

In the E-W direction, the main design concern is to provide displacement control. For this purpose, the fundamental period in this direction (T_{E-W}) needs to be reduced from 1.00 sec to about 0.5 sec if the current values of coefficient of distortion remain unchanged, as shown in Figure 3.9c. Nevertheless, the irregularities of stiffness and strength in height and plan are reduced by the introduction of the PT braces, and thus the value of coefficient of distortion diminishes, as reflected by the discontinuous horizontal line labeled as *braced* in Figure 3.9c. Once T_{E-W} is established from a displacement control point of view, it will be necessary to supply adequate lateral strength to the building according to Figure 3.9a. In the N-S direction, displacement control does not seem to be an issue, as shown in Figure 3.9c. Nevertheless it is necessary to increase the strength of the building to reduce its global μ demands (of about 3) and to reduce the existing irregularities of strength and stiffness. The problem is that when attempting to accomplish this, the fundamental period of the structure in this direction (T_{N-S}) diminishes from its initial value of 0.5 sec, and the seismic response for μ close to 1.0 in the N-S direction of the building increases considerably as T_{N-S} decreases from 0.5 towards the value of 0.4 sec, as shown in Figure 3.9a. In this context, it is important to note that from the point of view of strength and displacement demands (Figure 3.9a and 3.9c), base isolation by itself will not be very effective until T > 2.5 sec. Also, it should be noted that nonlinear behavior in the building will result in a significant reduction of the demanded strength. This emphasizes the need to provide the upgraded building with some plastic hysteretic energy dissipation capacity.

■ **Selection of layout (configuration) of bracing system.** An ideal solution is to place the PT braces in the perimeter of the building. However, aside from the structural properties of the bracing system, probably the most important consideration needed to determine its final configuration is related to the architectonic and functional integrity of the building. These types of considerations significantly influenced the proposed configuration of the PT bracing system. It should be mentioned that it was virtually impossible not to alter the existing distribution of space within the building.

Figure 3.11 shows a schematic plan view of the building, in which the resisting planes are identified with numbers in the N-S direction: 1, 23, 47 and 6; and with letters in the E-W direction: A, B, C, D, E and F. Figure 3.11 shows the proposed location in plan of the PT braces, while Figures 3.12a to 3.12e show schematically the location in height.

The properties and geometry of what was considered the best two alternatives for the PT bracing system are summarized in Tables 3.12 to 3.14 and Figures 3.11 and 3.12. As shown in Figure 3.12, the first option (configuration 1) consists in adding braces to four planes of resistance: 23 and 47 in the N-S direction, and C and E in the E-W direction; while the second option (configuration 2) consists in adding to the previous four planes one more plane of resistance in the E-W direction (one more braced bay located in Frame B). An asymmetric distribution of braces in the planes of resistance parallel to the N-S direction was provided to correct the large torsional response of the building when loaded in this direction (see Figure 2.42). Each diagonal in Figure 3.12 represents two braces, which were provided in this way as to avoid inducing large load eccentricity to the existing elements. As shown, each brace spans two stories, which results in angles α_i (Figure 3.10) that allow for an efficient solution. Four different types of braces were considered, as shown in Tables 3.12 to 3.14. As shown, the sizes of the braces in the lower two stories are considerably larger than those in the upper four stories, in such a way as to avoid the existence of a flexible and weak *first story*.

One of the problems that needs to be considered carefully with the proposed upgrading configurations is the need to strengthen some existing columns in such a way that they can resist adequately the increase in axial loads induced in them by the braces, particularly those columns that support braces in both directions, such as those in the intersection of the following frames: 23 and C, 23 and E, 47 and B, and 47 and E. Figures 3.12c and 3.12d illustrate the need to add new beams to frames C and E in such a way that the braces have enough support at the floor levels (i.e., to avoid the buckling of the slab).

In the next paragraphs, the use of the stick model (Figure 3.6) to estimate the response of the building when upgraded with brace configuration 1 will be illustrated. For this purpose, the stick model created before was slightly changed to include the bracing system, as shown in Figure 3.6b. The mass of the braces on this model were neglected, given that they are small when compared to the building's original total mass. Table 3.15 summarizes the dynamic characteristics of the first translational modes estimated from the stick models corresponding to the E-W and N-S directions.

Figure 3.9a illustrates the lateral strength of the building upgraded with brace configuration 1 (obtained by adding the strength of the original building plus that provided by the PT braces) relative to the design strength spectra for the safety limit state. As shown, in the N-S direction, the building is expected to dissipate some energy (μ slightly larger than 1). As mentioned before, this energy dissipation should be provided by the URM infills.

The values of the elastic coefficients of distortion in plan and height in both directions were reduced considerably by introducing the PT braces, as reflected by the following values: 1.5 and 1.6 in the E-W and N-S directions, respectively. Because the value of the coefficient of distortion diminishes considerably, the SDOFS displacement, δ_{SDOFS}, can be larger than that corresponding to the building without braces (see equation 3.8). According to the values of coefficient of distortion in the upgraded building, the new values of δ_{SDOFS} associated with IDI_{max} of 0.005 are about 2.2" and 2.6" in the E-W and N-S directions, respectively, which correspond to δ_{roof} of 2.8" and 3.2", respectively. To allow the performance criteria to be met through displacement control, **the building should be upgraded in such a way that the maximum δ_{roof} demands do not exceed values larger than 2.5" in both directions.** From Figures 3.9a and 3.9c, it can be concluded that the bracing system enhances considerably the seismic performance of the building in both directions, and that this performance can be considered adequate within the target performance for safety that has been specified before (Table 3.1). It should be noted that in all this, the energy dissipation provided by the URM infills has been neglected. One way in which this energy dissipation could have been included in the analysis of the upgraded building is by using an equivalent damping coefficient (ξ_{EQ}) that accounts for the viscous and hysteretic energy dissipated in the building ($\xi_{EQ} > \xi$). Nevertheless, a quantification of ξ_{EQ} is difficult due to the lack of research in this area -- future analytical and experimental research needs to be directed towards this issue). In the previous analyses ξ_{EQ} has been considered equal to ξ because it is a conservative assumption.

The stress on the braces (σ_{br}) for an IDI = 0.005 ranges from 71 to 74 ksi in different locations of the building. Considering that only **50% of the allowable yield stress will be used**, the yielding stress of the brace (f_y) should be about 150 ksi. The other **50% of f_y is left for post-tensioning**. Galvanized bridge wire was selected to size the braces. Tables 3.16 and 3.17 show the structural properties and sizes of galvanized bridge wire. From Table 3.16, it can be seen that the minimum f_y ranges from 140 to 160 ksi, which is very close to the required 150 ksi. The braces were sized using the properties given in Table 3.17. The selected sizes of the braces are summarized in Table 3.14.

3.2.4 SPECIAL CONSIDERATIONS IN THE DESIGN OF THE POST-TENSIONED BRACING SYSTEM

The design of the PT bracing scheme should not only consider the design of the braces themselves. It is necessary to assure the adequate behavior of the bracing system by avoiding the possible failure of the existing elements before the braces can reach their ultimate capacity.

■ **Existing frame members and URM infills.** As mentioned in Sections 1.3 to 1.5, the introduction of the PT braces in the structure will induce an initial state of compression in those infills and frame members that support the braces. Also, a change in the behavior of the frame members that support the braces should be considered when the building undergoes lateral deformation, i.e., a reduction in the flexural demands of these members will occur simultaneously with a significant increase of their axial forces. If the existing elements can not perform properly under the new loading conditions, it is necessary to upgrade them accordingly.

The existing columns need to be strengthened in such a way that they can receive the large axial forces induced in them by the braces. The nature of these axial forces is illustrated in Figure 3.13. Given that the braces are not attached to all the floor diaphragms, it is necessary to keep the stories that are not supported by the braces from developing local story mechanisms, as that shown in Figure 3.14.

It should be noted, as shown in Figure 3.14, that the support provided to an unattached floor will usually be provided by the infills and columns of the story immediately below it if there is no significant discontinuity in the lateral strength and stiffness between the stories above and below it. Thus, the columns that support the braces need to be strengthened in such a way that they can resist the forces schematically depicted in Figures 3.13 and 3.14. For this purpose, the columns can be jacketed with steel angles or channels, as illustrated in Figure 3.15a and 3.15b, respectively. The steel jackets and the columns need to work as one unit, which implies that any movement of the jacket relative to the existing column should be prevented. In this sense, it becomes important to provide some type of prestress to the jacket so that an adequate contact between the jacket and the existing element can be achieved. Sometimes, epoxy-like substances are added between the jacket and the existing element to further promote this contact. In the case illustrated in Figure 3.15a, this prestress can be achieved by preheating the horizontal steel straps before welding them to the steel angles that are added to the corners of the existing column. It is of great importance to avoid any movement in the steel angles when welding the steel straps. This can be done in the field by strongly tieing with wire these angles to the columns before welding the straps. Figure 3.16 and Table 3.18 summarize the size of the steel jackets used in the upgrading of the columns of the existing building.

The beams of the building do not need to be strengthened given their usually large dimensions and the existence of the slab. The beams that need to be added to frames C and E were sized so that their properties were equal to those of existing neighboring beams.

■ **Existing foundation.** The original foundation of the building consists on isolated square footings for all the columns of the building and a perimetral footing to support the RC perimetral walls. Given the large axial forces that the columns of the building develop due to post-tensioning and lateral loads (see Figure 3.13), it was necesary to check that the foundation of the building was able to deliver these forces safely to the soil. First, it was necesary to compute the maximum axial force demands in the columns that support the braces. These axial forces were estimated conservatively by considering the gravity loads and the maximum axial forces that can be developed at the base of the columns when the PT braces in both directions reach their ultimate strength simultaneously. Then, these axial force demands were compared to the maximum axial force that can be delivered to the columns according to the capacity of their respective footings. This capacity was computed in a simple manner given that the soil properties were not available. The ultimate load capacity of the soil at the site was estimated, based on simplified assumptions regarding its mechanical properties, to be 15 kg/cm^2 at the horizontal plane at the base of the footing. A safety factor of three was used to estimate the ultimate bearing capacity of the soil to the effects of load combinations considering only gravity loads, and of two for load combination considering gravity plus lateral loads.

It was found that the compresion and tension axial force demands in several of the columns that provide support to the PT braces was considerably larger than the counterpart supply provided by the foundation. In particular, the most critical column was that located in the intersection of Frames E and 47. This column has a maximum axial force demand of 4500 kips in compresion while the supply provided by its footing is only 1500 kips. For tension, the maximum demand is 1500 kips and the supply might as well be considered null. Although a detailed upgrading strategy for the foundation will not be presented in this report, the analysis of the foundation revealed the need to tie the isolated footings by means of foundation beams and the need to enhance the bearing capacity of four footings located in the intersections of Frames E and 47, B and 47, E and 23, and C and 23.

As mentioned in Section 1.3, any modification to the foundation is usually very expensive. Thus, the need to modify the foundation in the Pomona building may be considered a big disadvantage when using PT braces to upgrade this building. Nevertheless, it should be mentioned that the existing foundation was designed for gravity loads only, and does not have an adequate capacity to resists the effects of high and even moderate lateral loads. In this sense, practically any upgrading technique used to upgrade the Pomona building will at least require tieing the isolated footings of the foundation. The need to improve the bearing capacity of four footings is a consequence of the large overturning moments produced by the PT bracing system, which has been designed to resist very large lateral forces (usually associated to a μ close or equal to 1). The applicability of PT braces to upgrade an existing building may be limited by the height of the building, that is, **the need to upgrade the foundation due to the large axial force demands induced by the PT braces in the existing columns may limit the applicability of these braces to low and moderately low buildings.**

3.3 SEISMIC PERFORMANCE OF THE UPGRADED POMONA BUILDING

Once a few promising upgrading configurations are identified, it is necessary to assess the performance of the upgraded building in more detail (i.e., using more sophisticated methods of analysis). Before carrying out nonlinear analyses, it was considered convenient to perform some 3D elastic analyses. The PT braces, designed to carry the majority of the lateral loads, have been designed to remain elastic and maintain the existing frame members elastic (with small nonlinear demands). Therefore, it is believed that an elastic analysis of the upgraded building can provide a reasonable estimate of its maximum response.

In the elastic analyses summarized in this section, the energy dissipation provided by the URM infills has been neglected. As mentioned before, one way in which this energy dissipation could have been included in the analysis is by introducing ξ_{EQ}. Given that it is a conservative assumption, ξ_{EQ} has been considered equal to ξ.

3.3.1 ELASTIC ANALYSIS OF UPGRADED BUILDING

Several elastic analyses of the retrofitted building were carried out using the program SAP90. For this purpose, a 3D elastic model of the upgraded building was created by modeling the existing elements according to the guidelines discussed in Section 2.3.1, while modeling the PT braces as truss elements. First, two response spectra analyses of the building upgraded with brace configuration 1 were performed using the elastic design spectrum shown in Figure 3.9a as seismic input. One response spectrum analysis considered 100% of the EQGM input in the N-S direction plus 30% of this input in the E-W direction. To perform the second, this input was rotated 90 degrees (i.e., 30% in N-S and 100% in E-W). Figures 3.17 and 3.18 show the IDI envelopes for the four perimetral frames of the Pomona building upgraded with brace configuration 1. Figure 3.17 shows results corresponding to the response spectra analysis in which 100% of the EQGM was input in the N-S direction and 30% in the E-W direction. As shown, the torsional effects are not large and brace configuration 1 can control the IDI in the N-S and E-W directions to values less than 0.004, while the IDI distribution over height is fairly regular in both directions. Nevertheless, as shown in Figure 3.18, when the input is rotated 90 degrees, the maximum IDI value is around 0.007, and the building exhibits a significant torsional response (compare the IDI demands at the two end frames in the E-W direction, i.e. Frames A and F). Brace configuration 1 has added enough lateral stiffness to the building, but has not been capable of correcting its excessive torsional response. Although the maximum IDI exceeds the value of 0.005 in Frame A, Figure 3.2d shows that the IDI demand in this frame during the Upland EQ reached values close to 0.007. No damage was reported during this event in Frame A. From this point of view, the behavior of the building braced with configuration 1 may be considered acceptable. One more observation needs to be made regarding the results obtained from the elastic response spectra analyses: the energy dissipating capacity provided by the URM infills has been neglected. If the energy dissipation is considered, the response of the building will probably diminish. Although the performance of the building upgraded with brace configuration 1 can be considered adequate, the large torsional response of the building when loaded in the E-W direction remains an issue.

Adding some extra braces to Frame B (configuration 2), as shown in Figures 3.11 and 3.12e, is a good idea from a structural point of view. The addition of braces to Frame B should reduce the torsional response of the building, as well as adding lateral stiffness in the E-W direction. Nevertheless, introducing braces in this location disrupts the distribution of internal space in the building (divides the office of the president of the bank housed by the Pomona building).

Figures 3.19 and 3.20 show the IDI demands for the response spectra analyses of the building upgraded with brace configuration 2. By comparing Figures 3.17 and 3.19, it can be concluded that when 100% of the seismic excitation is input in the N-S direction and 30% in the E-W direction, the response of the building practically does not change. Nevertheless, by comparing Figures 3.18 and 3.20, it can be concluded that when the seismic input is rotated 90 degrees, the response in the N-S direction is slightly reduced, while the influence that torsion has on the response of the upgraded building in the E-W direction is reduced considerably. By introducing the braces in Frame B, the behavior of the upgraded building is enhanced, and the IDI is controlled effectively within the 0.005 limit.

Table 3.19 shows the base shear demands in both directions for all response spectrum analysis. By recalling that the ultimate strength of the building is about 0.98 W in the N-S direction and 0.56 W in the E-W direction (Tables 3.12 and 3.13), it can be concluded that the elastic base shear demands obtained from the response spectra analysis are within expected limits.

The fundamental translational periods estimated from the stick models (T_{N-S} = 0.38 sec and T_{E-W} = 0.55 sec) are compared to those obtained from the eigenvalue analyses of the 3D elastic models of the two upgraded versions of the building (configuration 1 and 2) in Table 3.20. As shown, both 3D elastic models yield a value of T_{N-S} that is close to that predicted by the stick model. Nevertheless, the 3D elastic model of brace configuration 1 yields a T_{E-W} that is larger than that of the stick model, while the 3D elastic model of brace configuration 2 yields a similar T_{E-W} to that of the stick model. It can be concluded that the actual lateral stiffness of the braces in the N-S direction match their target counterparts well, while the lateral stiffness of the braces in the E-W direction was somewhat overpredicted by the stick model.

Figures 3.21 to 3.24 show the IDI envelopes for the four perimetral frames of the 3D elastic models of the two upgraded versions of the building obtained from 3D time-history analyses using the two components of the Landers and Upland EQs. These EQGMs were scaled up in such a way that the component with the largest peak ground acceleration (PGA) would have a PGA of 0.38g. For instance, the Landers EQ components were scaled up by a factor of 6, in such a way that the PGA in N-S direction was equal to 0.38g, while that in the E-W direction was 0.30g. The Upland EQ components were scaled up by a factor of 3, in such a way that the N-S and E-W PGAs were also equal to 0.38 and 0.30, respectively. As shown in Figures 3.21 and 3.22, obtained for brace configuration 1, the maximum IDI is slightly larger than 0.005 and the overall performance of the building can be considered satisfactory. Nevertheless, two observations need to be made: first, the PGA of the E-W component of both EQs is 0.3g; and second, the upgraded versions of the building were designed using the mean spectra shown in Figures 3.9a and 3.9c (instead of using the mean plus one standard deviation spectra). If the maximum IDI in the E-W direction of the building increases linearly with respect to the PGA in this direction, a PGA of 0.38g in this direction will produce a maximum IDI of .0068.

Figures 3.23 and 3.24 summarize the results obtained for brace configuration 2. Assuming that the maximum IDI in the E-W direction of the building increases linearly with respect to the PGA in this direction, the maximum IDI is close to 0.005 for a PGA of 0.38g in the E-W direction. Table 3.19 summarizes the base shear demands in the building obtained from the different elastic time-history analyses and both brace configurations.

From the above results, it can be concluded that both upgrade configurations control the lateral deformation of the building within acceptable limits. Configuration 2 offers several structural advantages, especially the fact that it reduces considerably the torsional response of the building when it is loaded in the E-W direction.

3.3.2 Two Dimensional Nonlinear Analysis of Upgraded Building

Nonlinear 2D analyses were performed on a model of the building upgraded with brace configuration 1 to study its behavior in the E-W direction (the building has smaller lateral strength and stiffness in this direction as compared to those corresponding to the N-S direction). This was done to assess, within a relatively simple framework, the nonlinear behavior of the braced building when subjected to the safety level of EQGM. The analyses were carried out using the program DRAIN 2DX.

To carry out a 2D pushover and time-history analyses of brace configuration 1, PT braces were introduced to the DRAIN 2DX model described in Section 2.3.2. The PT braces were modeled using truss elements, while their prestress was modeled as initial axial fixed end forces acting on them. For the time-history analysis, a $\xi = 0.05$ was considered for the first two translational modes.

A 2D pushover analysis, considering P-Δ effects, was carried out to determine the lateral deformation vs. lateral load characteristics of the building (neglecting torsion), as well as to establish the distribution of nonlinear demands among the elements of the building. Because it yielded practically the same story shear distribution over height than that obtained from the response spectra analysis of the building, the distribution of lateral loads over height for the pushover analysis was obtained by assuming a triangular distribution of accelerations through height.

Two different nonlinear models of the building upgraded with brace configuration 1 were created to illustrate some relevant issues:

■ **Braced with lateral support (to unattached floor diaphragms).** As mentioned in Section 3.2.4 and shown in Figure 3.14, it is necessary to avoid the creation of partial mechanisms produced by the fact that not all floor diaphragms are attached to the bracing system. In this model (denoted as *braced with lateral support*), the model of the columns take into account the mechanical properties of their jackets. These jackets were designed to provide sufficient axial strength and stiffness to allow the PT braces to develop their full lateral stiffness and strength, while providing the unattached floors with sufficient lateral support to avoid the formation of story mechanisms.

■ **Braced.** In the second model (denoted as *braced*), the model of the jacketed columns only accounted for the upgrade of the axial stiffness and strength provided by the jackets, neglecting their contribution to the lateral strength and stiffness of the jacketed columns.

Figure 3.25 shows the δ_{roof} vs. V_b curves for the two different DRAIN 2DX models of the building upgraded with brace configuration 1, and how these curves compare to that corresponding to the DRAIN 2DX model of the original building. As shown in the figure, if the columns that support the braces are not axially strengthened, the first column will fail under compressive stresses at a $\delta_{roof} \approx 1.5$". The δ_{roof} vs. V_b curves corresponding to the two DRAIN 2DX models of the building upgraded with the brace configuration 1 show very similar ***global*** behavior up to a δ_{roof} of 3.5". At that δ_{roof}, all the PT braces spanning the second and third stories (attached to the second and fourth floors) of the **braced model** either buckle or yield. This is reflected in the curve denoted **braced** in Figure 3.25 with a large decrease in stiffness. Nevertheless, the curve denoted as **braced + lat. supp.**, which corresponds to the **braced with lateral support model**, does not show this decrease until δ_{roof} is around 4.3". At this point, all the PT braces spanning the second and third stories yield or buckle. The first PT brace yields or buckles at $\delta_{roof} \approx$ 3.4" and 4.1" in the **braced** and **braced with lateral support models**, respectively. The ultimate base shears that the DRAIN 2DX models develop are around 4000 kip (0.62W) for the **braced model** and 4500 kip (0.69W) for the **braced model with lateral support**. These values are similar to the value of 0.56 W which was previously estimated for the building upgraded with brace configuration 1 (see last column of Table 3.13). Note that the PT bracing system has been designed to limit the maximum δ_{roof} demand to 2.5".

As shown in Figure 3.25, the lateral stiffness and strength of the Pomona building are considerably enhanced by upgrading the building with PT braces.

Figures 3.26 and 3.27 show the distribution of story displacements and IDI over height for different values of δ_{roof}, obtained from the pushover analysis of the two DRAIN 2DX models of the building upgraded with brace configuration 1. To interpret the results obtained in these figures, it is necessary to recall that the PT braces are attached to the structure every two stories as shown in Figure 3.12 and 3.14, that is, they are attached to the second, fourth and sixth floors; while the mezzanine, third and fifth floors are free from the braces. In Figures 3.26 and 3.27, the continuous lines correspond to the displacement and IDI distributions over height obtained by considering the lateral displacements of all floors, while the discontinuous lines correspond to the respective distributions obtained by only considering the floors to which the braces are attached (second, fourth and sixth). For small values of δ_{roof}, the lateral deformation is more or less uniformly distributed throughout the height of the different models. Nevertheless, as δ_{roof} increases, it is very noticeable that the lateral displacement corresponding to the mezzanine floor decreases, and those corresponding to the third and fifth floors increase relative to those of the other floors. By comparing in Figure 3.27 the IDI distributions given by the continuous and discontinuous lines, it can be concluded that a significant concentration of lateral deformation occurs in stories whose floor is not attached to the bracing system. By comparing the results obtained using both models, it can be concluded that this concentration is smaller in the **braced model with lateral support**. Figures 3.26 and 3.27 illustrate the importance of controlling the lateral displacement of all the floors, including those that are not attached to the braces.

The above brings attention to the configuration used for the PT bracing system. It was mentioned in Section 3.2.3 that for efficient and economical design it was convenient to configure the braces in such a way that they span two stories. Nevertheless, as previously remarked in Section 3.2.4 and confirmed by the results of the pushover analyses, the designer has to recognize and analyze the consequences of not attaching all the floors to the bracing system.

Figures 3.28 to 3.31 show how nonlinear behavior progresses in the elements of the **braced model**. These figures follow the same conventions described in Section 2.4.1. In Figures 3.28 to 3.31, the PT braces are represented in the first and third bays of Frames C and E with diagonals that span two stories. As shown in Figure 3.28, for δ_{roof} = 1" some plastic hinges have appeared in some of the RC members of the building. Note that some columns that support the PT braces in the third bay of Frame E have developed plastic hinges (in the second and fourth stories). It was mentioned before that the axial strength and stiffness of the columns of the **braced model** were axially upgraded to allow them to receive the PT braces. The plastic hinges in the columns of Frame E are flexural hinges (as opposed as tensile or compressive hinges) and produced by the lateral displacement of the unsupported floors. Figures 3.29 and 3.30 show how the nonlinear behavior progresses for δ_{roof} = 2" and 3". As shown, RC members continue to develop plastic hinges, especially in the perimetral frames (A and F). It is interesting to note that plastic hinges have developed in the majority of the columns in Frame A (as opposed to the beams). Several columns located on the upper stories of Frame F also develop plastic hinges. Note that a large number of flexural plastic hinges develop in the columns that support the PT braces. As mentioned before, the PT braces have been designed to control the displacement of the structure within a δ of 2.5" for the safety EQGM; thus, with the exception of higher mode effects, the hinging in structural elements at safety level should be similar to that shown in Figure 3.29. As δ_{roof} increases towards a value of 4", it is noticeable that a global and some local mechanisms start to develop in the building, as shown in Figure 3.31. A very large percentage of the columns located in the fourth story have hinged at both ends, which explains the increase in IDI in the fourth story shown in Figure 3.27a. In Figure 3.31, it can be seen that there are circles in the intersection of the diagonals representing the PT braces in the second and third stories. These circles represent that the braces have either buckled in compression or yielded in tension. Note that buckling and/or yielding occurs in all the braces spanning the second and third stories, which imply that these are the critical stories (stories in which the failure actually occurs) for the failure of the upgraded building. The location of the critical stories obtained from the pushover analysis is consistent with the location of these stories presented in Table 3.13.

Figures 3.32 to 3.35 show how nonlinear behavior progresses in the elements of the **braced with lateral support model**. As shown in Figure 3.32, for δ_{roof} = 1" practically no hinging have developed in the existing RC members of the building, and no hinging occurs in the columns of Frame C and E (these frames support the PT braces). These columns have been upgraded to take the axial and lateral demands produced by the braces and the lateral displacement of the floors that are not attached to the braces. Figures 3.33 and 3.34 show how the nonlinear behavior progresses for δ_{roof} = 2" and 3". As shown, a few RC members develop plastic hinges, especially in the perimetral frames (A and F). Nevertheless, note that now the hinging of the frame members on Frames C and E concentrate in the beams as opposed to the columns. In Frames C and E, hinging occurs at the beams located in their central bay, possibly because of the weak coupling they provide to the first and third bays. The PT braces have been designed to control the displacement of the structure within a δ of 2.5" for the safety EQGM; thus, with the exception of higher mode effects, the hinging in structural elements at safety level should be similar to that shown in Figure 3.33. As δ_{roof} increases towards a value of 4", a few flexural hinges start to develop in the columns of Frames C and E. In Figure 3.35, it can be seen that there are circles in the intersection of the diagonals representing the PT braces in the second and third stories. Note that buckling and/or yielding concentrates exclusively in the braces spanning the second and third stories, which imply that these are the critical stories. The location of the critical stories obtained from the pushover analysis is consistent with the location of these stories presented in Table 3.13.

The same two DRAIN 2DX models used for the pushover analyses were used to perform time-history analyses using an EQGM that is supposed to represent the safety level EQGM. For this purpose, the E-W component of the Landers EQGM was scaled up by a factor of 6.

Figures 3.36 and 3.37 summarize the results obtained from the time-history analyses. These figures show in discontinuous lines the results obtained from the pushover analyses, while the positive and negative envelopes obtained from the time-history analyses are shown with continuous lines. Note that both the positive and the negative envelopes are plotted in the positive side of the displacement and IDI axis. As shown in Figure 3.36, the shapes for the displacement envelopes obtained from the time-history analyses are very similar to those obtained from the pushover analyses. The maximum δ_{roof} for both models change considerably, going from 2.8" for the **braced model** to 2.2" in the **braced model with lateral support**. Figure 3.37 shows the IDI demands for both models. The IDI distribution over height obtained from the time-history analyses has a similar shape to the IDI distribution obtained from the corresponding pushover analyses at a comparable δ_{roof}. The IDI in the **braced model with lateral support** is fairly constant over height, while there is a noticeable concentration of deformation in the second and fourth stories of the **braced model**. Note that the maximum IDI demands in the **braced model** are around 0.005 while those in the **braced model with lateral support** are around 0.003. It should be noted that all of these results have been obtained without accounting for torsional effects. Although it is difficult to assess how much the IDI demands will increase once torsion is accounted for, it can be said that the **braced model with lateral support** will probably satisfy the performance criteria established for the upgraded building. The same is not necessarily true for the **braced model**, in which inadequate concentration of deformation can be noticed.

The fairly large difference between the floor displacement and IDI demands in both models should also be noted. From analysis of Figure 3.37a, it is clear that the IDI in the second and fourth story of the **braced model** is large. This is a consequence of the relatively large motion of the fifth floor (which is the diaphragm on top of the fourth story) with respect to the fourth and sixth floors, which leads to a significant increase in global and local deformation demands in the **braced model.** The above results suggest that it is necessary to control adequately the response of the floor diaphragms that are not attached to the braces. Further research needs to be carried out to understand this large difference in behavior so that unadequate performance due to insufficient lateral support of the unattached floors can be prevented.

The **braced model** can be considered an abstraction and was developed to illustrate the need to avoid overlooking the formation of local failure mechanisms. The analysis of this model allows the detection of some problems associated with the response of the floors that are not attached to the bracing syst. .ı that can be detrimental to the global response of the building.

3.3.3 THREE-DIMENSIONAL NONLINEAR ANALYSIS OF UPGRADED BUILDING

Several nonlinear 3D analyses of models of different versions of the upgraded building were carried out to assess their behavior and performance when their torsional response is included. For this purpose, the DRAIN 3DX program was used. The elements of the original building were modeled according to the considerations made in Section 2.5, while the PT braces were modeled using truss elements.

Several 3D pushover analyses (the floor diaphragms are allowed to rotate in plan) considering P-Δ effects were carried out to determine the lateral displacement vs. lateral load behavior of the different versions of the upgraded building, as well as to establish the distribution of global displacement demands throughout the building. Because it yielded practically the same story shear distribution through height than that obtained from the response spectra analysis of the building, the distribution of lateral loads through height for the pushover analyses was obtained by assuming a triangular distribution of accelerations over height.

First, 3D pushover analyses in the E-W direction of two different versions of the upgraded building were carried out. Figures 3.38 to 3.42 summarize the results obtained from a 3D pushover analysis in the E-W direction of the building upgraded with brace configuration 1. Figure 3.38 and Figures 3.43 to 3.46 show the results from a 3D pushover analysis in the E-W direction of the building upgraded with a slightly modified version of brace configuration 2. This new version consists in eliminating one of the five braced bays in the E-W direction of the building shown in Figure 3.11. To obtain modified configuration 2, the braces located in Frame E and spanning from Frame 47 to Frame 6 were eliminated (the jackets in the columns were adjusted accordingly). Figure 3.38 and Figures 3.47 to 3.50 summarize the results of a 3D pushover analysis in the N-S direction of the building upgraded with brace configuration 1.

Figure 3.38 establishes a comparison between the δ_{roof} vs. V_b curves obtained from pushover analyses of the E-W direction of the DRAIN 2DX **braced with lateral support model** (configuration 1) and two DRAIN 3DX models (brace configuration 1 and modified brace configuration 2). The curves that have been plotted for the DRAIN 3DX models correspond to the node that is closest to the geometric centroid of the roof diaphragm. The initial lateral stiffness and ultimate strength in the E-W direction predicted by DRAIN 3DX for the building upgraded with brace configuration 1 are slightly smaller than the corresponding estimates obtained using the DRAIN 2DX **braced with lateral support model**. Note the similitude between the δ_{roof} vs. V_b curves in the E-W direction obtained from these two analyses of the building upgraded with the brace configuration 1. The δ_{roof} vs. V_b curve in the E-W direction obtained from the DRAIN 3DX model of the building upgraded with modified brace configuration 2 is practically equal to that obtained from the DRAIN 3DX analysis of the building upgraded with brace configuration 1, although the lateral stiffness and ultimate V_b predicted by the former analysis are slightly larger than those predicted by the latter one. Figure 2.38 also establishes a comparison between the ultimate V_b in the E-W direction predicted in Section 3.2.3 for the building upgraded with brace configuration 1 (see last column of Table 3.13) and that predicted by the 3D pushover analyses. As shown, the ultimate V_b in the E-W direction predicted using a simplified approach is a good estimate of the ultimate V_b estimated from a sophisticated 3D nonlinear analysis.

Figure 3.39 shows four δ_{roof} vs. V_b curves, one for each corner of the building upgraded with brace configuration 1, obtained from a 3D pushover analysis in the E-W direction. It is clear from these curves that there is a significant torsional response when this version of the upgraded building is loaded in the E-W direction. As shown, the corners located in the south end of the building (Frame A) have a δ_{roof} demand that is roughly twice that corresponding to the corners located in the north end (Frame F). It can be observed that the difference between the δ_{roof} demands of the south and north corners tends to increase with increasing δ_{roof}. Note that the 3D elastic analyses of Section 3.3.1 were able to detect this problem (see Figures 3.18b, 3.21b and 3.22b). Figures 3.40 and 3.41 show a comparison between the displacement and IDI distributions over height corresponding to the four corners of the DRAIN 3DX model of the building upgraded with brace configuration 1 (curves with continuous line) and those obtained using the DRAIN 2DX model of the same version of the upgraded building (curves with discontinuous line). The distributions corresponding to the four corners of the DRAIN 3DX model and labeled as δ_{roof} equal to 1", 2", 3", 4" and 5" are the distributions that occur at that corners when the displacement of the node closest to the geometric centroid of the roof diaphragm is equal to these values of δ_{roof} (i.e., 1", 2", 3", 4" and 5"). As shown in Figure 3.40, due to the large torsional effects, the displacement distributions over height obtained from the DRAIN 3DX model for the two corners located in Frame A (southeast and southwest corners) have different shapes than those obtained from the DRAIN 2DX model. Also, these south corners have considerably larger displacements than those of DRAIN 2DX model. The displacement distributions over height obtained from this same DRAIN 3DX model for the corners located in Frame F (northeast and northwest corners) have very similar shapes to those obtained from the DRAIN 2DX model, although due to torsional effects the displacements of these corners are considerably smaller. Figure 3.41 emphasizes the different deformation distributions over height between the corners located in Frame A of the DRAIN 3DX model and those obtained from the DRAIN 2DX model. As shown, the DRAIN 3DX model has large IDI demands in the ground and fifth stories of the corners located in Frame A, while the DRAIN 2DX model exhibits a large IDI demand in the second story. To help explain such differences, Figure 3.42 has been included. This figure shows how the six floor diaphragms of the DRAIN 3DX model move relative to each other and to the ground as δ_{roof} increases in the E-W direction. For a given δ_{roof}, the discontinuous rectangle represents the position of the ground floor, while the other six continuous rectangles represent the floor diaphragms of the building. The diaphragms' displacements illustrated in Figure 3.42 have been scaled up by a factor of 50 so that the relative movements between the floors can be perceptible. As shown in Figure 3.42, as δ_{roof} increases, the floor diaphragms tend to rotate around Frame F. Note that the rotations of the two lower stories (ground and mezzanine stories) and of the top story tend to be considerably larger than those of the other stories. In fact, the interstory rotation of the second, third and fourth stories is very small (this part of the building is rotating as a rigid body). Considering the large rotations in the ground, mezzanine and roof stories, it is possible to explain the large displacement and IDI demands in these stories of the corners located in Frame A. Note in Figure 3.41 that the IDI distributions over height of the corners in Frame F of the DRAIN 3DX model have similar shapes to those obtained from the DRAIN 2DX model, although, as expected, the IDI demands are smaller due to torsional effects.

Figures 3.43 to 3.46 show the results from the 3D pushover of the E-W direction of the DRAIN 3DX model of the building upgraded with modified brace configuration 2. Before discussing the results summarized in these figures, it should be noted that brace configuration 1 and modified configuration 2 have the same number of braced bays in the E-W direction: four. The only difference between these two configurations is that one of the braced bays in Frame E of brace configuration 1 has been translated to Frame B to obtained modified brace configuration 2. By comparing Figures 3.43 to 3.46 to those corresponding to the DRAIN 3DX model of the building upgraded with brace configuration 1 (Figures 3.39 to 3.42), it can be concluded that the torsional response of the upgraded building is reduced considerably. As shown in Figure 3.43, the δ_{roof} demands in the corners located in the south end of the building (Frame A) are now roughly 1.3 times the δ_{roof} demands corresponding to the corners located in the north end (Frame F), and this ratio remains fairly constant with increasing δ_{roof}. Figure 3.44 shows that now the displacement distributions of the four corners of the DRAIN 3DX model of the building upgraded with modified brace configuration 2 have similar shapes to those obtained from the DRAIN 2DX model for the building upgraded with configuration 1. Nevertheless, the DRAIN 3DX model still tends to have larger displacement demands in the ground, mezzanine and roof stories of the corners located in Frame A (although this deformation concentration has been reduced considerably with respect to that shown in Figure 3.41). The displacement distributions over height of the corners located in Frame F of the DRAIN 3DX model have now almost exactly the same shapes as those corresponding to the DRAIN 2DX model. Figure 3.45 shows that although the IDI concentration in the two bottom and roof stories of the corners located in Frame A has not disappeared completely, a significant improvement in the response of the upgraded building has been achieved with respect to that illustrated in Figure 3.41. Figure 3.46, which emphasizes that the torsional response of the upgraded building has been reduced considerably, shows that as the δ_{roof} in the E-W direction of the building increases, the building still rotates around Frame F. Although not as noticeable as before, the rotations in the two bottom and roof diaphragms is larger than that corresponding to the other diaphragms.

Figure 3.38 shows the δ_{roof} vs. V_b curves obtained from the 3D pushover analysis in the N-S direction of the DRAIN 3DX model of the building upgraded with brace configuration 1. As shown, the lateral strength and stiffness of the upgraded building is considerably higher in the N-S direction than in the E-W direction. The upgraded building is capable of developing an ultimate V_b in the N-S direction that is larger than the value of 0.98 W estimated in Section 3.2.3 (see last column of Table 3.12). Figure 3.47 shows the V_b vs. δ_{roof} curves for the four corners of the DRAIN 3DX model obtained from the 3D pushover analysis in the N-S direction. As shown, the torsional response of the building when loaded in the N-S direction has been reduced considerably with respect to that of the original building. Figures 3.48 and 3.49 show the displacement and IDI distributions over height for the four corners of the building upgraded with brace configuration 1, obtained from the 3D pushover analysis in the N-S direction. As shown in Figure 3.48 and 3.49, although the δ_{roof} demands are similar for all four corners, the displacement demands over height vary considerably from corner to corner. In particular, those corners located in Frame 1 (southwest and northwest) tend to accumulate large displacement and IDI demands in the third story, where this frame exhibits large irregularities in height of lateral stiffness and strength. The building eventually fails in this story, which becomes the critical story (story in which the failure actually occurs) for the failure of the upgraded building. The location of the critical story obtained from the pushover analysis is consistent with the location of this story presented in Table 3.12. Finally, Figure 3.50 gives an insight into the torsional response of the upgraded building when loaded in the N-S direction.

Results for the 3D time-history analyses of the different upgraded models of the building were not available. Nevertheless, from the results obtained in the 2D nonlinear time-history analyses of the upgraded building, and by considering that the torsional response in the building upgraded with modified brace configuration 2 is not large, it can be concluded that if the building is upgraded with the original or modified brace configuration 2, it will probably satisfy the performance criteria established for the safety limit state (see Table 3.1). Although with a significant torsional response when loaded in the E-W direction, the building upgraded with brace configuration 1 will also probably satisfy these performance criteria, although, as suggested by the 3D pushover results, the IDI demands in the ground and mezzanine will be considerably larger than the IDI demands on other frames and stories.

Nevertheless, one of the aspects of the upgraded building response that can not be studied without a 3D nonlinear time-history analysis is the magnitude of the floor accelerations. One of the drawbacks of upgrading an existing framed building with URM infills by introducing PT braces to this building is the fact that the floor accelerations in the upgraded building may be considerably higher that those occurring in the original building when subjected to similar EQGMs. It is believed that the nonlinear behavior of the URM infills should somehow damp the global response of the upgraded building in such a way that the building is provided with an internal mechanism to reduce the values of these story accelerations. In this sense, the results obtained from the 3D elastic analyses carried out in this study do not provide a fair estimate of the story accelerations, given that the contribution of the URM infills to damp the response of the building has been neglected. This issue needs further research. A new series of 3D analysis will be carried out in the future with the help of a new program for the nonlinear 3D analysis of RC structures (Filippou, 1995).

Response Condition: SAFETY	Performance criteria
State of RC members	Elastic (IDI not known)
Performance of URM infills	stable hysteretic behavior ($IDI \leq 0.005$)
State (response) of PT braces	Elastic
Damage to nonstructural elements	pre-collapse ($IDI \leq 0.0125$)

Table 3.1 Safety limit state design criteria

Story	Weight (kip)	Height (ft)	Stiffness from existing model for SAP90 (k/in)	
			N-S direction	E-W direction
ground	584	13	7613	1808
mezzanine	1121	12.5	4767	1429
2	1050	10.5	8852	3421
3	1050	10.5	7592	3125
4	1050	10.5	6258	2423
5	1284	13.5	5426	1130

Table 3.2 Story stiffness estimated from static analysis of 3D elastic model

Stories	Stiffness of building from SAP90 (k/in) (1)		Stiffness of frame only from SAP90 (k/in) (2)		Stiffness of URM walls (k/in) (1) - (2)	
	N-S	E-W	N-S	E-W	N-S	E-W
G	7613	1808	982	955	6631	853
Mz	4767	1429	951	762	3816	667
2	8852	3421	2800	1625	6052	1796
3	7592	3125	2403	1414	5189	1711
4	6258	2423	1689	992	4569	1431
5	5426	1130	661	333	4765	797

Table 3.3 URM infill stiffness estimated from static analysis of 3D elastic model

Stories	URM INFILLS STIFFNESS (K/in)				
	SAP90 (1)	Simplified for estimated IDI (2)	Correction factor[a] (3) = (1)/(2)	Simplified for IDI=0.005 (4)	Corrected for IDI = 0.005 (3)x(4)
G	6631	5954	1.00	2550	2550
Mz	3816	3848	0.99	1672	1655
2	6052	7546	0.80	2052	1646
3	5189	6092	0.85	1742	1484
4	4569	6092	0.75	1742	1307
5	4765	6092	0.78	1742	1362

[a] correction factor always less than 1.0

Table 3.4 URM infill stiffness in N-S direction obtained from simplified procedure

Stories	URM INFILL STIFFNESS (K/in)				
	SAP90 (1)	Simplified for estimated IDI (2)	Correction factor[a] (3) = (1)/(2)	Simplified for IDI=0.005 (4)	Corrected for IDI = 0.005 (3)x(4)
G	853	700	1.00	467	467
Mz	667	700	0.95	467	444
2	1796	2169	0.83	570	472
3	1711	2169	0.79	570	450
4	1431	2169	0.66	570	376
5	797	2169	0.37	570	209

[a] correction factor always less than 1.0

Table 3.5 URM infills stiffness in E-W direction obtained from simplified procedure

Factor	Concept	value of q_i		
		0.80	0.90	1.00
q_1 (1)	Irregularity in plan	$\Delta A > 30\%$ $e/B > 20\%$	$10\% < \Delta A \leq 30\ \%$ $10\% < e/B \leq 20$	$\Delta A \leq 10\%$ $e/B \leq 10\%$
q_2 (2)	Irregularity in elevation	$\Delta A > 30\%$	$10\% < \Delta A \leq 30\%$	$\Delta A \leq 10\%$
q_3 (3)	Tilt	$D > 2\%$	$1\% < D < 2\%$	$D \leq 1\%$
q_4	Impact with neighboring buildings	Heavy damage	Moderate damage	Light damage
q_5 (4)	Deterioration	Age > 30 minor repair	10 ≤ Age ≤ 30 major repair	Age ≤ 10 no previous damage

(1) ΔA is the area delimited by reentrant corners as a percentage of the total area. e/B is the ratio between the eccentricity in plan and the plan dimension that is parallel to the direction in which that eccentricity is measured
(2) ΔA is the largest percentual change of plan area or the sum of areas of the structural elements from one story to the next
(3) D is the tilt angle in degrees
(4) Age in years. Major repair is that that attempts the reestructuration and stiffening of the existing building

Table 3.6 Corrective factors

Story	Strength of masonry infills (kip)		Strength of RC columns (kip)	Total story strength (kip)	Critical story and V_b (kip)
	@ Cracking	@ Ultimate			
G	1974	2806	568	2159	
Mz	1423	2024	524	1681	<= 1729(1)
2	1593	2264	500	1769	
3	1593	2264	410	1711	
4	1593	2264	308	1646	
5	1593	2264	207	1581	

(1) 1729 kip = 0.28 W

Table 3.7 Estimated ultimate story strength in the N-S direction

Story	Strength of masonry infills (kip)		Strength of RC columns (kip)	Total story strength (kip)	Critical story and V_b (kip)
	@ Cracking	@ Ultimate			
G	551	782	568	863	<= 863(1)
Mz	621	881	524	899	
2	663	943	500	923	
3	663	943	410	866	
4	663	943	308	801	
5	663	943	207	736	

(1) 863 kip = 0.14 W

Table 3.8 Estimated ultimate story strength in the E-W direction

Floor	Centers of mass (ft)		Centers of stiffness formal method (ft)		Centers of stiffness simplified method (ft)	
	N-S	E-W	N-S	E-W	N-S	E-W
Mz	74	45	n.d. [a]	55	88	55
2	58	32	n.d. [a]	45	86	55
3	57	30	50	45	56	48
4	57	30	50	45	55	39
5	57	30	50	45	53	42
6(roof)	49	38	50	45	53	46

[a] n.d. (not defined), the center of resistance is not located within the floor diaphragm

Table 3.9 Location of centers of mass and resistance of existing building

Direction	Period (sec)	Mass corresponding to first mode		Equivalent height corresponding to first mode	
		(kip-sec^2/in)	% of total mass	(ft)	% of total height
N-S	0.55	14.3202	90	50.4	71
E-W	1.01	14.6915	92	49.6	70

Table 3.10 Dynamic properties of first translational mode of simplified models

Direction	$\Gamma\phi_1(H)$	$(c.o.d.)_H$	$(c.o.d.)_\theta$	c.o.d.
N-S	1.51	1.45	1.84	2.7
E-W	1.25	1.85	1.39	2.6

Table 3.11 Coefficients of distortion from simplified procedure

stories	number of braces	Stiffness (kip/in)		Strength @ IDI = 0.005		Critical Stories (Failure)
		Braces	Total	Braces	Total	
G-Mz	8 type 1 + 12 type 3	4,200	7,130	1.02 W	1.30 W	
2-3	8 type 2 + 12 type 4	2,800	6,880	0.56 W	0.85 W	V_{bx}=0.98W
4-5	8 type 2 + 12 type 4	2,800	5,700	0.56 W	0.83 W	

Table 3.12 Characteristics of proposed bracing system for configuration 1, N-S direction.

stories	number of braces	Stiffness (kip/in)		Strength @ IDI = 0.005		Critical Stories (Failure)
		Braces	Total	Braces	Total	
G-Mz	16 type 5	2,520	3,320	0.62 W	0.75 W	
2-3	16 type 2	1,680	3,310	0.34 W	0.49 W	V_{by}=0.56W
4-5	16 type 2	1,680	2,450	0.34 W	0.47 W	

Table 3.13 Characteristics of proposed bracing system for configuration 1, E-W direction.

Brace type	Required area (in^2)	Nominal diam. (in)	Provided area (in^2)
1	5.2	3 1/8	5.86
2	2.6	2 1/8	2.71
3	7.0	3 1/2	7.35
4	3.5	2 7/16	3.57
5	5.6	3 1/8	5.86

Table 3.14 Sizes of PT braces

Direction	Period (sec)	Mass corresponding to first mode		Equivalent height corresponding to first mode	
		(kip-sec^2/in)	% of total mass	(ft)	% of total height
N-S	0.38	13.8989	87	51.3	73
E-W	0.55	14.0414	88	51.1	72

Table 3.15 Dynamic properties of stick model of upgraded building

Coating class	Diam, in	Min tensile strength, ksi	Min yield strength* at 0.7 % extension under load, ksi	Min total elongation in 10 in, %
A	0.041 and over	220	160	4
B	All	210	150	4
C	All	200	140	4

* For actual cross section including zinc coating.

Table 3.16 Properties of galvanized bridge wire

Nominal diam, in	Class A coating throughout	Class A coating inner wires, class B coating outer wires	Class A coating inner wires, class C coating outer wires	Approx metallic area, in²	Approx weight per ft, lb
1/2	15.0	14.5	14.2	0.150	0.52
9/16	19.0	18.4	18.0	0.190	0.66
5/8	24.0	23.3	22.8	0.234	0.82
11/16	29.0	28.1	27.5	0.284	0.99
3/4	34.0	33.0	32.3	0.338	1.18
13/16	40.0	38.8	38.0	0.396	1.39
7/8	46.0	44.6	43.7	0.459	1.61
15/16	54.0	52.4	51.3	0.527	1.85
1	61.0	59.2	57.9	0.600	2.10
1 1/16	69.0	66.9	65.5	0.677	2.37
1 1/8	78.0	75.7	74.1	0.759	2.66
1 3/16	86.0	83.4	81.7	0.846	2.96
1 1/4	96.0	94.1	92.2	0.938	3.28
1 5/16	106.0	104.0	102.0	1.03	3.62
1 3/8	116.0	114.0	111.0	1.13	3.97
1 7/16	126.0	123.0	121.0	1.24	4.34
1 1/2	138.0	135.0	132.0	1.35	4.73
1 9/16	150.0	147.0	144.0	1.47	5.13
1 5/8	162.0	159.0	155.0	1.59	5.55
1 11/16	176.0	172.0	169.0	1.71	5.98
1 3/4	188.0	184.0	180.0	1.84	6.43
1 13/16	202.0	198.0	194.0	1.97	6.90
1 7/8	216.0	212.0	207.0	2.11	7.39
1 15/16	230.0	226.0	221.0	2.25	7.89
2	245.0	241.0	238.0	2.40	8.40
2 1/16	261.0	257.0	253.0	2.55	8.94
2 1/8	277.0	273.0	269.0	2.71	9.49
2 3/16	293.0	289.0	284.0	2.87	10.05
2 1/4	310.0	305.0	301.0	3.04	10.64
2 5/16	327.0	322.0	317.0	3.21	11.24
2 3/8	344.0	339.0	334.0	3.38	11.85
2 7/16	360.0	355.0	349.0	3.57	12.48
2 1/2	376.0	370.0	365.0	3.75	13.13
2 9/16	392.0	386.0	380.0	3.94	13.80
2 5/8	417.0	411.0	404.0	4.13	14.47
2 11/16	432.0	425.0	419.0	4.33	15.16
2 3/4	452.0	445.0	438.0	4.54	15.88
2 7/8	494.0	486.0	479.0	4.96	17.36
3	538.0	530.0	522.0	5.40	18.90
3 1/8	584.0	575.0	566.0	5.86	20.51
3 1/4	625.0	616.0	606.0	6.34	22.18
3 3/8	673.0	663.0	653.0	6.83	23.92
3 1/2	724.0	714.0	702.0	7.35	25.73
3 5/8	768.0	757.0	745.0	7.88	27.60
3 3/4	822.0	810.0	797.0	8.44	29.53
3 7/8	878.0	865.0	852.0	9.01	31.53
4	925.0	911.0	897.0	9.60	33.60

Table 3.17 Minimum breaking strength of bridge strand in tons (2.2 kip)

Location	Jacket Type 1	Jacket Type 2	Jacket Type 3
Floors 1-2	four 8 x 8 x 1 1/8 angles	four 6 x 6 x 5/8 angles	four 5 x 5 x 3/8 angles
Floors 3-4	four 6 x 6 x 5/8 angles	four 5 x 5 x 3/8 angles	four 5 x 5 x 3/8 angles
Floors 5-6	four 6 x 6 x 5/8 angles	four 5 x 5 x 3/8 angles	four 5 x 5 x 3/8 angles

Table 3.18 Jacket sizes

Direction and Upgrade	EQGM input (1):	EQGM input (2):	EQGM input (3):	EQGM input (4):
N-S, configuration 1	0.90 W	0.19 W	1.09 W	1.28 W
E-W, configuration 1	0.45 W	0.55 W	0.37 W	0.37 W
N-S, configuration 2	0.90 W	0.20 W	1.08 W	1.28 W
E-W, configuration 2	0.33 W	0.54 W	0.44 W	0.34 W

input (1) Response spectrum analysis, 100% EQ input N-S + 30% EQ input E-W
input (2) Response spectrum analysis, 30% EQ input N-S + 100% EQ input E-W
input (3) Time-history analysis, Landers EQGMs scaled up by a factor of six
input (4) Time-history analysis, Upland EQGMs scaled up by a factor of three

Table 3.19 Base shears obtained from elastic 3D model (SAP90)

Direction	Simplified model (sec)	3D elastic model (sec)	
		Configuration 1	Configuration 2
N-S	0.38	0.41	0.41
E-W	0.55	0.70	0.63

Table 3.20 Comparison of dynamic properties of first translational mode in simplified and 3D elastic models

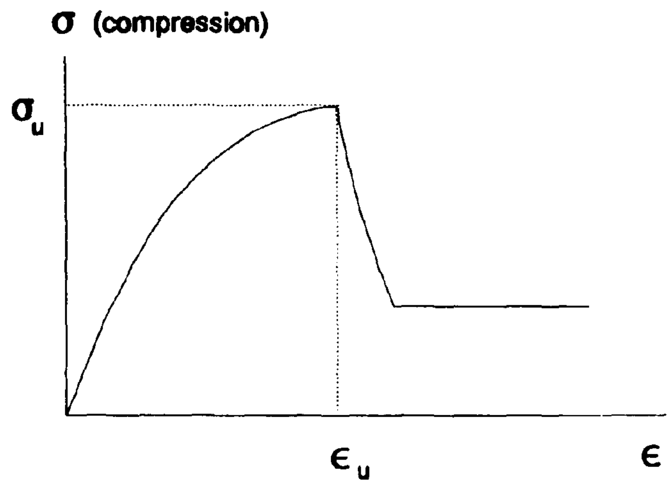

a) Typical axial stress vs. axial strain relationship in brick masonry

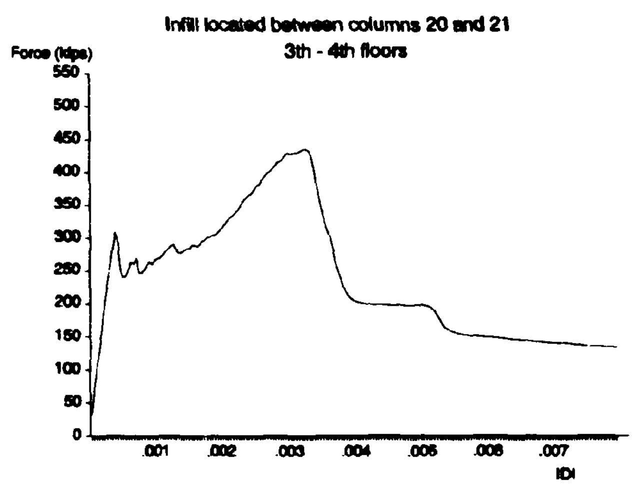

b) Lateral force vs. IDI curve in URM infill located in Frame 1

Figure 3.1 Force vs. deformation curves for URM and URM infill

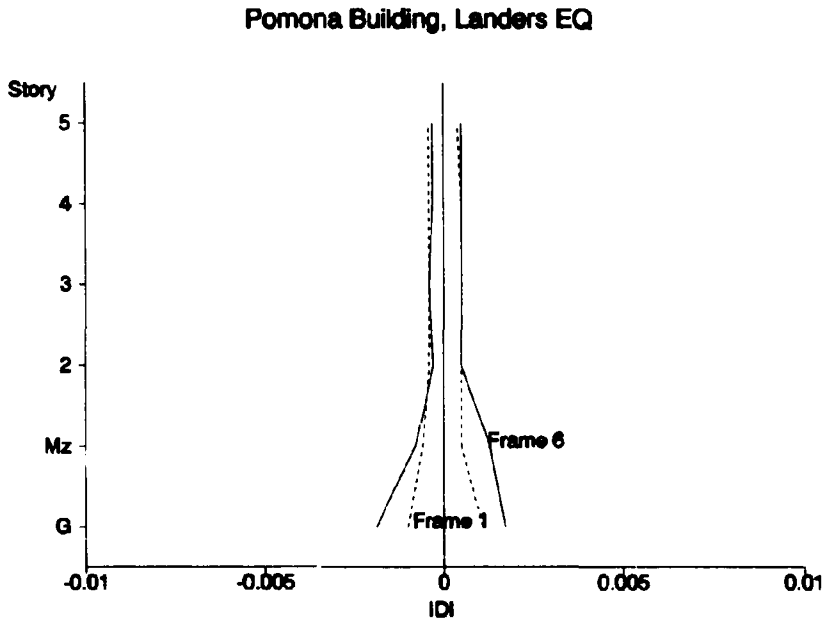

a) N-S direction

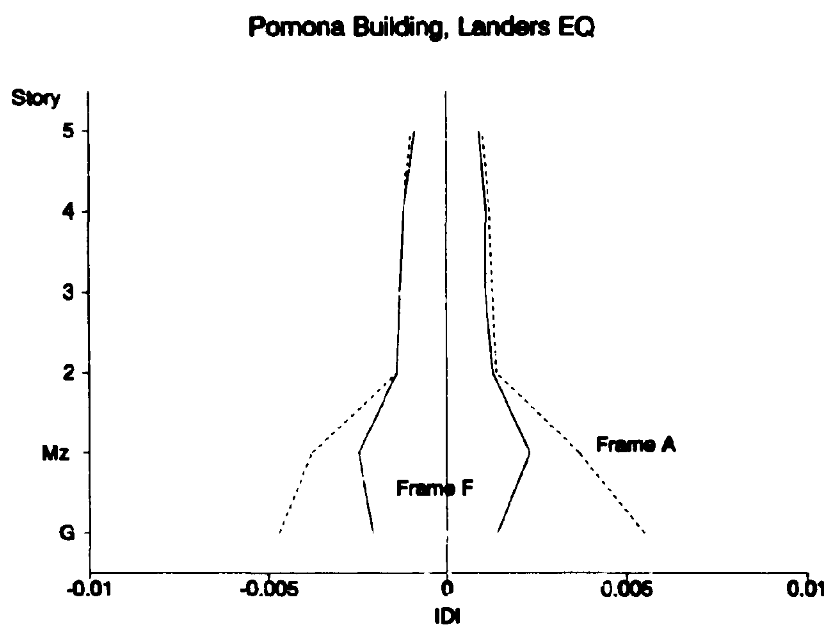

b) E-W direction

Figure 3.2 IDI obtained from elastic time-history analysis of building subjected to Landers EQ

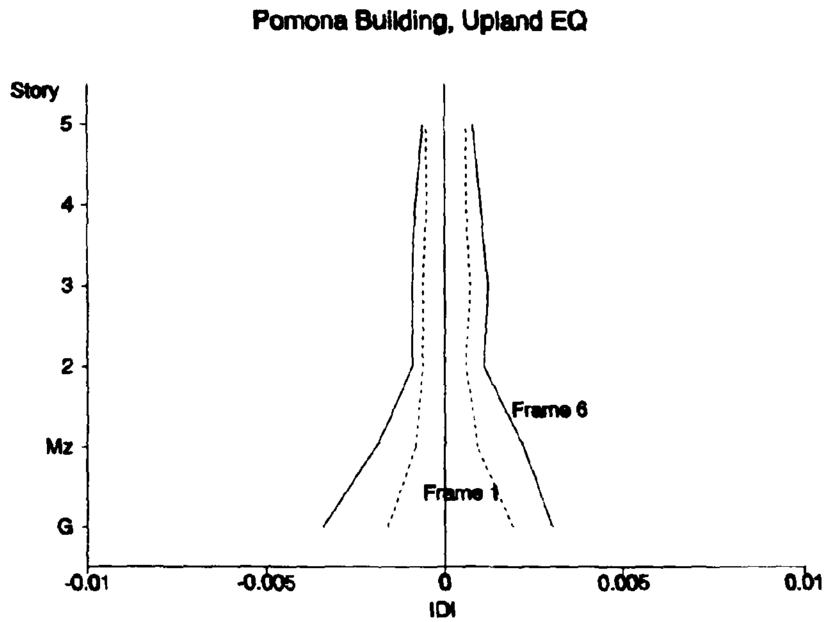

c) N-S direction

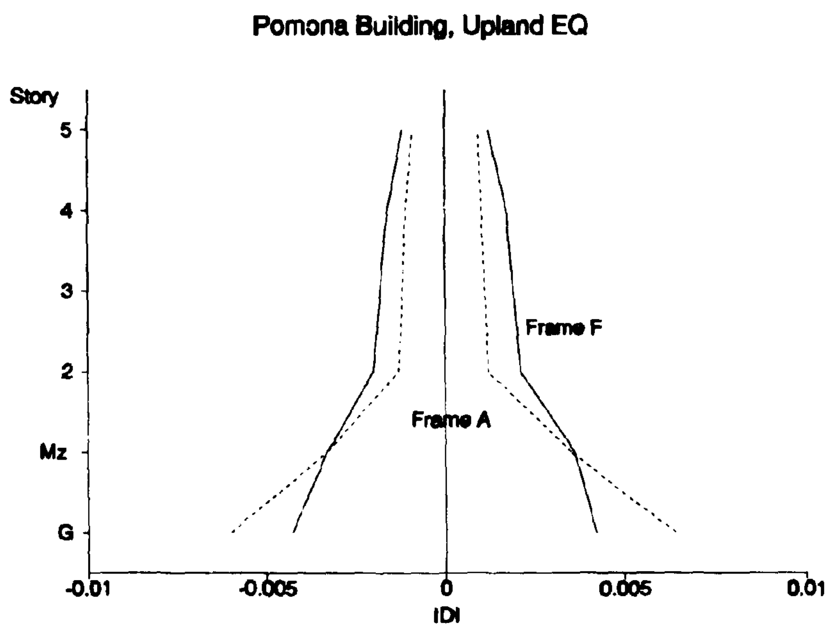

d) E-W direction

Figure 3.2 continued, IDI obtained from elastic time-history analysis of building subjected to Upland EQ

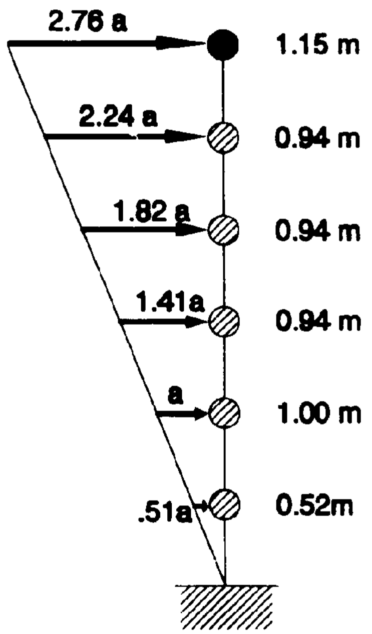

Story	F	V
6	3.17ma	3.17ma
5	2.10ma	5.27ma
4	1.71ma	6.98ma
3	1.33ma	8.31ma
2	1.00ma	9.31ma
1	0.27ma	9.58ma

Figure 3.3 Story forces and shears, assuming a linear distribution of accelerations through height, in terms of the mass (m) and acceleration (a) at the second floor

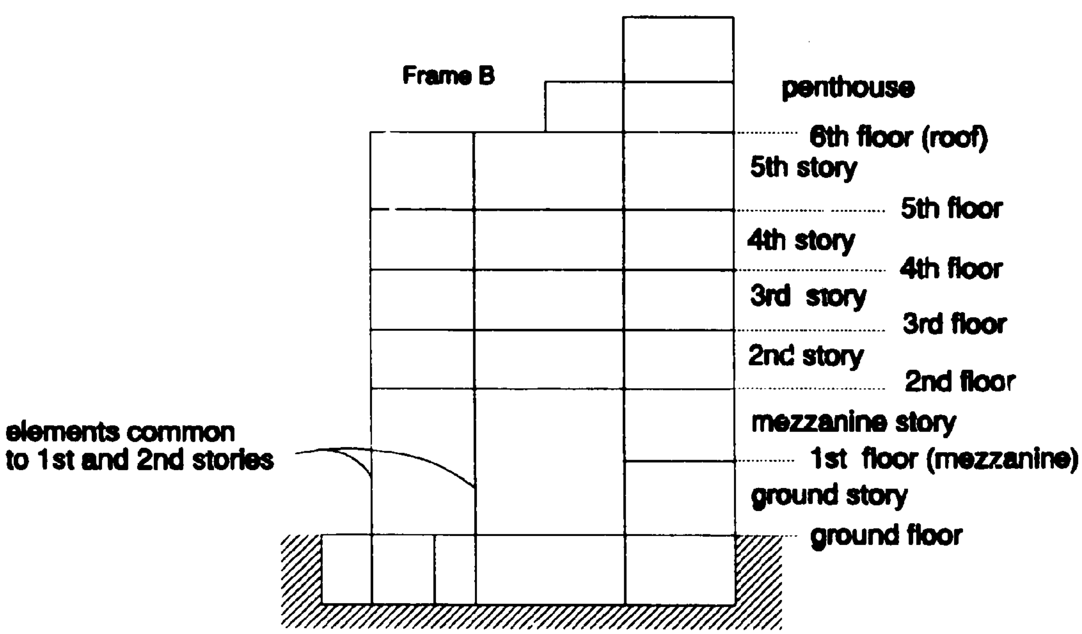

Figure 3.4 Identification of stories and floors

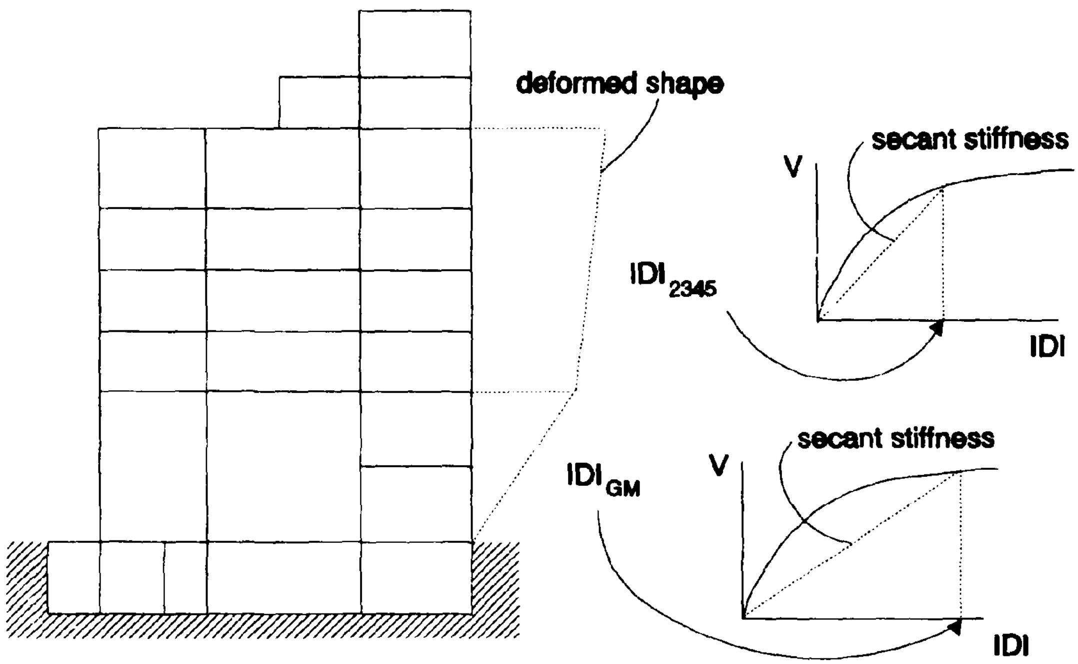

Figure 3.5 Difference between secant stiffness of the two lower stories and that of the four upper stories

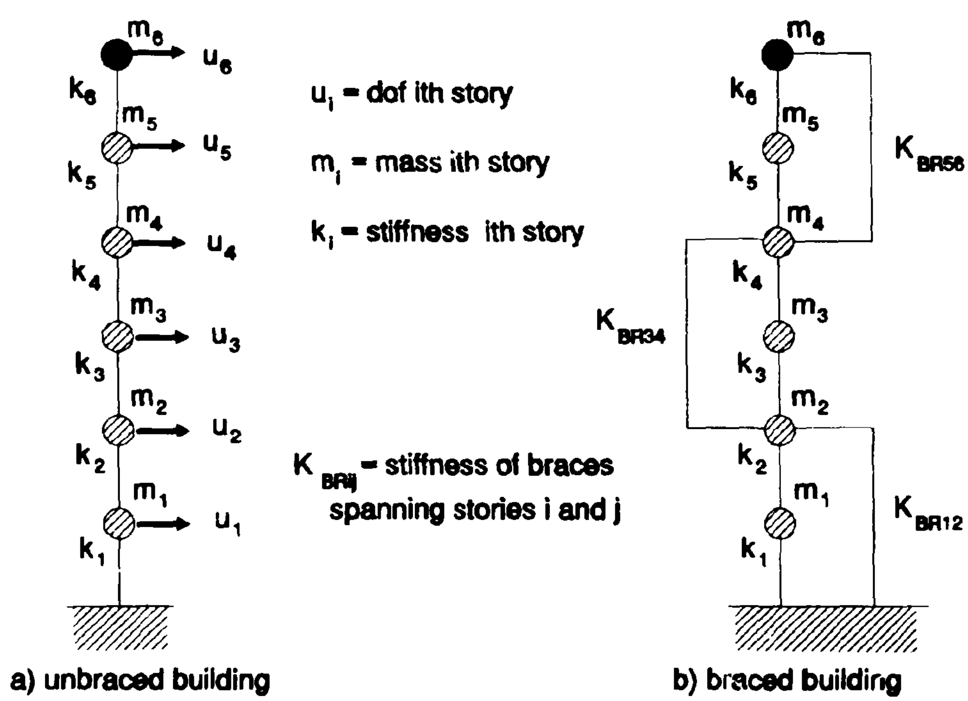

Figure 3.6 Stick models of braced and unbraced building

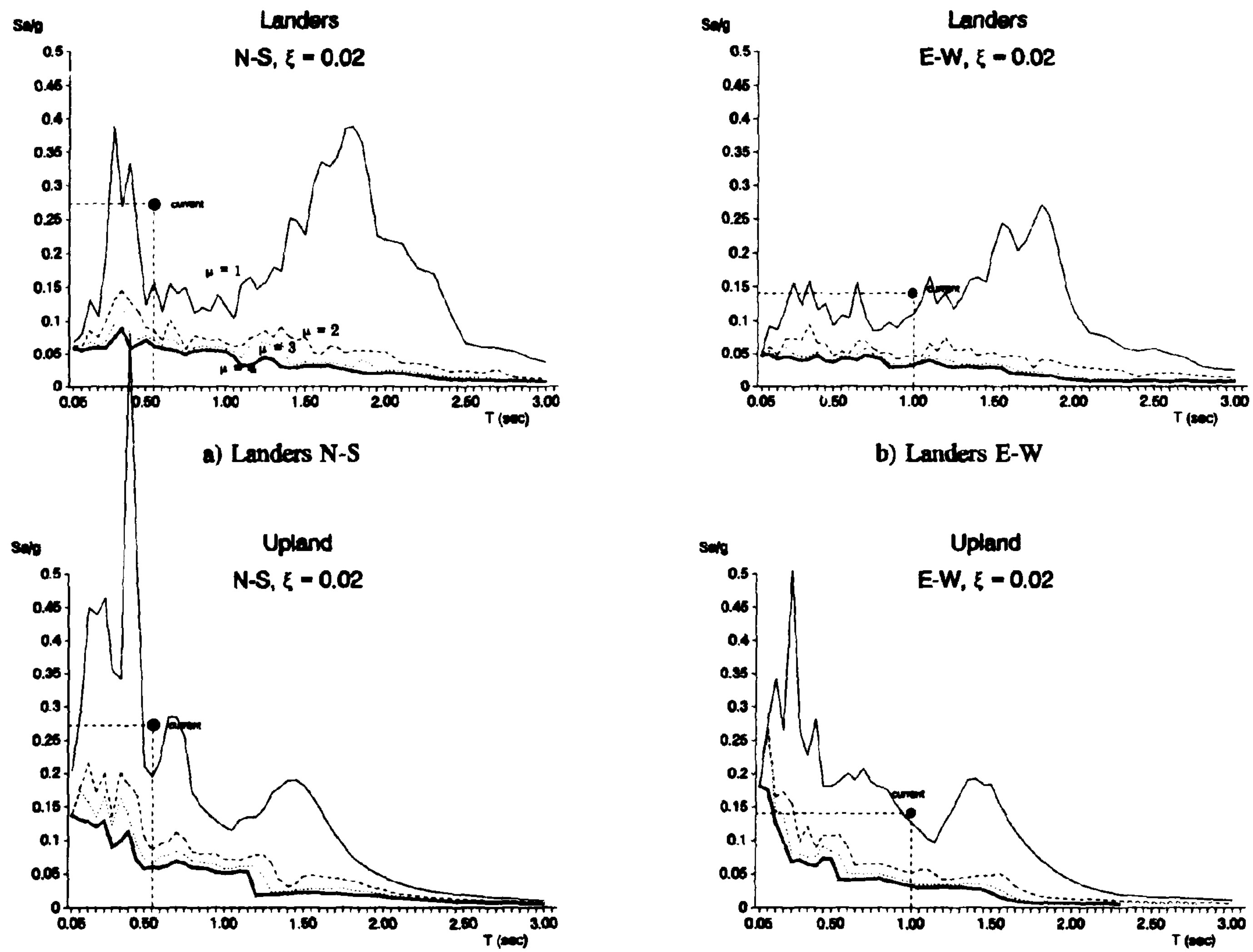

a) Landers N-S

b) Landers E-W

c) Upland N-S

d) Upland E-W

Figure 3.7 Strength Spectra for recorded ground motions

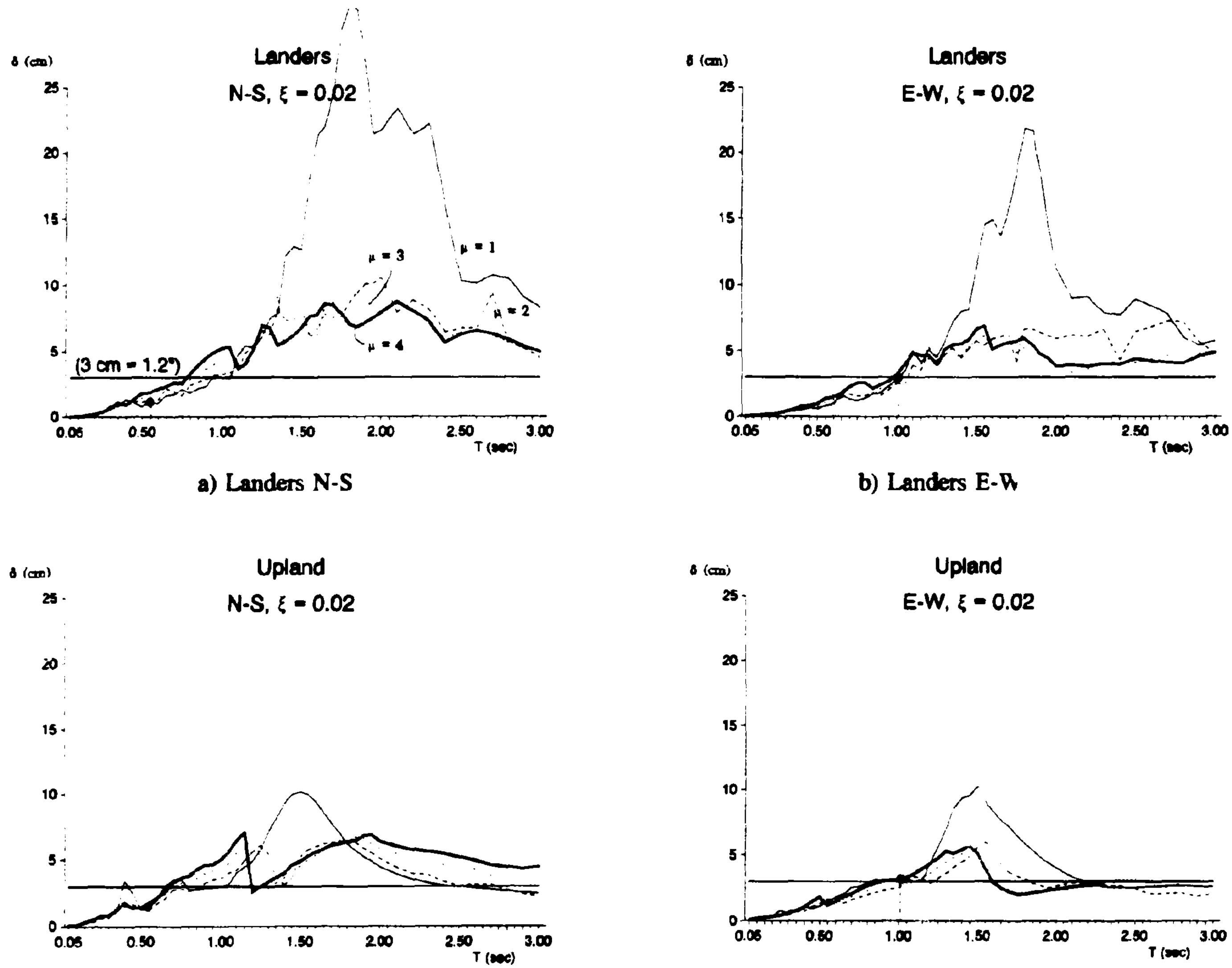

a) Landers N-S

b) Landers E-W

c) Upland N-S

d) Upland E-W

Figure 3.8 Displacement Spectra for recorded ground motions

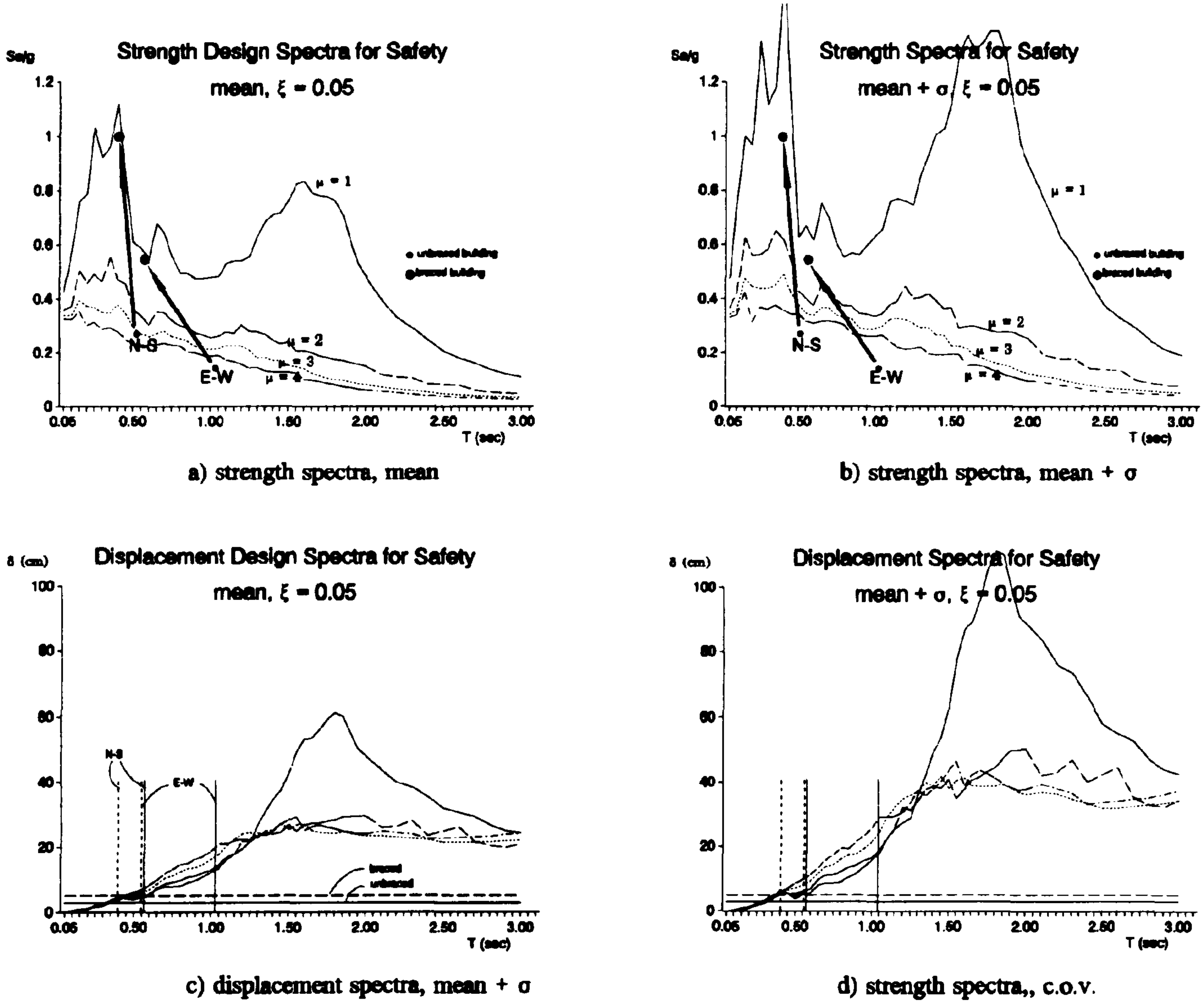

Figure 3.9 Design Spectra for Safety

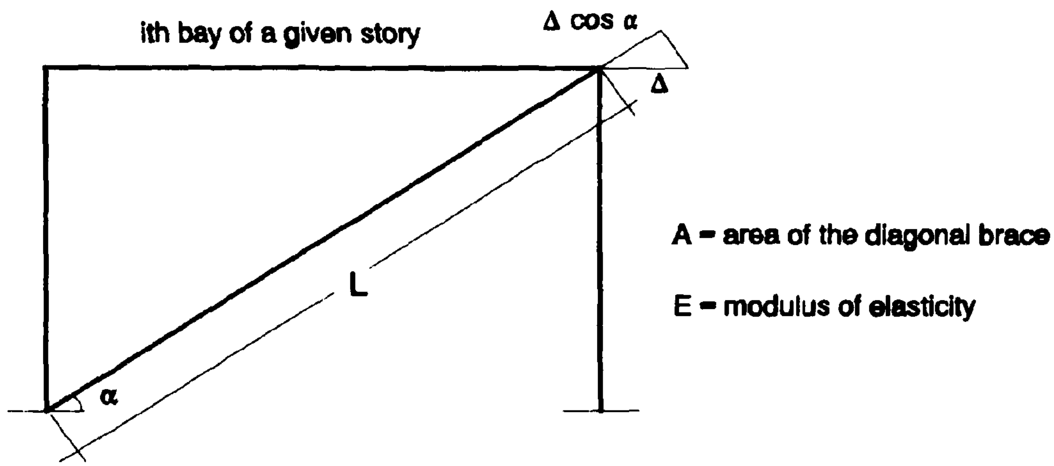

Figure 3.10 Definition of α, L, A and E

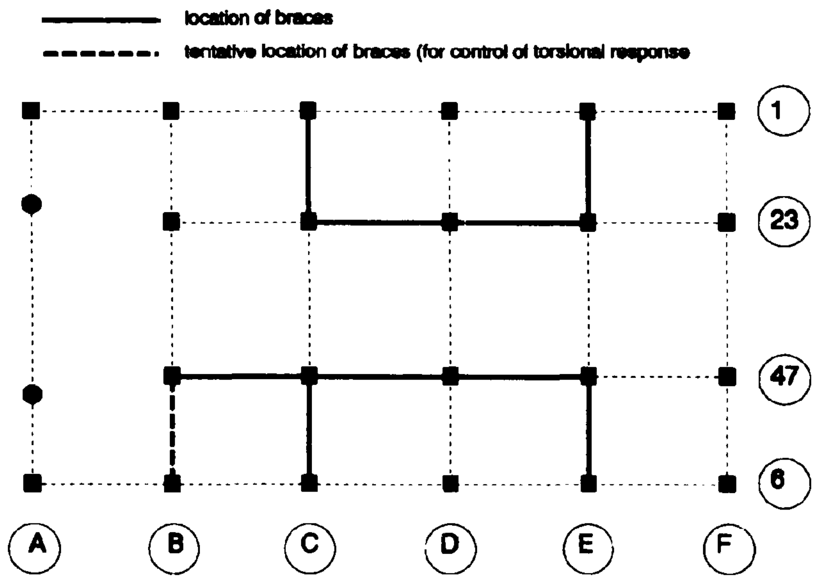

a) first two stories

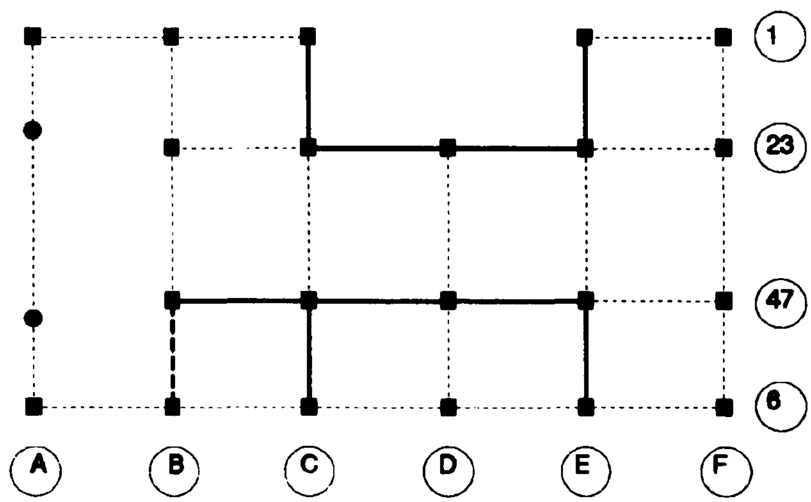

b) upper stories

Figure 3.11 Plan view of PT bracing system

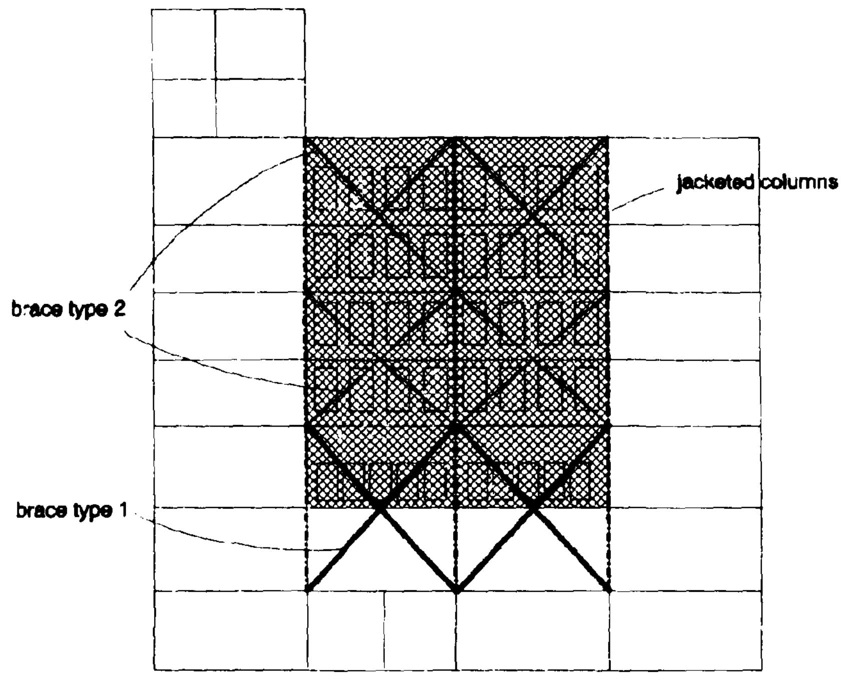

a) Frame 23

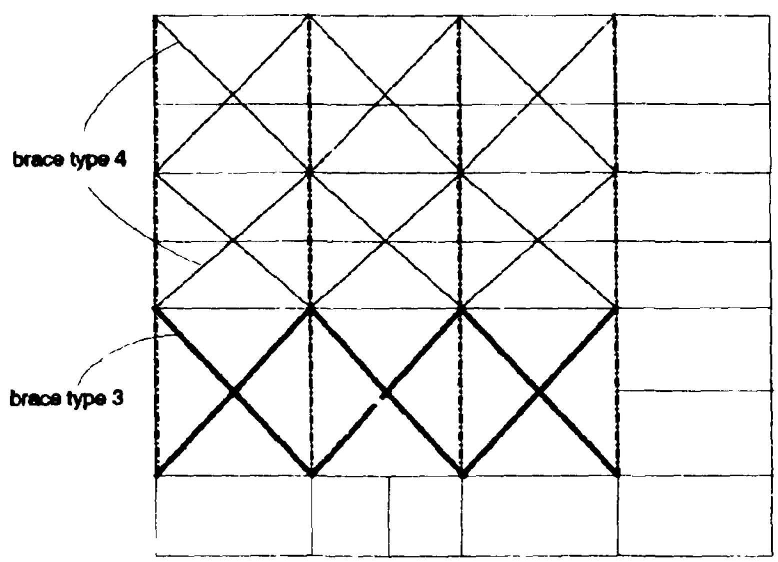

b) Frame 47

Figure 3.12 Elevation view of PT bracing system

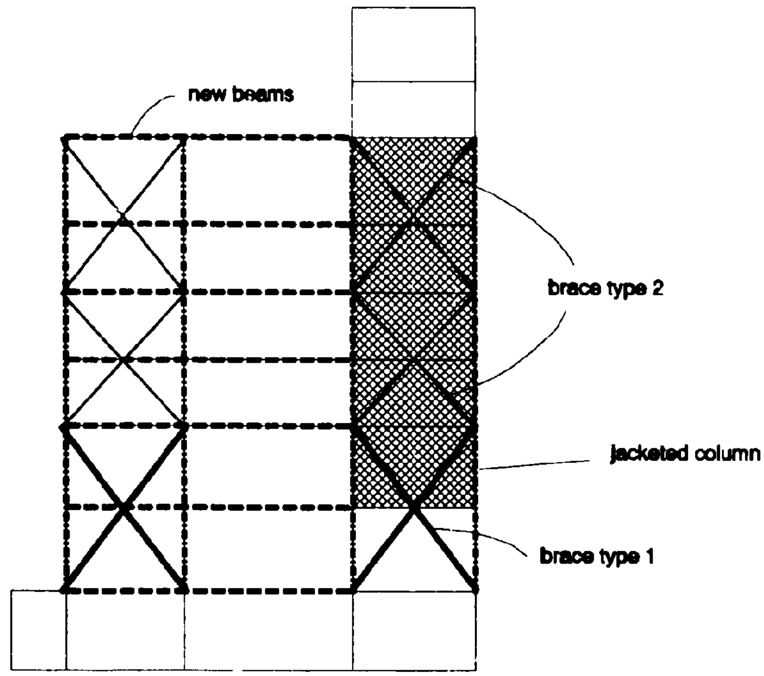

c) Frame C

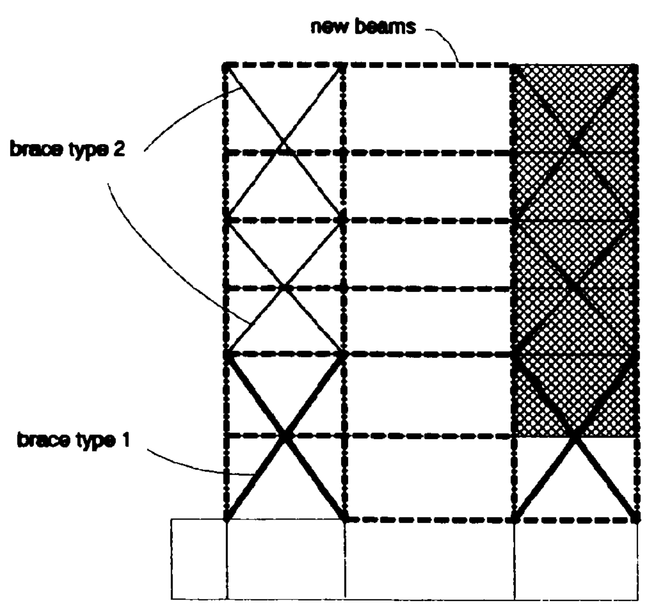

d) Frame E

Figure 3.12 continued

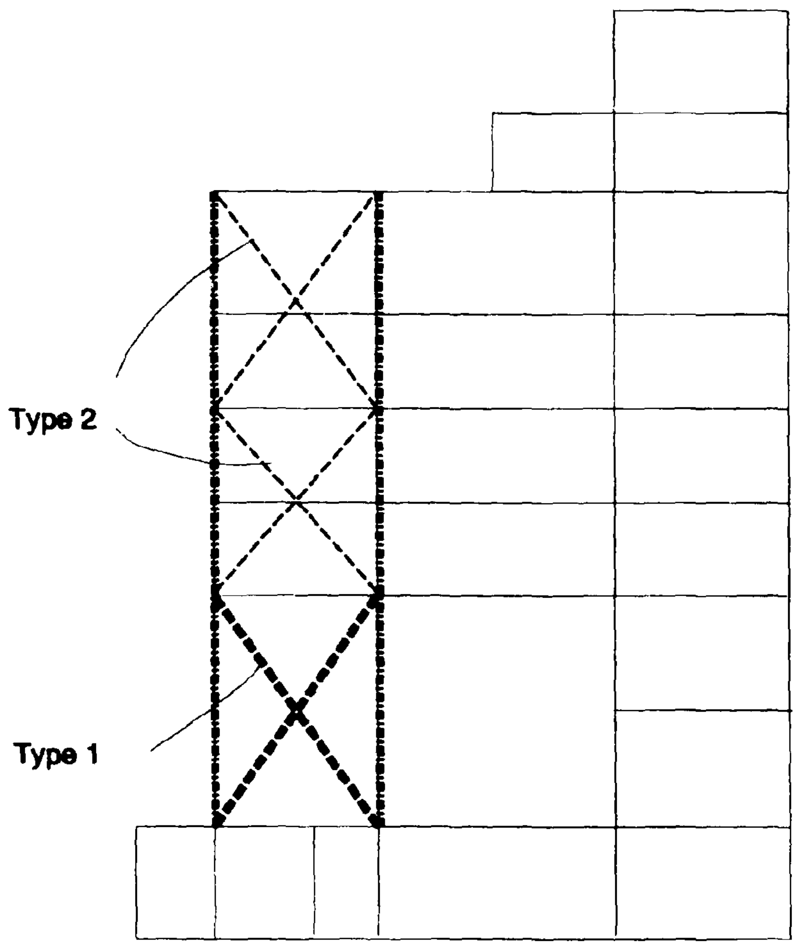

e) Frame B

Fig.ure 3.12 continued

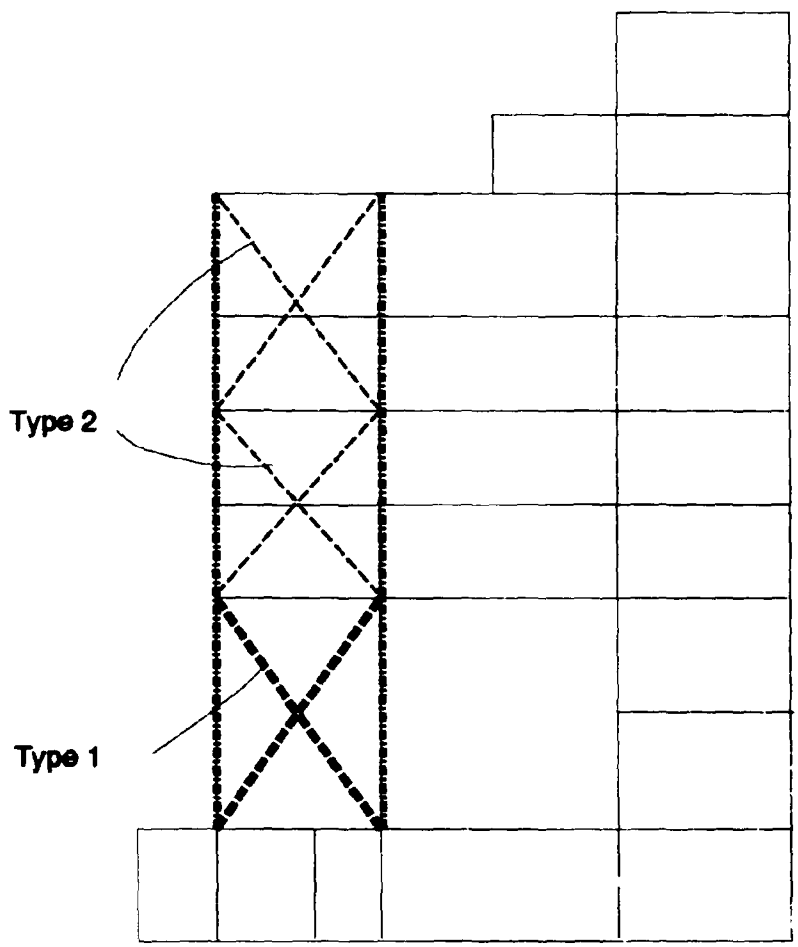

e) Frame B

Figure 3.12 continued

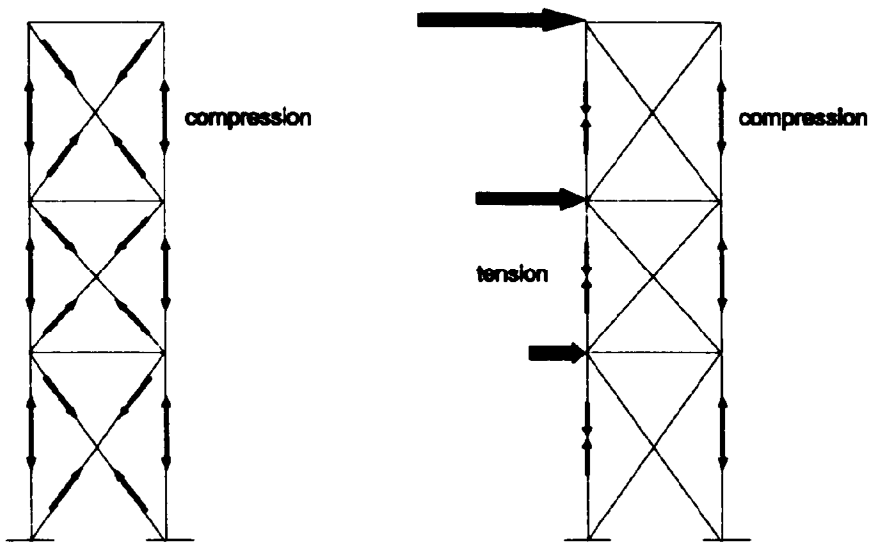

a) postensioning

b) lateral loads

Figure 3.13 Axial forces induced in columns by the PT braces

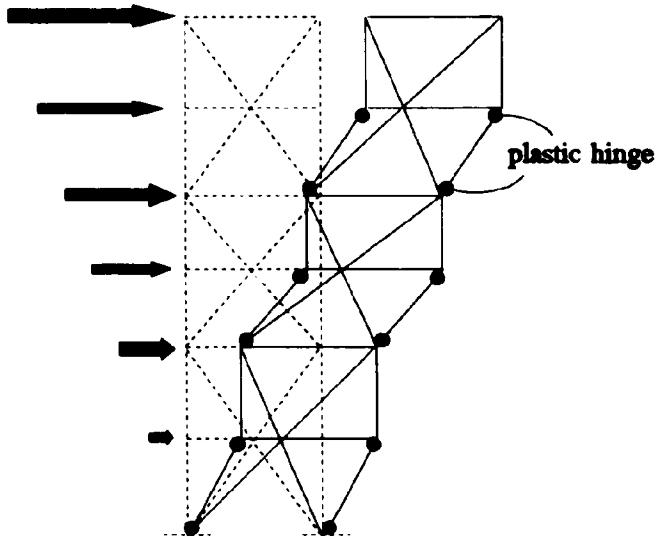

Figure 3.14 Local story mechanism

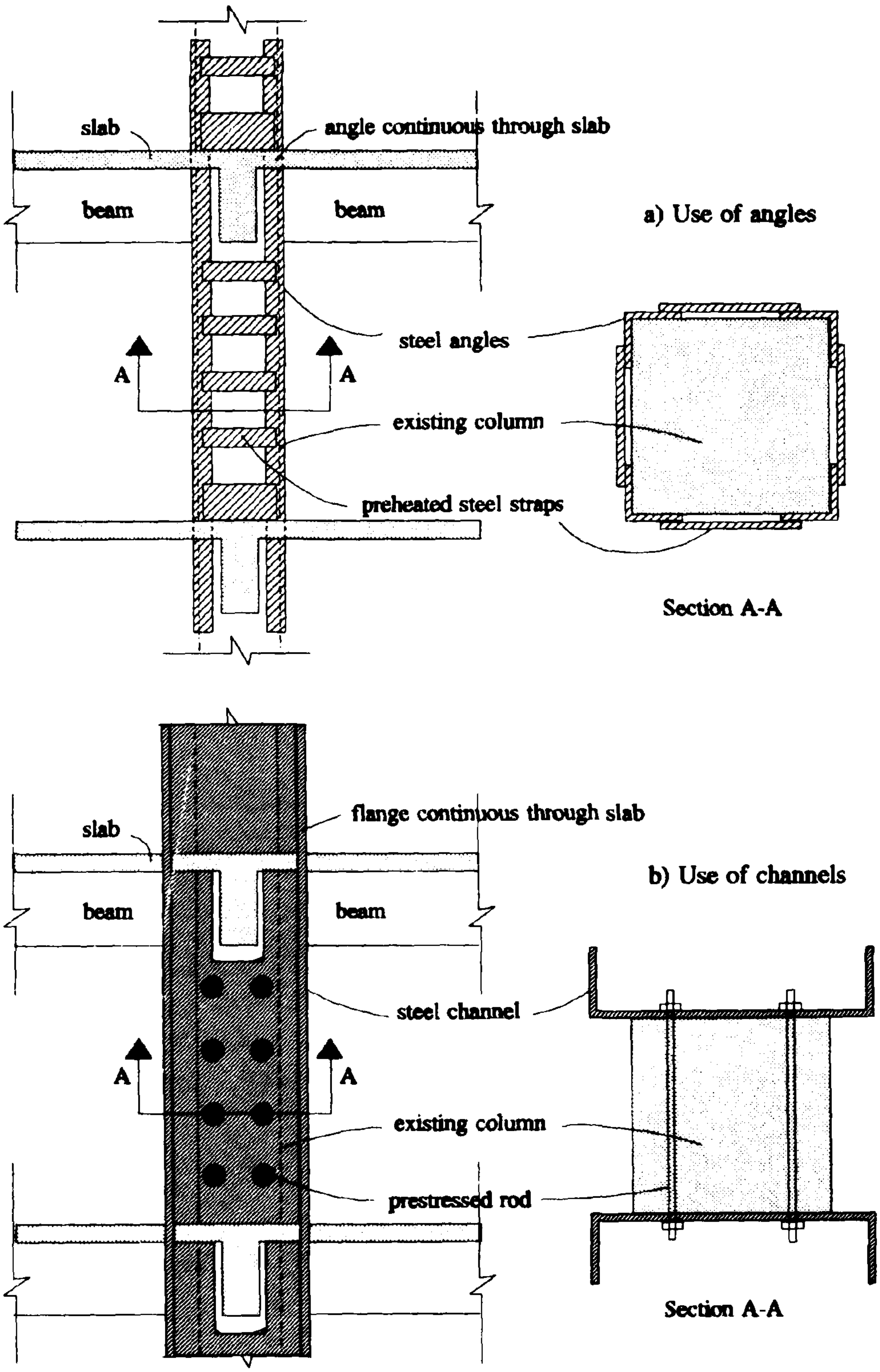

Figure 3.15 Steel jacketing of RC columns

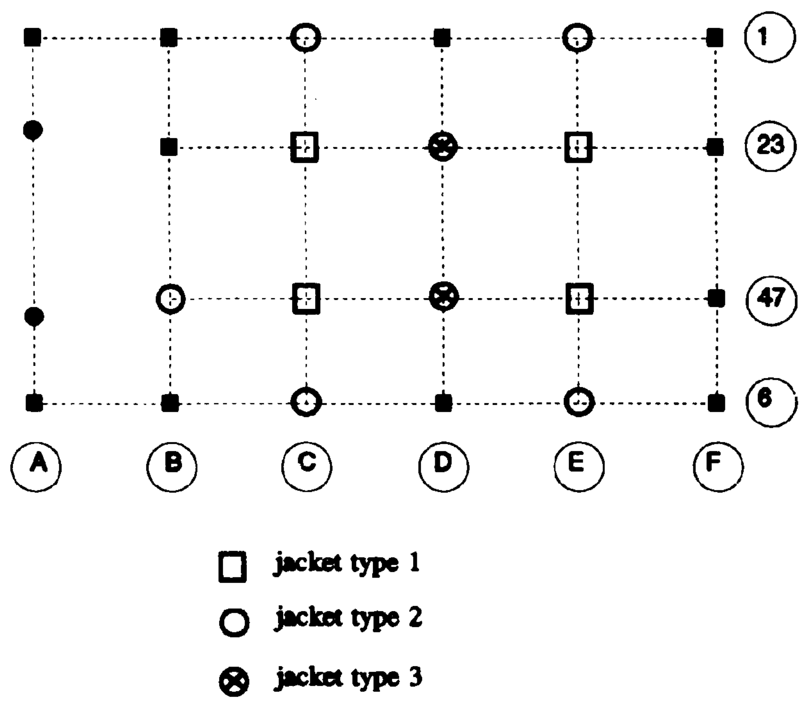

Figure 3.16 Types of steel jacket

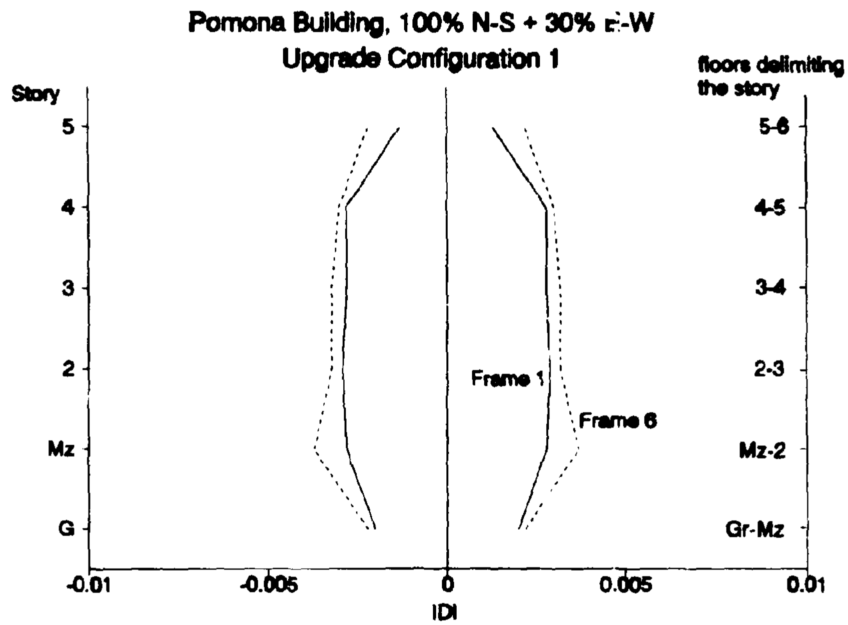

a) N-S direction

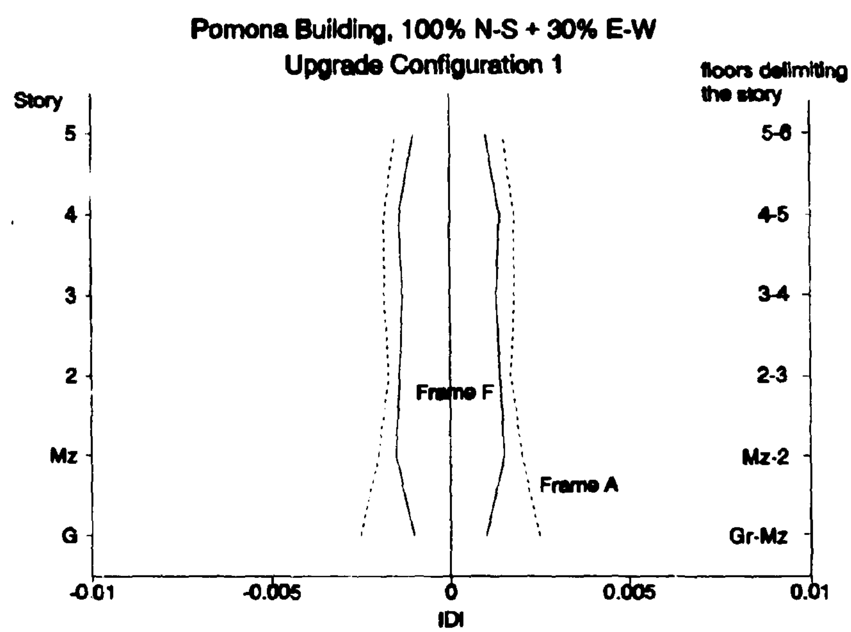

b) E-W direction

Figure 3.17 IDI obtained from elastic response spectra analysis of configuration 1 using 100% and 30% input in N-S and E-W directions, respectively

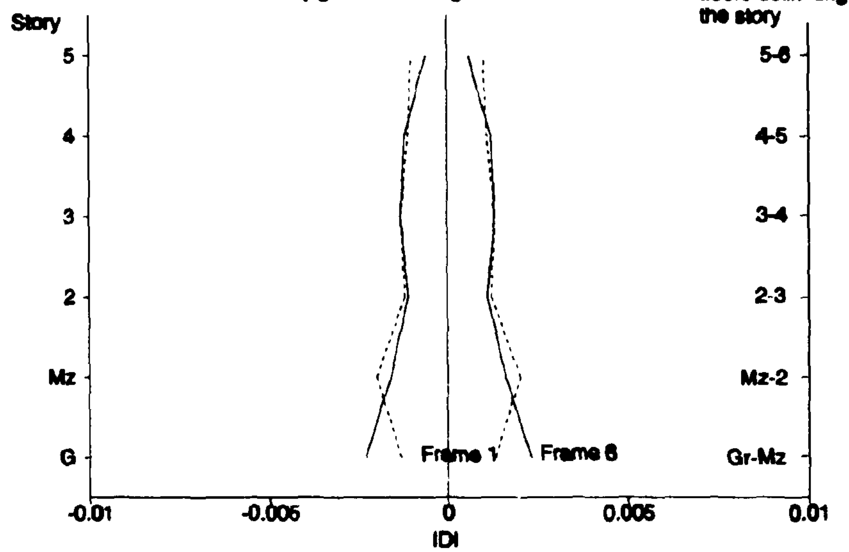

a) N-S direction

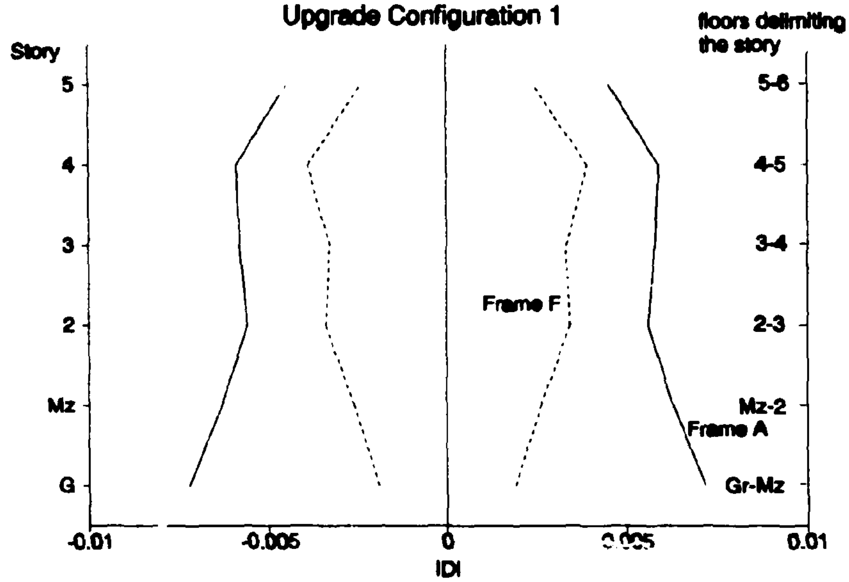

b) E-W direction

Figure 5.18 IDI obtained from elastic response spectra analysis of configuration 1 using 30% and 100% input in N-S and E-W directions, respectively

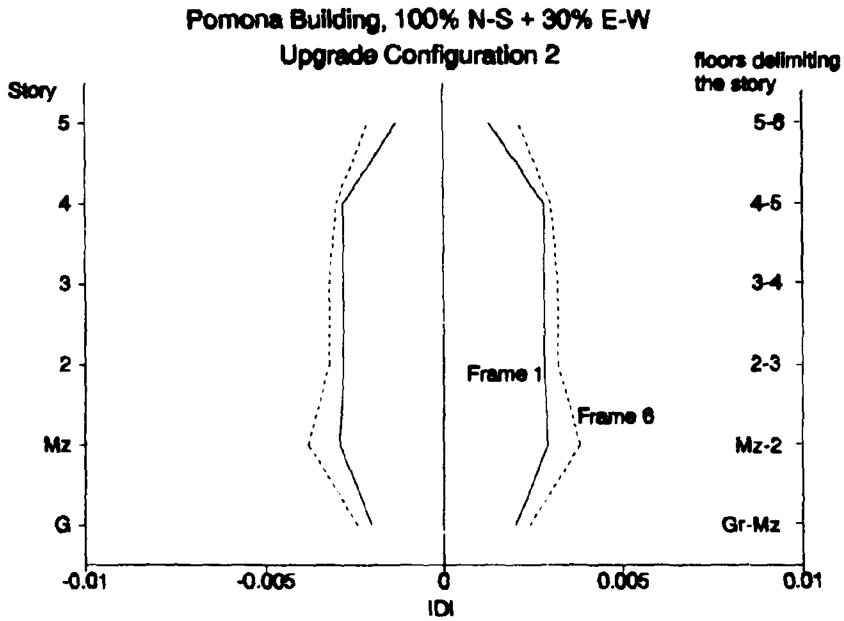

a) N-S direction

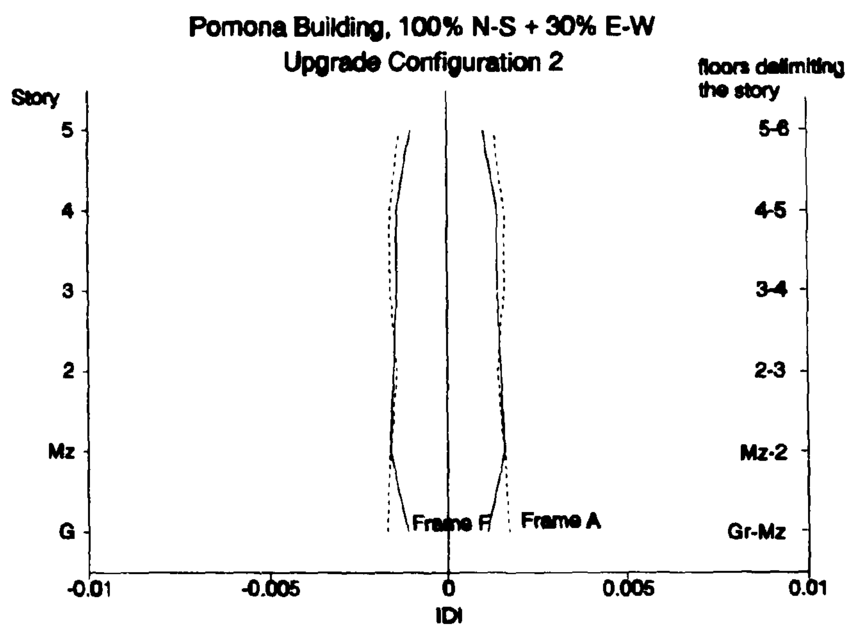

b) E-W direction

Figure 3.19 IDI obtained from elastic response spectra analysis of configuration 2 using 100% and 30% input in N-S and E-W directions, respectively

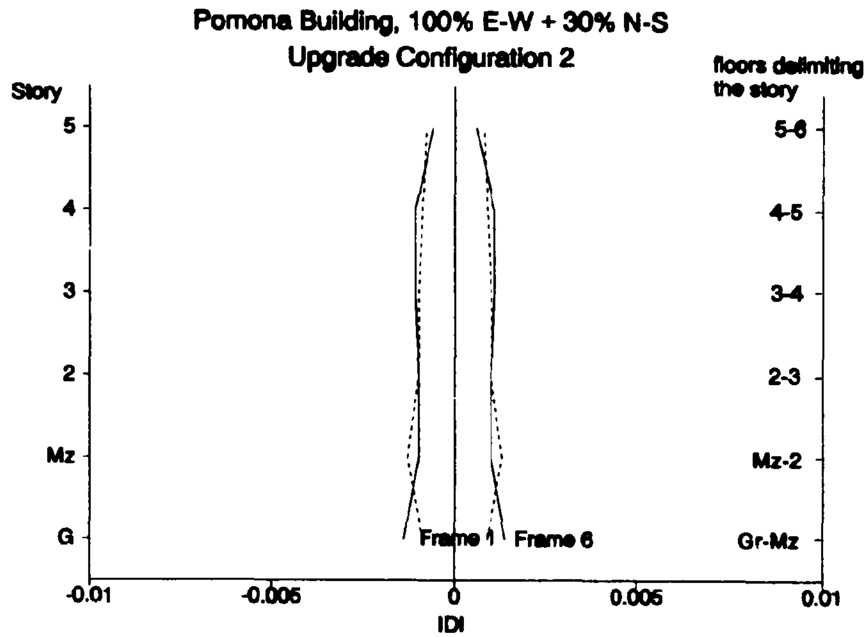

a) N-S direction

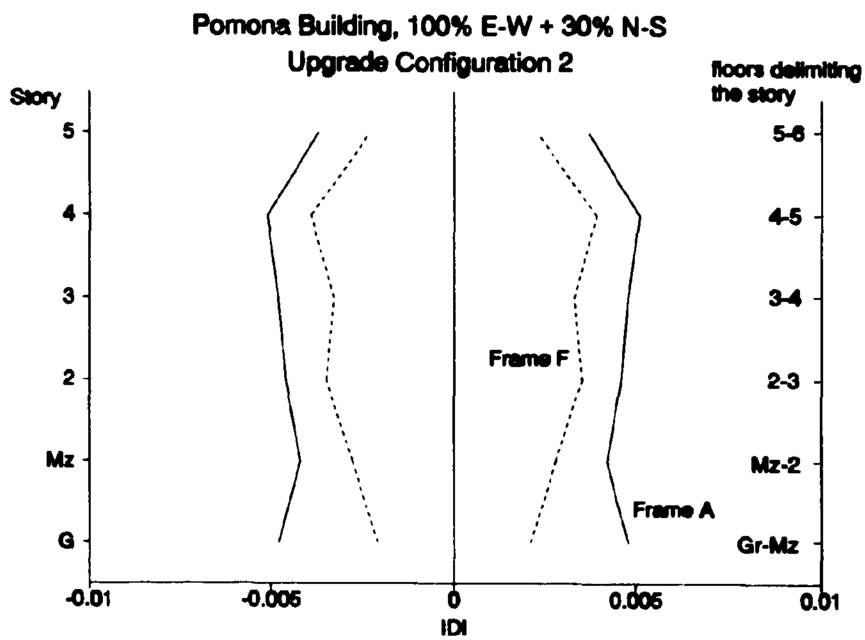

b) E-W direction

Figure 3.20 IDI obtained from elastic response spectra analysis of configuration 2 using 30% and 100% input in N-S and E-W directions, respectively

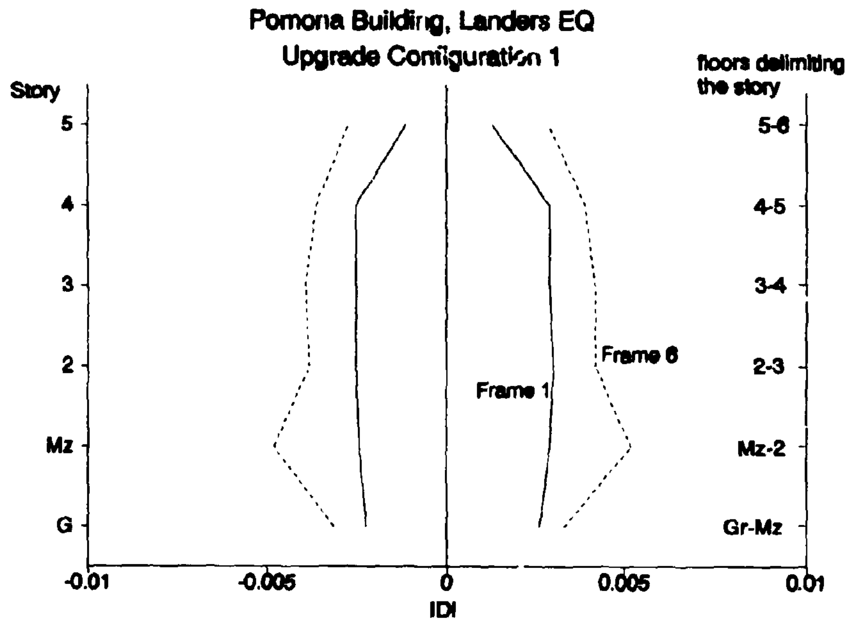

a) N-S direction

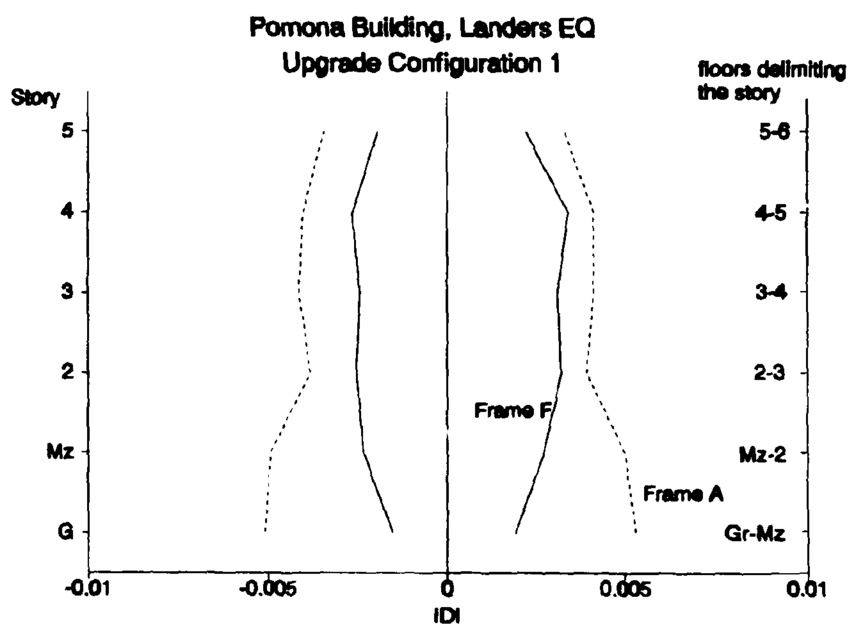

b) E-W direction

Figure 3.21 IDI obtained from elastic time-history analysis of configuration 1 subjected to Landers EQGMs scaled up by a factor of six

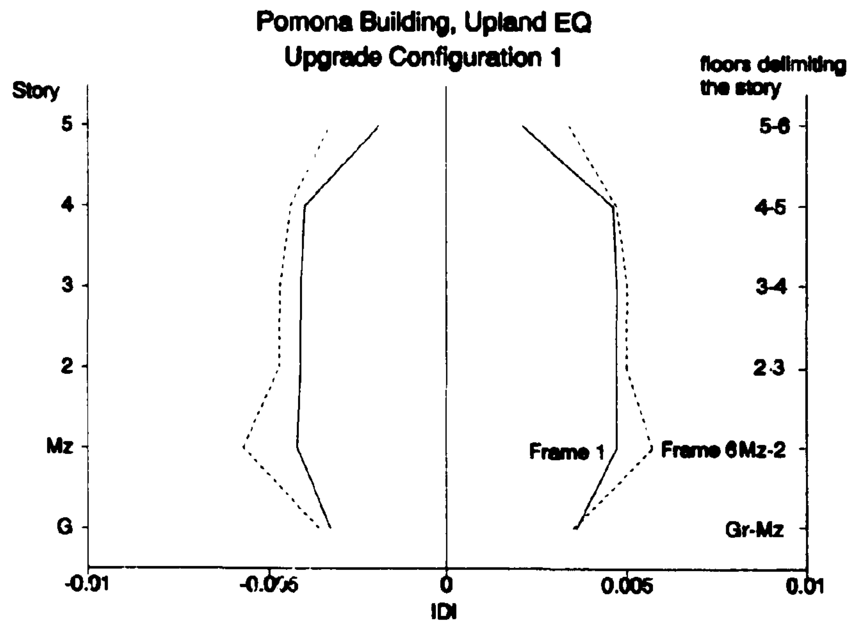

a) N-S direction

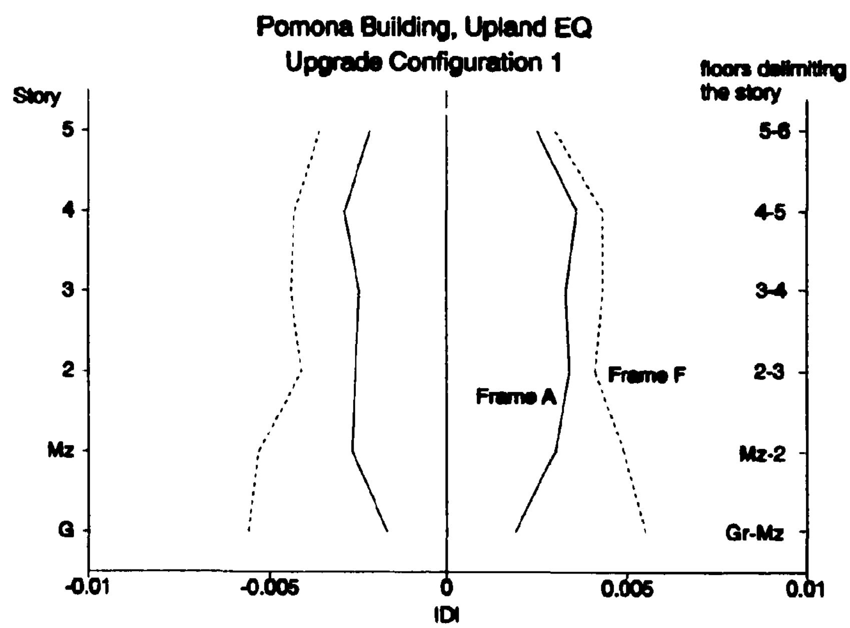

b) E-W direction

Figure 3.22 IDI obtained from elastic time-history analysis of configuration 1 subjected to Upland EQGMs scaled up by a factor of three

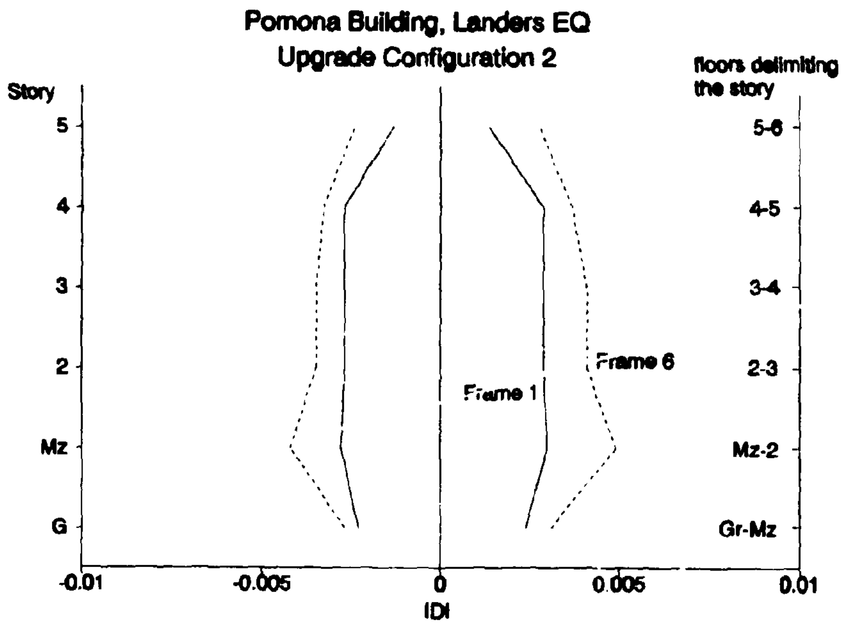

a) N-S direction

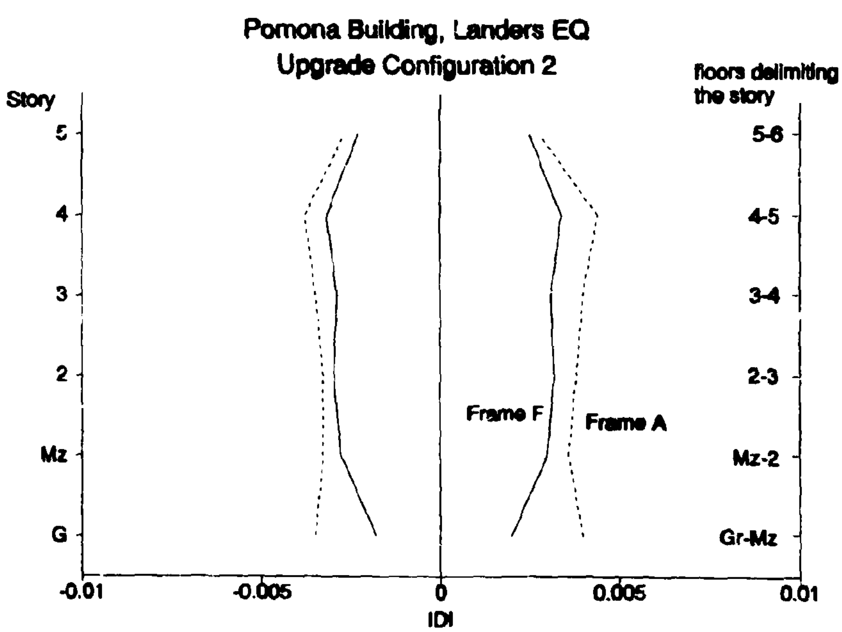

b) E-W direction

Figure 3.23 IDI obtained from elastic time-history analysis of configuration 2 subjected to Landers EQGMs scaled up by a factor of six

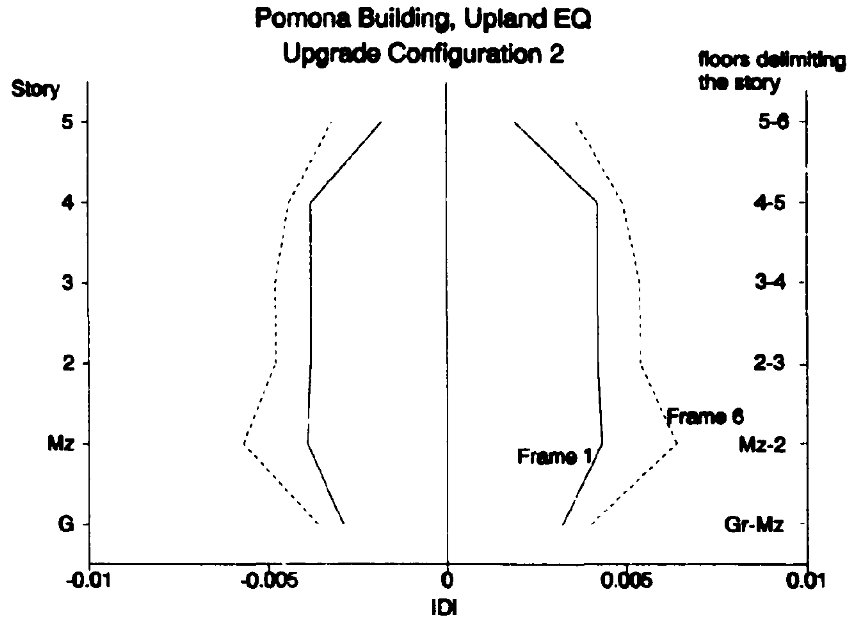

a) N-S direction

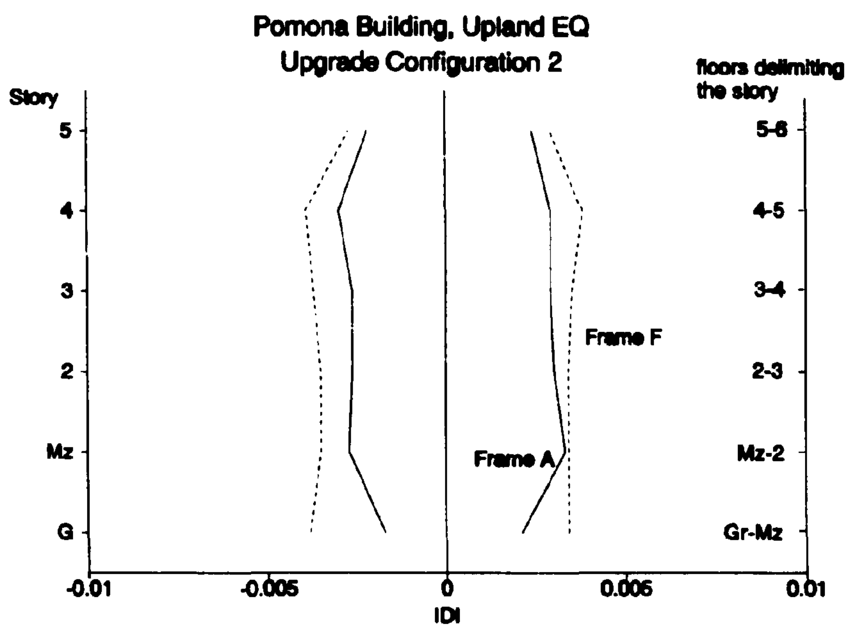

b) E-W direction

Figure 3.24 IDI obtained from elastic time-history analysis of configuration 2 subjected to Upland EQGMs scaled up by a factor of three

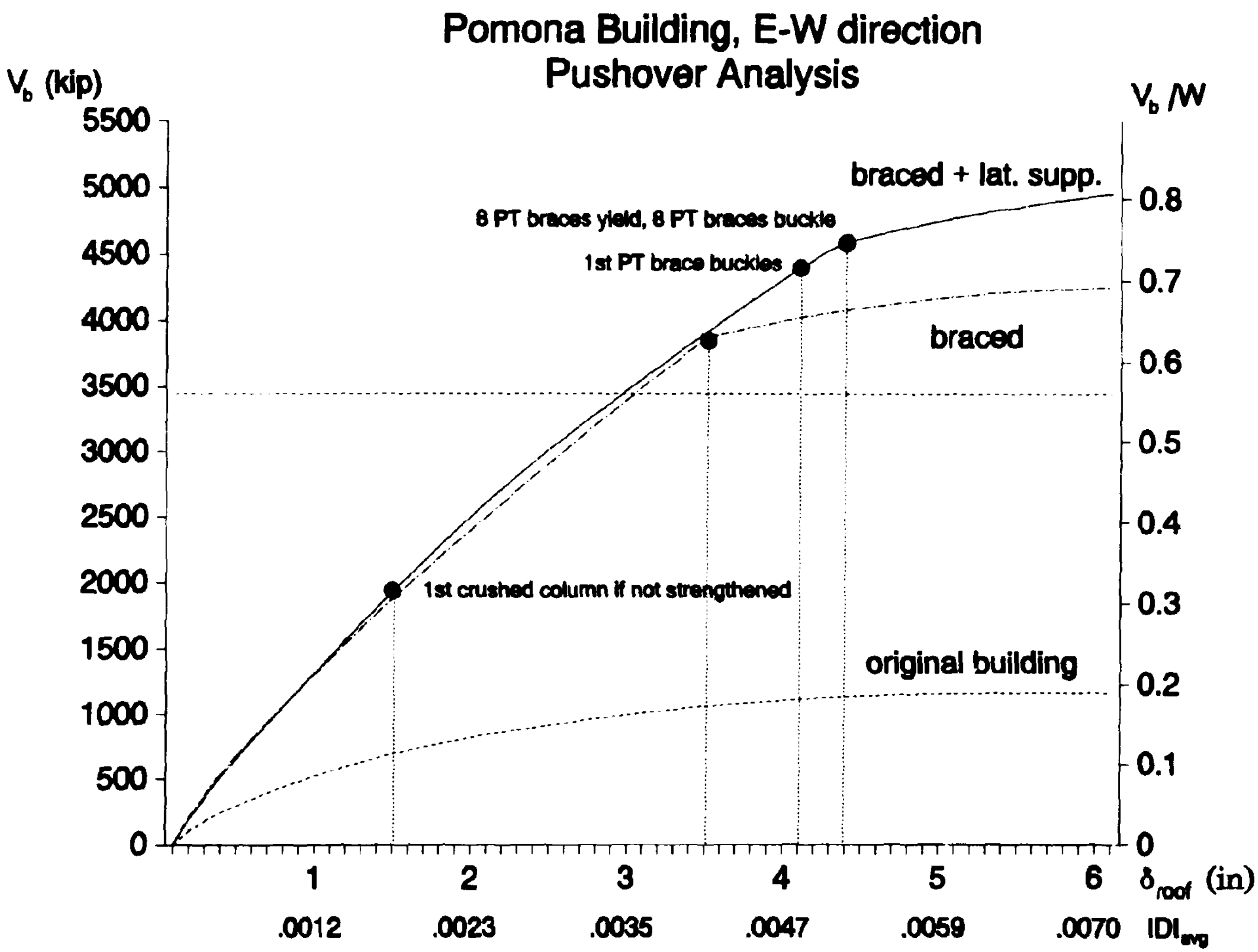

Figure 3.25 Roof displacement vs. base shear curves obtained from 2D pushover analysis of E-W direction

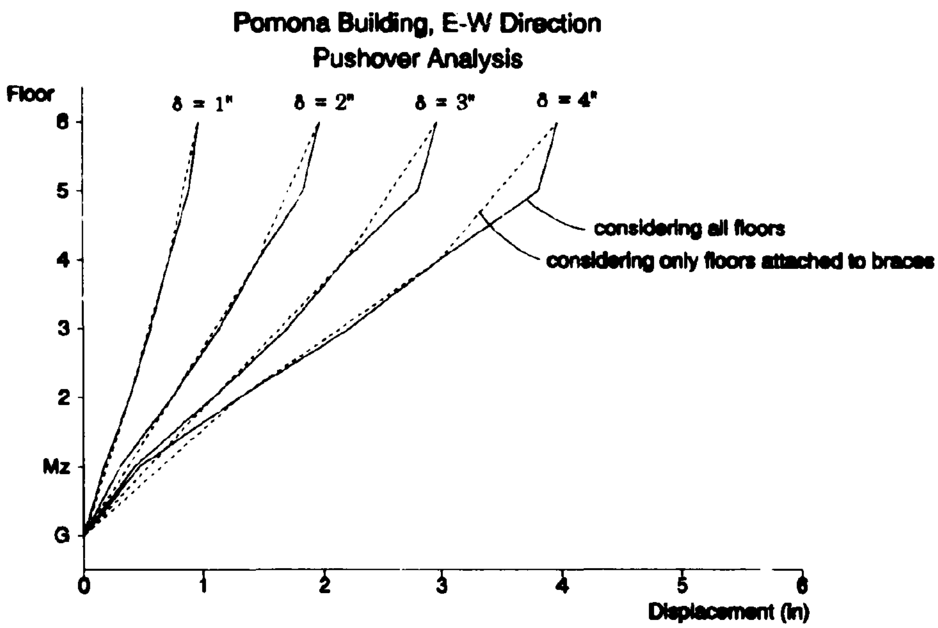

a) Without lateral support

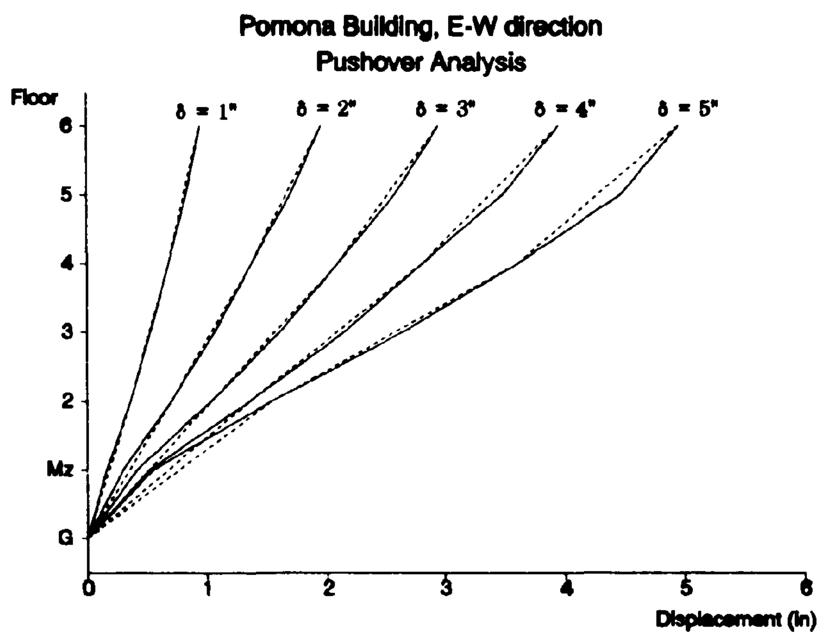

b) With lateral support

Figure 3.26 Floor displacements obtained from 2D pushover analysis of upgraded building with and without lateral support, E-W direction

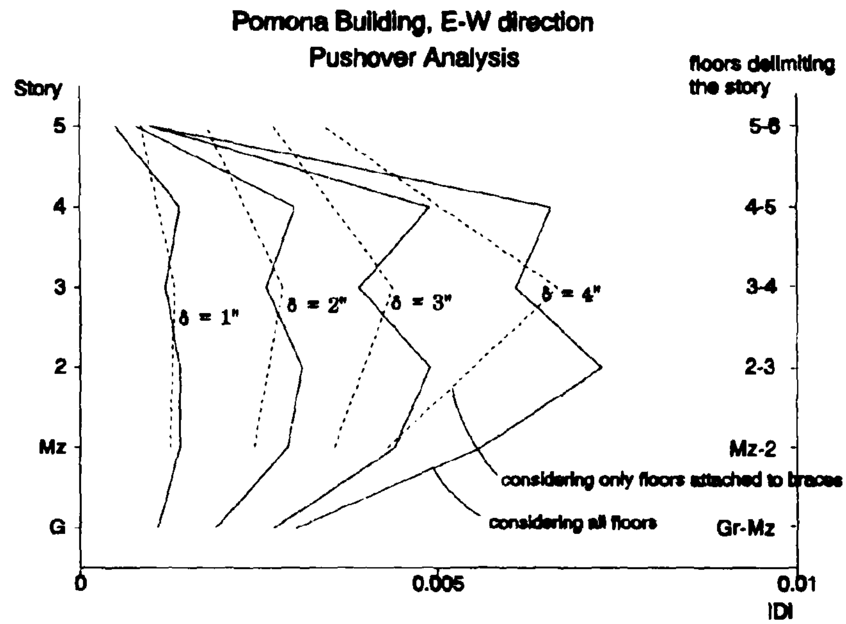

a) Without lateral support

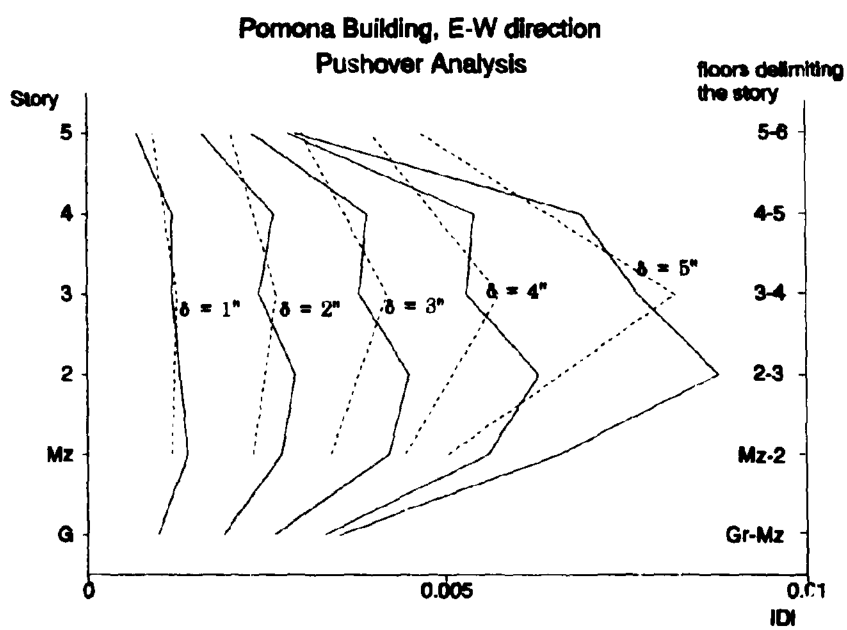

b) With lateral support

Figure 3.27 IDI obtained from 2D pushover analysis of upgraded building with and without lateral support, E-W direction

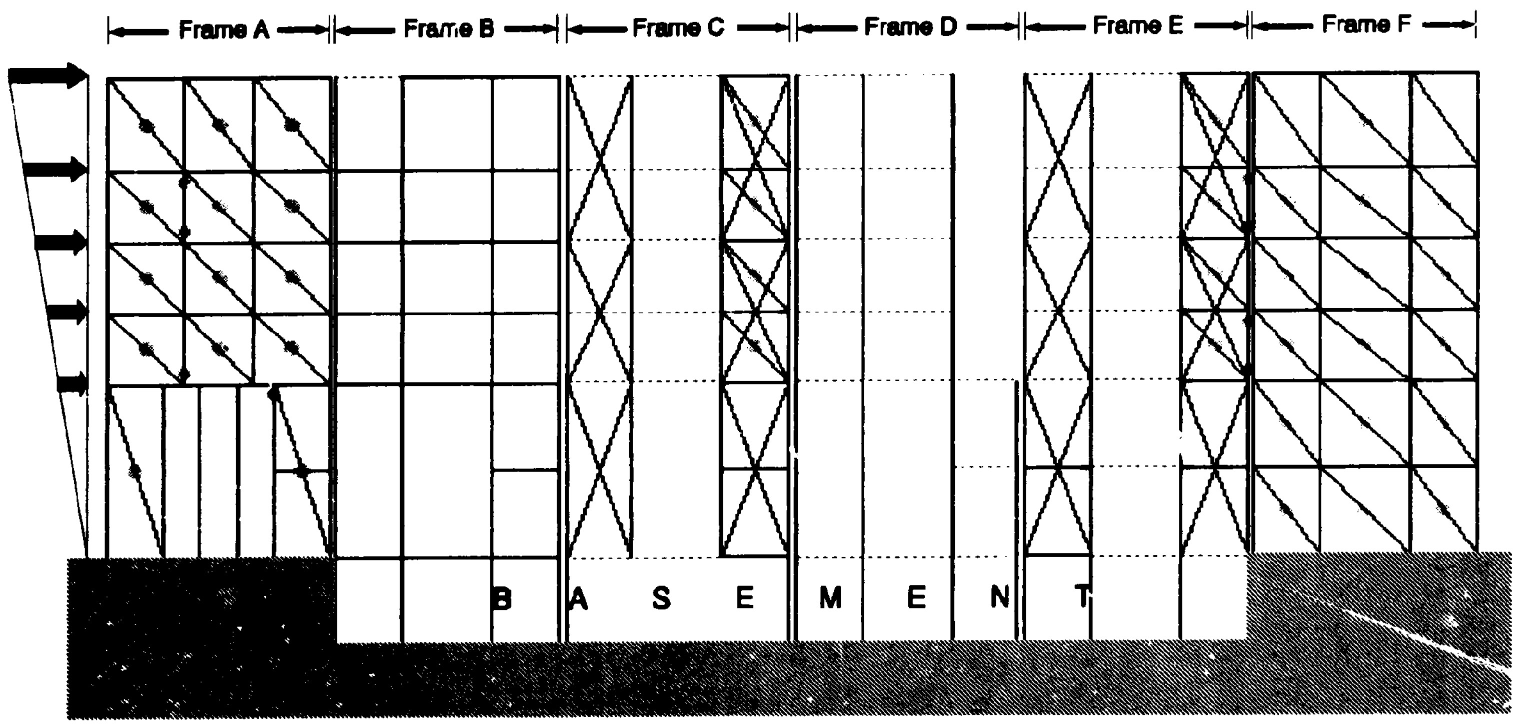

Figure 3.28 State of the E-W direction at δ_{roof} = 1" according to 2D pushover analysis of braced building without additional lateral stiffness

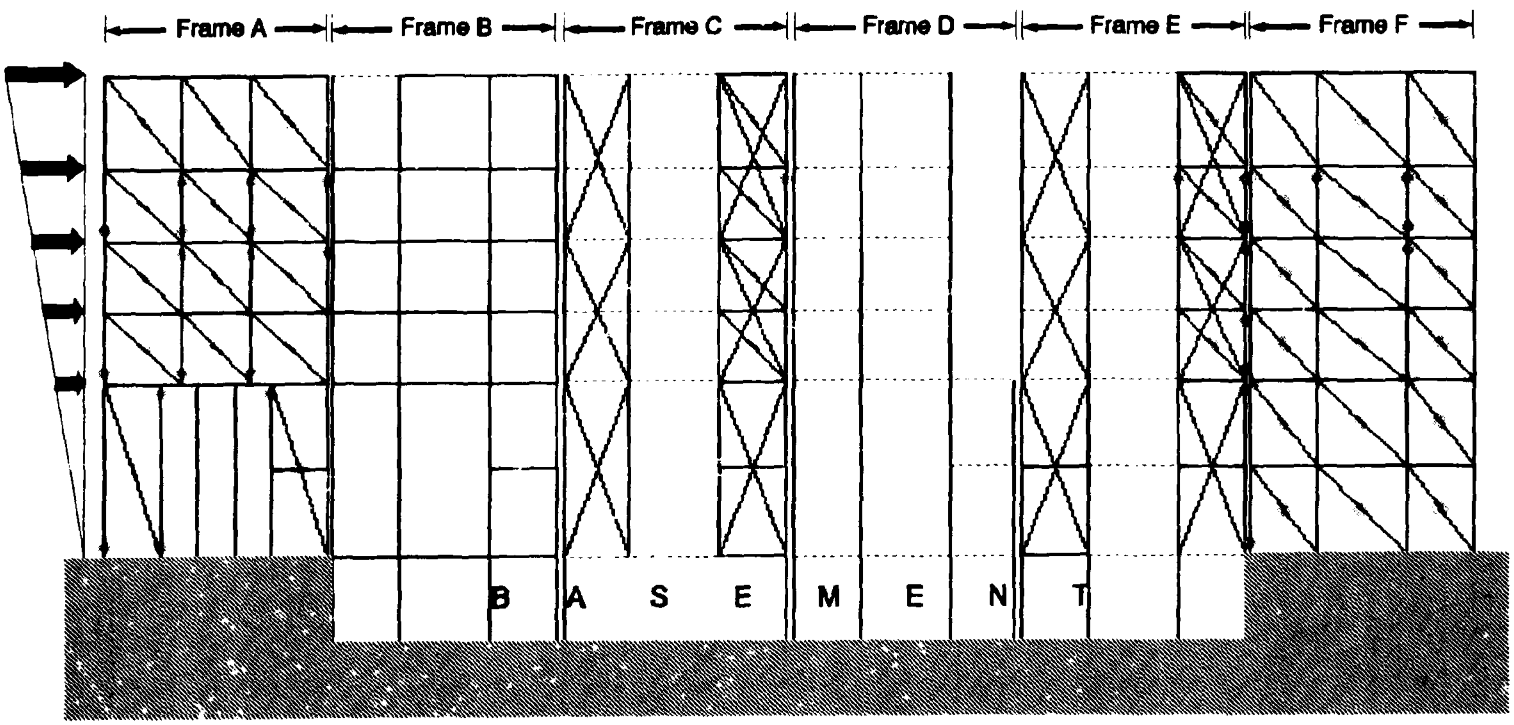

Figure 3.29 State of the E-W direction at $\delta_{roof} = 2''$ according to 2D pushover analysis of braced building without additional lateral stiffness

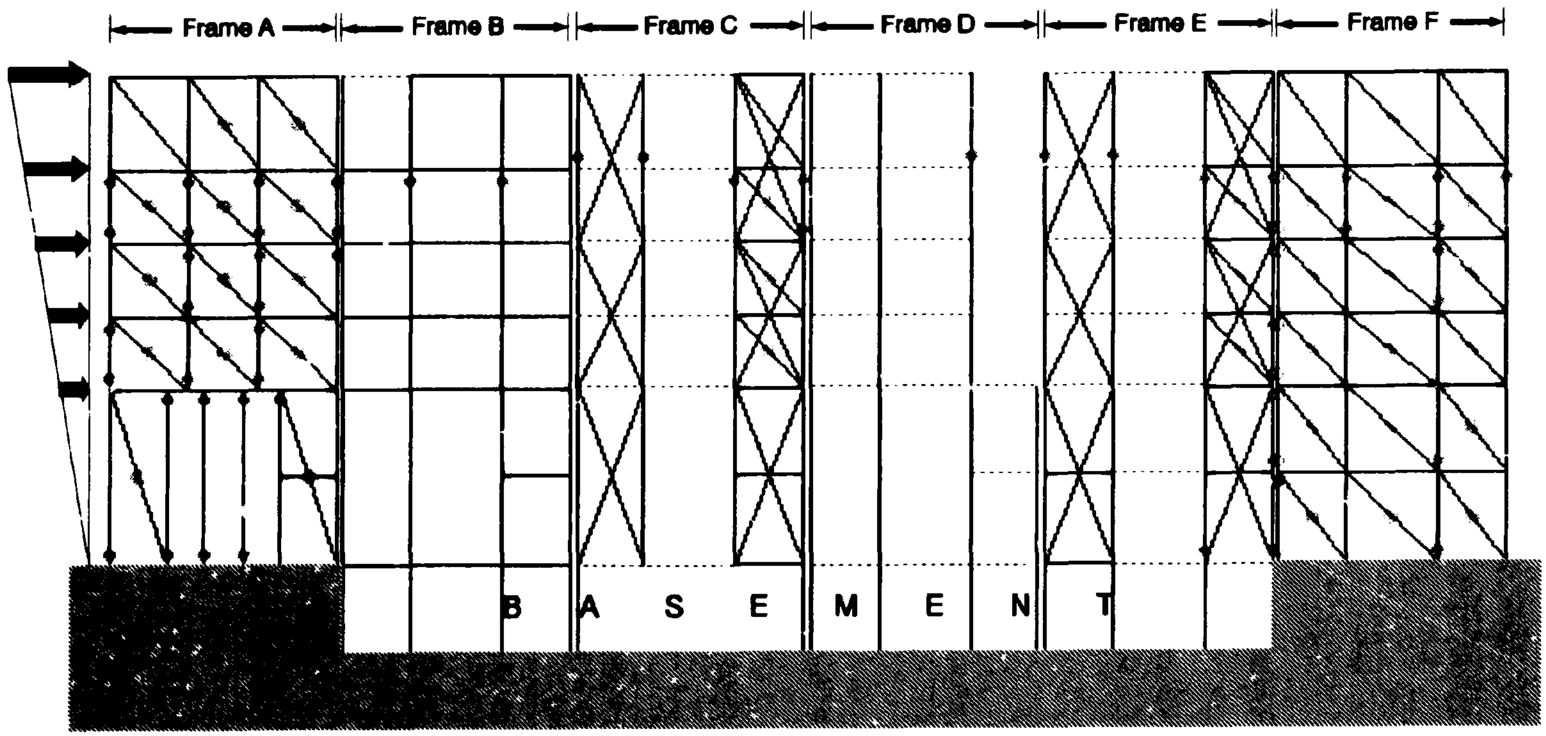

Figure 3.30 State of the E-W direction at δ_{roof} = 3" according to 2D pushover analysis of braced building without additional lateral stiffness

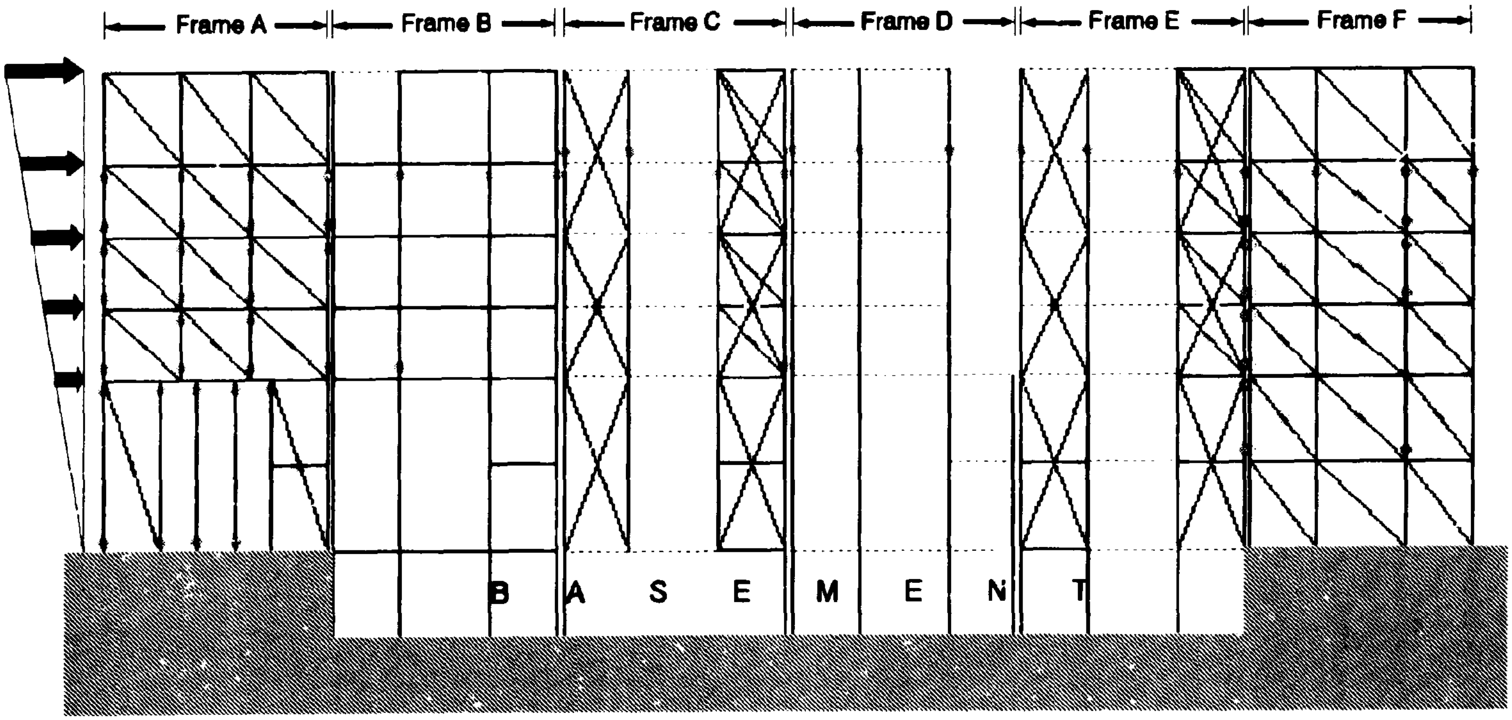

Figure 3.31 State of the E-W direction at δ_{roof} = 4" according to 2D pushover analysis of braced building without additional lateral stiffness

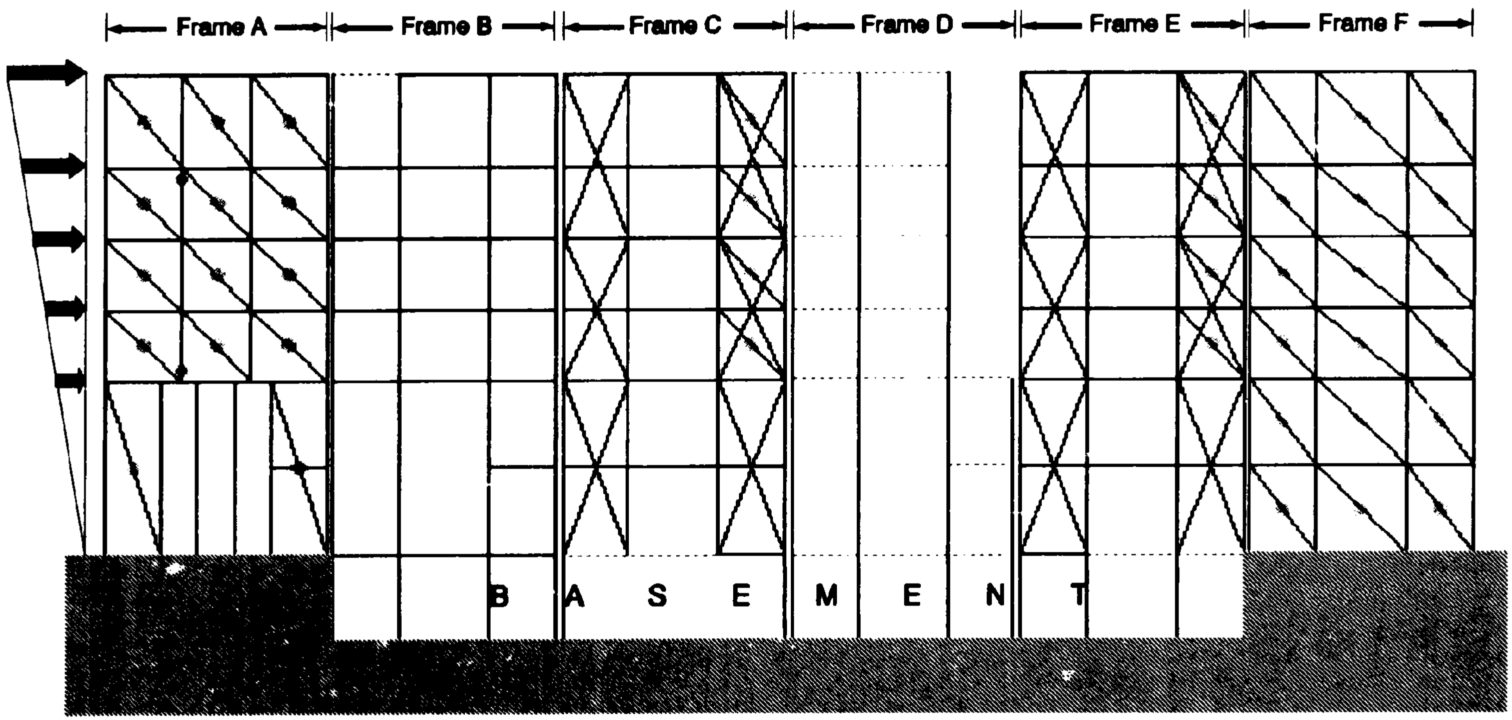

Figure 3.32 State of the E-W direction at $\delta_{roof} = 1''$ according to 2D pushover analysis of braced building with additional lateral stiffness

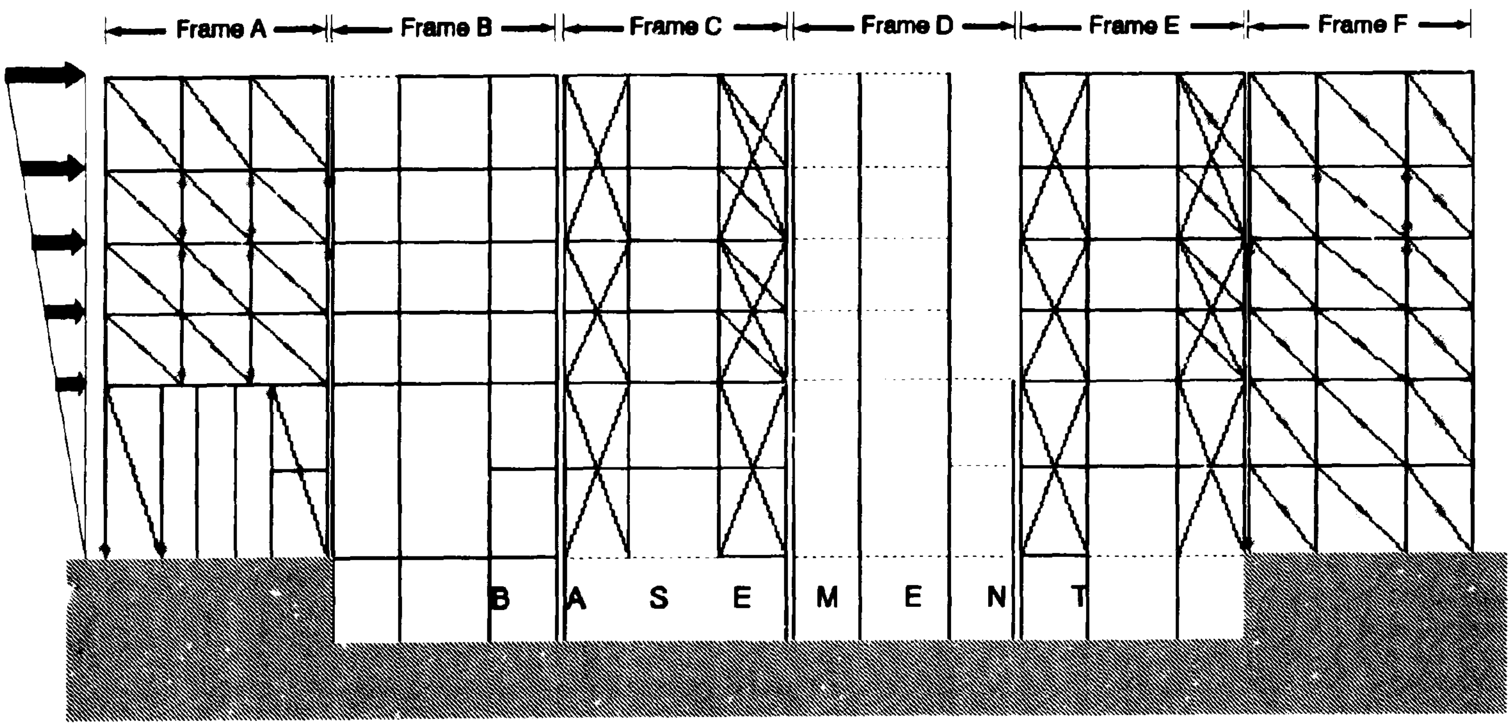

Figure 3.33 State of the E-W direction at δ_{roof} = 2″ according to 2D pushover analysis of braced building with additional lateral stiffness

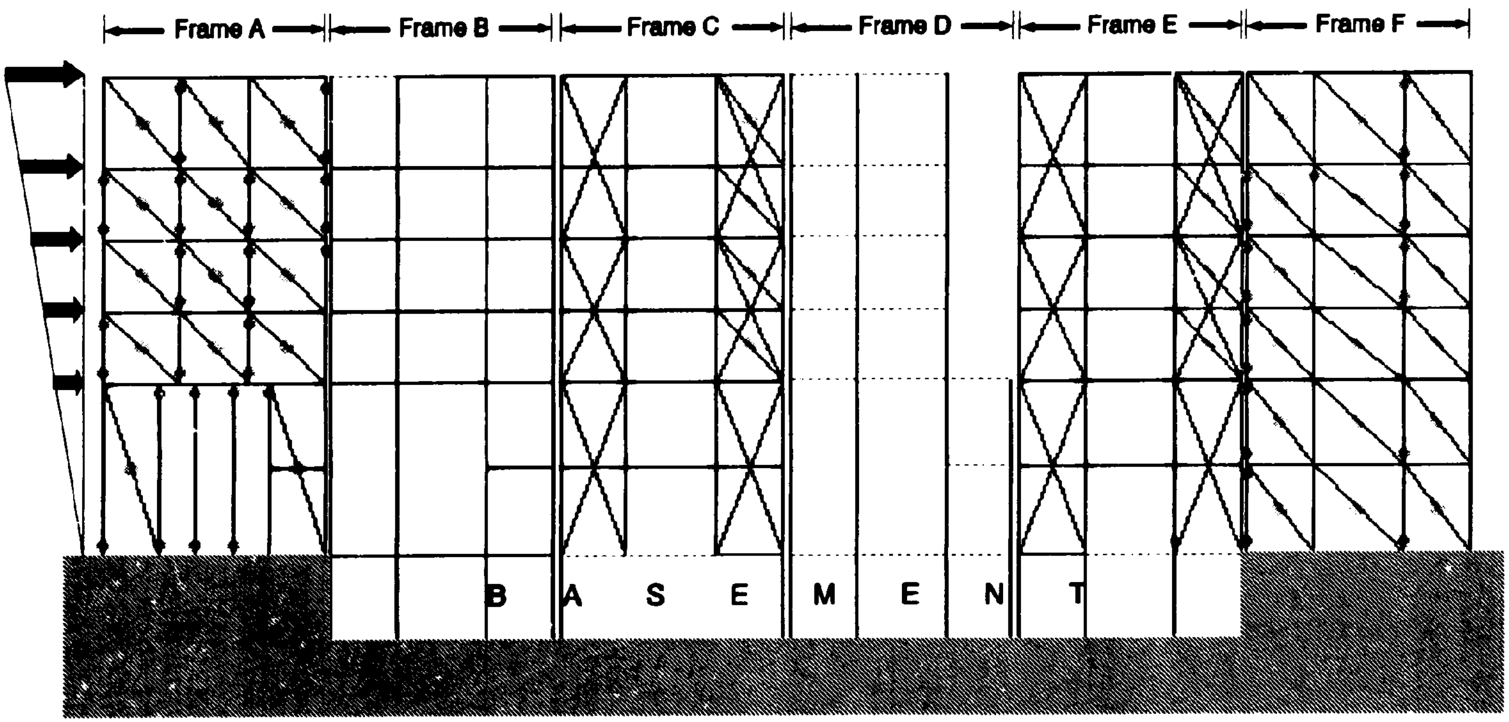

Figure 3.34 State of the E-W direction at δ_{roof} = 3" according to 2D pushover analysis of braced building with additional lateral stiffness

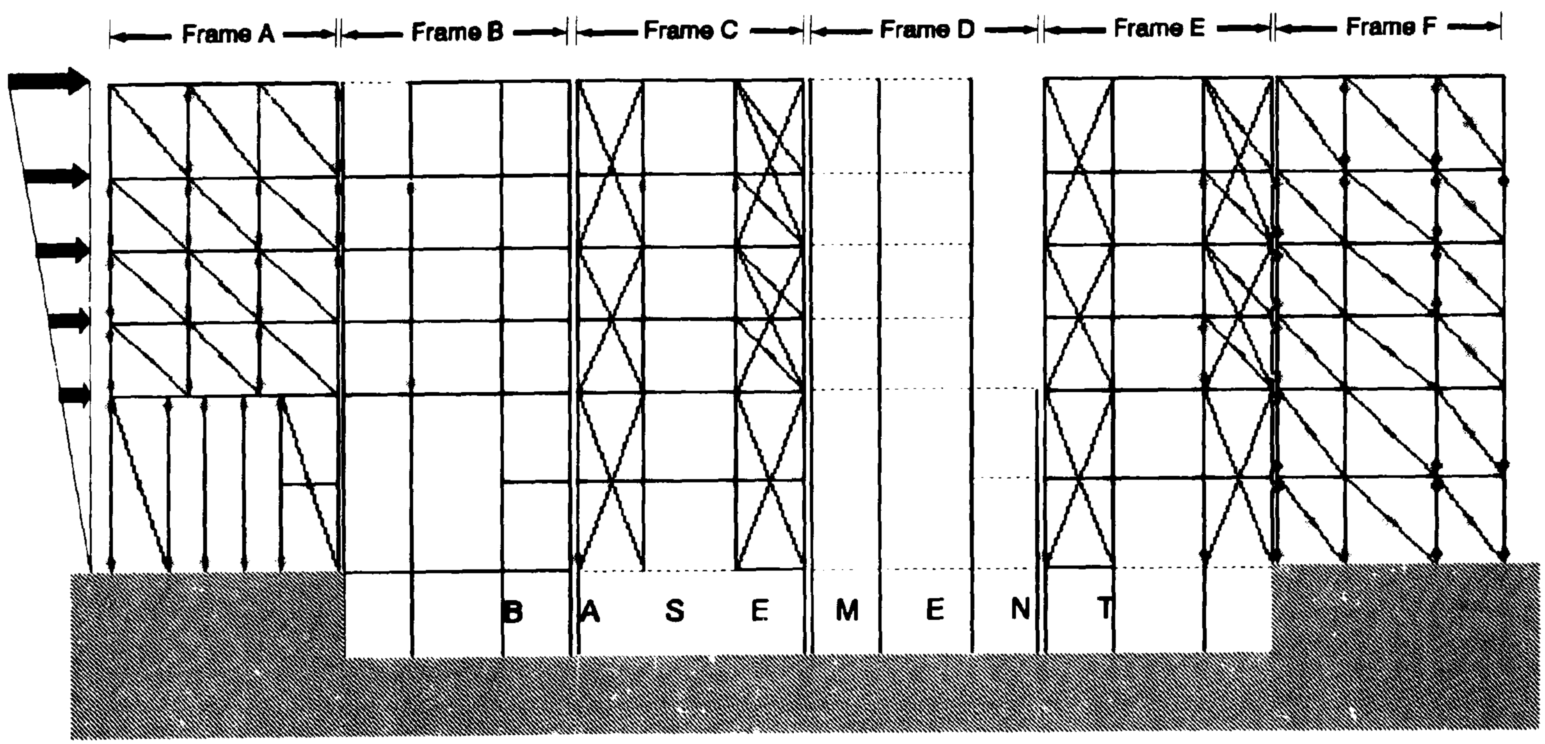

Figure 3.35 State of the E-W direction at δ_{roof} = 4″ according to 2D pushover analysis of braced building with additional lateral stiffness

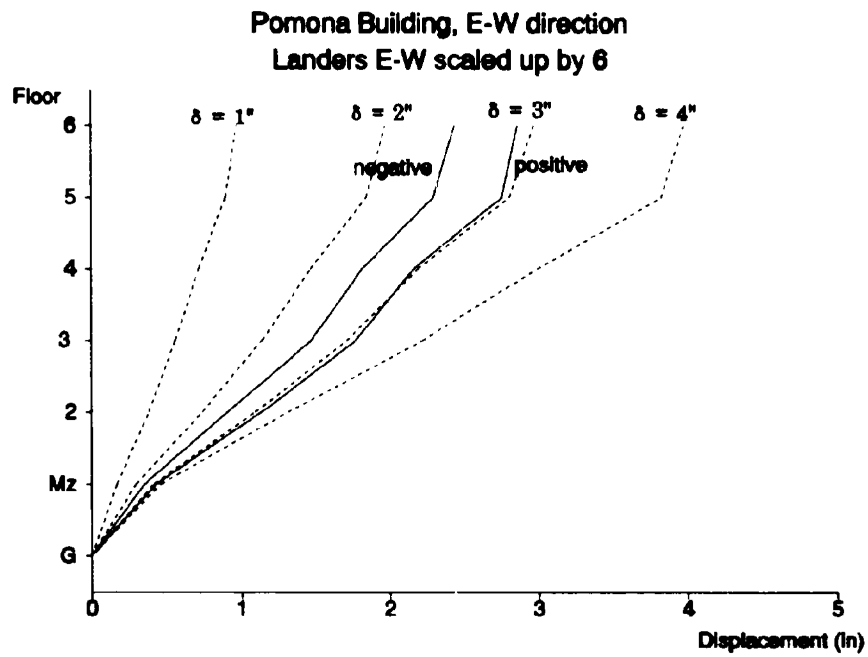

a) Without lateral support

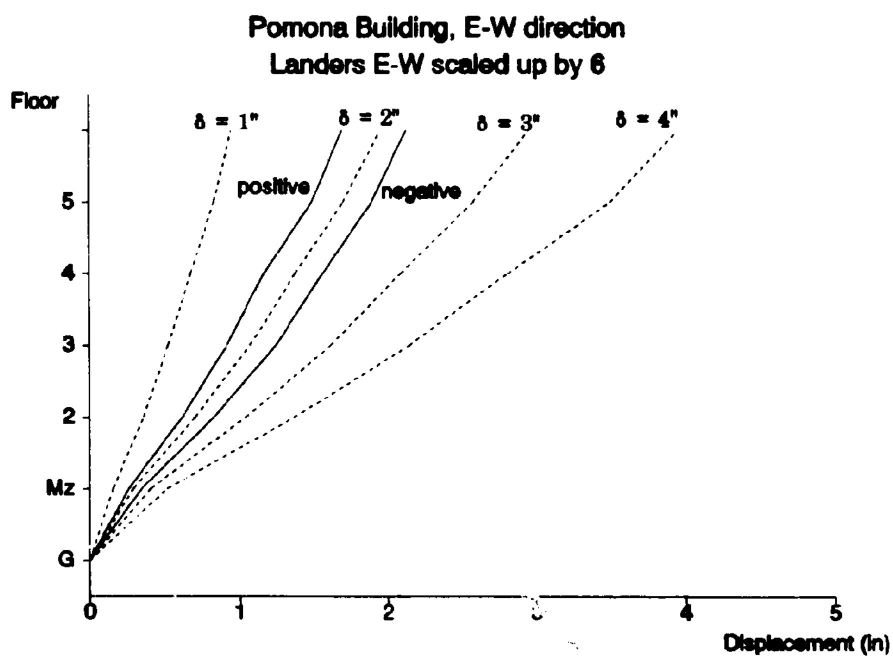

b) With lateral support

Figure 3.36 Floor displacements obtained from 2D time-history analysis of upgraded building with and without lateral support, E-W direction

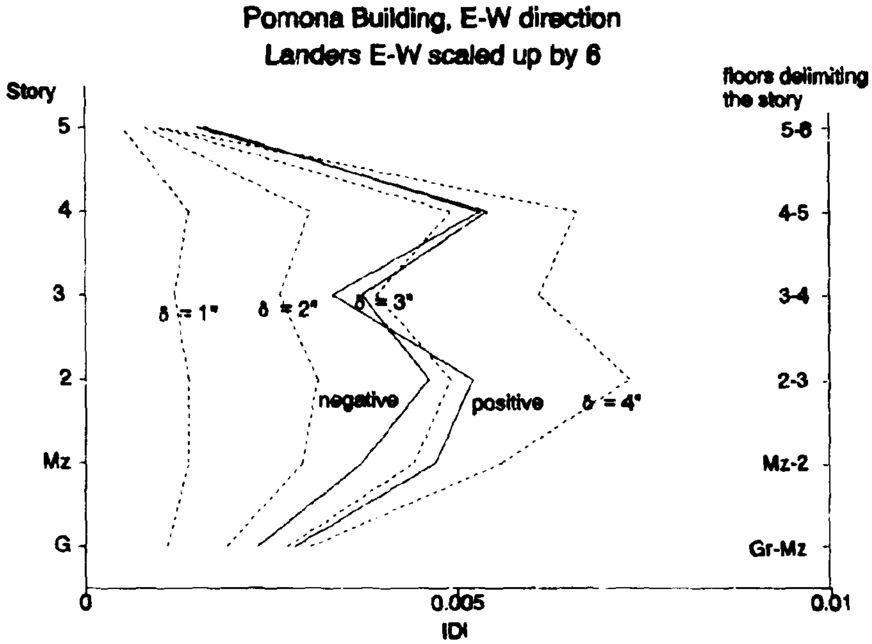

a) Without lateral support

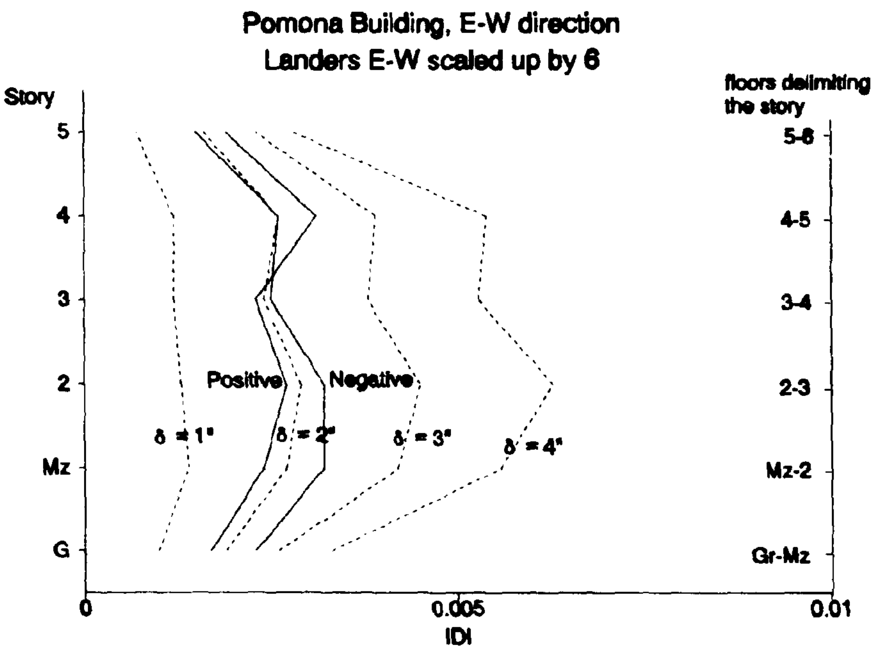

b) With lateral support

Figure 3.37 IDI obtained from 2D time-history analysis of upgraded building with and without lateral support, E-W direction

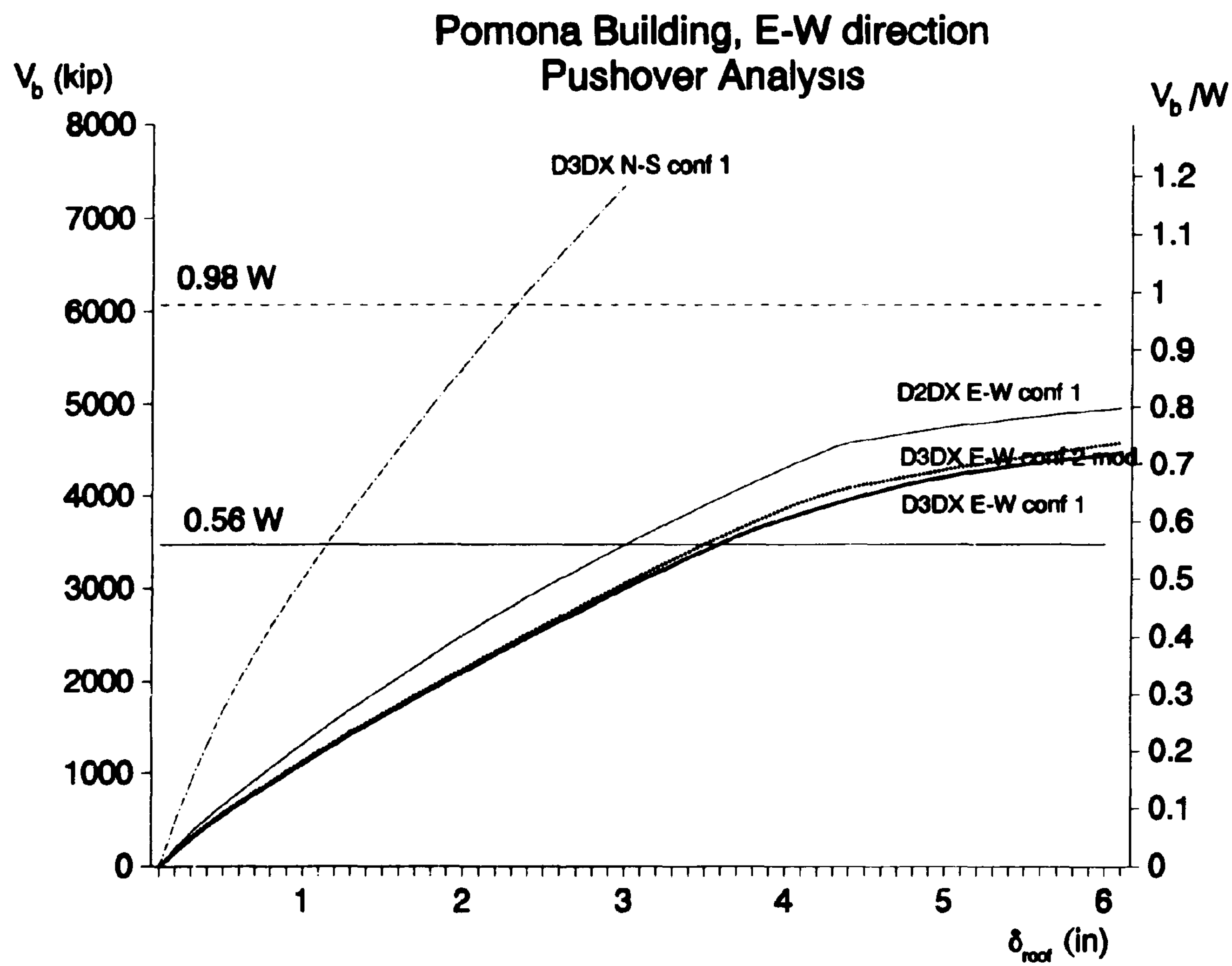

Figure 3.38 Roof displacement vs. base shear curves obtained from 2D and 3D pushover analyses

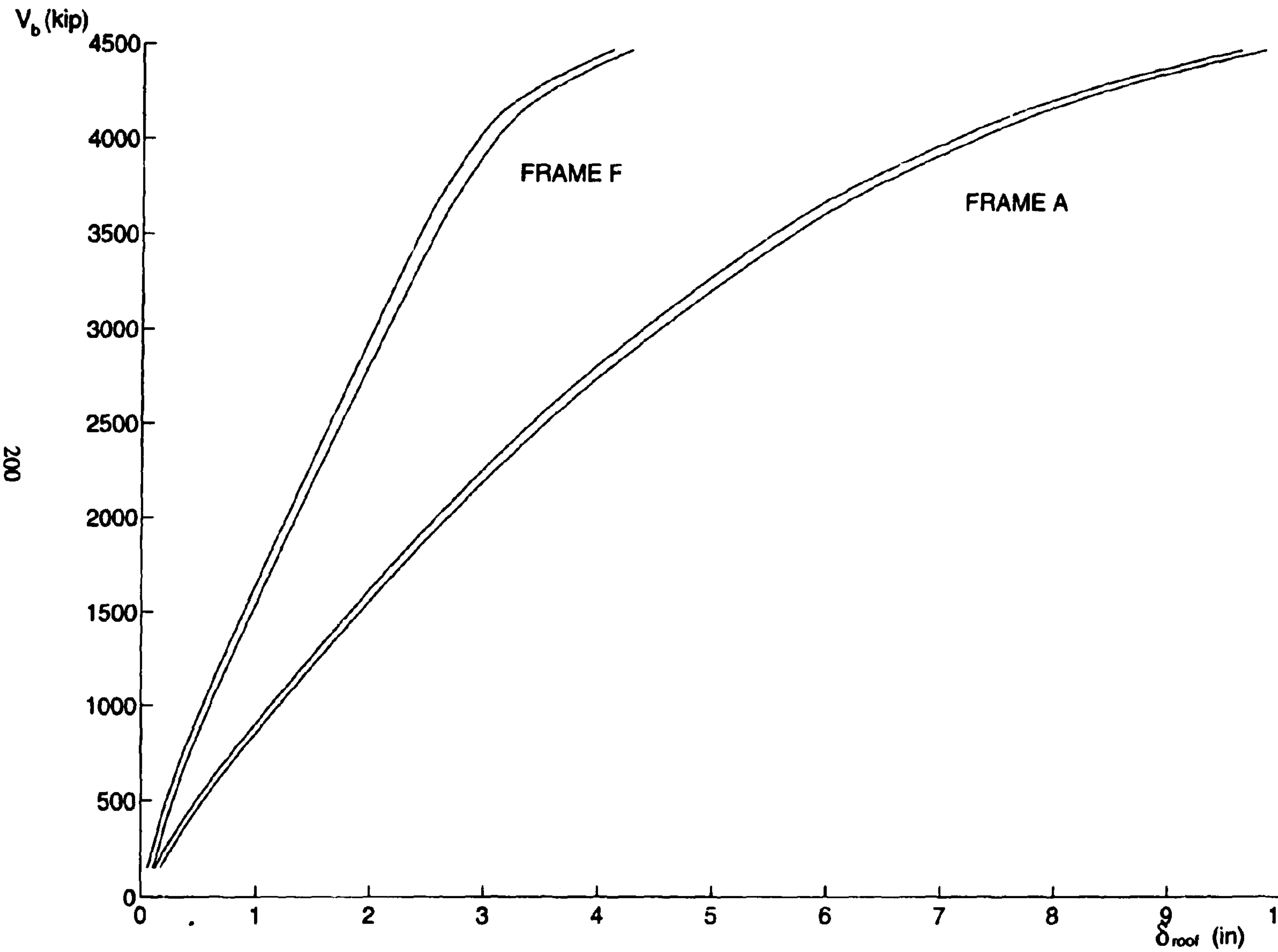

Figure 3.39 Roof displacement vs base shear curves from 3D pushover analysis of E-W direction of configuration 1

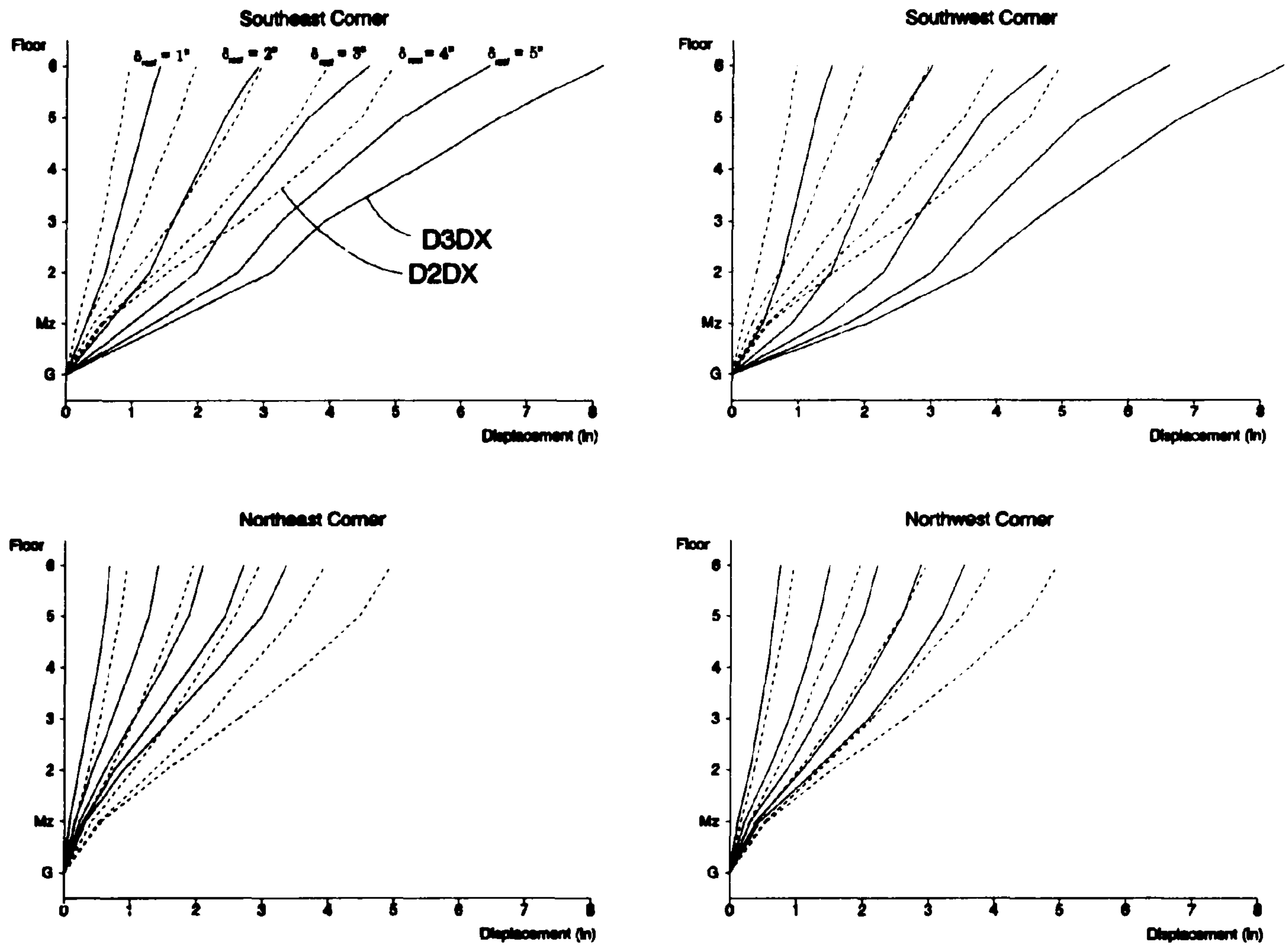

Figure 3.40 Comparison of floor displacements obtained from 2D and 3D pushover analysis of configuration 1, E-W direction

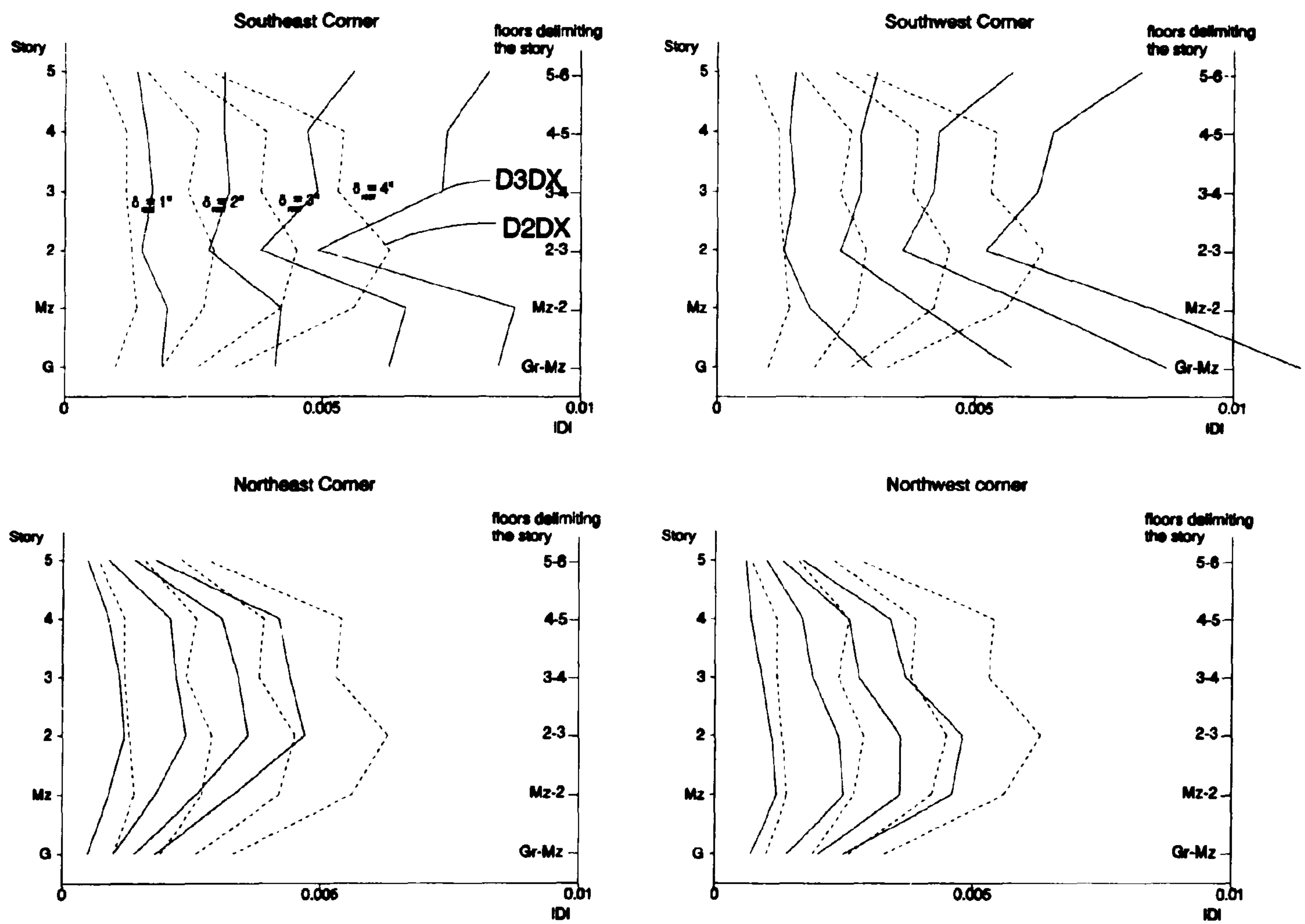

Figure 3.41 Comparison of IDI obtained from 2D and 3D pushover analyses of configuration 1, E-W direction

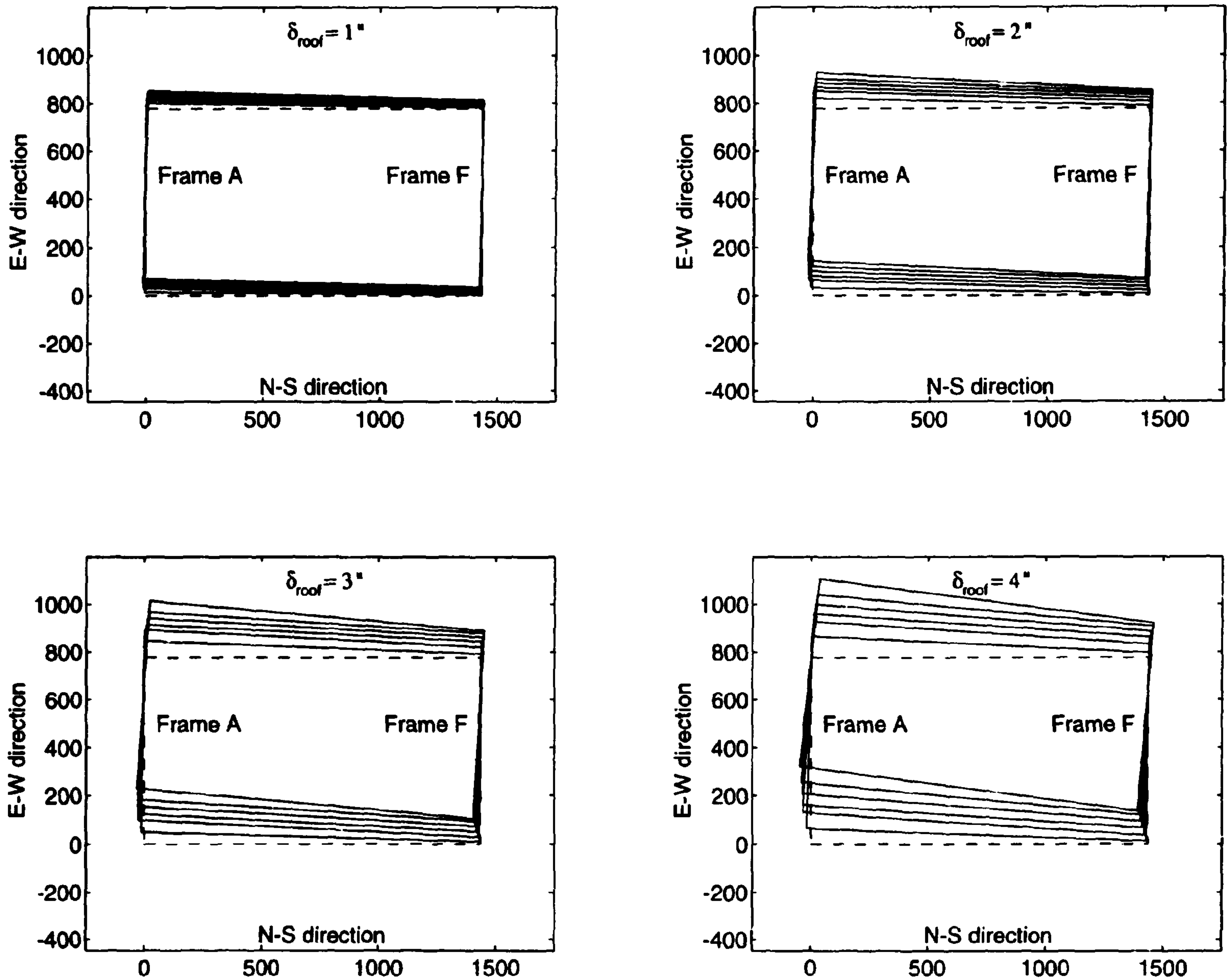

Figure 3.42 Displaced floor diaphragms from 3D pushover analysis of E-W direction of configuration 1

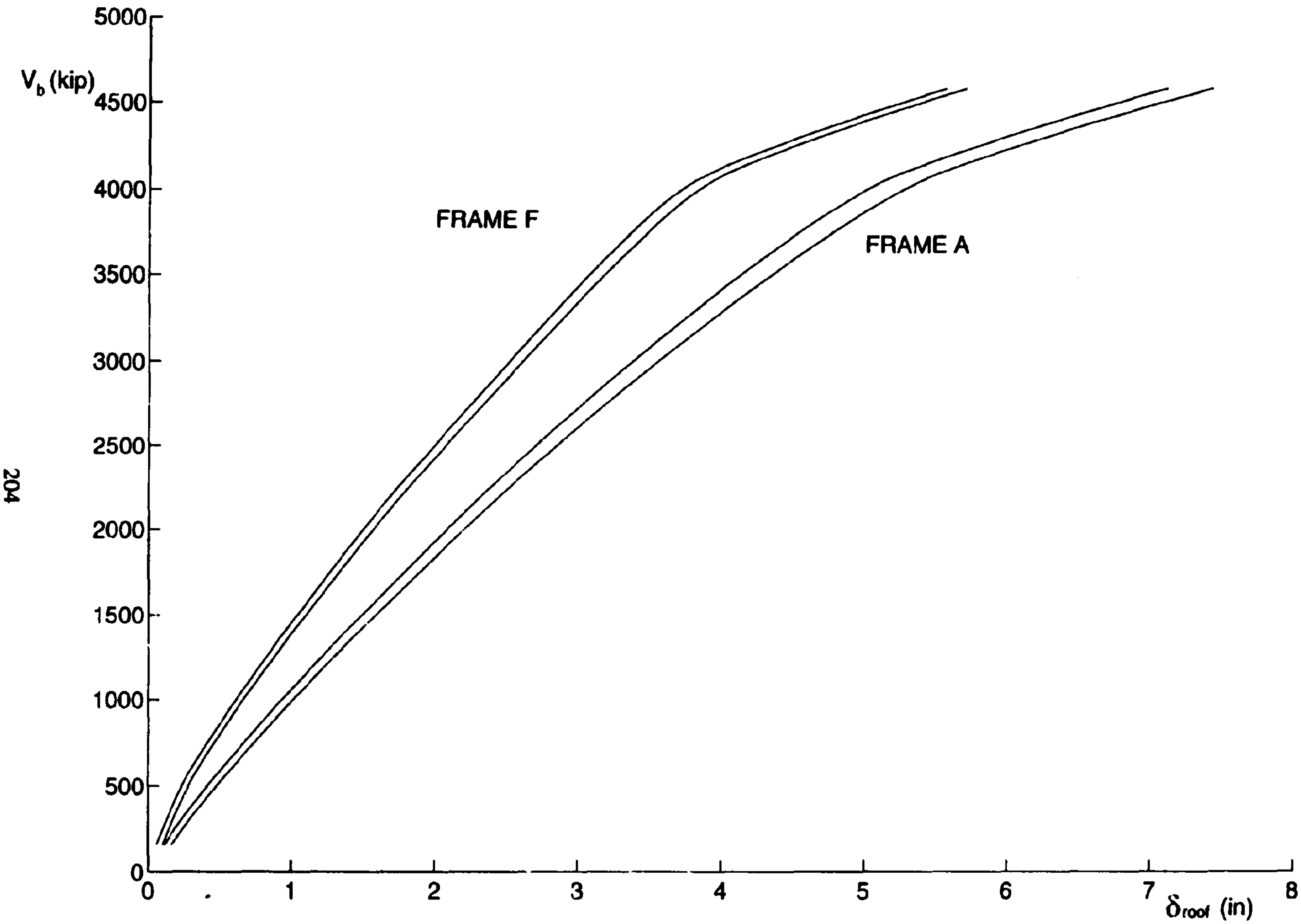

Figure 3.43 Roof displacement vs base shear curves from 3D pushover analysis of E-W direction of configuration 2

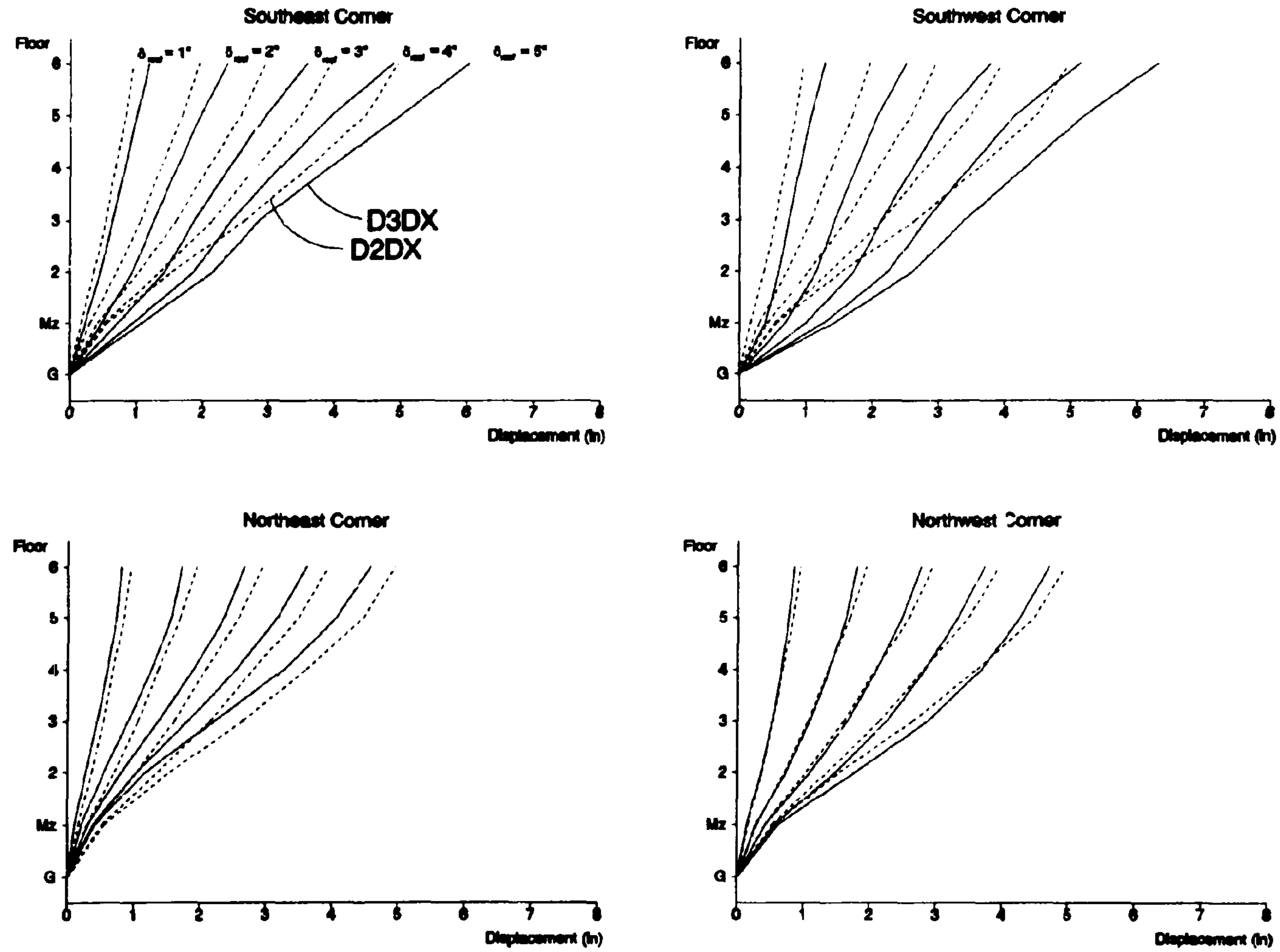

Figure 3.44 Comparison of floor displacements obtained from 2D pushover analysis of configuration 1 and 3D pushover analysis of configuration 2, E-W direction

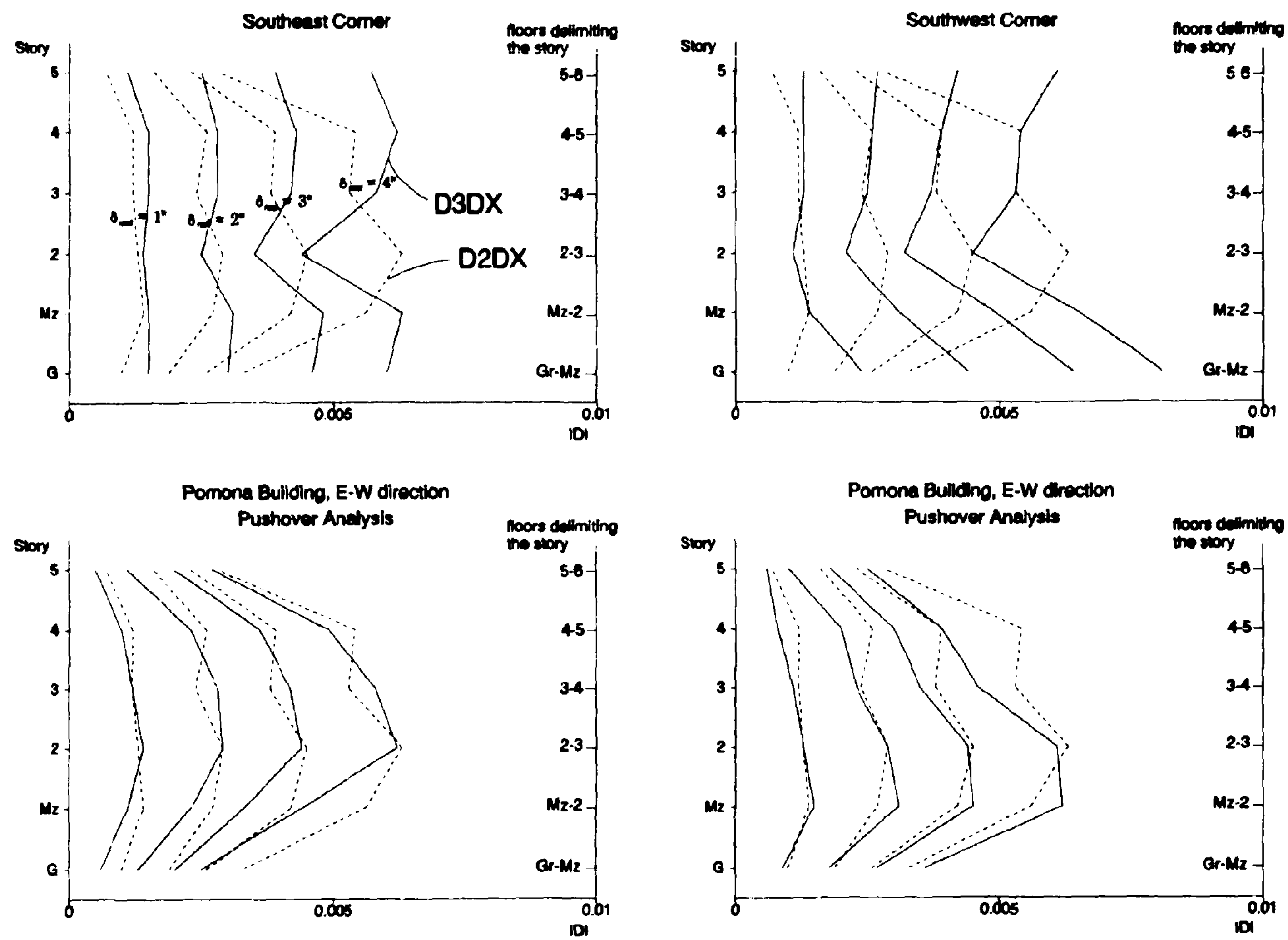

Figure 3.45 Comparison of IDI obtained from 2D pushover analysis of configuration 1 and 3D pushover analysis of configuration 2, E-W direction

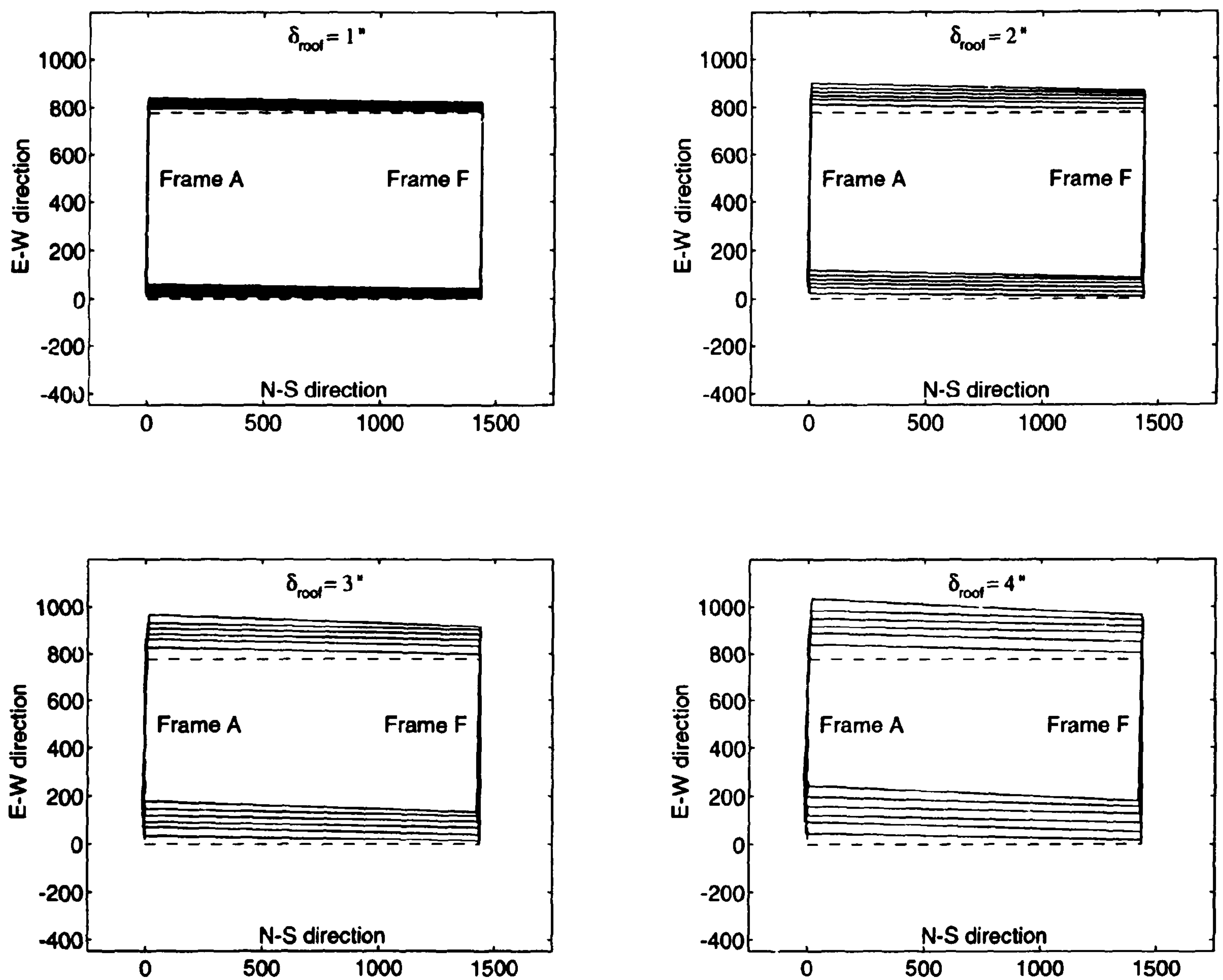

Figure 3.46 Displaced floor diaphragms from 3D pushover analysis of E-W direction of configuration 2

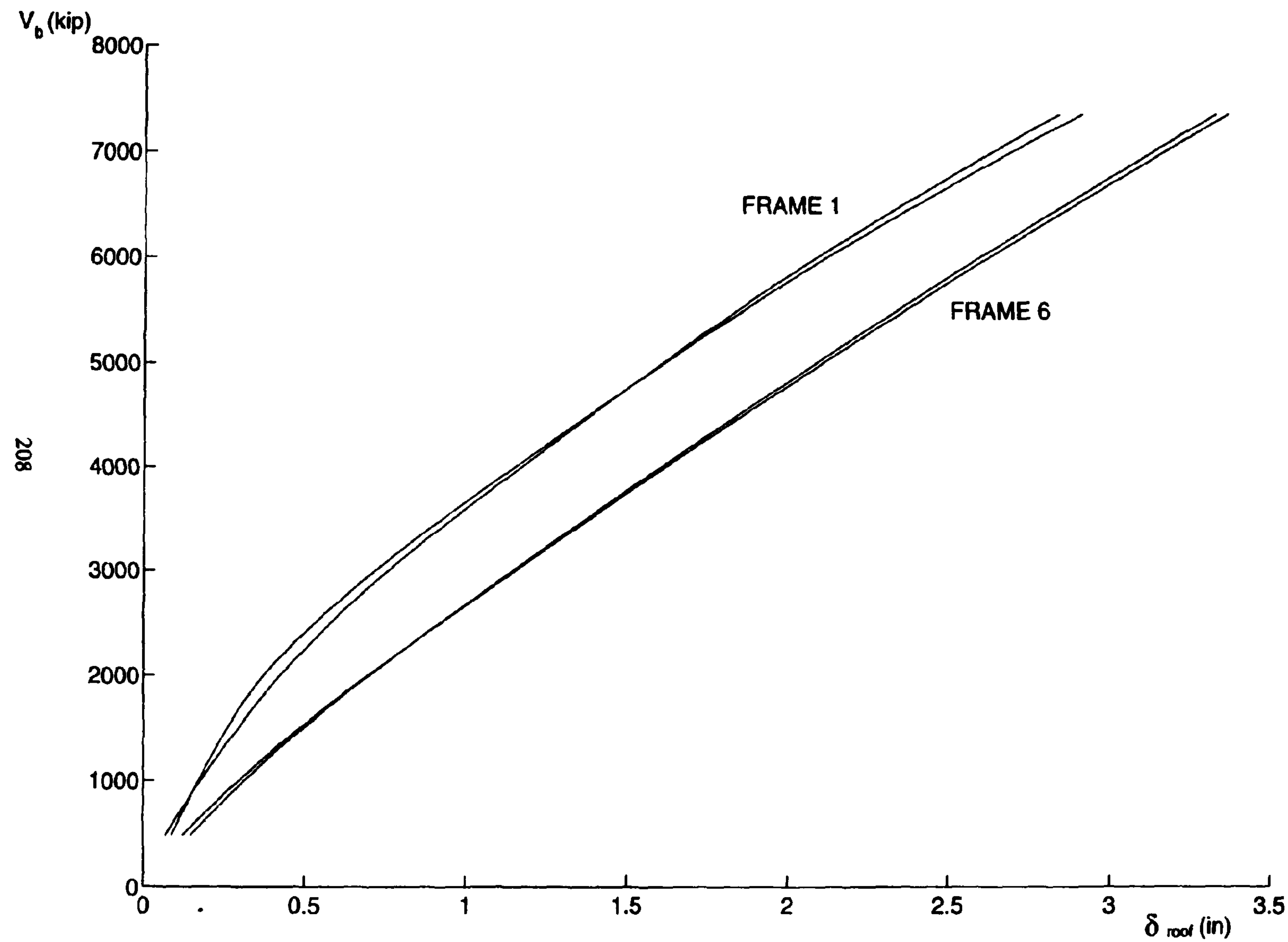

Figure 3.47 Roof displacement vs base shear curves from 3D pushover analysis of N-S direction of configuration 1

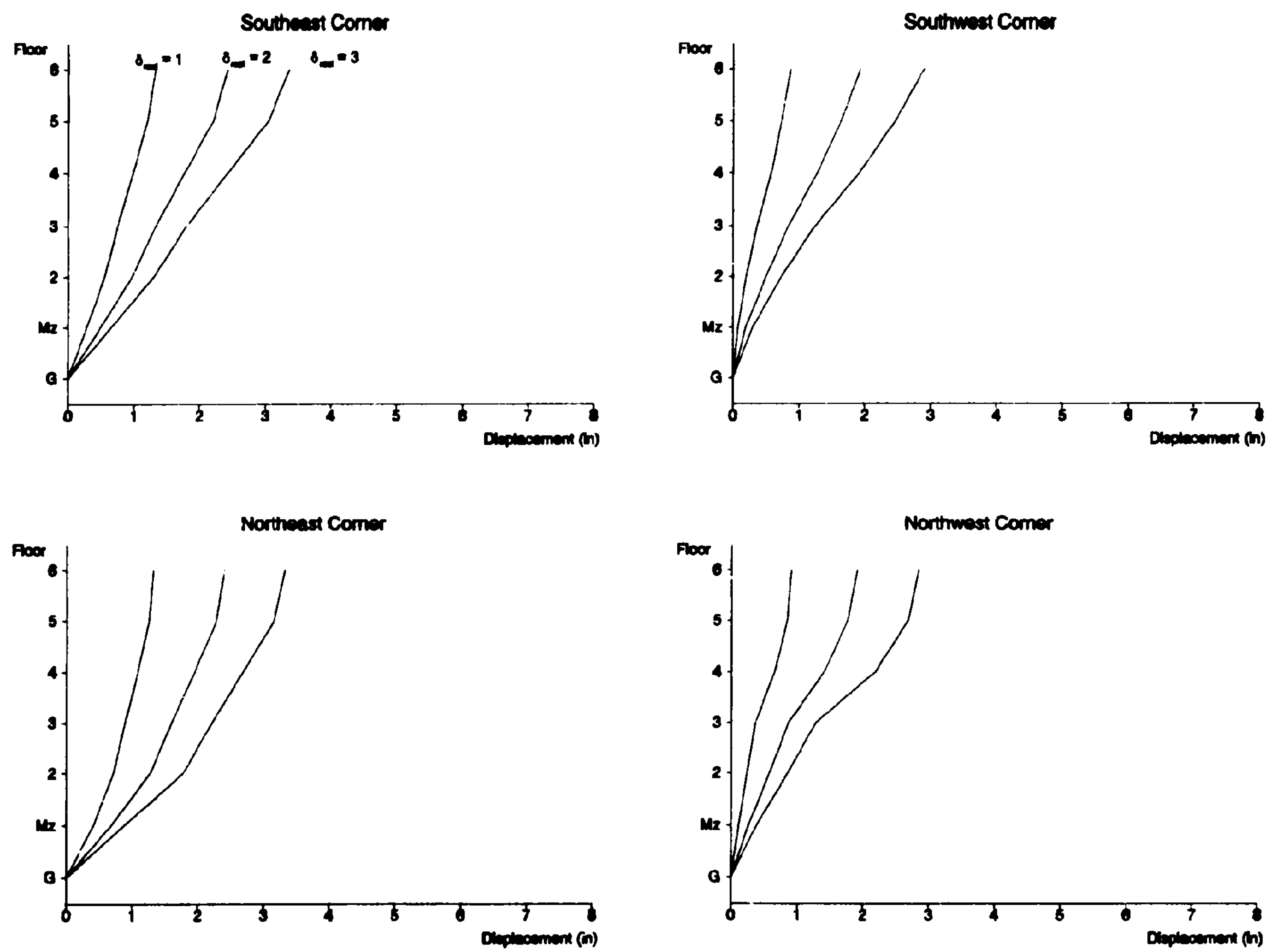

Figure 3.48 Floor displacements obtained from 3D pushover analysis of configuration 1, N-S direction

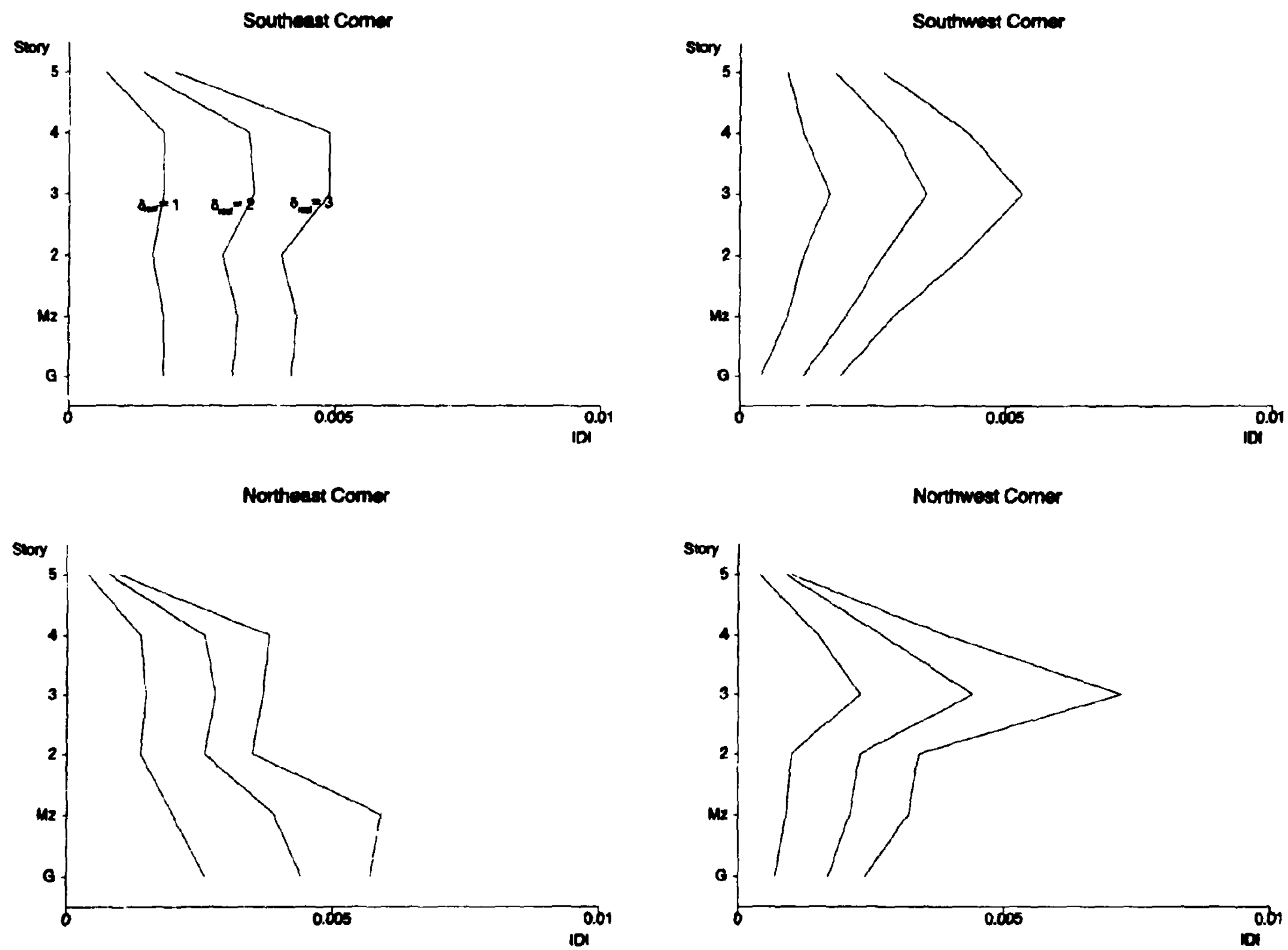

Figure 3.49 IDI obtained from 3D pushover analysis of configuration 1, N-S direction

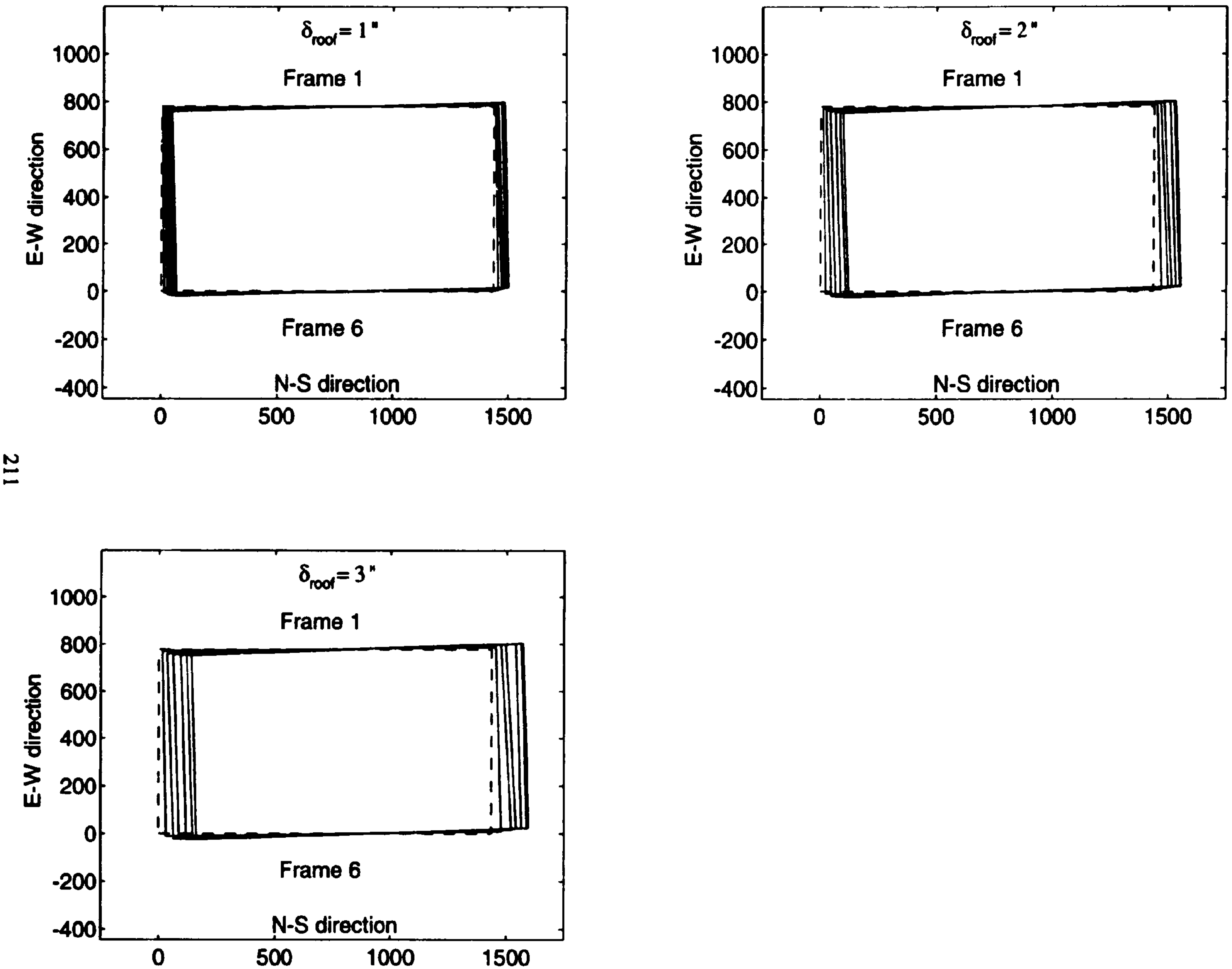

Figure 3.50 Displaced floor diaphragms from 3D pushover analysis of N-S direction of configuration 1

4 SUMMARY, CONCLUSIONS AND RECOMMENDATIONS

4.1 INTRODUCTORY REMARKS

The most significant seismic hazards in our urban and rural areas result from the interaction between the seismic activity at a given site and the local built environment (all human-made facilities). Given our inability to control the seismic activity that affects a given region, the most effective way to reduce its seismic hazards to an acceptable level is the upgrading (retrofitting) of existing hazardous structures. The urgency of the need to carry out this upgrading has been emphasized by the occurrence in recent years of moderate earthquake ground motions (EQGMs) in California, such as the Loma Prieta 1989 and Northridge 1994 events.

Unreinforced masonry (URM) buildings and framed buildings infilled with URM walls, which were designed and constructed before the development and flourishing of seismic design, constitute an important part of the vast inventory of high-risk structures in many cities of California. Currently, there is a need to develop simple and efficient retrofitting strategies and techniques to upgrade these buildings so that they can have adequate performance during strong EQGMs.

In recent years, several researchers and practitioners have shown that the seismic performance of existing buildings when subjected to strong EQGMs can be enhanced considerably by bracing them with post-tensioned (PT) rods or cables. The studies reported herein have discussed the possibility of rational application of this technique to existing framed buildings infilled with URM walls. In this chapter, a summary of some of the most relevant issues involved in this application, preliminary conclusions regarding the proposed solutions to address such issues, and recommendations for research needs to improve such solutions are presented.

4.2 SUMMARY AND CONCLUSIONS

4.2.1 PERFORMANCE OF FRAMED BUILDINGS INFILLED WITH UNREINFORCED MASONRY WALLS

Experimental tests carried out by several researchers around the world have consistently shown that URM walls and infills possess considerable capacity for inelastic deformation independently of their in-plane failure mode (i.e., diagonal tension, flexural tension, etc., for URM walls; and sliding shear, diagonal tension, compressive crushing, etc., for URM infills). It has been observed in the majority of these tests that URM walls and infills are able to undergo large inelastic deformations (large drift indexes, .005 and larger) without suffering very large deterioration in their maximum (ultimate) lateral load carrying capacity. In particular, it has been recognized that the presence of masonry infills that are not isolated from the structural elements can have a beneficial effect on the seismic performance of existing framed buildings. By properly introducing such elements within the bare frames of a building, a considerable increase in the ultimate strength and stiffness, as well as energy dissipation capacity of the building, can be achieved as it has been consistently shown in experimental tests and analytical studies.

- From the above observations, it can be concluded that, if certain conditions are met, the URM infills can enhance considerably the strength, stiffness and energy dissipation capacity of an existing framed building. The URM infills may be used to dissipate energy through stable hysteretic behavior (several researchers agree on the fact that URM infills can undergo relatively high inelastic deformations while showing adequate hysteretic behavior). Nevertheless, to accomplish this stable behavior, the in-plane drift index in the elements needs to be carefully controlled and certain modes of failure (for instance, brittle failure in the existing frame members) should be prevented. Furthermore, of particular importance is the fact that URM infills can create large stiffness and strength irregularities in plan and along the height of the building, which in turn can induce large torsional response and/or the creation of soft stories, thereby creating loading conditions on structural elements for which they were not designed.

4.2.2 USE OF POST-TENSIONED BRACES TO UPGRADE EXISTING BUILDINGS

The rehabilitation of an existing building using PT braces is an attractive option. Usually it is possible to achieve large and economic increases in the stiffness and lateral load strength of an existing building. The use of this technique offers several structural as well as non-structural advantages, such as: wide range of lateral stiffness and deformability capacity that can be considered in the design of the bracing system, that the loads induced in the foundation can be distributed along the whole foundation system (to avoid modifying the existing foundation), that the weight of the braces is usually small compared to that of the existing structure (does not add reactive mass), clean and fast construction process, etc.

Usually, the PT braces in a rehabilitated frame building are designed to limit considerably the displacement demand in the upgraded structure while increasing considerably its lateral strength. Thus, the introduction of the PT braces to an existing building diminishes considerably the flexural demands on the existing and possibly non-ductile frame members. To assure that the bracing system can achieve adequate displacement control throughout the ground motion, it is necessary to prevent the PT braces from becoming slack due to yielding or buckling in compression. Thus, a relevant consideration in the design of the PT braces is that their excessive yielding or buckling needs to be avoided at all cost. As with the use of any rehabilitation technique, it is necessary to check several aspects of the global and local behavior of the upgraded structure, such as: change of behavior of the existing structural elements, change in the dynamic characteristics of the building, connection of braces to the existing structure and possible effects on the foundation system, nonstructural components and contents.

4.2.3 PHILOSOPHY OR DESIGN CRITERIA FOR RETROFITTING USING A POST-TENSIONED BRACING SYSTEM

One of the main problems involved in upgrading an existing framed building with URM infills lies in defining what is to be considered an adequate overall seismic performance, and in particular, what constitutes adequate seismic performance for the URM infills. Currently, there is a need to define this rationally, so that performance-based EQ-RD methods can be implemented taking into account the real deformation, strength, stability and energy dissipation capacities of URM elements.

Given that the existing URM infills can enhance considerably the mechanical characteristics of an existing framed building (increase in strength, stiffness and energy dissipation capacity), rational performance criteria for framed buildings with URM infills should be based on allowing the infills to contribute to the global lateral load resistance of the building in a controlled manner (i.e., without suffering excessive damage and/or degradation of their mechanical characteristics).

A large percentage of infilled frame buildings have non-ductile frames. Performance criteria involving these frame members should focus on avoiding their non-ductile (brittle) failure, which implies limiting them to their elastic range of behavior. It has been suggested before that the PT braces should remain essentially elastic during a seismic event. It follows from the above observations that the PT braces should be designed and introduced into the building in such a way that they and the frame members remain esentially elastic. Given that the infilled framed building has a large natural source of viscous and hysteretic energy dissipating capacity in the URM infills, it would seem appropriate to supply hysteretic energy dissipating capacity to the upgraded building by using the URM infills as "energy dissipators". It is necessary to make sure the URM infills can provide this dissipation in a stable manner throughout the ground motion by controlling their in-plane deformation.

The proposed performance criteria for the upgraded building can be summarized as:

- Non-ductile frame members should not develop brittle failure.
- URM infills should not collapse.
- The PT bracing system should not lose stiffness or develop soft stories (prevent PT braces from significant yielding and/or buckling in compression).
- The above criteria can be complemented with performance criteria for nonstructural elements as well as contents.

To achieve the above performance criteria, the following philosophy of design is suggested:

- Keep the PT braces and non-ductile frame members in their elastic range of behavior.
- The PT braces should control the maximum IDI in the building in such a way as to achieve a stable hysteretic behavior in the URM infills.

From the above, it can be concluded that in selecting the *overall* stiffness of the PT bracing system, the following requirements or needs have to be considered:

• The bracing system should have stiffness such that the existing URM infills can contribute to carry an important percentage of the lateral load. In this way, the URM infills can dissipate part of the energy input to the building.
• The stiffness of the bracing system needs to control the lateral displacement as well as the rate of deformations in the building in order to control structural and non-structural damage, and allow for stable hysteretic behavior in the URM infills.
• The *relative* stiffness of the bracing system in plan and height should attempt to correct the existing lateral stiffness and strength irregularities.

■ It should be strongly emphasized that good performance of the upgraded building can only be achieved by controlling its response. It is not enough to meet the strength demands in the building to achieve such control. Thus, the design of the PT braces can not be based on a strength demand-supply approach, such as those stressed by current EQ-RD codes. The PT bracing system **should be configured and designed taking into account simultaneously the expected strength, displacement, and hysteretic energy dissipation demands.**

4.2.4 PRACTICAL APPLICATION

To illustrate the potential use of PT braces to rehabilitate hazardous non-ductile frame buildings infilled with URM walls, this technique was applied to an existing building (Pomona building). The Pomona building, built in 1923, is a non-ductile reinforced concrete framed building infilled with URM walls. After assessing the performance of this building with the use of two-dimensional (2D) and three-dimensional (3D) elastic and nonlinear analyses, it was possible to conclude that this building would probably collapse when subjected to the design earthquake ground motion derived for the site. This building exhibited insufficient lateral strength and stiffness, as well as large irregularities of mass and lateral stiffness and strength through plan and height. From the application of URM braces to the Pomona building, the following observations and conclusions can be made:

- A significant increase in the lateral strength and lateral stiffness of framed buildings with URM infills can be achieved by introducing PT braces into their frames. In the specific case of the Pomona building, the ultimate base shear in both directions of the upgraded building was about three times those corresponding to the existing building, as reflected by increases from 0.15 W to 0.50 W in the E-W direction, and from 0.40 W to 1.20 W in the N-S direction. Large increases in the lateral stiffness were also achieved by introducing PT braces to this building, as reflected by the fact that the lateral stiffness in the upgraded building is about three times that of the existing building in the E-W direction (decrease in the fundamental period of translation from 1.0 sec to around 0.6 sec) in the upgraded building, and about one and a half times that of the existing building in the N-S direction (decrease in the fundamental period of translation from 0.5 sec to 0.4 sec).

- Proper selection of the layout of the PT braces to be introduced into the existing building would allow considerable reduction in the strength and stiffness irregularities in plan and height of the building. An indirect way to measure the above irregularities, and thus a possible improvement, is by means of a coefficient of distortion, which is defined as the ratio between the maximum to average interstory drift index demands in the building. An idea of the improvements attained by introducting PT braces into the Pomona building can be provided by the fact that the coefficient of distortion in both directions was reduced from a value of about 3.0 in the existing building to about 1.5 in the upgraded building.

- The diameter of the PT braces in the upgraded Pomona building ranged from 1/8" to 3 1/2". It was proposed to fabricate the PT braces of galvanized bridge wire with a yielding stress of 150 ksi. For the PT braces in the Pomona building, fifty percent of the available yield stress is used for post-tensioning, which implies that fifty percent is available to resist the effects of lateral loads.

- The use of PT braces to upgrade non-ductile frame buildings with URM infills may be limited to low-rise and squat medium-rise buildings. This is because the PT braces are usually designed to resist very high lateral forces, which in turn is a consequence of designing them to remain elastic while keeping the frame members from having significant nonlinear demands (i.e., basically elastic). The large forces that can be generated in the PT braces when the building is subjected to lateral loads induce large axial forces in the existing columns and the foundation system, which can create structural problems that may be very expensive to fix. Among such problems, the need to upgrade the mechanical properties of the existing columns and foundation can be mentioned. In the case of the Pomona building, the upgrading of its existing columns and foundation according to the proposal made in this report would probably increase considerably the cost of the upgrading project. Not only that, but the constructability of the upgrading strategy becomes an issue.

Besides the observations and conclusions that were drawn directly from the use of PT braces to upgrade the Pomona building, it was possible during the EQ-RD of this upgrading strategy to gather other information that is relevant to its application, as reflected by the following.

- In this report, a quantitative measure of the qualitative definition of damage in the elements of the Pomona building was established by setting limits to the maximum IDI in the building. The controlling IDI at safety level for the Pomona building was imposed by the need to achieve stable hysteretic behavior in the URM infills. In particular, this limiting value of IDI was equal to 0.005. Although a multi-limit state performance criteria needs to be established to allow for a rational performance-based earthquake-resistant design, the seismic rehabilitation of this existing building using PT braces has been based exclusively on the safety limit state.

- In a practical context, it may be desirable to analyze not just one, but several alternatives to upgrade a building. If many alternatives are considered at the beginning of the EQ-RD process, it may be impossible to analyze each one in detail. In this case, it is desirable to establish simple preliminary analysis procedures that allow for the identification of the most promising alternatives. In this report, the use of a simplified analysis procedure based on a stick and single-degree-of-freedom models to assess the performance of the existing and upgraded building was discussed. It was found that simple methods to quantify the lateral

lateral stiffness and strength, as well as the irregularities in plan and height of the building, provided reasonable estimates.

- The simple models of the original building were used successfully for the preliminary design of several alternatives of the bracing system, as well as for the preliminary assessment of the performance of the building upgraded using these alternatives. Simple methods like the ones discussed are invaluable tools for the simple and rational EQ-RD of upgrading schemes.

- After some promising alternatives were identified using the simplified methodology, the performance of the upgraded building was assessed from 2D and 3D elastic and nonlinear analyses of complex models of the building. The results of these analyses showed that the upgraded building satisfied the preestablished performance criteria, suggesting that PT braces can be used efficiently in the upgrading of existing infilled buildings with URM walls. The structural soundness achieved in the upgraded building shows the versatility of the PT bracing technique if one considers the multiple structural deficiencies existing in the original building.

- Given that the PT braces, which provide the majority of lateral stiffness and strength in the upgraded building, and the existing frame members should remain elastic, it was found that using the results obtained from detailed elastic analyses is a reasonable and conservative way of assessing the performance of the upgraded building.

- In the elastic analyses carried out in this report, the energy dissipation provided by the URM infills has been neglected. One way in which this energy dissipation could have been included in the analysis is by introducing an equivalent damping coefficient (ξ_{EQ}) to account for the viscous and inelastic (plastic) hysteretic energy dissipated by the URM infills.

- The design of the PT bracing scheme should not only consider the design of the braces themselves, but the possible failure of the existing elements or the formation of local mechanisms before the braces can reach their ultimate capacities. The upgrading of the existing elements should be carried accordingly.

- In many cases, structural considerations do not determine the final configuration of the PT bracing system. Other constraints (architectonic, space, constructability, etc.) can have as much or more influence in determining such configuration.

4.3 RECOMMENDATIONS FOR RESEARCH NEEDS

- Several issues in the in-plane behavior of URM elements are yet to be understood. Among them, it is necessary to gain a better understanding of the cyclic behavior of URM walls and infills. Special consideration should be given to the way in which degradation of stiffness and strength occurs in the infill as a function of its maximum deformation and cumulative hysteretic energy dissipation demands. A damage index to use these demands to provide a quantitative measure to the qualitative description of different levels of damage should be established to allow the use of performance-based methods in the EQ-RD of upgrading schemes of buildings with URM infills. The possible effect that the maximum deformation demand in one direction has in the strength and stiffness that an URM infill can develop in the opposite direction needs to be clarified.

- Another issue that deserves consideration is the in-plane behavior of URM infills with openings. Although some analytical and experimental efforts have been carried out to assess the effect that a large opening can have on the in-plane mechanical characteristics of an URM infill, there is very little information about this topic if one considers the large percentage of real URM infills that have openings.

- Further research needs to be devoted to obtaining simple but reliable mathematical models of URM infills. These models should incorporate a good understanding of the cyclic behavior of URM infills with and without openings.

- The results presented in this report suggest that an elastic analysis should yield reasonable estimates of the global response of an infilled frame building upgraded with PT braces when subjected to the design earthquake ground motion for the safety limit state. In general, no consideration should be given to the service limit state to achieve a sound design of the PT brace configuration. Research needs to be carried out to quantify the possible reduction of the global response of the building due to the damping effects created by the viscous and inelastic (plastic) hysteretic energy dissipation provided by the URM infills. The possibility of representing these effects by using an equivalent damping coefficient (ξ_{EQ}), that is larger than the damping coefficient used in the analysis of the original building, needs to be assessed.

- The effect that the introduction of PT braces to the original building has on the magnitude of the floor accelerations in the upgraded building still needs to be studied. Also, the possible reduction in their magnitude due to the damping effects created by the hysteretic energy dissipation provided by the URM infills need to be studied. According to the results obtained from these studies, the implications to the out-of-plane behavior of the URM infills should be assessed.

REFERENCES

ABK, A Joint Venture 1984; "Methodology of mitigation of seismic hazards in existing unreinforced masonry buildings: The Methodology ABK-TR-08"; El Segundo, California.

Abrams, D.P. 1992; "Strength and behavior of unreinforced masonry elements"; Proceedings of the Tenth World Conference on Earthquake Engineering, Vol. 6, pp. 3475-3480; Madrid, Spain.

Algermissen S.T., et al. 1990; "Probabilistic earthquake acceleration and velocity maps for the United States and Puerto Rico"; Department of the Interior, U.S. Geological Survey.

Angel, R. and Abrams, D.P. 1994; "Out-of-plane strength evaluation of URM infill panels"; Technical Report NCEER-94-0004; National Center for Earthquake Engineering Research; State University of New York at Buffalo.

Astaneh, A. 1991; "Notes on comprehensive design of structures"; Department of Civil Engineering, University of California at Berkeley.

Atkinson, R.H. and Yan G.G. 1990; "Results of a statistical study of masonry deformability"; *The Professional Journal of the Masonry Society*, Volume 9, Number 1; Boulder, Colorado.

Badoux, M., and Jirsa, J.O. 1987; "Seismic retrofitting of reinforced concrete frame structures with steel bracing systems"; Proceedings of the IABSE Symposium; Paris, France.

Beavers, J.E., et al. 1992; "A hollow clay tile wall seismic performance program overview"; Proceedings of the Tenth World Conference on Earthquake Engineering, Vol. 6, pp. 3505-3510; Madrid, Spain.

Bertero, R.D. and Bertero, V.V. 1992; "Tall reinforced concrete buildings: conceptual earthquake-resistant design methodology"; *Report No. UCB/EERC 92/16*; Earthquake Engineering Research Center; University of California at Berkeley.

Bertero, V.V. et al. 1991; "Design guidelines for ductility and drift limits: review of the state-of-the-practice and state-of-the-art in ductility and drift-based earthquake-resistant design of buildings"; *Report No. UCB/EERC 91/15*; Earthquake Engineering Research Center; University of California at Berkeley.

Bertero, V.V. 1992a; "Seismic upgrading of existing structures"; Proceedings of the Tenth World Conference on Earthquake Engineering, Vol. 9, pp. 5101-5106; Madrid, Spain.

Bertero, V.V. 1992b; "Main issues and future directions on earthquake resistant design"; Keynote Lecture, Tenth World Conference on Earthquake Engineering; Madrid, Spain.

Bonilla M.G. et al. 1984; "Statistical relations among earthquake magnitude, surface rupture length, and surface rupture displacement"; *Bulletin of the Seismological Society of America*, Vol. 74, No. 6, pp. 2379-2411.

Brokken, S.T. and Bertero, V.V. 1981; "Studies on effects of infills in seismic resistant R/C construction"; *Report No. UCB/EERC 81/12*; Earthquake Engineering Research Center; University of California at Berkeley.

Boussabah, L. and Bruneau, M. 1992; "Review of the seismic performance of unreinforced masonry walls"; Proceedings of the Tenth World Conference on Earthquake Engineering, Vol. 8, pp. 4537-4540; Madrid, Spain.

Building Laws of San Francisco 1926; Mercury Press; San Francisco.

California Strong Motion Instrumention Program Staff 1990; "Quick report om CSMIP strong-motion records for the february 28, 1900 earthquake near Upland, California"; Division of Mines and Geology, California Department of Conservation; Sacramento, California.

Chrysostomou, C.Z., et al. 1988; "Preliminary studies of the effects of degrading infill walls on the nonlinear seismic response of steel frames"; *Technical Report NCEER-88-0046*, National Center for Earthquake Engineering Research; State University of New York at Buffalo.

Chrysostomou, C.Z., et al. 1992; "Nonlinear seismic response of infilled steel frames"; Proceedings of the Tenth World Conference on Earthquake Engineering, Vol. 8, pp. 4435-4437; Madrid, Spain.

Cosenza, E. et al. 1990; "An evaluation of the use of damage functionals in earthquake-resistant design"; Proceedings of the IX European Conference on Earthquake Engineering, Vol. 9, pp. 303-312; Moscow, Russia.

Cruz, Z.E. et.al. 1988; "Lecciones del sismo del 3 de marzo de 1985"; Instituto Chileno del Cemento y del Hormigon; Santiago, Chile.

Durrani, A.J. and Luo, Y.H. 1994; "Seismic retrofit of flat-slab buildings with masonry infills"; *Technical Report NCEER-94-0004*; National Center of Earthquake Engineering Research; State University of New York at Buffalo; Buffalo, NY.

EEFIT 1986; "The Mexican earthquake of 19 september 1985"; A field report by EEFIT; Cambridge, England.

Ewing, R.D. et al. 1990; " FEM/I a finite element computer program for the nonlinear static analysis of reinforced masonry building components"; *Report No. 2.2-1*, U.S.-Japan Coordinated Program for Masonry Building Research; California.

Filippou, F.C. 1987; "Electronic spreadsheets in reinforced and prestressed concrete design";

SEMM Report No. 87-01, University of California at Berkeley.

Filippou, F.C. 1995; personal communication

French, C.W. and Moehle, J.P. 1991; "Effect of floor slab on behavior of slab-beam-column connections"; American Concrete Institute, *ACI SP-123*; Michigan.

Fricke, K.E. et al. 1992; "In situ lateral load testing of an unreinforced masonry hollow clay tile wall"; Proceedings of the Sixth Canadian Masonry Symposium, Vol.2, pp. 519-530; Saskatchewan, Canada.

Fumal, T.E. and Tinsley, J.C. 1985; "Mapping quaternary sedimentary deposits for areal variations in shaking response"; *U.S. Geological Survey Professional Paper 1360*, pp. 101-126; Washington, D.C.

Gaylord, E.H. and Gaylord, C.H. 1990; Structural Engineering Handbook; Third Edition, McGraw-Hill; Hightown, New Jersey

Gere, J.M. and Shah, H.C. 1984; Terra non firma -- understanding and preparing for earthquakes; W.H. Freeman and Company; New York.

Gergely, P. et al. 1994; "Evaluation and modelling of infilled frames"; *Technical Report NCEER-94-0004*; National Center of Earthquake Engineering Research; State University of New York at Buffalo.

Guh, T.J. 1989; "Seismic upgrading of buildings structures using post-tensioning"; thesis submitted to the University of California at Berkeley in partial fulfillment of the requirements for the degree of Doctor of Philosophy.

Habibullah, A. and Wilson, E.L. 1989; "SAP90 A series of computer programs for the static and dynamic finite element analysis of structures"; Computers and Structures, Inc.; Berkeley, California.

Hata, O. 1993; communication by fax.

Hejal, R. and Chopra, A.K. 1987; "Earthquake response of torsionally-coupled buildings"; *Report No. UCB/EERC-87/20*; Earthquake Engineering Research Center; University of California at Berkeley.

Hirao, K. et al. 1988; "The effect of duration and frequency content of earthquake motion on energy responses of SDOF structures"; Proceedings of the Ninth World Conference on Earthquake Engineering, Vol. V, pp. 141-146; Tokyo, Japan.

Idriss, I.M. 1990; "Response of soft soil sites during earthquakes"; H. Bolton Seed Memorial Symposium Proceedings, Editor J. Michael Duncan, Volume 2, pp. 273-289; Vancouver, Canada.

Iglesias J., et al. 1986; "Intensidad del sismo de 1985 en la Ciudad de Mexico"; Sociedad Mexicana de Ingenieria Sísmica, Publicación Especial; Mexico, D.F.

Jamal, B.D., et al. 1992; "Numerical Analysis for in-plane behavior of infilled frames"; Proceedings of the Sixth Canadian Masonry Symposium, pp. 609-620; Canada.

Jirsa, J.O., and Badoux, M. 1990; "Strategies for seismic redesign of buildings"; Proceedings of the Fourth U.S. National Conference on Earthquake Engineering, Vol. 3, pp. 343-352; Palm Springs, California.

Kariotis, J., et al. 1993; "Unreinforced masonry (URM) infill buildings"; SMIP Directed Research Project, California.

Kariotis, J., et al. 1994; "Simulation of the recorded response of unreinforced (URM) infill buildings"; *Technical Report NCEER-94-0004*; National Center of Earthquake Engineering Research; State University of New York at Buffalo.

Kiremdjian, A.S. 1975; "Seismic hazard mapping of California"; *Report No. 21*, J.A. Blume Earthquake Engineering Center, Department of Civil Engineering; Stanford University; California.

Klingner, R.E. and Bertero, V.V. 1976; "Infilled frames in earthquake-resistant construction"; *Report No. EERC 76-32*; Earthquake Engineering Research Center; University of California at Berkeley.

Klingner, R.E. 1980; "Mathematical modelling of infilled frames"; American Concrete Institute; *ACI SP 63-1*; Michigan.

König, G. et al. 1988; "Experimental investigations of the behavior of unreinforced masonry walls under seismically induced loads and lessons derived"; Proceedings of the Ninth World Conference on Earthquake Engineering, Vol. 8, pp. 1117-1122; Tokyo-Kyoto, Japan.

Kusukawa, K. et al. 1992; "Investigation of damages on reinforced concrete buildings caused by the 1990 Philippine-Luzon earthquake"; Proceedings of the Tenth World Conference on Earthquake Engineering, Vol. 1, pp. 103-108; Madrid, Spain.

Kwok, Y.-H. and Ang, A. H.-S. 1987; "Seismic damage analysis and design of unreinforced masonry buildings"; *Report UILU-ENG-87-2007*, University of Illinois at Urbana-Champaign.

Langenbach, R. 1990; "Traditional and contemporary construction practices utilizing unreinforced masonry in seismic areas"; Proceedings of the Fourth U.S. National Conference on Earthquake Engineering, Vol. 3, pp. 263-272; Palm Springs, California.

Liauw, T.C. and Kwan, A.K.H. 1992; "Experimental study of shear wall and infilled frame on shake-table"; Proceedings of the Tenth World Conference on Earthquake Engineering, Vol. 5, pp. 2659-2664; Madrid, Spain.

MacGregor, J.G. 1988; Reinforced Concrete: Mechanics and Design; Prentice-Hall, Englewood, New Jersey.

Mahin, S.A. and Bertero, V.V. 1977; "RCCOLA User's Manual and Documentation"; Department of Civil Engineering; University of California at Berkeley.

Mahin, S.A. and Bertero, V.V. 1981; "An evaluation of inelastic seismic design spectra"; *Journal of Structural Engineering*; ASCE Vol. 107; pp. 1777-1795.

Mander, J.B. et al. 1994; "Physical and analytical modeling of brick infilled steel frames"; *Technical Report NCEER-94-0004*; National Center for Earthquake Engineering Research; State University of New York at Buffalo.

Mehrabi, A.B. and Shing, P.B. 1994; "Performance of masonry-infilled R/C frames under in-plane lateral loads: analytical modeling"; *Technical Report NCEER-94-0004*; National Center for Earthquake Engineering Research; State University of New York at Buffalo.

Meli, R., et al. 1992; "Experimental study on earthquake-resistant design of confined masonry structures"; Proceedings of the Tenth World Conference on Earthquake Engineering, Vol. 6, pp. 3469-3474 ; Madrid, Spain.

Merz, K. 1977; "The problem of damage to nonstructural components and equipment"; Proceedings of a Workshop on Earthquake-Resistant Reinforced Concrete Building Construction, Vol. III, pp. 1098-1127; University of California at Berkeley.

Miranda, E. 1991; "Seismic evaluation and upgrading of existing buildings"; Ph.D. dissertation; Department of Civil Engineering; University of California at Berkeley.

Miranda, E. and Bertero, V.V. 1989; "Performance of low rise buildings in Mexico City"; *Earthquake Spectra*, Volume 5, Number 1, pp. 121-143; Earthquake Engineering Research Institute; Oakland, California.

Miranda, E. and Bertero, V.V. 1990; "Post-tensioning technique for seismic upgrading of existing low-rise buildings"; Proceedings of the Fourth U.S. National Conference on Earthquake Engineering, Vol. 3, pp. 393-402; Palm Springs, California.

Moehle, J.P. et al. 1994; "Preliminary report on the seismological and engineering aspects of the January 17, 1994 Northridge Earthquake"; *Report No. UCB/EERC 94/01*; Earthquake Engineering Research Center; University of California at Berkeley.

Molavi, M. and Fshghi, S. 1992; "Structural damage from Manjil-Iran earthquake of June 1990"; Proceedings of the Tenth World Conference on Earthquake Engineering, Vol. 1, pp. 91-97; Madrid, Spain.

Naiem, F. 1989, The Seismic Design Handbook; Structural Engineering Series, Van Nostrand Reinhold; New York.

NBS Building Science Series 165, 1987; "Engineering aspects of the September 19, 1985 Mexico earthquake"; U.S. Department of Commerce, National Bureau of Standards.

Park, R., et al. 1975; Reinforced Concrete Structures; John Wiley & Sons; New York.

Park, R., et al. 1982; "Stress-strain behavior of concrete confined by overlapping hoops at low and high strain rates"; *Journal of the American Concrete Institute*, No.1 V.79; pp. 13-27.

Park Y.J., et.al. 1984; "Seismic damage analysis and damage-limiting design of R.C. buildings"; *Report UILU-ENG-84-2007*, University of Illinois at Urbana-Champaign.

Paulay, T. and Priestley, M.J.N. 1992; Seismic Design of Reinforced Concrete and Masonry Buildings; John Wiley & Sons, New York.

Pincheira, J.A. and Jirsa, J.O. 1992; "Post-tensioned bracing for seismic retrofit of RC frames"; Proceedings of the Tenth World Conference on Earthquake Engineering, Vol. 9, pp. 5199-5204; Madrid, Spain.

Pires, F. and Cansado, C.E. 1992; "The behavior of infilled reinforced concrete frames under horizontal cyclic loading"; Proceedings of the Tenth World Conference on Earthquake Engineering, Vol. 6, pp. 3419-3422; Madrid, Spain.

Powell, G.H., et al. 1992; "Drain-2DX Version 1.00, User Guide Sections"; Department of Civil Engineering, University of California at Berkeley.

Powell, G.H. et al. 1994; "Drain-3DX Version 1.10, User Guide"; Department of Civil Engineering, University of California at Berkeley.

Qi, X. and Moehle, J.P. 1991; "Displacement design approach for reinforced concrete structures subjected to earthquakes"; *Report No. UCB/EERC-91/02*; Earthquake Engineering Research Center; University of California at Berkeley.

Riddell, R. and Vásquez, J. 1984; "Existence of centers of resistance and torsional uncoupling of earthquake response of buildings"; Proceedings of the Eighth World Conference on Earthquake Engineering, Vol. IV, pp. 187-194; San Francisco, California.

Rioobo, J.M. 1989; "Sistema de rigidización y refuerzo de estructuras mediante cables de presfuerzo"; Proceedings of the VIII Congreso Nacional de Ingeniería Sísmica, Vol. III, G74-

G82; Acapulco, Mexico.

Sakamoto, I. 1978; "Seismic performance of nonstructural and secondary structural elements"; *Report No. UCB/EERC-78/10*; Earthquake Engineering Research Center; University of California at Berkeley.

Sanchez, P.E., et al. 1991; "Seismic zonation of the Los Angeles Region"; Proceedings of the Fourth International Conference on Seismic Zonation, Volume I, pp. 797-844; Stanford, California.

Scaletti, H., et al. 1992; "Pseudo dynamic tests of confined masonry buildings"; Proceedings of the Tenth World Conference on Earthquake Engineering, Vol. 6, pp. 3493-3498; Madrid, Spain.

Schuller, M. et al. 1994; "Performance of masonry-infilled R/C frames under in-plane lateral loads: experiments"; *Technical Report NCEER-94-0004*; National Center for Earthquake Engineering Research; State University of New York at Buffalo

SEAOC's Hazardous Building Subcommittee for Infilled Frames 1993; "Guidelines for analysis of existing frame structures with concrete or masonry infill"; Structural Engineers Association of Southern California.

Seed, H.B., and Idriss, I.M. 1982; "Ground motions and soil liquefaction during earthquakes"; Earthquake Engineering Research Institute; Oakland, California.

Shakal, et al. 1992; "Strong-motion records from the Landers, California earthquake of June 28, 1992"; *Report OSMS 92-09*, Division of Mines and Geology, California Department of Conservation; Sacramento, California.

Shimizaki, K. 1988; "Strong ground motion drift and base shear coefficient for R/C structures";

Proceedings of the Ninth World Conference on Earthquake Engineering, Vol. V, pp. 165-170; Tokyo, Japan.

Terán-Gilmore, A. 1993; "On the design of RC buildings located on soft soils using an energy approach"; CE299 Report; University of California at Berkeley.

Tinsley, J.C., et al. 1985; "Evaluating liquefaction potential"; U.S. Geological Survey *Professional Paper 1360*, pp. 101-126; Washington, D.C.

Trifunac, M.D. and Brady, A.G. 1975; "A study on the duration of strong earthquake ground motion"; *Bulletin of the Seismological Society of America*, Vol. 65, No. 3, pp. 581-626.

UBC 1991; Uniform Building Code; International Conference of Building Officials; Whittier, California.

Wakabayashi M. and Martinez, R.E. 1988; "Design of earthquake-resistant buildings"; McGraw-Hill; Hightown, New Jersey.

Wallace, J.W. 1992; "Biax: Revision 1, a computer program for the analysis of reinforced concrete and reinforced masonry sections"; *SEMM Report No. CU/CEE-92/4*, Clarkson University; New York.

Wesnousky, S.G. 1986; "Earthquakes, quaternary faults, and seismic hazard in California"; *Journal of Geophysical Research*, Vol. 91, No. B12; pp. 12587-12631.

Zagajeski, S.W. and Bertero, V.V. 1977; "Computer-aided optimum seismic design of ductile reinforced concrete moment-resisting frames"; *Report No. UCB/EERC-77/16*; Earthquake Engineering Research Center; University of California at Berkeley.

Ziony, J.I., and Yerkes, R.F. 1985; "Evaluating earthquake and surface-faulting potential"; U.S. Geological Survey *Professional Paper 1360*, pp. 43-92; Washington, D.C.

APPENDIX A. DESIGN EARTHQUAKE GROUND MOTION

As mentioned in section 1.4, when post-tensioned (PT) braces are used to upgrade an existing structure, it is important to estimate, with reasonable reliability, the maximum and minimum axial forces acting on the braces in order to avoid their excessive yielding and/or buckling. Therefore, a reliable design of the bracing system should be based on the use of a reliable seismic input, i.e., design earthquake ground motions (EQGMs), rather than on using code-prescribed design EQGMs (which at present is done defining reduced smoothed linear elastic design response spectra).

This brings considerable importance to the definition and determination of the EQGMs used to design and assess the performance of the upgraded building. Bertero (1992b) and Bertero and Bertero (1992) offer a detailed discussion of the issues involved in controlling the seismic risk of the built environment and the problems involved in determining the design EQGMs.

The framed building with URM infills that is described in section 2.1 is located in the Los Angeles metropolitan area (LA), specifically in the city of Pomona. Figure A.1 shows the location of this city on the map of California, which also shows the location of the major faults and the epicenters of the major earthquakes that have occurred in California (Gere and Shah 1984). Figure A.2 shows an illustrative block diagram of the major tectonic features and geomorphic provinces of LA county. Figure A.3 gives a closer look at the significant faults and earthquakes in the LA basin. By studying the previous figures, an idea of the tremendous complexity involved in trying to establish the seismic risk for the LA area is obtained. This complexity is produced not only because of the complex dynamics of the faulting system itself, but also because of the very large number of small, medium and large faults (many of whose existence have not yet been identified) that can be relevant to the seismic risk of a given site.

It is not the purpose of this report to establish in detail the seismic risk to the site where the Pomona building is located. It should be clearly stated that to do so, there is a need to have access to information that is not currently available or is not reliable enough (such as the exact soil profile at the site, the effect of the local soil on the amplification or deamplification of the motion in rock, adequate historical information concerning the behavior and historical seismic activity of all relevant faults, attenuation relationships, etc). Nevertheless, it is important to establish these risks in a reasonable manner to allow for the rational design of the PT bracing system. In general, the information concerning the seismic risk that the city of Pomona faces has been studied by several researchers in the more general context of the LA metropolitan area. Thus, the information provided in this section regarding the seismic risk of Pomona has not been obtained specifically for this city, but as a part of a considerably larger context. In other words, although the information can be considered to be realistic, it has not been derived from specific and/or detailed information obtained from the Pomona building site.

In the last two decades, the US Geological Survey and the Division of Mines and Geology of the California Department of Conservation have concentrated attention on improving the mapping and forecasting of the LA area earthquake risk. It has been considered that the critical first step in this seismic zonation is the analysis of the distribution and character of late quaternary faulting in the region. From surface and near-surface geologic evidence, Ziony and Yerkes (1985) identified nearly **100 potential EQ sources** in the LA area. To establish the seismic risk associated with each particular fault, recent zonation efforts have considered three types of evidence (Sanchez et al. 1991): the average rate of slip along the fault in the recent geological past, the average recurrence interval (in years) between previous events along the fault, and the maximum length or dimensions of the potential rupture segment. Nevertheless, as noted by Sanchez et al. (1991), the record of historical seismicity in the LA region is generally inadequate to infer actual seismic hazard levels. For example, reliable estimates of geologically determined slip rates are available only for a few major faults in the region (Wesnousky 1986). Also, estimates of the maximum credible EQs for faults is based primarily on the potential rupture length of an identified segment (Bonilla et al. 1984), but accepted segmentation models exist for only the most active faults in the LA region, and some of these segmentation schemes can be considered tentative and beset by large uncertainties. Also, as noted by Sanchez et al. (1991) hidden seismogenic sources could be present elsewhere, adding a new element of uncertainty to the location and magnitude of potential EQ sources. Other sources of uncertainty do not correspond to the seismic sources themselves but are introduced in the modeling of the fault system, such as: seismic source modelling (point, line or area); frequency of occurrences for each source; attenuation relationships; local soil effects, etc. The reader can find a comprehensive introduction to some of these topics in Naiem (1989).

Taking into consideration the above discussion, it is not difficult to understand why Sanchez et al. (1991) concluded that the feasibility of a reliable, frequency-dependent and probability-derived ground shaking hazard zonation scheme remains an issue, especially because methods for characterizing the ground-shaking hazard are still being debated in the scientific and engineering communities.

The seismic hazard at a given site has usually been established by means of its peak ground acceleration (PGA). To determine the PGA at the Pomona building site for the design of the upgrading scheme, two different seismic zonation maps of the state of California were used (Kiremidjian et al. 1975 and Algermissen et al. 1990). According to SEAOC's Hazardous Building Subcommittee for Infilled Frames (1993), the EQGM spectral data for design shall as a minimum be the mean response having 10% probability of being exceeded in 50 years (return period of 475 years). Figures A.4 and A.5 show PGA zonation maps obtained according to the above probability of exceedence in 50 years, and although both zonations differ (in some locations considerably), the PGAs obtained for the site of the Pomona building are similar: Kiremidjian et al. zonation yields a PGA around 0.4g, while the Algermissen et al. zonation yields values around 0.45-0.50 g. It should be mentioned that the PGA obtained from Kiremidjian et al. corresponds to an "average" or "firm" soil (shear wave velocity is 1500 ft/sec or above) and that of Algermissen et al. to rock. Considering the tremendous uncertainty involved in defining these PGAs, the difference between them is more than acceptable.

To estimate the PGA at the site of the building, it is necessary to consider the influence of the local soil conditions. Seed and Idriss (1982) conclude from the detailed study of several EQGMs that, at comparable distances from the source, the PGAs recorded on rock are somewhat higher than those recorded on deep alluvium (typically in the case of accelerations greater than about 0.1g). They observed that at lower acceleration levels accelerations on deep soil deposits seem to be higher than those on rock. Figure A.6 shows these tendencies, which were observed from the results of detailed studies of the PGA developed on four different types of soil deposits:

1. Rock
2. Stiff soil deposits involving cohesionless soils or stiff clays to about 200 ft (60 m) in depth.
3. Deep cohesionless soil deposits with depths greater than about 250 ft (75 m).
4. Deposits of soft to medium stiff clays and sands

As can be concluded from the above classification of soils, the "softness" of the soil increases from 1 to 4. Although Seed and Idriss did not have any intention of classifying soils according to the above four categories, in this paper the above categories will be denominated as Seed and Idriss soil categories. Available information regarding the conditions of the soil at the site of the Pomona building describe it as (Hata O. 1993): alluvial, silty sand/sandy silt. It was considered necessary to learn a little more about the soil before attempting to use Figure A.6 to determine the local PGA.

Figure A.7 shows the textural character of the surficial geologic materials in the San Gabriel Valley (Fumal and Tinsley 1985). The location of the Pomona building is shown in the figure. As shown, the soil at the site can be classified as type Q_{ym} (medium-grained Holocene Alluvium), which has been characterized by Fumal and Tinsley (1985) as: loose, moderately well drained, moderately sorted to well-sorted sand and silty sand forming alluvial plains and natural leeves along streams; locally contains thin beds of well-sorted clay, silt, gravel, and occasional cobbles and boulders; contains freshwater pelecypod and gastropod shells; intermediate in character and lateral extent between fine- and coarse-grained alluvium with which it interfingers; generally overlies late Pleistocene alluvium; generally less than 50 m thick in coastal basins and less than 10 m thick in inland basins. This description of the local soil conditions coincides with the available information for the soil at the site.

The soil at the site does not match exactly any of the Seed and Idriss soil categories, and without any detailed study to determine its properties, it is not possible to attempt a formal categorization. Nevertheless, according to the above description of the soil, it would seem reasonable to classify the soil at the site within Seed and Idriss soil types 3 and 4.

In recent years, the shear-wave velocity of the soil has been identified as a useful property to study and possibly predict within reasonable limits the shaking response of a site during an EQGM (Fumal and Tinsley 1985). The importance of shear-wave velocity can be shown by noting the way UBC 1991 uses it in its definition of soil type S4: a soil profile containing more than 40 feet (12 meters) of soft clay characterized by a shear wave velocity less than 500 ft per second (150 meter/second). In other words, shear wave can provide an idea of the degree of "softness" of the soil. Figure A.8 shows the generalized shear-wave velocity map in the San Gabriel Valley (Fumal and Tinsley 1985). This map was obtained assuming that the surficial textural characteristics extend to depths of significance to shaking response. According to the figure, the building is located in zone I, which is characterized by shear-wave velocities ranging from 150 to 285 m/s. By comparing these values of shear-wave velocity to those specified by UBC 1991 for soil type S4 (150 m/s), the high degree of "softness" of the soil at the site of the Pomona building is confirmed.

Using Figure A.6 with the PGAs obtained from Kiremdjian and Algermissen, and assuming the soil can be categorized within the third Idriss and Seed category (deep cohesionless soil), the following is obtained: a PGA of 0.5 in rock leads to a PGA around 0.38g in the soil; while considering a PGA of 0.4g in firm soil leads to a PGA of around 0.34g. It should be mentioned that the curve shown for soft soils in Figure A.6 has recently been actualized and corrected by Idriss (1990), as shown in Figure A.9. In the latter figure, a PGA ranging from 0.40 to 0.50g will lead to a PGA in soft soil around 0.40g. The difference between the values obtained for the PGA at the site is not significant, in spite of the different assumptions made to obtain them. A PGA of 0.38g was considered for the design of the building.

Once the maximum PGA has been obtained, it is necessary to define other characteristics of the EQGM that are relevant for the design of the building, such as the frequency content and duration of the EQGM at the site. For this purpose, it is necessary to study the dynamic characteristics of the ground-shaking at the site. Fortunately, there are four recorded EQGMs at the base of the Pomona building. Its accelerographs were triggered in the past during two earthquakes (two horizontal directions, N-S and E-W, for each earthquake):

■ **Upland 1990** (California Strong Motion Instrumentation Program 1990). The Upland EQ occurred on February 28, 1990 and had a local magnitude (M_L) of 5.5. Its epicenter was located at 34.140^0 N and 117.688^0 W, and had a focal depth of 10 km. CSMIP station 23544 (Pomona building) recorded at its base the EQGM produced by the Upland EQ, whose epicenter was 10 km away. At the site, the EQGM has an horizontal PGA of 0.13g and a strong-motion duration (defined according to Trifunac and Brady 1975) of about 10 sec. After this EQ, some damage was observed in the Pomona building: broken windows, cracked partitions walls and veneer.

■ **Landers 1992** (Shakal et al. 1992). The Landers EQ occurred on June 28, 1992 and had a surface-wave magnitude (M_S) of 7.5. Its epicenter was located at 34.217^0 N and 116.433^0 W, and had a local depth of 9 km. CSMIP station 23544 recorded at its base the EQGM produced by the Landers EQ, whose epicenter was 123 km away. At the site, the EQGM has an horizontal PGA of 0.07g and a strong-motion duration of about 30 sec.

General information regarding the four recorded EQGMs is summarized in Table A.1. Although these EQGMs are not enough to determine all of the relevant characteristics (frequency content, duration, input energy, etc.) that future EQGMs occurring at the site of the Pomona building can have, the information that each provides complements the others', because the Upland motions represent near-source EQGMs with moderate magnitude, while the Landers motions represent the effects of a distant source EQGM with large magnitude.

Figures A.10 and A.11 show the strength and displacement spectra for $\xi = 0.05$ and the four

EQGMs recorded at the base of the building. As shown in Figure A.10 all four strength (S_a) spectra tend to peak at periods between 0.3-0.4 sec and 1.5-1.8 sec. The peaks in the 0.3-0.4 sec range are very large for the Upland EQGMs (S_a = 0.57g and 0.37g in the N-S and E-W directions, respectively) while the peaks in the 1.5-1.8 sec range tend to be larger for the Landers EQGMs (S_a = 0.25g and 0.17g in the N-S and E-W directions, respectively). Figure A.11 shows that the displacement (δ) demands for the Landers EQGMs are larger than those imposed by the Upland EQGMs for T larger than 1 sec and $\mu = 1$, while for other T and μ, these demands are fairly similar.

A better understanding of the soil and its dynamic characteristics can be obtained by studying the input energy per unit mass (E_I) spectra corresponding to the four recorded EQGMs. Studying the E_I spectra shown in Figure A.12, it is very noticeable that the elastic E_I spectra corresponding to the four EQGMs peak in a period range going from 1.5 to 1.8 sec. Hirao et al. (1988) have discussed the possibility of estimating the frequency content of an EQGM from its E_I spectra corresponding to small values of ξ. By noticing the large and fairly narrow peaks in the E_I spectra, it is possible to conclude that all four EQGMs have a narrow frequency content around a T of 1.5-1.8 sec, which can be defined as the fundamental period of excitation for the EQGMs (T_g). The large value of T_g and the narrow band of the E_I spectra confirm the "softness" of the soil. Given the strong influence that the soil at the site shows on the frequency content of the four recorded EQGMs, it is possible to conclude that for EQGMs generated from seismic events that occur at large epicentral distances, the frequency content will be very likely to have a narrow band around a T_g ranging from 1.5 to 1.8 sec, as shown in Figures A.12a and A.12b. Nevertheless, EQGMs generated from seismic events occurring at small epicentral distances will not only show the influence of the dynamic characteristics of the soil at the site, but the dynamic characteristics of the fault movement as well, which considerably complicates the possible determination of the frequency content of such motions. For instance, Figure A.12c shows an E_I spectra that peaks at two locations (one at $T \approx 0.4$ sec and another at $T \approx 1.5$ sec). In spite of the fact that the Upland EQGMs have larger PGAs than the Landers EQGMs (see Table A.1) and that the Upland EQGMs strength spectra peak at considerably larger values of S_a than the Landers EQGMs (see Figure A.10), the E_I spectra corresponding to the Upland EQGMs peak at considerably lower values than those corresponding to the Landers EQGMs. For instance, the E_I spectra for Landers EQGMs peaks at values around 10000 and 5000 cm^2/sec^2 in the N-S and E-W directions, respectively, while the Upland EQGMs peak at 2500 and 1750 respectively. This can be explained by noting the considerably larger duration for the Landers EQGMs (23 and 28 sec) with respect to that of the Upland EQGMs (5 and 11 sec).

Other characteristics of EQGMs relevant to EQ-RD are the plastic hysteretic energy ($E_{H\mu}$) dissipation demands and the duration of strong motion. According to the philosophy of design for the PT bracing system (see section 1.5), the PT braces should be designed and introduced within the existing frame in such a way that them and existing frame members remain elastic, while the maximum deformation in the URM infills is limited in such a way that these infills can have stable hysteretic behavior through several load cycles. Under the above conditions, the duration of EQGM becomes less relevant, although it is undeniable that it influences the performance of the URM infills. In this report, the influence of the duration of ground motion was neglected not only because it is believed to have small influence, but because there is no way of quantifying its effect on the URM infills of the Pomona building. There is still a need to fully understand how the repetition of load cycles affect the performance of URM infills (with and without openings) as a function of the maximum displacement demands on them.

The safety design strength spectra was estimated according to the recommendations given by SEAOC's Hazardous Building Subcommittee for Infilled frames (1993): use of a mean response spectra rather than the mean plus one sigma used for new buildings. The mean strength and displacement response spectra were obtained using the four EQGMs recorded at the site scaled up so that their PGAs were equal to 0.38g. Figure A.13 shows the strength and displacement safety design spectra (mean), as well as the coefficient of variation of the strength spectra. As shown, the mean strength spectra has retained the frequency content of the EQGMs recorded at the site.

The design and assessment of the seismic performance of a building should be carried out using a multi-limit state behavioral criterion. Usually it is enough to use a two-limit state approach: serviceability and safety. The advantages of developing a design method based on two limit states have been discussed by Zagajeski and Bertero (1977) and Bertero and Bertero (1992). Besides the safety design EQGM, in some cases it is necessary to develop a service design EQGM. Nevertheless, two facts should be noted:

■ According to the strength and displacement demands shown in Figures A.10 and A.11, the Landers and Upland EQGMs can be classified somewhere in between serviceability and damageability type of EQGMs. The performance of the building during these EQGMs can be considered acceptable from the point of view of structural and nonstructural damage (little damage was observed after the Upland EQGM while no damage was reported after the Landers EQGMs). Thus, a point can be made about the adequacy of the building to resist EQGMs of moderate intensity associated with the serviceability (and even damageability) limit state. Once the structure is upgraded, there is reason to believe the building should perform adequately during EQGMs similar to those recorded during the Upland and Landers EQs.

■ In the case of a framed building with URM infills upgraded with PT braces, adequate performance has been associated with the elastic behavior of the braces and existing frame elements, no matter what limit state is considered. The building is supposed to exhibit a behavior close to elastic during the safety EQGM (the behavior will not be linear elastic because moderate nonlinear demands are expected on the URM infills); therefore, the strength and displacement demands imposed by the safety EQGM will be considerably larger than those imposed by the service EQGM. Thus, the design of the PT bracing system and the assessment of the building's seismic performance will be based only on the design spectra for the safety limit state.

In some cases, it is also convenient to verify the potential for hazards other than those due to vibration of the building, such as those that occur as a consequence of the ground failure, such as liquefaction and landslides. Given the unconsolidated and uncemented nature of the soil at the site, it was considered necessary to check the liquefaction potential at the site. As shown in Figure A.14, this potential ranges from low to very low, which indicates that liquefaction should not be of concern in the seismic performance of the building.

■ **Concluding Remarks.** From the discussions presented in this chapter, it is possible to conclude that the feasibility of establishing a reliable design seismic input a the site of the Pomona building remains an issue, especially because methods for characterizing the ground-shaking hazard are still being debated in the scientific and engineering communities.

In spite of the above, an attempt was carried to establish in a reasonable manner design spectra for the EQ-RD design of the Pomona building. The values of PGA at the site obtained using different PGA zonation maps ranged from 0.4g (in firm soil) to 0.5g (in rock). Considering the tremendous uncertainty involved in defining these PGAs, the difference between them is considered to be more than acceptable.

To estimate the PGA of the EQGMs at the base of the Pomona building, it was necesary to establish, in a general manner, some of the properties of the soil at the site. In particular, it was concluded that the soil has a high degree of "softness". Based on this characteristic, a PGA of 0.38g was considered for the design of the Pomona building.

The safety design strength spectra was estimated according to the recommendations given by SEAOC's Hazardous Building Subcommittee for Infilled frames (1993). Accordingly, the safety design spectra was assumed equal to the mean strength spectra of the four EQGMs that have been recorded at the site. To obtain this mean spectra, all four EQGMs were scaled up so that their PGAs were equal to 0.38g. Given the importance of displacement control for the EQ-RD of the upgraded Pomona building, a safety design displacement spectra was also established using the same considerations done to obtain the design strength spectra.

Other characteristics of EQGMs relevant to EQ-RD are the plastic hysteretic energy dissipation demands and the duration of strong motion. According to the philosophy of design for the PT bracing system, the PT braces and the frame members should remain elastic, while the maximum deformation in the URM infills should be limited so that they can exhibit stable hysteretic behavior. Under the above conditions the duration of EQGM becomes less relevant, although its influence in the performance of the URM infills can not be denied. In this report, the influence of the duration of ground motion was neglected.

Ground Motion	distance from epicenter (km)	PGA (in/sec^2)	PGV (in/sec)	PGD (in)	duration of strong motion (sec)
Lander N-S	123	26.4 = 0.07g	4.4	1.2	23.3
Lander E-W	123	19.3 = 0.05g	3.8	1.0	28.4
Upland N-S	10	49.2 = 0.13g	4.0	0.7	4.6
Upland E-W	10	37.8 = 0.10g	3.0	0.6	10.9

PGA = peak ground acceleration
PGV = peak ground velocity
PGD = peak ground displacement

Table A.1 Characteristics of EQGMs recorded at the base of the Pomona building

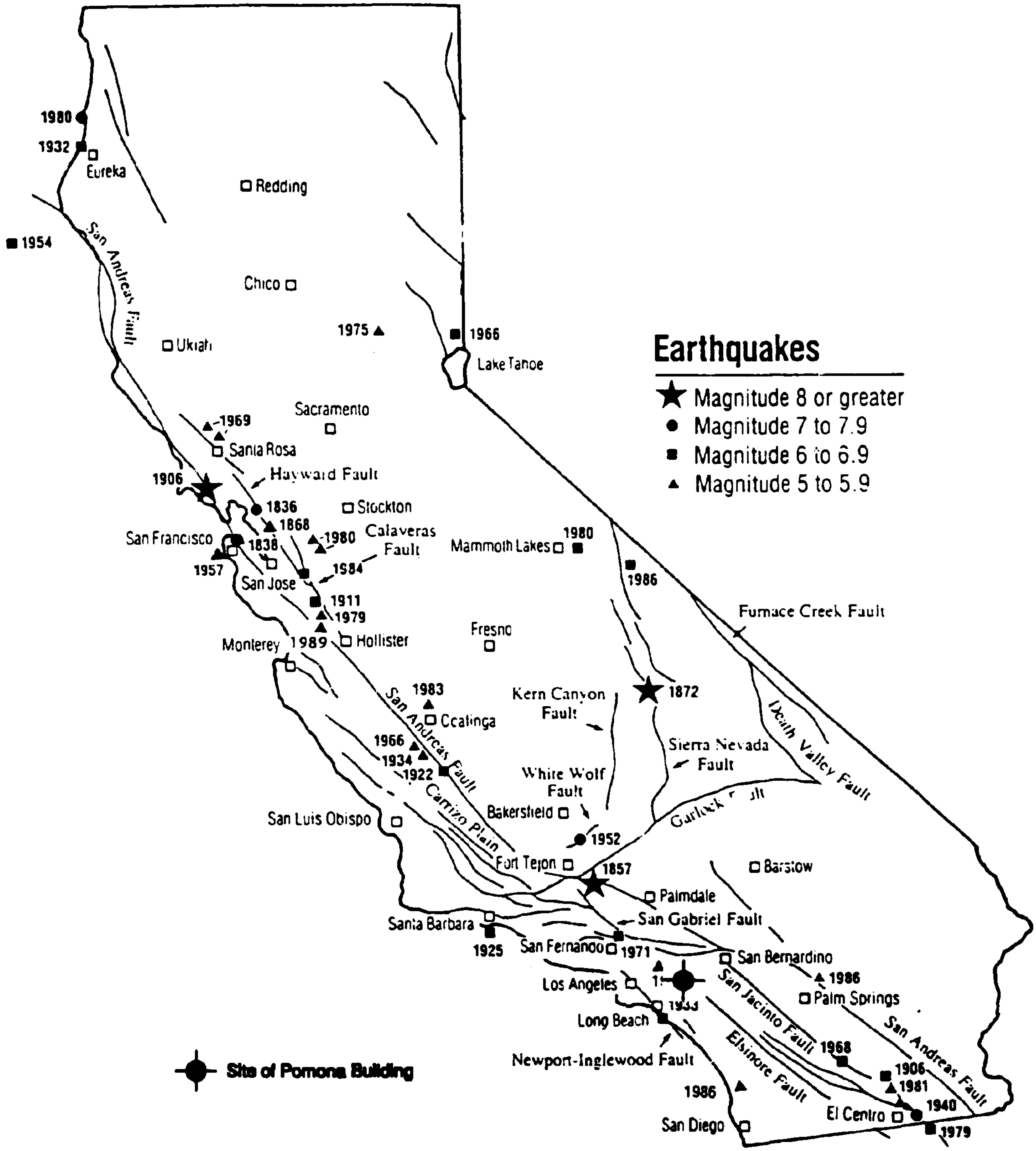

Figure A.1 Major Faults and Significant Earthquakes of California 1836-1987

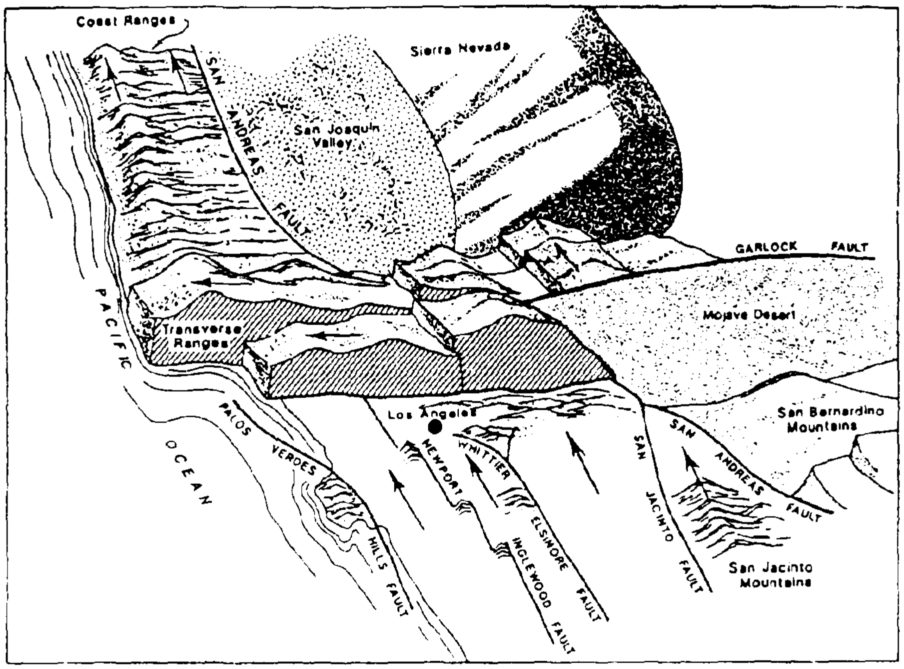

Figure A.2 Illustrative block diagram of major tectonic features and geomorphic provinces of Los Angeles County

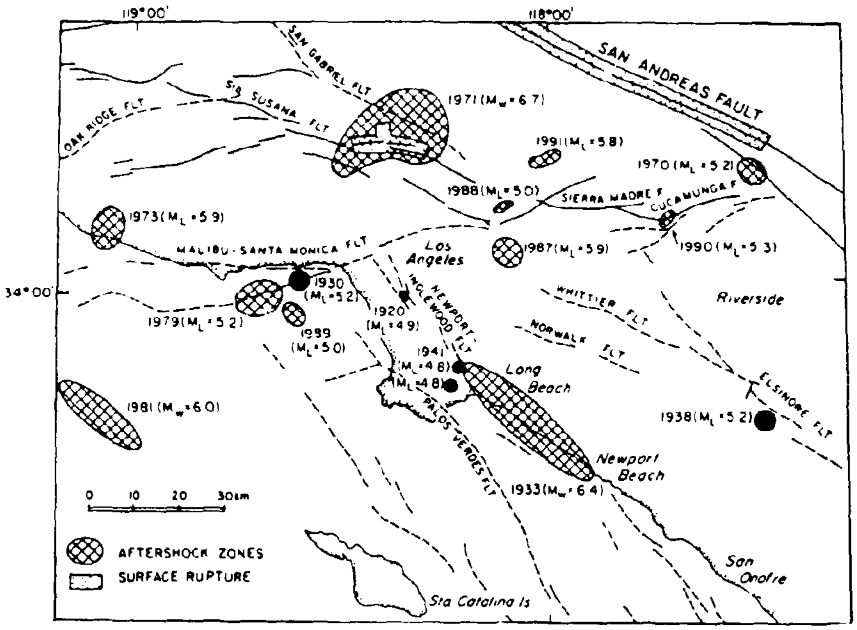

Figure A.3 Significant EQs of M 4.8 that have occurred in the greater LA basin area since 1920. Aftershock zones are shaded with cross hatching. Dotted areas indicate surface rupture

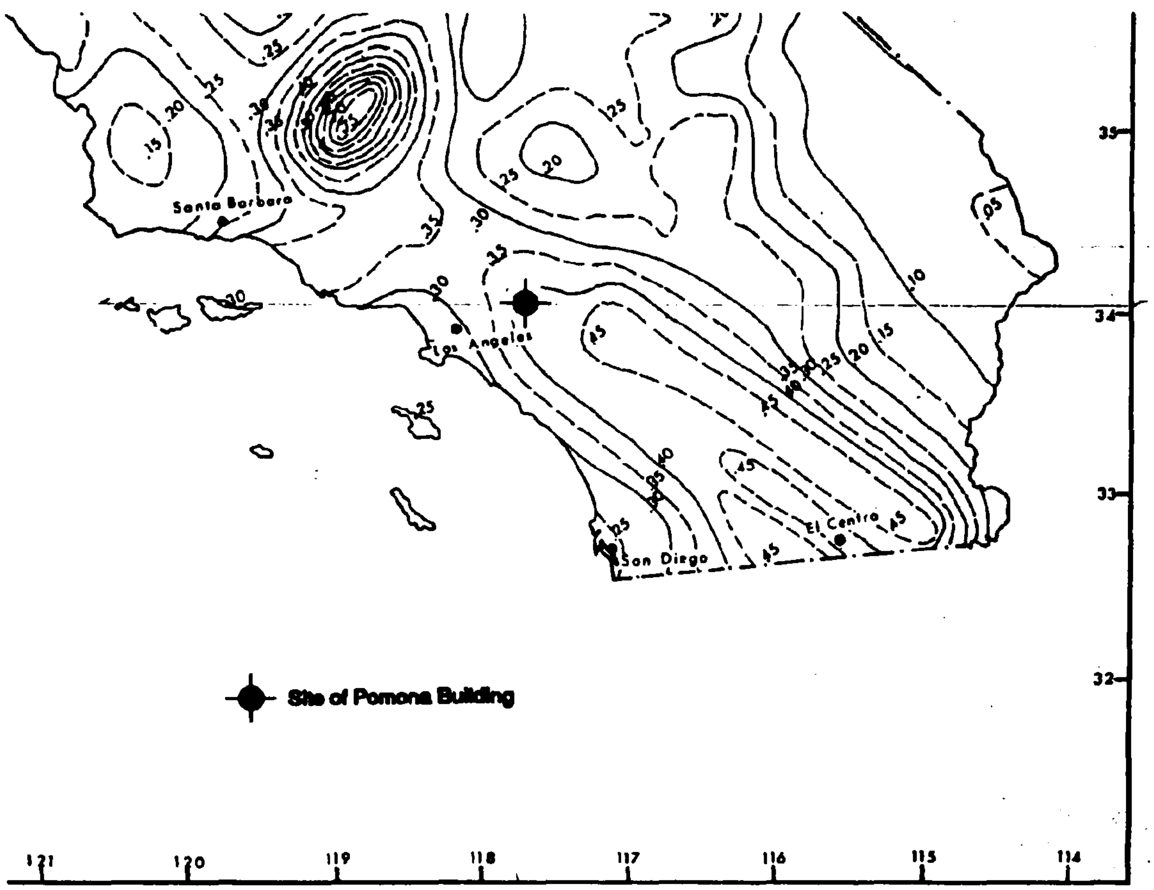

Figure A.4 Seismic hazard map for southern California for a return period of 475 years (Kiremidjian et al. 1975).

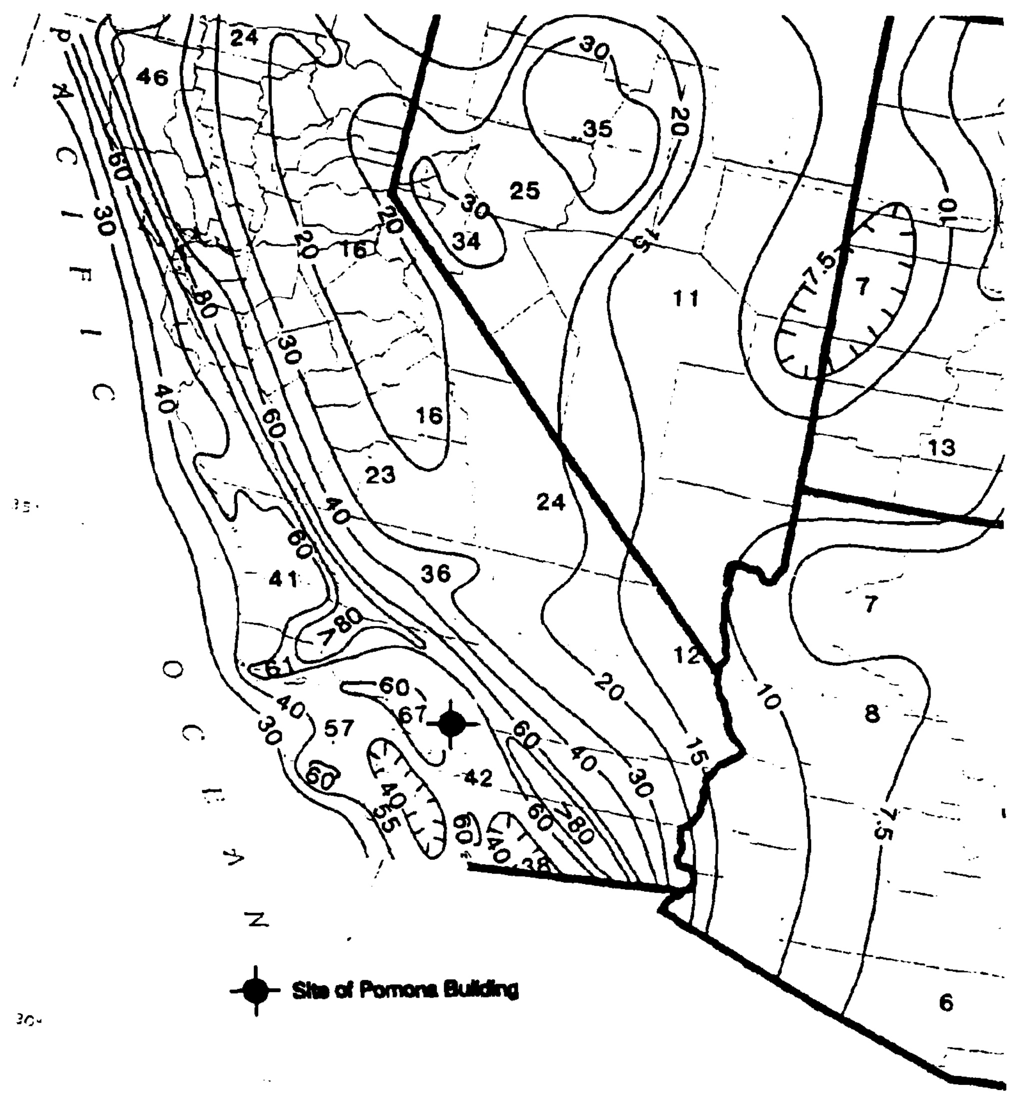

Figure A.5 Seismic hazard map for southern California for a return period of 475 years (Algermissen et al. 1990).

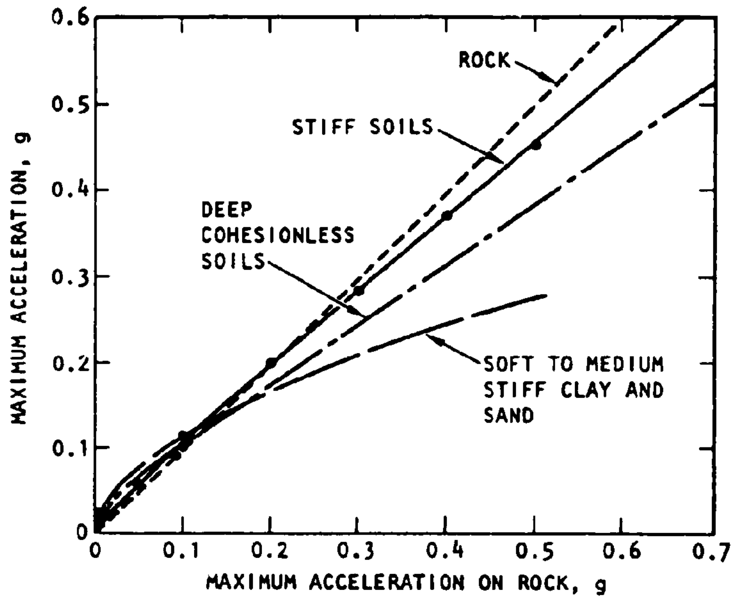

Figure A.6 Approximate relationships between PGA on rock and other local site conditions (Seed and Idriss, 1982)

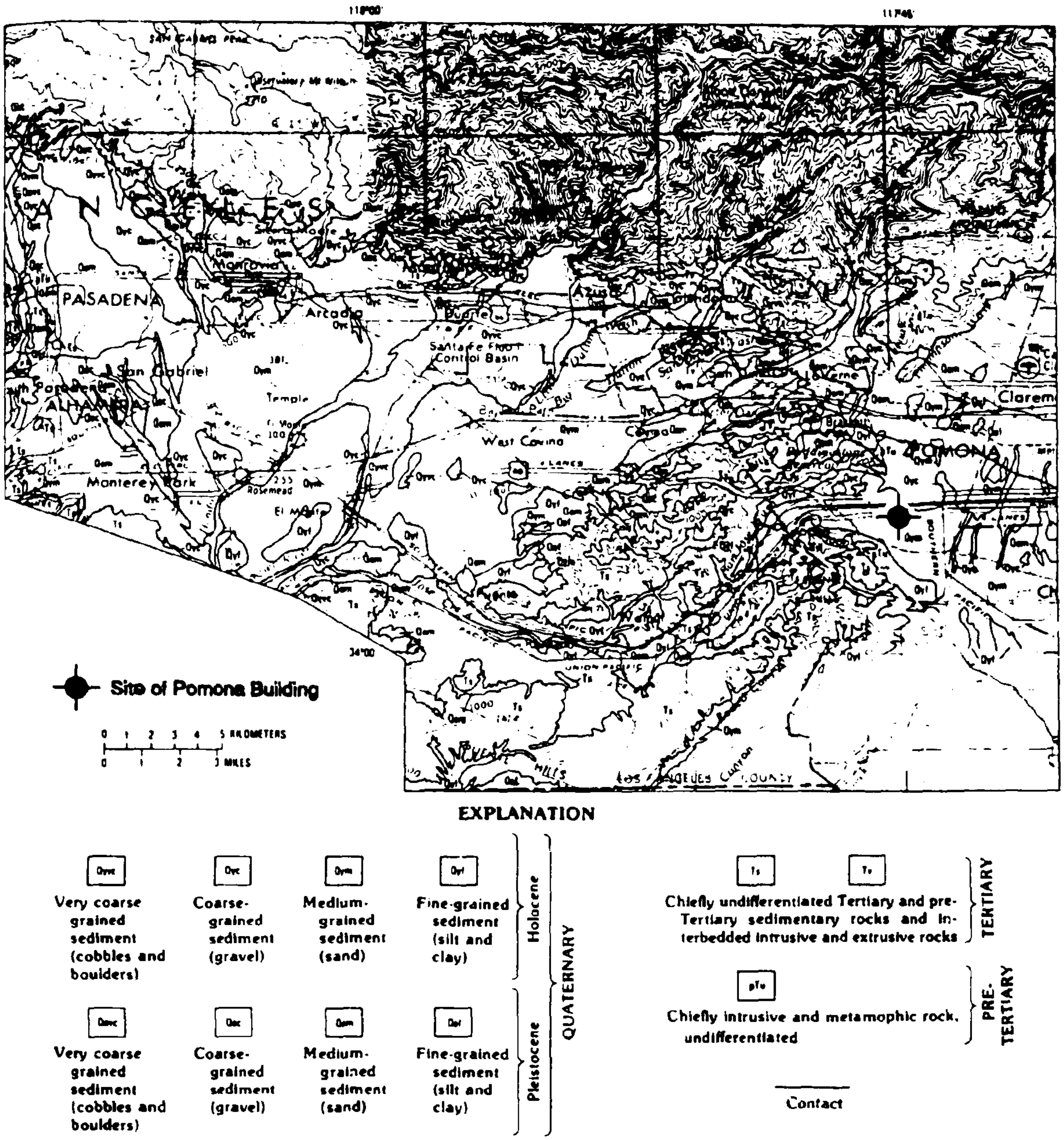

Figure A.7 Age and textural character of surficial geologic materials in the San Gabriel Valley (Fumal and Tinsley 1985)

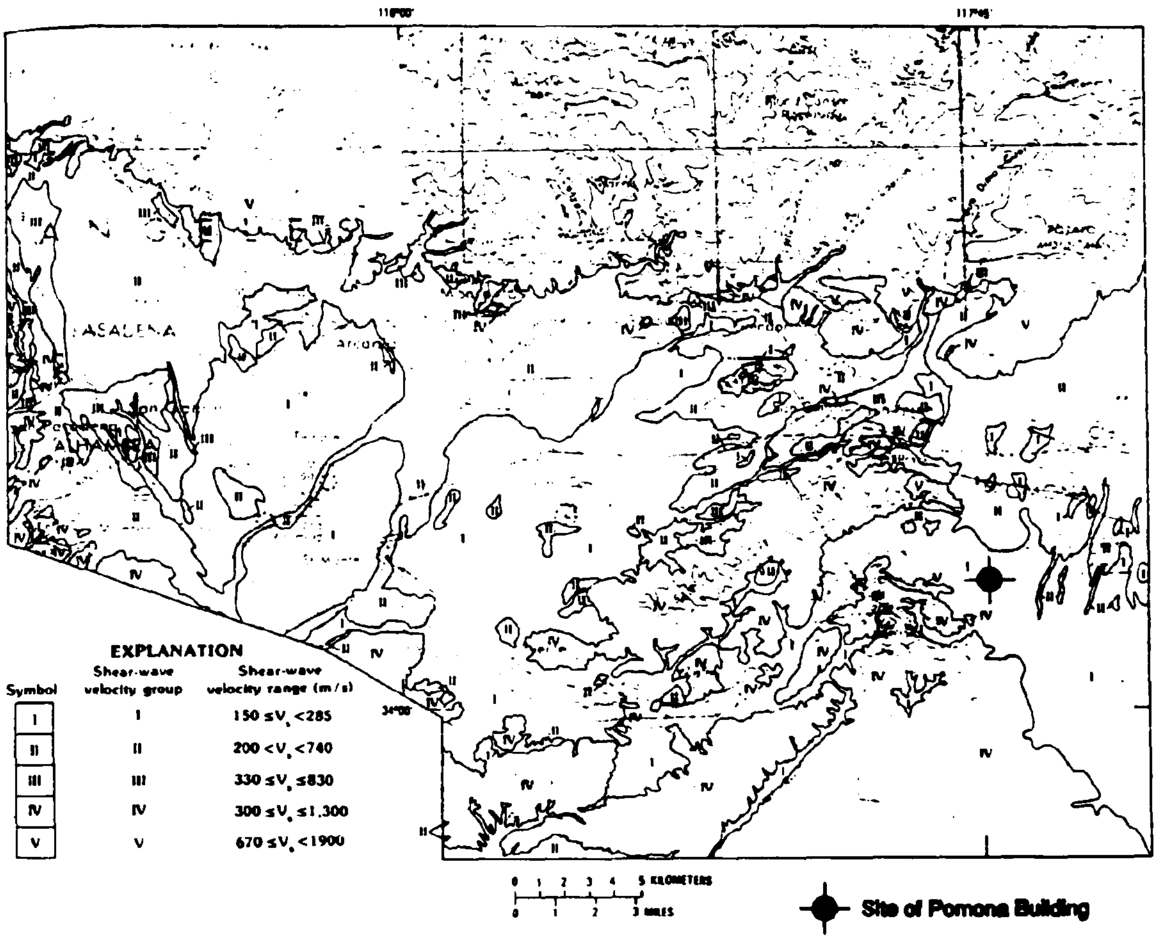

Figure A.8 Generalized shear-wave velocity groups in the San Gabriel Valley. (Fumal and Tinsley 1985)

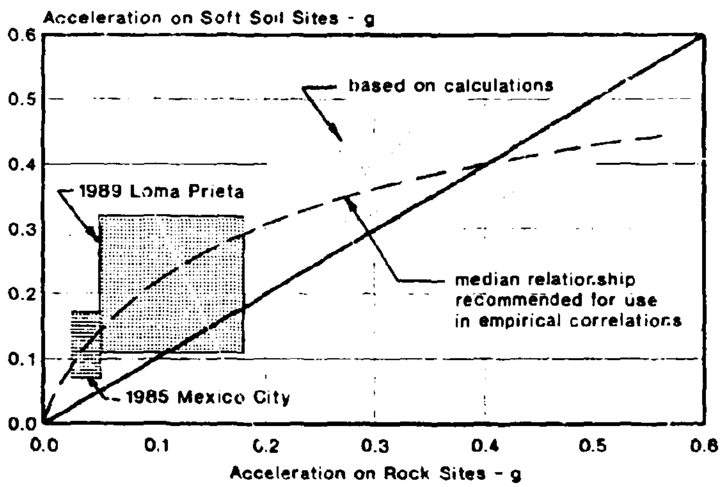

Figure A.9 Variations of PGA on soft soil sites vs. rock sites (Idriss 1990)

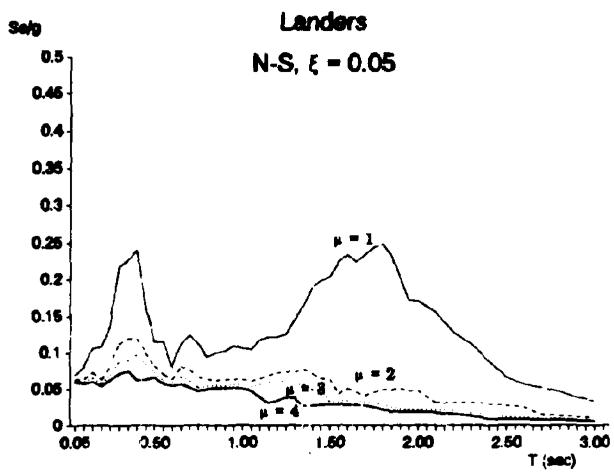

a) Landers N-S

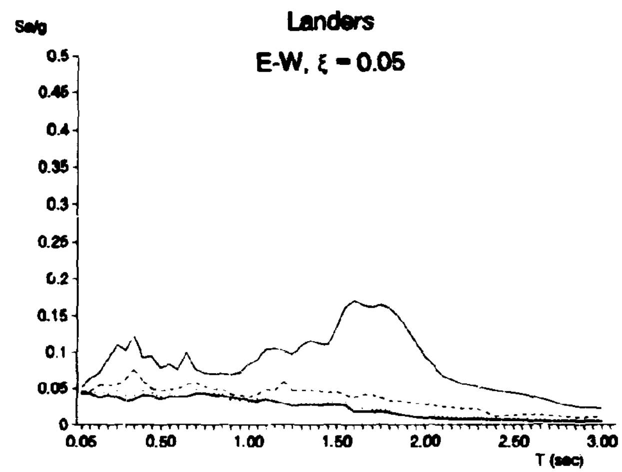

b) Landers E-W

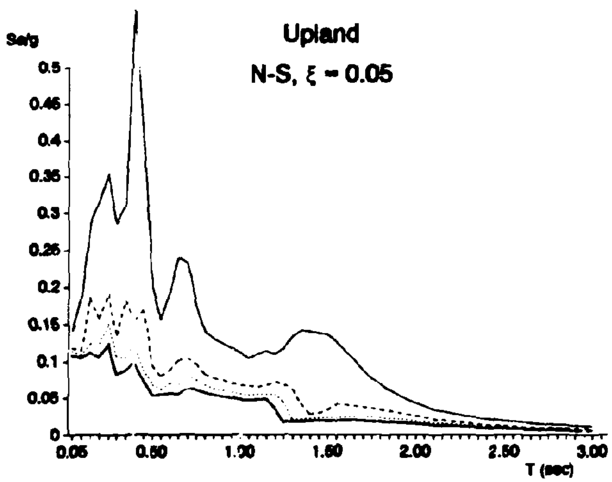

c) Upland N-S

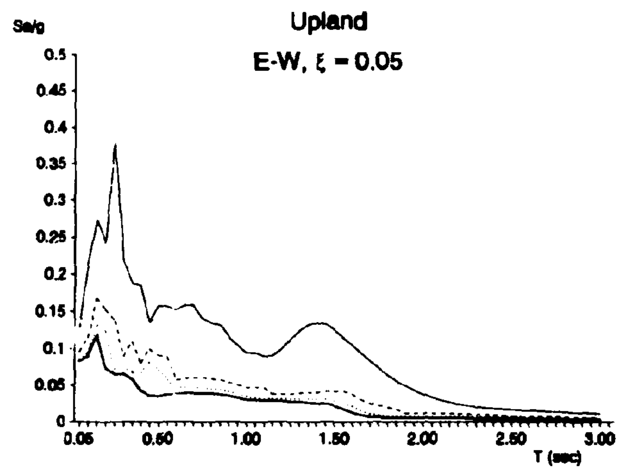

d) Upland E-W

Figure A.10 Strength spectra for recorded ground motions

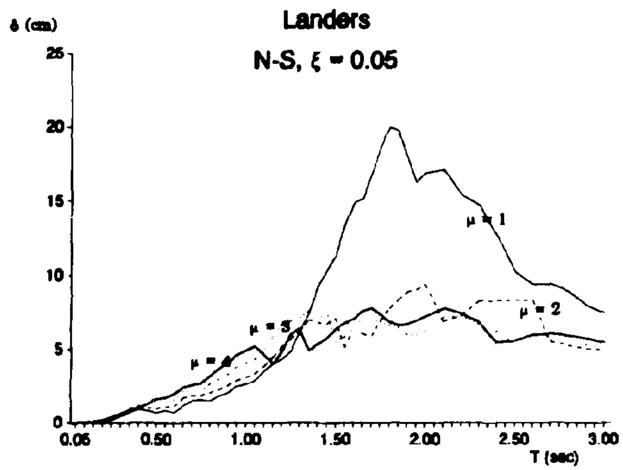

a) Landers N-S

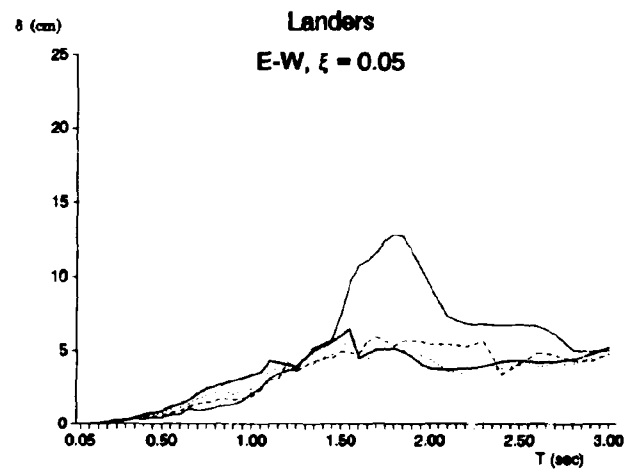

b) Landers E-W

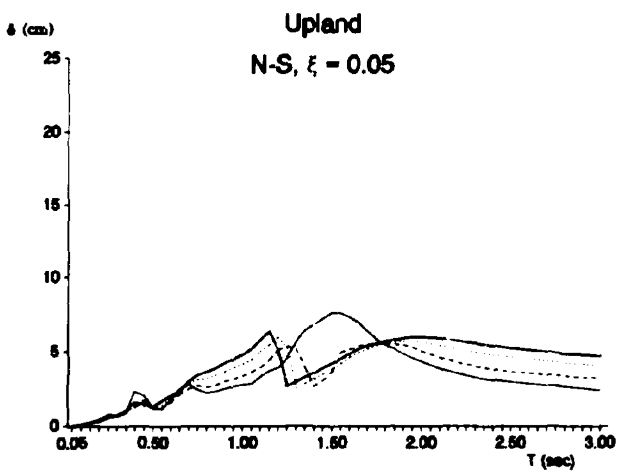

c) Upland N-S

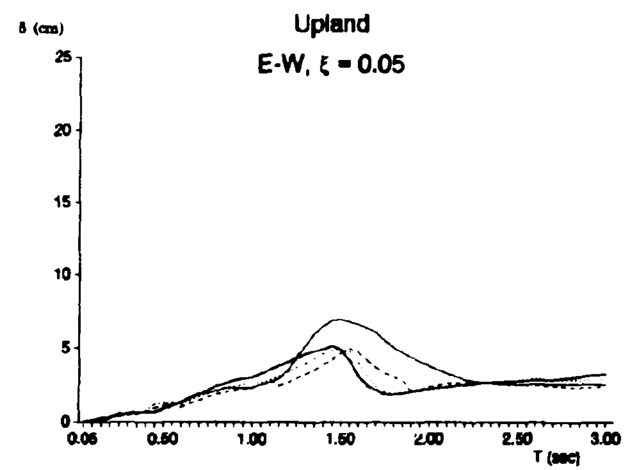

d) Upland E-W

Figure A.11 Displacement spectra for recorded ground motions

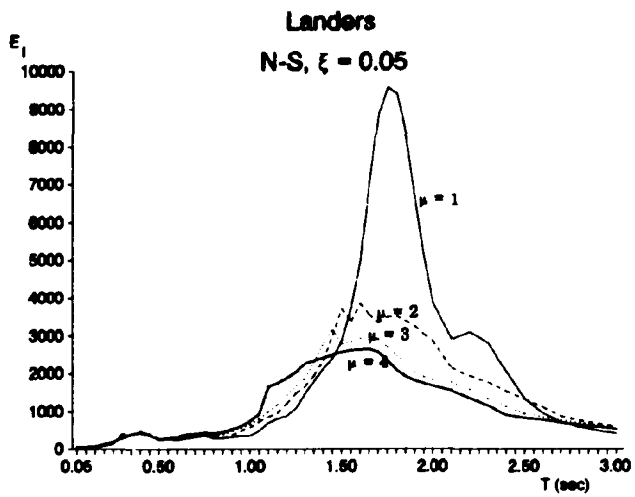

a) Landers N-S

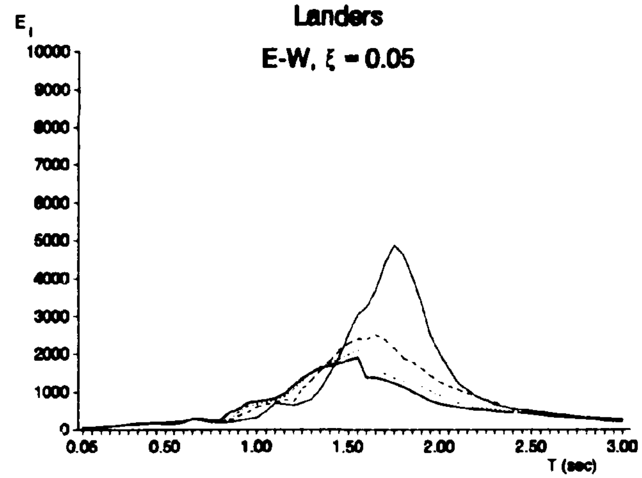

b) Landers E-W

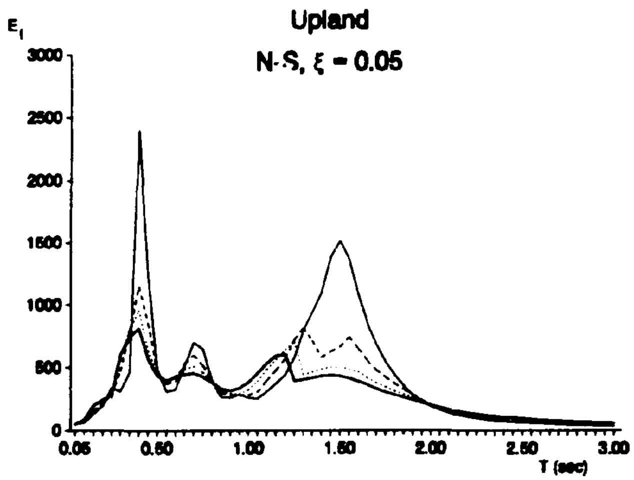

c) Upland N-S

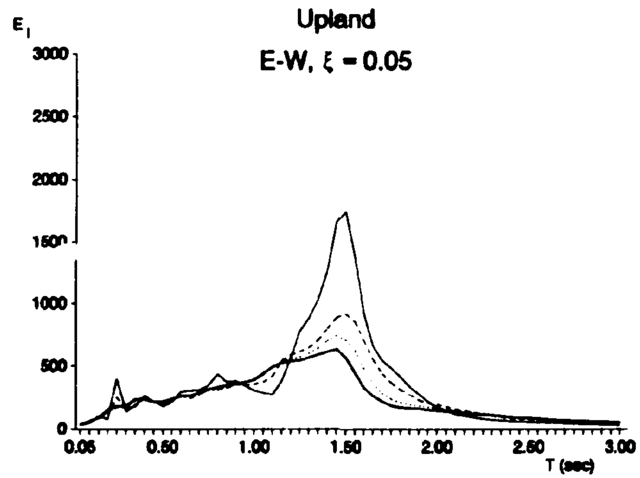

d) Upland E-W

Figure A.12 Normalized input energy spectra for recorded ground motions (cm^2 / sec^2)

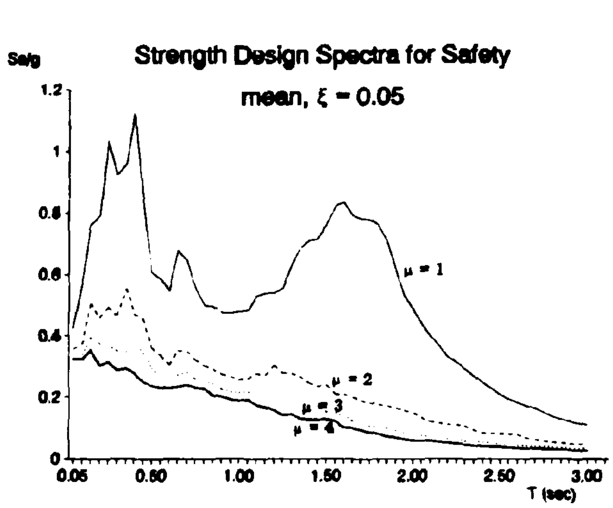

a) strength spectra, mean

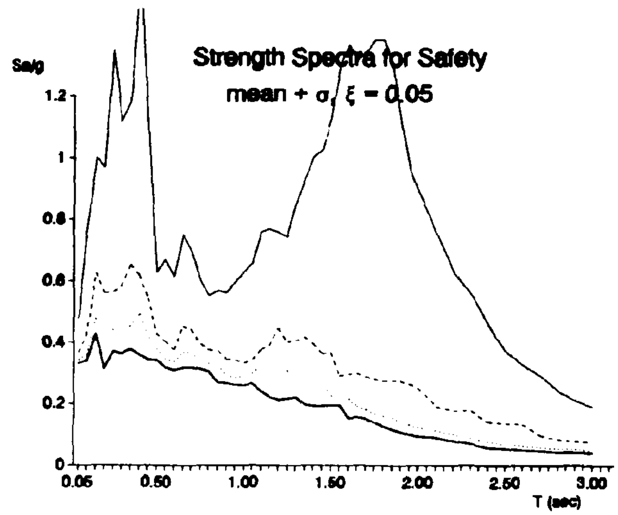

b) strength spectra, mean + σ

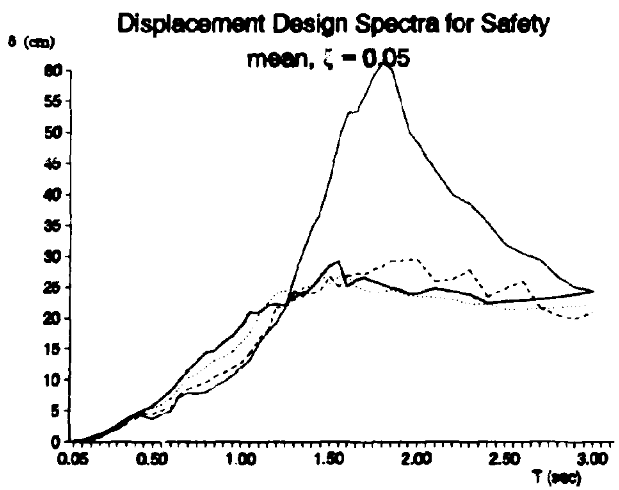

c) displacement spectra, mean

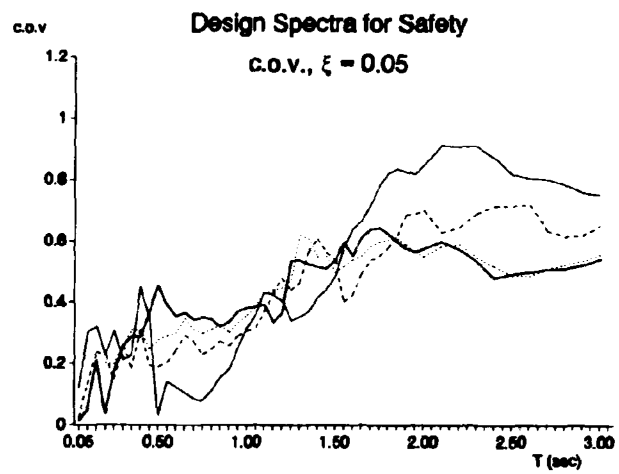

d) strength spectra, c.o.v.

Figure A.13 Design spectra for safety

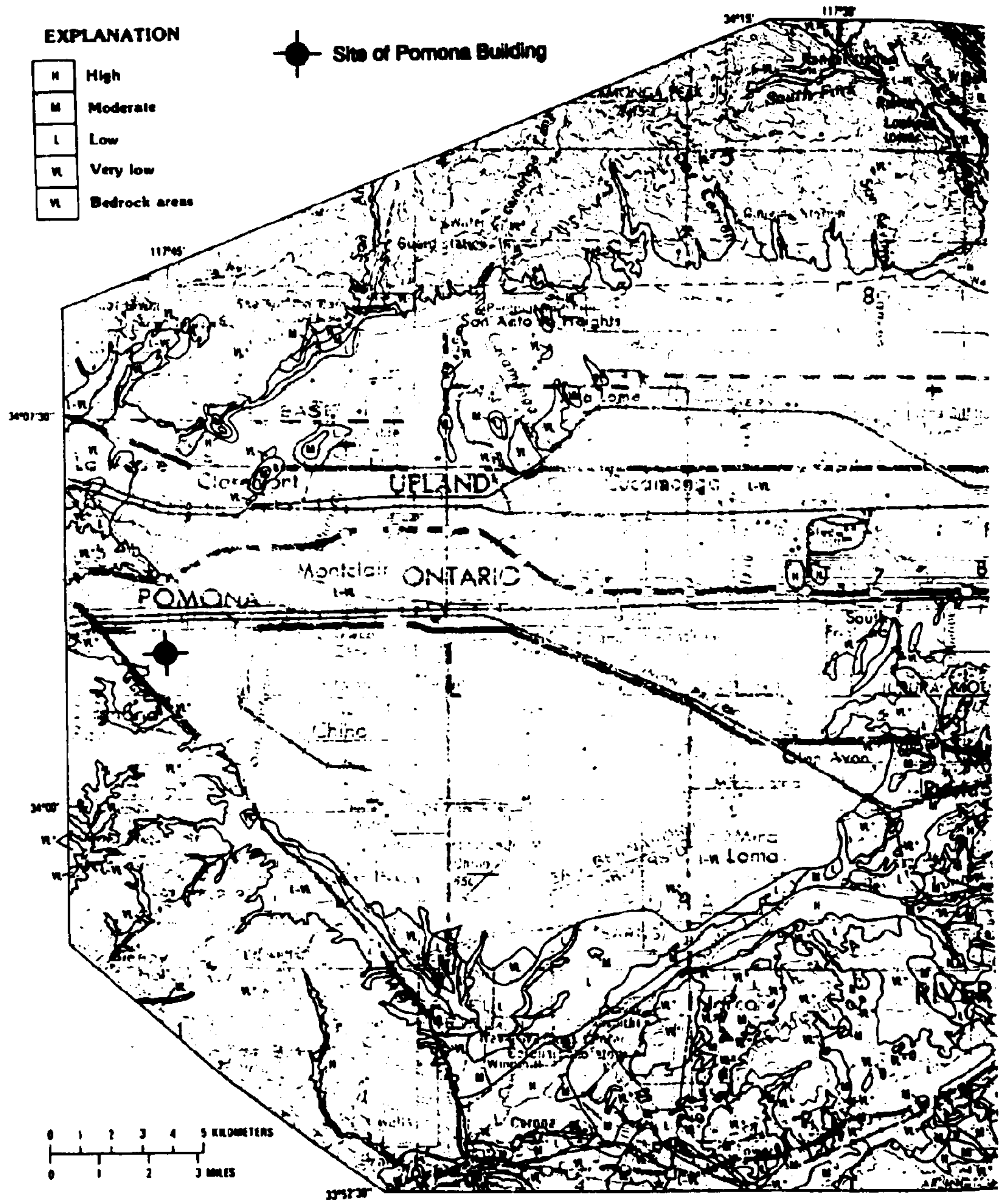

Figure A.14 Relative liquefaction susceptibility in the upper Santa Ana River basin (Tinsley et al. 1985)

EARTHQUAKE ENGINEERING RESEARCH CENTER REPORT SERIES

EERC reports are available from the National Information Service for Earthquake Engineering (NISEE) and from the National Technical Information Service (NTIS). Numbers in parentheses are Accession Numbers assigned by the National Technical Information Service; these are followed by a price code. Contact NTIS, 5285 Port Royal Road, Springfield Virginia, 22161 for more information. Reports without Accession Numbers were not available from NTIS at the time of printing. For a current complete list of EERC reports (from EERC 67-1) and availablity information, please contact University of California, EERC, NISEE, 1301 South 46th Street, Richmond, California 94804-4698.

UCB/EERC-84/01 "Pseudodynamic Test Method for Seismic Performance Evaluation: Theory and Implementation," by Shing, P.-S.B. and Mahin, S.A., January 1984, (PB84 190 644)A08.

UCB/EERC-84/02 "Dynamic Response Behavior of Kiang Hong Dian Dam," by Clough, R.W., Chang, K.-T., Chen, H.-Q. and Stephen, R.M., April 1984, (PB84 209 402)A08.

UCB/EERC-84/03 "Refined Modelling of Reinforced Concrete Columns for Seismic Analysis," by Kaba, S.A. and Mahin, S.A., April 1984, (PB84 234 384)A06.

UCB/EERC-84/04 "A New Floor Response Spectrum Method for Seismic Analysis of Multiply Supported Secondary Systems," by Asfura, A. and Der Kiureghian, A., June 1984, (PB84 239 417)A06.

UCB/EERC-84/05 "Earthquake Simulation Tests and Associated Studies of a 1/5th-scale Model of a 7-Story R/C Frame-Wall Test Structure," by Bertero, V.V., Aktan, A.E., Charney, F.A. and Sause, R., June 1984, (PB84 239 409)A09.

UCB/EERC-84/06 "Unassigned," by Unassigned, 1984.

UCB/EERC-84/07 "Behavior of Interior and Exterior Flat-Plate Connections Subjected to Inelastic Load Reversals," by Zee, H.L. and Moehle, J.P., August 1984, (PB86 117 629/AS)A07.

UCB/EERC-84/08 "Experimental Study of the Seismic Behavior of a Two-Story Flat-Plate Structure," by Moehle, J.P. and Diebold, J.W., August 1984, (PB86 122 553/AS)A12.

UCB/EERC-84/09 "Phenomenological Modeling of Steel Braces under Cyclic Loading," by Ikeda, K., Mahin, S.A. and Dermitzakis, S.N., May 1984, (PB86 132 198/AS)A08.

UCB/EERC-84/10 "Earthquake Analysis and Response of Concrete Gravity Dams," by Fenves, G.L. and Chopra, A.K., August 1984, (PB85 193 902/AS)A11.

UCB/EERC-84/11 "EAGD-84: A Computer Program for Earthquake Analysis of Concrete Gravity Dams," by Fenves, G.L. and Chopra, A.K., August 1984, (PB85 193 613/AS)A05.

UCB/EERC-84/12 "A Refined Physical Theory Model for Predicting the Seismic Behavior of Braced Steel Frames," by Ikeda, K. and Mahin, S.A., July 1984, (PB85 191 450/AS)A09.

UCB/EERC-84/13 "Earthquake Engineering Research at Berkeley - 1984," by EERC, August 1984, (PB85 197 341/AS)A10.

UCB/EERC-84/14 "Moduli and Damping Factors for Dynamic Analyses of Cohesionless Soils," by Seed, H.B., Wong, R.T., Idriss, I.M. and Tokimatsu, K., September 1984, (PB85 191 468/AS)A04.

UCB/EERC-84/15 "The Influence of SPT Procedures in Soil Liquefaction Resistance Evaluations," by Seed, H.B., Tokimatsu, K., Harder, L.F. and Chung, R.M., October 1984, (PB85 191 732/AS)A04.

UCB/EERC-84/16 "Simplified Procedures for the Evaluation of Settlements in Sands Due to Earthquake Shaking," by Tokimatsu, K. and Seed, H.B., October 1984, (PB85 197 887/AS)A03.

UCB/EERC-84/17 "Evaluation of Energy Absorption Characteristics of Highway Bridges Under Seismic Conditions - Volume I (PB90 262 627)A16 and Volume II (Appendices) (PB90 262 635)A13," by Imbsen, R.A. and Penzien, J., September 1986.

UCB/EERC-84/18 "Structure-Foundation Interactions under Dynamic Loads," by Liu, W.D. and Penzien, J., November 1984, (PB87 124 889/AS)A11.

UCB/EERC-84/19 "Seismic Modelling of Deep Foundations," by Chen, C.-H. and Penzien, J., November 1984, (PB87 124 798/AS)A07.

UCB/EERC-84/20 "Dynamic Response Behavior of Quan Shui Dam," by Clough, R.W., Chang, K.-T., Chen, H.-Q., Stephen, R.M., Ghanaat, Y. and Qi, J.-H., November 1984, (PB86 115177/AS)A07.

UCB/EERC-85/01 "Simplified Methods of Analysis for Earthquake Resistant Design of Buildings," by Cruz, E.F. and Chopra, A.K., February 1985, (PB86 112299/AS)A12.

UCB/EERC-85/02 "Estimation of Seismic Wave Coherency and Rupture Velocity using the SMART 1 Strong-Motion Array Recordings," by Abrahamson, N.A., March 1985, (PB86 214 343)A07.

UCB/EERC-85/03 "Dynamic Properties of a Thirty Story Condominium Tower Building," by Stephen, R.M., Wilson, E.L. and Stander, N., April 1985, (PB86 118965/AS)A06.

UCB/EERC-85/04 "Development of Substructuring Techniques for On-Line Computer Controlled Seismic Performance Testing," by Dermitzakis, S. and Mahin, S., February 1985, (PB86 132941/AS)A08.

UCB/EERC-85/05 "A Simple Model for Reinforcing Bar Anchorages under Cyclic Excitations," by Filippou, F.C., March 1985, (PB86 112 919/AS)A05.

UCB/EERC-85/06 "Racking Behavior of Wood-framed Gypsum Panels under Dynamic Load," by Oliva, M.G., June 1985, (PB90 262 643)A04.

UCB/EERC-85/07 "Earthquake Analysis and Response of Concrete Arch Dams," by Fok, K.-L. and Chopra, A.K., June 1985, (PB86 139672/AS)A10.

UCB/EERC-85/08 "Effect of Inelastic Behavior on the Analysis and Design of Earthquake Resistant Structures," by Lin, J.P. and Mahin, S.A., June 1985, (PB86 135340/AS)A08.

UCB/EERC-85/09 "Earthquake Simulator Testing of a Base-Isolated Bridge Deck," by Kelly, J.M., Buckle, I.G. and Tsai, H.-C., January 1986, (PB87 124 152/AS)A06.

UCB/EERC-85/10 "Simplified Analysis for Earthquake Resistant Design of Concrete Gravity Dams," by Fenves, G.L. and Chopra, A.K., June 1986, (PB87 124 160/AS)A08.

UCB/EERC-85/11 "Dynamic Interaction Effects in Arch Dams," by Clough, R.W., Chang, K.-T., Chen, H.-Q. and Ghanaat, Y., October 1985, (PB86 135027/AS)A05.

UCB/EERC-85/12 "Dynamic Response of Long Valley Dam in the Mammoth Lake Earthquake Series of May 25-27, 1980," by Lai, S. and Seed, H.B., November 1985, (PB86 142304/AS)A05.

UCB/EERC-85/13 "A Methodology for Computer-Aided Design of Earthquake-Resistant Steel Structures," by Austin, M.A., Pister, K.S. and Mahin, S.A., December 1985, (PB86 159480/AS)A10.

UCB/EERC-85/14 "Response of Tension-Leg Platforms to Vertical Seismic Excitations," by Liou, G.-S., Penzien, J. and Yeung, R.W., December 1985, (PB87 124 871/AS)A08.

UCB/EERC-85/15 "Cyclic Loading Tests of Masonry Single Piers: Volume 4 - Additional Tests with Height to Width Ratio of 1," by Sveinsson, B., McNiven, H.D. and Sucuoglu, H., December 1985, (PB87 165031/AS)A08.

UCB/EERC-85/16 "An Experimental Program for Studying the Dynamic Response of a Steel Frame with a Variety of Infill Partitions," by Yanev, B. and McNiven, H.D., December 1985, (PB90 262 676)A05.

UCB/EERC-86/01 "A Study of Seismically Resistant Eccentrically Braced Steel Frame Systems," by Kasai, K. and Popov, E.P., January 1986, (PB87 124 178/AS)A14.

UCB/EERC-86/02 "Design Problems in Soil Liquefaction," by Seed, H.B., February 1986, (PB87 124 186/AS)A03.

UCB/EERC-86/03 "Implications of Recent Earthquakes and Research on Earthquake-Resistant Design and Construction of Buildings," by Bertero, V.V., March 1986, (PB87 124 194/AS)A05.

UCB/EERC-86/04 "The Use of Load Dependent Vectors for Dynamic and Earthquake Analyses," by Leger, P., Wilson, E.L. and Clough, R.W., March 1986, (PB87 124 202/AS)A12.

UCB/EERC-86/05 "Two Beam-To-Column Web Connections," by Tsai, K.-C. and Popov, E.P., April 1986, (PB87 124 301/AS)A04.

UCB/EERC-86/06 "Determination of Penetration Resistance for Coarse-Grained Soils using the Becker Hammer Drill," by Harder, L.F. and Seed, H.B., May 1986, (PB87 124 210/AS)A07.

UCB/EERC-86/07 "A Mathematical Model for Predicting the Nonlinear Response of Unreinforced Masonry Walls to In-Plane Earthquake Excitations," by Mengi, Y. and McNiven, H.D., May 1986, (PB87 124 780/AS)A06.

UCB/EERC-86/08 "The 19 September 1985 Mexico Earthquake: Building Behavior," by Bertero, V.V., July 1986.

UCB/EERC-86/09 "EACD-3D: A Computer Program for Three-Dimensional Earthquake Analysis of Concrete Dams," by Fok, K.-L., Hall, J.F. and Chopra, A.K., July 1986, (PB87 124 228/AS)A08.

UCB/EERC-86/10 "Earthquake Simulation Tests and Associated Studies of a 0.3-Scale Model of a Six-Story Concentrically Braced Steel Structure," by Uang, C.-M. and Bertero, V.V., December 1986, (PB87 163 564/AS)A17.

UCB/EERC-86/11 "Mechanical Characteristics of Base Isolation Bearings for a Bridge Deck Model Test," by Kelly, J.M., Buckle, I.G. and Koh, C.-G., November 1987, (PB90 262 668)A04.

UCB/EERC-86/12 "Effects of Axial Load on Elastomeric Isolation Bearings," by Koh, C.-G. and Kelly, J.M., November 1987, PB88-179015(A06).

UCB/EERC-87/01 "The FPS Earthquake Resisting System: Experimental Report," by Zayas, V.A., Low, S.S. and Mahin, S.A., June 1987, (PB88 170 287)A06.

UCB/EERC-87/02 "Earthquake Simulator Tests and Associated Studies of a 0.3-Scale Model of a Six-Story Eccentrically Braced Steel Structure," by Whittaker, A., Uang, C.-M. and Bertero, V.V., July 1987, (PB88 166 707/AS)A18.

UCB/EERC-87/03 "A Displacement Control and Uplift Restraint Device for Base-Isolated Structures," by Kelly, J.M., Griffith, M.C. and Aiken, I.D., April 1987, (PB88 169 933)A04.

UCB/EERC-87/04 "Earthquake Simulator Testing of a Combined Sliding Bearing and Rubber Bearing Isolation System," by Kelly, J.M. and Chalhoub, M.S., December 1990, PB92-192962(A09).

UCB/EERC-87/05 "Three-Dimensional Inelastic Analysis of Reinforced Concrete Frame-Wall Structures," by Moazzami, S. and Bertero, V.V., May 1987, (PB88 169 586/AS)A08.

UCB/EERC-87/06 "Experiments on Eccentrically Braced Frames with Composite Floors," by Ricles, J. and Popov, E., June 1987, (PB88 173 067/AS)A14.

UCB/EERC-87/07 "Dynamic Analysis of Seismically Resistant Eccentrically Braced Frames," by Ricles, J. and Popov, E., June 1987, (PB88 173 075/AS)A16.

UCB/EERC-87/08 "Undrained Cyclic Triaxial Testing of Gravels-The Effect of Membrane Compliance," by Evans, M.D. and Seed, H.B., July 1987, (PB88 173 257)A19.

UCB/EERC-87/09	"Hybrid Solution Techniques for Generalized Pseudo-Dynamic Testing," by **Thewalt, C. and Mahin, S.A., July 1987, (PB 88 179 007)A07.**
UCB/EERC-87/10	"Ultimate Behavior of Butt Welded Splices in Heavy Rolled Steel Sections,' by **Bruneau, M., Mahin, S.A. and Popov, E.P., September 1987, (PB90 254 285)A07.**
UCB/EERC-87/11	"Residual Strength of Sand from Dam Failures in the Chilean Earthquake of March 3, 1985," by **De Alba, P., Seed, H.B., Retamal, E. and Seed, R.B., September 1987, (PB88 174 321/AS)A03.**
UCB/EERC-87/12	"Inelastic Seismic Response of Structures with Mass or Stiffness Eccentricities in Plan," by **Bruneau, M. and Mahin, S.A., September 1987, (PB90 262 650/AS)A14**
UCB/EERC-87/13	"CSTRUCT: An Interactive Computer Environment for the Design and Analysis of Earthquake Resistant Steel Structures," by **Austin, M.A., Mahin, S.A. and Pister, K.S., September 1987, (PB88 173 339/AS)A06.**
UCB/EERC-87/14	"Experimental Study of Reinforced Concrete Columns Subjected to Multi-Axial Loading," by **Low, S.S. and Moehle, J.P., September 1987, (PB88 174 347/AS)A07**
UCB/EERC-87/15	"Relationships between Soil Conditions and Earthquake Ground Motions in Mexico City in the Earthquake of Sept. 19, 1985," by **Seed, H.B., Romo, M.P., Sun, J., Jaime, A. and Lysmer, J., October 1987, (PB88 178 991)A06.**
UCB/EERC-87/16	"Experimental Study of Seismic Response of R. C. Setback Buildings," by **Shahrooz, B.M. and Moehle, J.P., October 1987, (PB88 176 359)A16.**
UCB/EERC-87/17	"The Effect of Slabs on the Flexural Behavior of Beams," by **Pantazopoulou, S.J. and Moehle, J.P., October 1987, (PB90 262 700)A07.**
UCB/EERC-87/18	"Design Procedure for R-FBI Bearings," by **Mostaghel, N. and Kelly, J.M., November 1987, (PB90 262 718)A04.**
UCB/EERC-87/19	"Analytical Models for Predicting the Lateral Response of R C Shear Walls: Evaluation of their Reliability," by **Vulcano, A. and Bertero, V.V., November 1987, (PB88 178 983)A05.**
UCB/EERC-87/20	"Earthquake Response of Torsionally-Coupled Buildings," by **Hejal, R. and Chopra, A.K., December 1987, PB90-208638(A15).**
UCB/EERC-87/21	"Dynamic Reservoir Interaction with Monticello Dam," by **Clough, R.W., Ghanaat, Y. and Qiu, X-F., December 1987, (PB88 179 023)A07.**
UCB/EERC-87/22	"Strength Evaluation of Coarse-Grained Soils," by **Siddiqi, F.H., Seed, R.B., Chan, C.K., Seed, H.B. and Pyke, R.M., December 1987, (PB88 179 031)A04.**
UCB/EERC-88/01	"Seismic Behavior of Concentrically Braced Steel Frames," by **Khatib, I., Mahin, S.A. and Pister, K.S., January 1988, (PB91 210 898/AS)A11.**
UCB/EERC-88/02	"Experimental Evaluation of Seismic Isolation of Medium-Rise Structures Subject to Uplift," by **Griffith, M.C., Kelly, J.M., Coveney, V.A. and Koh, C.G., January 1988, (PB91 217 950/AS)A09.**
UCB/EERC-88/03	"Cyclic Behavior of Steel Double Angle Connections," by **Astaneh-Asl, A. and Nader, M.N., January 1988, (PB91 210 872)A05.**
UCB/EERC-88/04	"Re-evaluation of the Slide in the Lower San Fernando Dam in the Earthquake of Feb. 9, 1971," by **Seed, H.B., Seed, R.B., Harder, L.F. and Jong, H.-L., April 1988, (PB91 212 456/AS)A07.**
UCB/EERC-88/05	"Experimental Evaluation of Seismic Isolation of a Nine-Story Braced Steel Frame Subject to Uplift," by **Griffith, M.C., Kelly, J.M. and Aiken, I.D., May 1988, (PB91 217 968/AS)A07.**
UCB/EERC-88/06	"DRAIN-2DX User Guide.," by **Allahabadi, R. and Powell, G.H., March 1988, (PB91 212 530)A12.**
UCB/EERC-88/07	"Theoretical and Experimental Studies of Cylindrical Water Tanks in Base-Isolated Structures," by **Chalhoub, M.S. and Kelly, J.M., April 1988, (PB91 217 976/AS)A05.**
UCB/EERC-88/08	"Analysis of Near-Source Waves: Separation of Wave Types Using Strong Motion Array Recording," by **Darragh, R.B., June 1988, (PB91 212 621)A08.**
UCB/EERC-88/09	"Alternatives to Standard Mode Superposition for Analysis of Non-Classically Damped Systems," by **Kusainov, A.A. and Clough, R.W., June 1988, (PB91 217 992/AS)A04.**
UCB/EERC-88/10	"The Landslide at the Port of Nice on October 16, 1979," by **Seed, H.B., Seed, R.B., Schlosser, F., Blondeau, F. and Juran, I., June 1988, (PB91 210 914)A05.**
UCB/EERC-88/11	"Liquefaction Potential of Sand Deposits Under Low Levels of Excitation," by **Carter, D.P. and Seed, H.B., August 1988, (PB91 210 880)A15**
UCB/EERC-88/12	"Nonlinear Analysis of Reinforced Concrete Frames Under Cyclic Load Reversals," by **Filippou, F.C. and Issa, A., September 1988, (PB91 212 589)A07**
UCB/EERC-88/13	"Implications of Recorded Earthquake Ground Motions on Seismic Design of Building Structures," by **Uang, C.-M. and Bertero, V.V., November 1988, (PB91 212 548)A06.**
UCB/EERC-88/14	"An Experimental Study of the Behavior of Dual Steel Systems," by **Whittaker, A.S., Uang, C.-M. and Bertero, V.V., September 1988, (PB91 212 712)A16.**
UCB/EERC-88/15	"Dynamic Moduli and Damping Ratios for Cohesive Soils," by **Sun, J.I., Golesorkhi, R. and Seed, H.B., August 1988, (PB91 210 922)A04**

UCB/EERC-88/16 "Reinforced Concrete Flat Plates Under Lateral Load: An Experimental Study Including Biaxial Effects," by Pan, A. and Moehle, J.P., October 1988, (PB91 210 856)A13.

UCB/EERC-88/17 "Earthquake Engineering Research at Berkeley - 1988," by EERC, November 1988, (PB91 210 864)A10.

UCB/EERC-88/18 "Use of Energy as a Design Criterion in Earthquake-Resistant Design," by Uang, C.-M. and Bertero, V.V., November 1988, (PB91 210 906/AS)A04.

UCB/EERC-88/19 "Steel Beam-Column Joints in Seismic Moment Resisting Frames," by Tsai, K.-C. and Popov, E.P., November 1988, (PB91 217 984/AS)A20.

UCB/EERC-88/20 "Base Isolation in Japan, 1988," by Kelly, J.M., December 1988, (PB91 212 449)A05.

UCB/EERC-89/01 "Behavior of Long Links in Eccentrically Braced Frames," by Engelhardt, M.D. and Popov, E.P., January 1989, (PB92 143 056)A18.

UCB/EERC-89/02 "Earthquake Simulator Testing of Steel Plate Added Damping and Stiffness Elements," by Whittaker, A., Bertero, V.V., Alonso, J. and Thompson, C., January 1989, (PB91 229 252/AS)A10.

UCB/EERC-89/03 "Implications of Site Effects in the Mexico City Earthquake of Sept. 19, 1985 for Earthquake-Resistant Design Criteria in the San Francisco Bay Area of California," by Seed, H.B. and Sun, J.I., March 1989, (PB91 229 369/AS)A07.

UCB/EERC-89/04 "Earthquake Analysis and Response of Intake-Outlet Towers," by Goyal, A. and Chopra, A.K., July 1989, (PB91 229 286/AS)A19.

UCB/EERC-89/05 "The 1985 Chile Earthquake: An Evaluation of Structural Requirements for Bearing Wall Buildings," by Wallace, J.W. and Moehle, J.P., July 1989, (PB91 218 008/AS)A13.

UCB/EERC-89/06 "Effects of Spatial Variation of Ground Motions on Large Multiply-Supported Structures," by Hao, H., July 1989, (PB91 229 161/AS)A08.

UCB/EERC-89/07 "EADAP - Enhanced Arch Dam Analysis Program: Users's Manual," by Ghanaat, Y. and Clough, R.W., August 1989, (PB91 212 522)A06.

UCB/EERC-89/08 "Seismic Performance of Steel Moment Frames Plastically Designed by Least Squares Stress Fields," by Ohi, K. and Mahin, S.A., August 1989, (PB91 212 597)A05.

UCB/EERC-89/09 "Feasibility and Performance Studies on Improving the Earthquake Resistance of New and Existing Buildings Using the Friction Pendulum System," by Zayas, V., Low, S., Mahin, S.A. and Bozzo, L., July 1989, (PB92 143 064)A14.

UCB/EERC-89/10 "Measurement and Elimination of Membrane Compliance Effects in Undrained Triaxial Testing," by Nicholson, P.G., Seed, R.B. and Anwar, H., September 1989, (PB92 139 641/AS)A13.

UCB/EERC-89/11 "Static Tilt Behavior of Unanchored Cylindrical Tanks," by Lau, D.T. and Clough, R.W., September 1989, (PB92 143 049)A10.

UCB/EERC-89/12 "ADAP-88: A Computer Program for Nonlinear Earthquake Analysis of Concrete Arch Dams," by Fenves, G.L., Mojtahedi, S. and Reimer, R.B., September 1989, (PB92 139 674/AS)A07.

UCB/EERC-89/13 "Mechanics of Low Shape Factor Elastomeric Seismic Isolation Bearings," by Aiken, I.D., Kelly, J.M. and Tajirian, F.F., November 1989, (PB92 139 732/AS)A09.

UCB/EERC-89/14 "Preliminary Report on the Seismological and Engineering Aspects of the October 17, 1989 Santa Cruz (Loma Prieta) Earthquake," by EERC, October 1989, (PB92 139 682/AS)A04.

UCB/EERC-89/15 "Experimental Studies of a Single Story Steel Structure Tested with Fixed, Semi-Rigid and Flexible Connections," by Nader, M.N. and Astaneh-Asl, A., August 1989, (PB91 229 211/AS)A10.

UCB/EERC-89/16 "Collapse of the Cypress Street Viaduct as a Result of the Loma Prieta Earthquake," by Nims, D.K., Miranda, E., Aiken, I.D., Whittaker, A.S. and Bertero, V.V., November 1989, (PB91 217 935/AS)A05.

UCB/EERC-90/01 "Mechanics of High-Shape Factor Elastomeric Seismic Isolation Bearings," by Kelly, J.M., Aiken, I.D. and Tajirian, F.F., March 1990.

UCB/EERC-90/02 "Javid's Paradox: The Influence of Preform on the Modes of Vibrating Beams," by Kelly, J.M., Sackman, J.L. and Javid, A., May 1990, (PB91 217 943/AS)A03.

UCB/EERC-90/03 "Earthquake Simulator Testing and Analytical Studies of Two Energy-Absorbing Systems for Multistory Structures," by Aiken, I.D. and Kelly, J.M., October 1990, (PB92 192 988)A13.

UCB/EERC-90/04 "Unassigned," by Unassigned, 1990.

UCB/EERC-90/05 "Preliminary Report on the Principal Geotechnical Aspects of the October 17, 1989 Loma Prieta Earthquake," by Seed, R.B., Dickenson, S.E., Riemer, M.F., Bray, J.D., Sitar, N., Mitchell, J.K., Idriss, I.M., Kayen, R.E., Kropp, A., Harder, L.F., Jr. and Power, M.S., April 1990, (PB 192 970)A08.

UCB/EERC-90/06 "Models of Critical Regions in Reinforced Concrete Frames Under Seismic Excitations," by Zulfiqar, N. and Filippou, F.C., May 1990.

UCB/EERC-90/07 "A Unified Earthquake-Resistant Design Method for Steel Frames Using ARMA Models," by Takewaki, I., Conte, J.P., Mahin, S.A. and Pister, K.S., June 1990, PB92-192947(A06).

UCB/EERC-90/08 "Soil Conditions and Earthquake Hazard Mitigation in the Marina District of San Francisco," by Mitchell, J.K., Masood, T., Kayen, R.E. and Seed, R.B., May 1990, (PB 193 267/AS)A04.

UCB/EERC-90/09 "Influence of the Earthquake Ground Motion Process and Structural Properties on Response Characteristics of Simple Structures," by Conte, J.P., Pister, K.S. and Mahin, S.A., July 1990, (PB92 143 064)A15.

UCB/EERC-90/10 "Experimental Testing of the Resilient-Friction Base Isolation System," by Clark, P.W. and Kelly, J.M., July 1990, (PB92 143 072)A08.

UCB/EERC-90/11 "Seismic Hazard Analysis: Improved Models, Uncertainties and Sensitivities," by Araya, R. and Der Kiureghian, A., March 1988, PB92-193010(A08).

UCB/EERC-90/12 "Effects of Torsion on the Linear and Nonlinear Seismic Response of Structures," by Sedarat, H. and Bertero, V.V., September 1989, (PB92 193 002/AS)A15.

UCB/EERC-90/13 "The Effects of Tectonic Movements on Stresses and Deformations in Earth Embankments," by Bray, J. D., Seed, R. B. and Seed, H. B., September 1989, PB92-192996(A18).

UCB/EERC-90/14 "Inelastic Seismic Response of One-Story, Asymmetric-Plan Systems," by Goel, R.K. and Chopra, A.K., October 1990, (PB93 114 767)A11.

UCB/EERC-90/15 "Dynamic Crack Propagation: A Model for Near-Field Ground Motion.," by Seyyedian, H. and Kelly, J.M., 1990.

UCB/EERC-90/16 "Sensitivity of Long-Period Response Spectra to System Initial Conditions," by Blasquez, R., Ventura, C. and Kelly, J.M., 1990.

UCB/EERC-90/17 "Behavior of Peak Values and Spectral Ordinates of Near-Source Strong Ground-Motion over a Dense Array," by Niazi, M., June 1990, (PB93 114 833)A07.

UCB/EERC-90/18 "Material Characterization of Elastomers used in Earthquake Base Isolation," by Papoulia, K.D. and Kelly, J.M., 1990, PB94-190063(A08).

UCB/EERC-90/19 "Cyclic Behavior of Steel Top-and-Bottom Plate Moment Connections," by Harriott, J.D. and Astaneh-Asl, A., August 1990, (PB91 229 2[illegible]/AS)A05.

UCB/EERC-90/20 "Seismic Response Evaluation of an Instrumented Six Story Steel Building," by Shen, J.-H. and Astaneh-Asl, A., December 1990, (PB91 229 294/AS)A04.

UCB/EERC-90/21 "Observations and Implications of Tests on the Cypress Street Viaduct Test Structure," by Bollo, M., Mahin, S.A., Moehle, J.P., Stephen, R.M. and Qi, X., December 1990, (PB93 114 775)A13.

UCB/EERC-91/01 "Experimental Evaluation of Nitinol for Energy Dissipation in Structures," by Nims, D.K., Sasaki, K.K. and Kelly, J.M., 1991.

UCB/EERC-91/02 "Displacement Design Approach for Reinforced Concrete Structures Subjected to Earthquakes," by Qi, X. and Moehle, J.P., January 1991, (PB93 114 569/AS)A09.

UCB/EERC-91/03 "A Long-Period Isolation System Using Low-Modulus High-Damping Isolators for Nuclear Facilities at Soft-Soil Sites," by Kelly, J.M., March 1991, (PB93 114 577/AS)A10.

UCB/EERC-91/04 "Dynamic and Failure Characteristics of Bridgestone Isolation Bearings," by Kelly, J.M. April 1991, (PB93 114 528)A05.

UCB/EERC-91/05 "Base Sliding Response of Concrete Gravity Dams to Earthquakes," by Chopra, A.K. and Zhang, L., May 1991, (PB93 114 544/AS)A05.

UCB/EERC-91/06 "Computation of Spatially Varying Ground Motion and Foundation-Rock Impedance Matrices for Seismic Analysis of Arch Dams," by Zhang, L. and Chopra, A.K., May 1991, (PB93 114 825)A07.

UCB/EERC-91/07 "Estimation of Seismic Source Processes Using Strong Motion Array Data," by Chiou, S.-J., July 1991, (PB93 114 551/AS)A08.

UCB/EERC-91/08 "A Response Spectrum Method for Multiple-Support Seismic Excitations," by Der Kiureghian, A. and Neuenhofer, A., August 1991, (PB93 114 536)A04.

UCB/EERC-91/09 "A Preliminary Study on Energy Dissipating Cladding-to-Frame Connection," by Cohen, J.M. and Powell, G.H., September 1991, (PB93 114 510)A05.

UCB/EERC-91/10 "Evaluation of Seismic Performance of a Ten-Story RC Building During the Whittier Narrows Earthquake," by Miranda, E. and Bertero, V.V., October 1991, (PB93 114 783)A06.

UCB/EERC-91/11 "Seismic Performance of an Instrumented Six-Story Steel Building," by Anderson, J.C. and Bertero, V.V., November 1991, (PB93 114 809)A07.

UCB/EERC-91/12 "Performance of Improved Ground During the Loma Prieta Earthquake," by Mitchell, J.K. and Wentz, Jr., F.J., October 1991, (PB93 114 791)A06.

UCB/EERC-91/13 "Shaking Table - Structure Interaction," by Rinawi, A.M. and Clough, R.W., October 1991, (PB93 114 917)A13.

UCB/EERC-91/14 "Cyclic Response of RC Beam-Column Knee Joints: Test and Retrofit," by Mazzoni, S., Moehle, J.P. and Thewalt, C.R., October 1991, (PB93 120 277)A03.

UCB/EERC-91/15 "Design Guidelines for Ductility and Drift Limits: Review of State-of-the-Practice and State-of-the-Art in Ductility and Drift-Based Earthquake-Resistant Design of Buildings," by Bertero, V.V., Anderson, J.C., Krawinkler, H., Miranda, E. and The CUREe and The Kajima Research Teams,, July 1991, (PB93 120 269)A08.

UCB/EERC-91/16 "Evaluation of the Seismic Performance of a Thirty-Story RC Building," by Anderson, J.C., Miranda, E., Bertero, V.V. and The Kajima Project Research Team,, July 1991, (PB93 114 841)A12.

UCB/EERC-91/17	"A Fiber Beam-Column Element for Seismic Response Analysis of Reinforced Concrete Structures," by Taucer, F., Spacone, E. and Filippou, F.C., December 1991, (PB94 117 629AS)A07.
UCB/EERC-91/18	"Investigation of the Seismic Response of a Lightly-Damped Torsionally-Coupled Building," by Boroschek, R. and Mahin, S.A., December 1991, (PB93 120 335)A13.
UCB/EERC-92/01	"Studies of a 49-Story Instrumented Steel Structure Shaken During the Loma Prieta Earthquake," by Chen, C.-C., Bonowitz, D. and Astaneh-Asl, A., February 1992, (PB93 221 778)A08.
UCB/EERC-92/02	"Response of the Dumbarton Bridge in the Loma Prieta Earthquake," by Fenves, G.L., Filippou, F.C. and Sze, D.T., January 1992, (PB93 120 319)A09.
UCB/EERC-92/03	"Models for Nonlinear Earthquake Analysis of Brick Masonry Buildings," by Mengi, Y., McNiven, H.D. and Tanrikulu, A.K., March 1992, (PB93 120 293)A08.
UCB/EERC-92/04	"Shear Strength and Deformability of RC Bridge Columns Subjected to Inelastic Cyclic Displacements," by Aschheim, M. and Moehle, J.P., March 1992, (PB93 120 327)A06.
UCB/EERC-92/05	"Parameter Study of Joint Opening Effects on Earthquake Response of Arch Dams," by Fenves, G.L., Mojtahedi, S. and Reimer, R.B., April 1992, (PB93 120 301)A04.
UCB/EERC-92/06	"Seismic Behavior and Design of Semi-Rigid Steel Frames," by Nader, M.N. and Astaneh-Asl, A., May 1992, PB93-221760(A17).
UCB/EERC-92/07	"A Beam Element for Seismic Damage Analysis," by Spacone, E., Ciampi, V. and Filippou, F.C., August 1992, (PB95-192126)A06.
UCB/EERC-92/08	"Nonlinear Static and Dynamic Analysis of Reinforced Concrete Subassemblages," by Filippou, F.C., D'Ambrisi, A. and Issa, A., August 1992, PB95-192175(A09).
UCB/EERC-92/09	"Evaluation of Code Accidental-Torsion Provisions Using Earthquake Records from Three Nominally Symmetric-Plan Buildings," by De la Llera, J.C. and Chopra, A.K., September 1992, (PB94 117 611)A08.
UCB/EERC-92/10	"Slotted Bolted Connection Energy Dissipators," by Grigorian, C.E., Yang, T.-S. and Popov, E.P., July 1992, (PB92 120 285)A03.
UCB/EERC-92/11	"Mechanical Characteristics of Neoprene Isolation Bearings," by Kelly, J.M. and Quiroz, E., August 1992, (PB93 221 729)A07.
UCB/EERC-92/12	"Application of a Mass Damping System to Bridge Structures," by Hasegawa, K. and Kelly, J.M., August 1992, (PB93 221 786)A06.
UCB/EERC-92/13	"Earthquake Engineering Research at Berkeley - 1992," by EERC, October 1992, PB93-223709(A10).
UCB/EERC-92/14	"Earthquake Risk and Insurance," by Brillinger, D.R., October 1992, (PB93 223 352)A03.
UCB/EERC-92/15	"A Friction Mass Damper for Vibration Control," by Inaudi, J.A. and Kelly, J.M., October 1992, (PB93 221 745)A04.
UCB/EERC-92/16	"Tall Reinforced Concrete Buildings: Conceptual Earthquake-Resistant Design Methology," by Bertero, R.D. and Bertero, V.V., December 1992, (PB93 221 695)A12.
UCB/EERC-92/17	"Performance of Tall Buildings During the 1985 Mexico Earthquakes," by Terán-Gilmore, A. and Bertero, V.V., December 1992, (PB93 221 737)A11.
UCB/EERC-92/18	"Dynamic Analysis of Nonlinear Structures using State-Space Formulation and Partitioned Integration Schemes," by Inaudi, J.A. and De la Llera, J.C., December 1992, (PB94 117 702/AS/A05.
UCB/EERC-93/01	"Seismic Performance of an Instrumented Six-Story Reinforced-Concrete Building," by Anderson, J.C. and Bertero, V.V., 1993.
UCB/EERC-93/02	"Evaluation of an Active Variable-Damping-Structure," by Polak, E., Meeker, G., Yamada, K. and Kurata, N., 1993, (PB93 221 711)A05.
UCB/EERC-93/03	"An Experimental Study of Flat-Plate Structures under Vertical and Lateral Loads," by Hwang, S.-H. and Moehle, J.P., February 1993, (PB94 157 690/AS)A13.
UCB/EERC-93/04	"Seismic Performance of a 30-Story Building Located on Soft Soil and Designed According to UBC 1991," by Terán-Gilmore, A. and Bertero, V.V., 1993, (PB93 221 703)A17.
UCB/EERC-93/05	"Multiple-Support Response Spectrum Analysis of the Golden Gate Bridge," by Nakamura, Y., Der Kiureghian, A. and Liu, D., May 1993, (PB93 221 752)A05.
UCB/EERC-93/06	"On the Analysis of Structures with Viscoelastic Dampers," by Inaudi, J.A., Zambrano, A. and Kelly, J.M., August 1993, PB94-165867(A06).
UCB/EERC-93/07	"Earthquake Analysis and Response of Concrete Gravity Dams Including Base Sliding," by Chávez, J.W. and Fenves, G.L., December 1993, (PB94 157 658/AS)A10.
UCB/EERC-93/08	"Model for Anchored Reinforcing Bars under Seismic Excitations," by Monti, G., Spacone, E. and Filippou, F.C., December 1993, PB95-192183(A05).
UCB/EERC-93/09	"A Methodology for Design of Viscoelastic Dampers in Earthquake-Resistant Structures," by Abbas, H. and Kelly, J.M., November 1993, PB94-190071(A10).
UCB/EERC-93/10	"Tuned Mass Dampers Using Viscoelastic Dampers," by Inaudi, J.A., Lopez-Almansa, F. and Kelly, J.M., December 1993.

UCB/EERC-93/11 "Nonlinear Homogeneous Dynamical Systems," by Inaudi, J.A. and Kelly, J.M., December 1993.

UCB/EERC-93/12 "Synthesized Strong Ground Motions for the Seismic Condition Assessment of the Eastern Portion of the San Francisco Bay Bridge," by Bolt, B.A. and Gregor, N.J., December 1993, PB94-165842(A10).

UCB/EERC-93/13 "On the Analysis of Structures with Energy Dissipating Restraints," by Inaudi, J.A., Nims, D.K. and Kelly, J.M., December 1993, PB94-203619(A07).

UCB/EERC-94/01 "Preliminary Report on the Seismological and Engineering Aspects of the January 17, 1994 Northridge Earthquake," by EERC, January 1994, (PB94 157 666/AS)A05.

UCB/EERC-94/02 "Energy Dissipation with Slotted Bolted Connections," by Grigorian, C.E. and Popov, E.P., February 1994, PB94-164605.

UCB/EERC-94/03 "The Influence of Plate Flexibility on the Buckling Load of Elastomeric Isolators," by Kelly, J.M., March 1994, PB95-192134(A04).

UCB/EERC-94/04 "Insitu Test Results from Four Loma Prieta Earthquake Liquefaction Sites: SPT, CPT, DMT and Shear Wave Velocity," by Mitchell, J.K., Lodge, A.L., Coutinho, R.Q., Kayen, R.E., Seed, R.B., Nishio, S. and Stokoe II, K.H., April 1994, PB94-190089(A09).

UCB/EERC-94/05 "Seismic Response of Steep Natural Slopes," by Sitar, N. and Ashford, S.A., May 1994, PB94-203643(A10).

UCB/EERC-94/06 "Small-Scale Testing of a Self-Centering Friction Energy Dissipator for Structures," by Nims, D.K. and Kelly, J.M., August 1994.

UCB/EERC-94/07 "Accidental and Natural Torsion in Earthquake Response and Design of Buildings," by De la Llera, J.C. and Chopra, A.K., June 1994, PB94-203627(A14).

UCB/EERC-94/08 "Preliminary Report on the Principal Geotechnical Aspects of the January 17, 1994 Northridge Earthquake," by Stewart, J.P., Bray, J.D., Seed, R.B. and Sitar, N., June 1994, PB94203635(A12).

UCB/EERC-94/09 "Performance of Steel Building Structures During the Northridge Earthquake," by Bertero, V.V., Anderson, J.C. and Krawinkler, H., August 1994, PB95-112025(A10).

UCB/EERC-94/10 "Manual for Menshin Design of Highway Bridges: Ministry of Construction, Japan," by Sugita, H. and Mahin, S., August 1994, PB95-192100(A08).

UCB/EERC-94/11 "Earthquake Analysis and Response of Two-Level Viaducts," by Singh, S.P. and Fenves, G.L., October 1994, (A09).

UCB/EERC-94/12 "Response of the Northwest Connector in the Landers and Big Bear Earthquakes," by Fenves, G.L. and Desroches, R., December 1994, PB95-192001(A08).

UCB/EERC-95/01 "Seismological and Engineering Aspects of the 1995 Hyogoken-Nanbu Earthquake," by EERC, June 1995.

UCB/EERC-95/02 "The Attenuation of Strong Ground Motion Displacement," by Gregor, N.J., June 1995.

UCB/EERC-95/03 "Upgrading Bridge Outrigger Knee Joint Systems," by Stojadinovic, B. and Thewalt, C.R., June 1995.

UCB/EERC-95/04 "Earthquake Hazard Reduction in Historical Buildings Using Seismic Isolation," by Garevski, M., June 1995.

UCB/EERC-95/05 "Final Report on the International Workshop on the Use of Rubber-Based Bearings for the Earthquake Protection of Building," by Kelly, J.M., May 1995.

UCB/EERC-95/06 "Seismic Rehabilitation of Framed Buildings Infilled with Unreinforced Masonry Walls Using Post-Tensioned Steel Braces," by Terán-Gilmore, A., Bertero, V.V. and Youssef, N., June 1995.